1. Report No. FHWA/TX-99/1364-1	2. Government Accession No.	3. Recipient's Catalog No.	
4. Title and Subtitle **BEHAVIOR AND DESIGN OF LARGE STRUCTURAL** **CONCRETE BRIDGE PIER OVERHANGS**		5. Report Date July 1996 Revised: February 1997	
		6. Performing Organization Code	
7. Author(s) **Scott D. Armstrong, Reuben M. Salas, Brad Wood, John E. Breen and Michael E. Kreger**		8. Performing Organization Report No. Research Report 1364-1	
9. Performing Organization Name and Address Center for Transportation Research The University of Texas at Austin 3208 Red River, Suite 200 Austin, TX 78705-2650		10. Work Unit No. (TRAIS)	
		11. Contract or Grant No. Research Study 0-1364	
12. Sponsoring Agency Name and Address Texas Department of Transportation Research and Technology Transfer Office P.O. Box 5080 Austin, TX 78763-5080		13. Type of Report and Period Covered Interim	
		14. Sponsoring Agency Code	

15. Supplementary Notes

Study conducted in cooperation with the U. S. Department of Transportation, Federal Highway Administration.
Research study title: "Design of Large Structural Members Utilizing Partial Prestressing"

16. Abstract

In designing large cantilever bent caps for use on recent projects under current AASHTO design specifications, designers were faced with considerable uncertainties. Questions arose when designers attempted to satisfy both serviceability and strength requirements for a series of cap designs that mixed both non-prestressed and prestressed concrete solutions. The problems were complicated because of uncertainty whether AASHTO corbel or deep beam provisions would apply. The resulting designs were highly congested, had poor constructibility and high costs.

This report outlines development of a new design approach involving use of strut-and-tie models (STM), as well as a mix of prestressed and non-prestressed main flexural reinforcement. A series of sixteen bent cap overhangs were designed, built at a reduced scale, and loaded to failure. Deflections, crack patterns and widths, reinforcement strains, and overall behavior were observed. Economic and constructibility issues were examined. The use of T-headed anchorages was explored.

A comprehensive design approach that considers both serviceability issues (deflections, cracking, crack widths, fatigue stress ranges, and side face crack control) and strength issues (ductility, adequacy of STM design and analysis of flexural capacity) was developed. Recommendations for design and detailing to improve behavior, reduce congestion and improve constructibility are provided.

17. Key Words Bridge repair, cantilever bridge piers, reinforced concrete bents, cantilever bents	18. Distribution Statement No restrictions. This document is available to the public through the National Technical Information Service, Springfield, Virginia 22161.		
19. Security Classif. (of report) Unclassified	20. Security Classif. (of this page) Unclassified	21. No. of pages 278	22. Price

Form DOT F 1700.7 (8-72)   Reproduction of completed page authorized

BEHAVIOR AND DESIGN OF LARGE STRUCTURAL CONCRETE BRIDGE PIER OVERHANGS

by

SCOTT D. ARMSTRONG, REUBEN M. SALAS, BRAD WOOD, JOHN E. BREEN AND MICHAEL E. KREGER

Research Report No. 1364-1

February 1997

This report was prepared in cooperation with the Texas Department of Transportation and the U.S. Department of Transportation, Federal Highway Administration.

DISCLAIMERS

The contents of this report reflect the views of the authors, who are responsible for the facts and the accuracy of the data presented herein. The contents do not necessarily reflect the official views or policies of the Federal Highway Administration or the Texas Department of Transportation. This report does not constitute a standard, specification, or regulation.

There was no invention or discovery conceived or first actually reduced to practice in the course of or under this contract, including any art, method, process, machine, manufacture, design or composition of matter, or any new and useful improvement thereof, or any variety of plant which is or may be patentable under the patent laws of the United States of America or any foreign country.

NOT INTENDED FOR CONSTRUCTION,
BIDDING, OR PERMIT PURPOSES

John E. Breen, Texas PE# 18479
Michael E. Kreger, Texas PE# 65541

Research Supervisors

The contents of this report reflect the views of the authors, who are responsible for the facts and accuracy of the data presented herein. The contents do not necessarily reflect the views of the Texas Department of Transportation. This report does not constitute a standard, specification, or regulation.

ACKNOWLEDGMENTS

TABLE OF CONTENTS

LIST OF FIGURES

LIST OF TABLES

SUMMARY

In designing large cantilever bent caps for use on recent projects under current AASHTO design specifications, designers were faced with considerable uncertainties. Questions arose when designers attempted to satisfy both serviceability and strength requirements for a series of cap designs which mixed both non-prestressed and prestressed concrete solutions. The problems were complicated because of uncertainty whether AASHTO corbel or deep beam provisions would apply. The resulting designs were highly congested, had poor constructibility and high costs.

This report outlines development of a new design approach involving use of strut-and-tie models (STM) as well as a mix of prestressed and non-prestressed main flexural reinforcement. A series of sixteen bent cap overhangs were designed, built at a reduced scale, and loaded to failure. A detailed explanation of the STM design for a typical specimen is given in Section 2.4.4. Deflections, crack patterns and widths, reinforcement strains and overall behavior were observed. Economic and constructibility issues were examined. The use of T-headed anchorages was explored.

A comprehensive design approach which considers both serviceability issues such as deflections, cracking, crack widths, fatigue stress ranges and side face crack control, as well as strength issues such as ductility, adequacy of STM design, and analysis of flexural capacity was developed. Recommendations for design and detailing to improve behavior, reduce congestion and improve constructibility are provided.

CHAPTER ONE

INTRODUCTION

1.1 BACKGROUND

1.1.1 Large Cantilever Bridge Piers Used on San Antonio Downtown "Y" Project

The need for this research stems from problems experienced by the Texas Department of Transportation Bridge Division when large cantilever piers were designed as substructure elements for segmental box girder bridges in the San Antonio "Y" project. This project involved the construction of an elevated freeway over an existing section of at-grade freeway. Frontage roads paralleled the lower level mainlanes and access to and from the lower level freeway was provided by entrance and exit ramps. The large cantilever piers were required where entrance or exit ramps prevented positioning the bridge piers directly below the superstructure. Figure 1.1 illustrates the typical situation where the large cantilever piers were used.

A large number of cantilever overhang lengths were required to accommodate the variety of relative positions of the superstructure, lower level mainlanes, frontage roads, and entrance and exit ramps. Loads were transferred from the superstructure through two transversely spaced bearings at the end of each span. Thus, each pier was loaded with two left bearings and two right bearings. For shorter overhangs, only the two left bearings loaded the overhang. These bearings were close to the column. For longer overhangs, both the left bearing and right bearings loaded the overhang, and these could be at a considerable distance from the column.

Figure 1. 1   Typical cantilever bridge pier

The conventional AASHTO Standard Specification for Highway Bridges (1) requires the use of corbel provisions when the shear span to depth ratio (a/d) is less than one. For shorter overhangs where all bearings were within this limit, it was appropriate to apply the AASHTO corbel provisions providing reinforcement to resist a shear-friction failure through the overhang at the face of the column. In the case of longer overhangs, where all bearings were outside this limit, AASHTO provisions could reasonably be applied to the member by treating the overhang as a beam, although very often they would be deep beams because of the low span to depth ratios.

However, because of the variety of pier sizes needed to accommodate the overall roadway geometrics, many overhangs had lengths for which the appropriate AASHTO design provisions were not obvious. Several overhangs had an a/d ratio for the inside bearing less than one and an a/d ratio for the outside bearing greater than one. In

these instances, reinforcement was provided for both deep beam provisions as well as resistance to a shear-friction failure even though it may not have been necessary. Consequently, reinforcing cages were heavily congested and difficult to construct, and may have been significant over-designed. Figure 1.2 shows an example of a typical TxDOT bent cap design.

The design of the overhangs was further complicated by the use of reinforced (i.e., Non-prestressed) concrete for some structures and post-tensioned concrete for others. The current non-LRFD AASHTO bridge design specification places different strength and serviceability requirements on each, treating them in separate chapters as essentially separate and unique materials.

For reinforced concrete, only mild reinforcement is used and the design is largely in accordance with an ultimate strength design philosophy. The serviceability provisions guard against fatigue failure of the reinforcement, excessive crack widths, and excessive deflections. Fatigue failure of the reinforcement is prevented by providing sufficient reinforcement to control the range of stress experienced by the steel as loads cycle on and off the member. Crack widths are controlled by providing the required area of steel, but also by using a large enough number of bars so that the crack width formulae are indirectly satisfied. This leads to cracking patterns in which the cracks are well distributed and in which crack widths are acceptably small. However, the required number of bars to satisfy the crack width provisions can become quite numerous, leading to highly congested reinforcing cages which are difficult to assemble and which create problems with the placement and consolidation of concrete. Furthermore, the cracking can significantly reduce the stiffness of the member and can lead to difficulties in obtaining acceptable service load deflections.

Post-tensioned concrete, on the other hand, is designed under the AASHTO criteria primarily in accordance with a service load, or work stress, design philosophy. Members are required to be "fully post-tensioned" which means that the tensile stresses in the concrete under service loads are limited to levels below which cracking would be expected to occur. This results in quantities of post-tensioning which are much greater than would be required if an ultimate strength design approach governed. Excessive camber of a member can be a problem when the large amounts of post-tensioning required by service load stress criteria are used. The high camber occurs over time with creep and shrinkage of the concrete under the large post-tensioning force. In the even that a fully post-tensioned member does crack due to poor construction or an extreme overload, a sufficient number of non-prestressed reinforcing elements often may not be present to control the cracking. Additionally, fully post-tensioned concrete exhibits considerably less ductility than reinforced concrete. This results in less warning of distress and less general structural integrity when the structure is subjected to unanticipated accidental loads.

As previously mentioned, some of the piers in San Antonio were designed using AASHTO reinforced concrete provisions while others were designed using AASHTO fully post-tensioned concrete provisions. Because of the greatly different design approaches required by the AASHTO provisions, it was not uncommon for two adjacent overhangs, having only slightly different strength requirements, to be designed with significantly different strengths and service load behavior. This would occur when one overhang was designed using reinforced concrete, but it would be then found not possible to provide enough mild reinforcement for strength in the
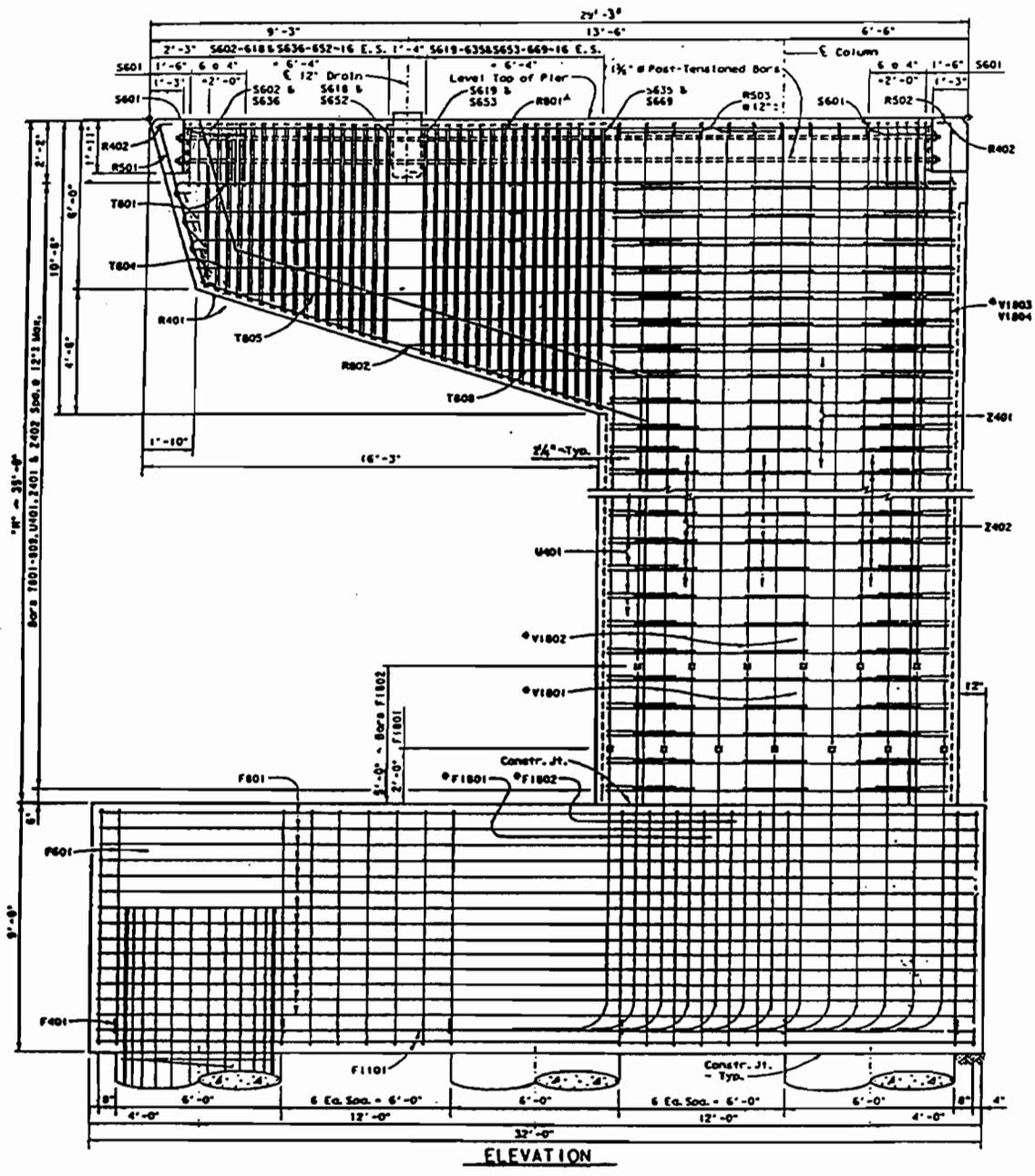
Figure 1. 2   Typical TxDOT bent cap design

3

second overhang because the cage would become excessively congested. The second overhang would have to be redesigned as a fully post-tensioned member, basically governed by the service load design provisions of AASHTO.

1.1.2 New Approaches

In order to find improved solutions for a rational design approach for such large irregular members, it is necessary to look at relatively new philosophies of design that have been developed and investigated during recent years. The general structural concrete approach presented by Schlaich et.al. (2), and endorsed by the IABSE Colloquium on Structural Concrete (3), is a logical way of providing a smooth transition between conventionally reinforced and fully prestressed structures. With the use of this concept, prestressed structures are designed for a mix of active (prestressed) and passive (non-prestressed) reinforcement without arbitrary requirements for limiting service level tensile stresses. The structures may be cracked under service loads but cracks are controlled. This results in a reduced consumption of prestressing steel and avoids unnecessarily high factors of safety against failure. With regard to the design of discontinuity regions such as those in corbel, bracket or deep beam structures, previous research conducted at The University of Texas at Austin (4), TxDOT Project 1127, highly recommended the use of strut-and-tie models as useful and rational detailing tools. As expressed in that report, the use of the method enables the designer to have a better understanding of the distribution of internal forces in the structure. In particular, it is of great assistance in proportioning reinforcement.

Concerning congestion in reinforcement development areas, the use of T-headed reinforcing bars has also been studied as a new technique that has been used with success in offshore structures, especially for shear reinforcement. This practice, which replaces hooked bars, not only reduces the congestion in problem regions, allowing for an adequate placement of the concrete mix, but also makes construction of the reinforcing cages much easier.

All of these approaches were investigated in this portion of the overall project.

1.1.3 Strut-and-Tie Modeling

The ambiguity associated with the design of the overhangs with intermediate a/d ratios (in which deep beam, corbel, and shear-friction provisions all were applied), and the highly congested reinforcing cages which resulted, could have been alleviated with the use of strut-and-tie modeling.

In strut-and-tie modeling (2), the designer is directed toward an approach which emphasizes tracing the flow of forces through a structure. The flow of forces, or load paths, are made up of zones of compressive and tensile stresses. The zones of compressive stresses are referred to as struts and the load carrying capacity of the struts is a function of the compressive strength of the concrete. The zones of tensile stresses are referred to as ties. The ties are made up of reinforcement which is provided in sufficient quantities to carry the tension forces.

4

The strut-and-tie modeling approach is in contrast to the section-by-section approach to design inherent in today's design codes. It is this section-by-section approach that caused the difficulty faced by the designers in determining whether overhangs with intermediate a/d ratios should be designed as corbels or as deep beams. Strut-and-tie modeling offers an approach which is transparent and allows the designer to visualize more clearly where reinforcement is needed, giving a more rational approach to the design of members for which application of more empirical code equations is not obvious. In order to assist designers not familiar with strut-and-tie modeling, considerable detail is given in section 2.4.4 for one of the overhangs

It is commonly recognized that the traditional section-by-section analysis and design works satisfactorily, and may be the preferred method of design, in those regions of a structure where the Bernouli assumption that plane sections remain plane is valid. These regions are referred to as B-regions. The longer cantilever overhangs in San Antonio could reasonably be treated as having a large portion of B-region.

The strut-and-tie approach is preferred in those regions of a structure where the Bernouli assumption is not valid and the appropriate application of existing and generally highly empirical code equations is not clear to the designer. These regions are referred to as Discontinuity regions or D-regions. The overhangs of the large cantilever piers in San Antonio with bearings close to the column should be treated as D-regions.

1.1.4 Structural Concrete

The situation described in Section 1.1.1, where two adjacent overhangs would have significantly different strengths and service load performance, is fundamentally irrational and is a consequence of the AASHTO treatment of reinforced concrete in one chapter as if one material, while post-tensioned concrete is treated in a separate chapter as if a separate material. A more reasonable approach would involve the use of what many researchers traditionally referred to as "partial prestressing," but which now is giving way to a more unified approach termed "structural concrete."

The term, partial prestressing, is not advocated here because it has historically been the source of confusion among researchers and structural engineers. The confusion has centered around the manner in which the degree of partial prestressing would be defined. Several different definitions have been proposed through the years but no single definition has earned universal acceptance and usage. One major usage of the term, partial prestressing, was to signify designs based on combinations of mild and pretensioned (or post-tensioned) reinforcement. An ultimate strength design approach is taken considering the contributions at ultimate of both non-prestressed and prestressed reinforcement so that the member strength is in proportion to the demand from factored loads. Secondary checks are made of serviceability conditions. This design approach is closely patterned after the procedure for a member designed with only mild reinforcement.

Members designed with combinations of non-prestressed and prestressed reinforcement offer many advantages over either reinforced concrete or fully post-tensioned concrete for cases like the large cantilever overhangs used in San Antonio. The highly congested cages of the reinforced concrete members could be greatly

5

reduced by substitution of post-tensioning for some of the mild reinforcement. This would lead to cages which would be much easier to assemble and to members for which good placement and consolidation of concrete would be easier to achieve. The overhangs might be expected to be cracked at loads below or slightly above service loads, but the mild reinforcement would be available to distribute the cracks and control the crack widths. The expected amount of cracking would be less than for the reinforced concrete overhangs, so greater member stiffness would be available to control service load deflections.

The reduction of post-tensioning offers advantages over fully post-tensioned members in that excessive cambering of the member could be avoided, ductility could be improved and cost savings are possible.

The proposed term "structural concrete" would apply to the full spectrum of concrete members carrying structural loads from plain concrete, to those with mild, prestressed, or mixed reinforcement. With this term, the need for a single, universally accepted, definition of the degree of prestressing is eliminated and the related confusion is avoided. Also embodied in the structural concrete approach is a unified design methodology which is applicable to all structural concrete, regardless of the type of reinforcement that is used. It is hoped that eventually this integrated approach will replace the current approach taken in AASHTO and other codes which treats reinforced and prestressed concrete in separate chapters and with different strength and serviceability criteria.

1.1.5 T-Headed Reinforcement

In recent years the extreme congestion of reinforcement in the cages for offshore concrete structures has led to the development of improved ways to anchor reinforcement. Hooks have been replaced by headed reinforcing bars wherein a plate is attached transversely to the bar at its ends to serve as an anchorage. The attachment is frequently done by friction welding. A major proponent of the use of such headed reinforcing bars has been the firm of Norwegian Contractors. While such headed bars are often used as shear reinforcement, they have also been used for anchorage of flexural reinforcement in areas of structures where insufficient lengths are available for straight bar development or standard hooks. Some applications are with stub cantilevers, corbels, brackets and daps.

1.2 RESEARCH PROJECT 1364

In order to address the overall problem of developing a safe, economical and rational design procedure for large, irregular bridge support structures such as the large cantilever bridge piers used in the San Antonio "Y", the Texas Department of Transportation and the Federal Highway Administration co-sponsored Research Project 1364 entitled, *"Design of Large Structural Members Utilizing Partial Prestressing,"* at the Center for Transportation Research of The University of Texas at Austin. Detailed tests and investigations were carried out at the University's Ferguson Structural Engineering Laboratory.

In order to investigate the problem systematically, the project was broken into three phases. This report specifically is restrictive to the first phase in which the continuity

Side View **End View**
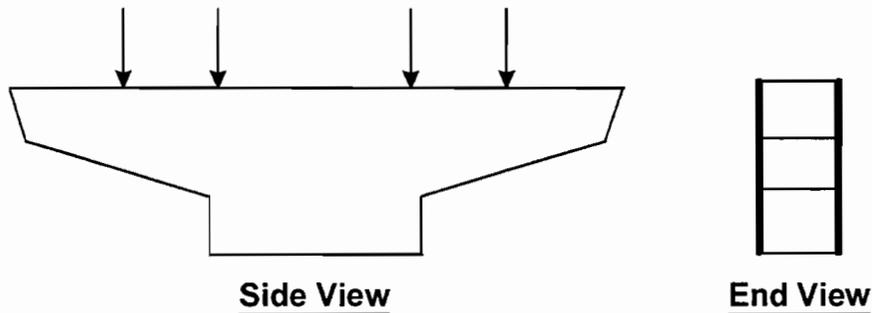
Figure 1. 3   Multiple overhang specimen

and anchorage conditions of the reinforcement in the connection zone, between the overhang and the prismatic pier shaft shown in Figure 1.1, was eliminated. Design and testing used the geometrically symmetrical reduced specimen shown in Figure 1.3. In this specimen, general actions in the overhang are similar to those in the prototype, although actions in the joint between the overhangs and the pier shaft greatly differ from conditions typical of Figure 1.1.

Later phases of the project, to be reported by Wood, Scott and Kreger, tested overall specimens similar to Figure 1.1 and will be reported in CTR Report 1364-2F.

1.3 OBJECTIVES

The overall objectives of the initial phase of Project 1364 reported herein are:

a) to develop a better understanding of the influence of post-tensioning on the requirements for non-prestressed reinforcement in large structural concrete members such as these cantilever overhangs.

b) to develop a rational unified design methodology for structural concrete that is envisioned to include applications of strut-and-tie models and to facilitate the efficient use of mixed prestressed and non-prestressed reinforcement for use on large cantilever bridge pier overhangs of intermediate length for which application of the current AASHTO provisions is ambiguous. The procedure should be rational, transparent, and easy to use. It should result in overhangs which have acceptable service load performance as well as ultimate strength, and which would be more easily constructed and economical than designs resulting from current AASHTO standards.

c) to make the finding of this study available for consideration by code and specification-writing bodies as soon as results of the research program are approved by TxDOT.

The specific objectives of this portions of the research program, Series 1364-1, are:

a) to design, build, and test under static loading, sixteen 1/5.5 scale post-tensioned cantilever overhangs with varying mixtures of prestressed and non-prestressed reinforcement using both conventional and strut-and-tie models for shear design, and to compare results with allowable and analytical performance;

b) to test T-headed reinforcing bars for flexure in some models to evaluate their performance in crack control, in reducing congestion in anchorage areas, and in

7

improving constructibility of the reinforcing cages when compared to companion specimens; and

c) to evaluate the use of different areas of skin reinforcement in controlling crack widths at service loads (minimum face steel and skin reinforcement as suggested by Frantz and Breen (5) as well as variations).

1.4 ORGANIZATION OF REPORT

This report is divided into seven chapters. The contents of Chapters 2 through 7 are briefly described here:

Chapter Two: Experimental Program — detailed description of specimen design, fabrication and testing.

Chapter Three: Test Results — presentation of data collected during the testing of each specimen.

Chapter Four: Analysis of Test Results — analysis and discussion of service load and ultimate load behavior of each specimen, as well as comparison between specimens.

Chapter Five: Overhang Constructibility — discussion of construction-related topics, material quantities, costs and economics.

Chapter Six: Design Recommendations — discussion of recommended design procedure.

Chapter Seven: Summary and Conclusions — summary of key elements of experimental program and significant findings from research

1.5 SOURCES

The test programs reported herein were carried out by three different members of the project team. Considerable detail on specimens, measurements, and observations beyond the summary of observations reported herein are available in two M.S.E. theses filed in the General Library of The University of Texas at Austin. They are:

1) Armstrong, Scott D., *"Design and Behavior of Large Concrete Cantilever Overhangs with Combinations of Prestressed and Non-Prestressed Reinforcement,"* MSE Thesis, The University of Texas at Austin, August 1994.

2) Salas Pereira, Ruben M., *"Behavior of Structura Concrete Cantilever Piers Using T-Headed Reinforcing Bars and Various Design Criteria,"* MSE Thesis, The University of Texas at Austin, August 1994.

CHAPTER TWO

EXPERIMENTAL PROGRAM

2.1 INTRODUCTION

The purpose of this experimental program was to study the behavior of varied mixtures of prestressed and non-prestressed reinforcement in design of large bridge support structures using an ultimate design approach, including the state-of-the-art in strut-and-tie modeling for shear, the state-of-the-art in T-headed reinforcement for non-prestressed flexural reinforcing steel, and varying amounts of skin reinforcement. All eight specimens (sixteen overhangs) were designed, fabricated, post-tensioned and tested at the Ferguson Structural Engineering Laboratory at The University of Texas at Austin.

Each specimen was loaded to failure with specific observation made of the service load behavior. Service loading of the test specimens simulated superstructure dead loads and traffic live loads.

2.2 DESIGN AND LOADING OF THE SPECIMENS

2.2.1 Specimen Dimensions

The dimensions of the specimen overhang was determined by examining typical cantilever piers utilized on the San Antonio Downtown "Y" project. Overhang lengths varied in these piers from less than two feet (0.6 m) to approximately 25 feet (7.6 m). The maximum depths of the caps, at the column face, varied from eight feet (2.4 m) to as much as 13 feet (4.0 m), and the widths of the piers ranged from eight (2.4 m) to 10 feet (3.0 m). The average distance between the left and right bearings was approximately 12 feet (3.6 m). Typical reinforcing bars used in those designs included #11 and #8 bars for flexural reinforcement, and #6 and #4 bars for shear reinforcement in the overhang structure. For the column section typical bars included #18 bars for the vertical (main) steel and #4 bars for the horizontal (stirrup) steel.

Each of these dimensions was considered to arrive at a typical prototype overhang of intermediate length for which design of the reinforcement by the current AASHTO provisions would be ambiguous. The overall dimensions of this overhang are shown in Figure 2.1.

2.2.2 Scale Factor Selection

Various geometric scale factors were studied based on economics, available materials, fabrication methods, and testing procedures. After this review, a scale factor of 5.5
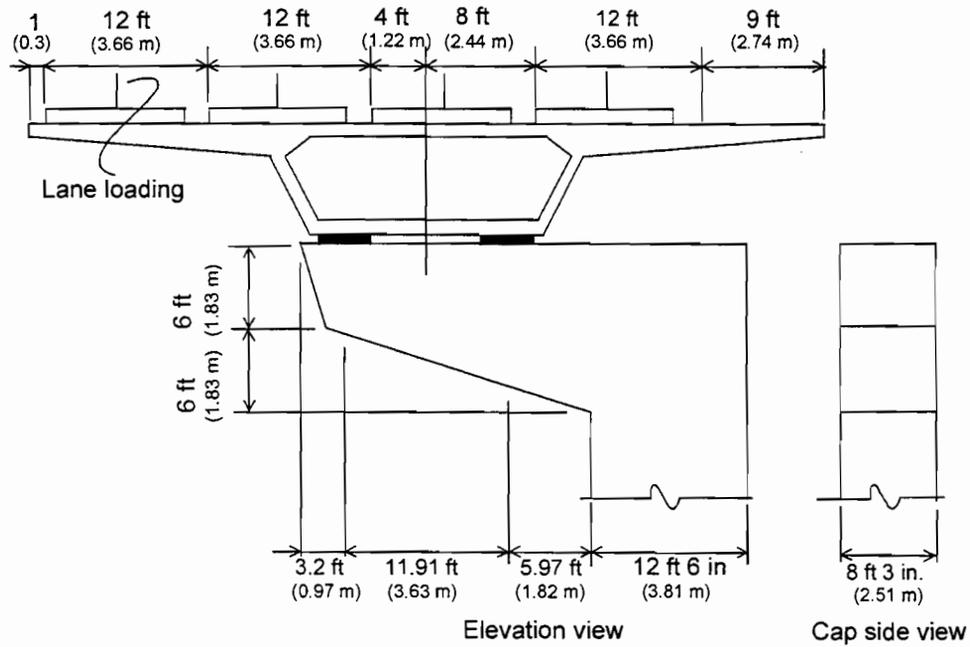
Figure 2. 1   Prototype structure and superstructure
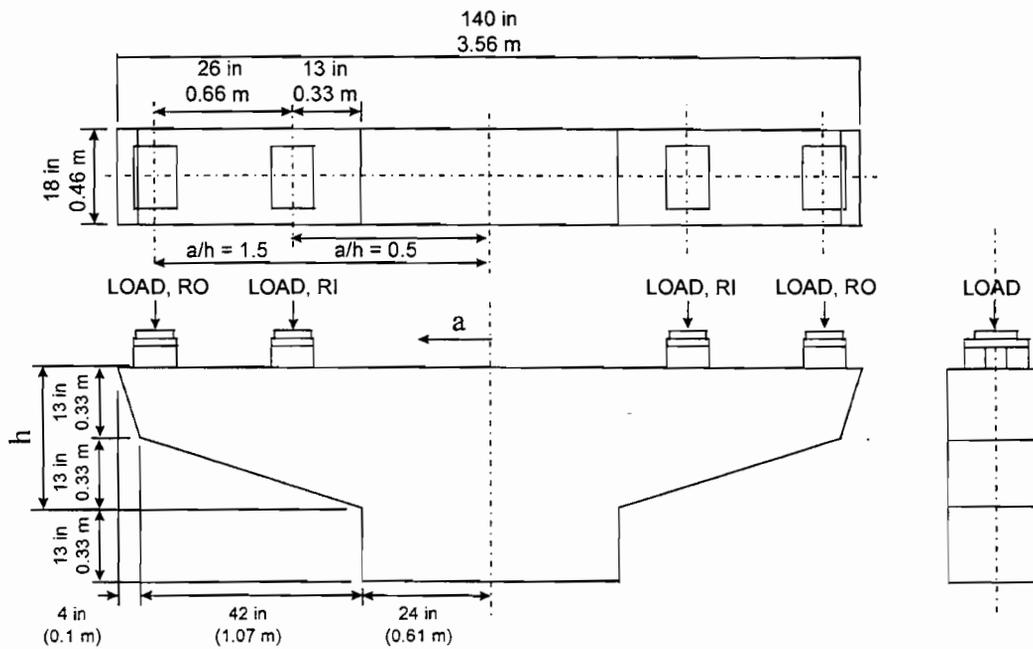
Figure 2. 2   Geometry of the scale specimens

10

was chosen. One of the major considerations was the ability to scale down the commonly used #11 and #8 reinforcing bars to available deformed #2 bars and 7-gage wire, respectively. In addition, this scale factor allowed for a modest size test set-up without exceeding the capacity of the available testing equipment.

2.2.3 Model Selection

The model geometry used for construction of test specimens is shown in Figure 2.2. This geometry was selected to simplify the loading arrangement by allowing testing of two cantilever overhangs simultaneously, providing a balanced moment at the column section. By loading "T"-shaped specimens symmetrically on both sides, the complicated details of anchoring the column of an "L" shaped specimen to develop the column moment were eliminated.

The resulting overall specimen dimensions are shown in Figure 2.2. The position of the bearings relative to the column face are also shown in Figure 2.2. The a/h ratios were 0.5 for the inside bearings and 1.5 for the outside bearings. At ultimate load levels it was recognized that only one overhang would fail. This was accepted since the focus of the experimental program was the performance of the models at service loads and full information at service load levels as well as factored load levels could be obtained for both overhangs.
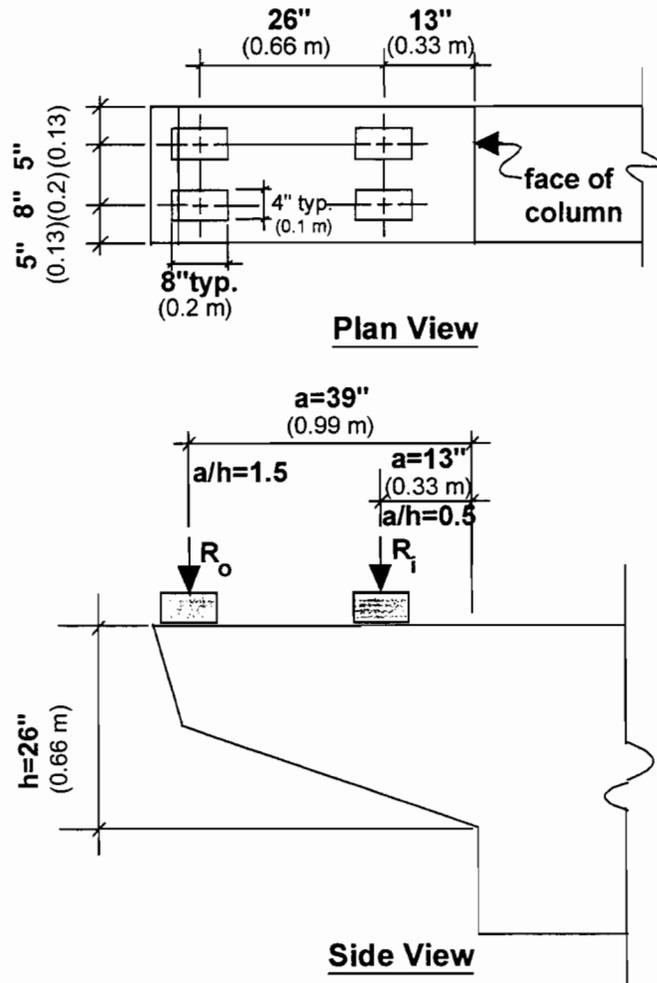
Figure 2. 3   Location of loads and bearing arrangement

2.2.4   Size and Arrangement of Bearings

The size and arrangement of bearings used was also derived from the typical full-scale bridge. Bearing sizes varied in the full-scale piers, depending on whether the bearing was fixed, sliding, or sliding at an expansion joint. The average dimensions and distances between these three bearing types was considered in the selection of

bearing sizes and arrangements to be used on the model piers. The size of the bearings used in the tests was 4-in x 8-in. (.10 m x .20 m).

Since each pier supported a back span and a forward span, each cantilever overhang had four bearing locations, as shown in Figure 2.3.

2.2.5 Materials Modeling

2.2.5.1 Concrete

The concrete mix design was carried out to provide a concrete strength at 28 days of 5000 psi (34.5 MPa), as commonly used by TxDOT in the full-size piers (see mix details in Section 2.5.1). The maximum aggregate size was limited to 3/8-in. (9.5 mm) to allow for adequate placement of the mix. With this design the stress-strain behavior of the concrete was assumed to be equal to that of the prototype, allowing for use of stress and strain scale factors equal to unity.

The typical concrete cover used in the specimens was 0.41 in. (10 mm). This is in direct scale with a cover of 2-1/4" (57 mm) which was typically used in the full-scale piers.

2.2.5.2 Reinforcing Bars

It was desired that the same number and equivalent size of bars be used in the models that would have been used if full-scale piers were being constructed. This was important because the distribution of the reinforcement was of primary concern for controlling crack widths.

An examination was made of the typical full-scale piers to determine the bar sizes that were used for each of the different types of mild reinforcement. Each model overhang was designed initially with the prototype dimensions giving the required number and size of each bar. Reinforcing bars or wires were then selected for the models by scaling each bar by using the closest available bar or wire diameter resulting when the full-scale diameter was divided by 5.5. A slight adjustment to the number of bars was permitted where the exact diameter was not available. Similarly, in most models, if the yield strength of the model reinforcement was significantly different than the assumed grade of the prototype reinforcement, 60 ksi (420 MPa), the number of bars or wires was again adjusted. This was the case for the #2 reinforcing bars and the 7- and 9-gauge wires. The #3 reinforcing bars and 10-guage wire had measured yield strengths close to 60 ksi (420 MPa) so no adjustment was made to the number of these on the basis of yield strength.

The adjustments ensure that the tensile yield provided by the reinforcement in the models was nearly equivalent to the tensile yield force in the prototype. Table 2.1 lists the size of reinforcement for the prototype design and the number of bars or wires used in the model specimens to substitute for each prototype bar.

Table 2. 1   Typical Mild Reinforcement in Models (CO-RU)

Type of Mild Reinforcement	Size of Prototype Reinforcement	Size of Model Reinforcement	Number of Model Bars or Wires Used for Each Prototype Bar
Moment Bars Top Bars Bottom Bars	No. 11	No. 2	0.86
Side Face Bars Shear-Friction Bars Horizontal Shear Bars Top Bars Bottom Bars	No. 8	7 ga. Wire	0.77
Double Shear Stirrups Anchorage Zone Stirrups	No. 6	10 ga. Wire	1.08
Vertical Column Steel Column Ties	No. 18 No. 4	No. 3 9 ga. Wire	1.20 0.61

The post-tensioning in the models was similar to what would have been used in a full-scale design. It was observed that the most common size of tendon used in the San Antonio project was a 19-strand, 0.6-in. diameter tendon. The required number of these tendons, with the effective depth at the location typically observed in the San Antonio designs, was determined for each overhang. The models were designed with approximately the same number of tendons at an equivalent effective depth by selecting appropriate combinations of 3/8-in. (9 mm), ½-in. (13 mm), and 0.6-in. (15 mm) diameter strands. In the models each tendon was a single strand of one of these sizes. The result was that each single strand tendon in the model represented approximately one 19-strand tendon in the prototype.

Double vertical shear stirrups were used as web reinforcement, as this was observed to be typical in the full-scale piers.

2.2.6 Load Similitude

Load relations between prototype and model were calculated based on scale factors as (6):

1. Loads distributed over an area:

Model load per unit area = prototype load per unit area   (2.1)

2. Load distributed over a length

Model load per unit length = $\dfrac{1}{5.5} \times$ prototype load per unit length   (2.2)

3. Concentrated loads

$$\text{Model load} \;=\; \frac{1}{5.5^2} \times \text{prototype load} \qquad\qquad (2.3)$$

4. Gravity loads

$$\text{Model density} \;=\; 5.5 \times \text{prototype density} \qquad\qquad (2.4)$$

Using these relations, the measured strain in the model was assumed equal to the prototype strain, and the model deflections were 1/5.5 type the prototype deflections.

The requirement for increased model density was overcome with the application of eternal loads from the loading rams as discussed later.

2.2.7 Critical Load Cases

Load Group I from the AASHTO Bridge Design Specifications was assumed to be critical for the member so only dead load (D) and live load plus impact (L + I) were considered.

A superstructure was assumed with similar characteristics to that used in San Antonio (Pier D36 - San Antonio "Y" Project III - C & D). The bridge was wide enough for four lanes of traffic. It was arbitrarily decided that the pier would be an interior pier in a four-span continuous unit with 110-ft. spans.

The dead load of the superstructure was taken as the weight of 110 feet of the typical superstructure increased by a continuity factor of 1.143 since an interior pier was assumed. This load was assumed to be split evenly between all bearings.

The live loading was based on AASHTO lane loads increased by a continuity factor of 1.223 for the case of the first, third, and fourth spans of the unit loaded. This was further increased by a factor of 1.213 to account for impact loading.

Two different live load cases were determined to be critical for the design of the specimen. The case of the outside three lanes loaded was found to produce the maximum moment at the column face. The case of all four lanes loaded was critical for producing the maximum shear at the column face. These two cases are referred to as flexure loading and shear loading, respectively.

Factored loads were determined by application of AASHTO code Equation (3-10):

$$\gamma[\beta_D \bullet D + \beta_L (L + I)] \qquad\qquad (2.5)$$

For flexural and tension members and a Group I load combination, this equation reduces to the following:

$$1.3[1.0D + 1.67(L + I)] = 1.3D + 2.17(L + I) \qquad (2.6)$$

Table 2.2 summarizes critical loads for the specimens.

The basic design for all specimens began with the same model loads at service load level. As indicated later in the text, various theories were used to design the individual models but always starting from the same service loads. In two specimens, the nominal yield point of the bars was used (as would be typical in design). All other specimens used actual yield points of the bars in calculating ultimate capacities. Thus if all design philosophies examined were equally valid and accurate, one would expect all of the specimens (except for the two based on nominal yield point) to have the same failure loads if they all failed in flexure or to have somewhat different loads if they failed in shear. (Note the difference between factored loads for flexure and for shear in Table 2.2).

2.3 OVERALL EXPERIMENT DESIGN

The sixteen cantilever overhangs tested in this phase were designed and tested progressively. Changes were made in approach in some cases as results from earlier tests were analyzed. In particular, examination of data indicated that some horizontal restraint at loading bearings was probably occurring in some of the initial models tested so elastomeric pads were introduced into the loading arrangement for later specimens. This has some effect on ultimate load conditions but negligible effect at service loads. Such changes will be clearly pointed out where germane to the discussion.

2.3.1 Specimen Identification Code

Each specimen overhang is given a distinctive six-part identification code as shown in Table 2.3.

2.3.2 Major Specimen Variables

The sixteen cantilever overhangs tested in this phase were constructed as eight individual bent-cap specimens, each with two symmetrically-loaded overhangs. All specimens had the same minimal compressive strength of 5000 psi (35 MPa) and the same external dimensions. The only variable in loading was that some specimens were loaded through steel bearings. When it was discovered that some lateral restraint might be present near ultimate loads, other specimens (1, 5, 7 and 8) were loaded with large elastomeric bearing pads to relieve such restraint possibilities. These cases will be clearly indicated when discussing ultimate moment capacities.

15

Table 2. 2   Prototype and Model Design Loads

Description		Prototype Load		Model Load	
		kips	kN	kips	kN
Flexure Design Loads					
Service Loads	Ro*	1680	7473	55.5	247
	Ri*	1031	4586	34.1	152
	Dead load cap***	220	979	1.32 model	5.87 model
				5.94 additional****	26.42 additional
Factored Loads**	Ro	2621	11658	86.6	385
	Ri	1212	5391	40.1	178
	Dead load cap	286	1272	1.7 model	7.56 model
				7.7 additional	34.25 additional
Shear Design Loads					
Service Loads	Ro	1276	6120	45.5	202
	Ri	1376	6120	45.5	202
	Dead load cap	220	979	1.32 model	5.87 model
				5.94 additional	26.42 additional
Factored Loads	Ro	1959	8714	64.8	288
	Ri	1959	8714	64.8	288
	Dead load cap	286	1272	1.7 model	7.56 model
				7.7 additional	34.25 additional

*   Ri and Ro include dead loads from superstructure, live load and impact
        Ro - outer bearing load
        Ri - inner bearing load (see Fig 2.3)
**   Load factors are based on Group I loading (AASHTO provisions)
***   Overhang dead load refers to the resultant dead load applied at the centroid of
        the structure
****   Additional dead loads (simulated dead loads) were applied to the models through
        the same loading rams used to apply the Ri and Ro loads. 75.4 percent of the
        additional dead load was applied in combination with Ri load (at 13 inches from
        the face of the column), while 24.6 percent was applied in combination with the
        Ro load (at 39 inches from the face of the column).

16

The major variables were in the design philosophies and reinforcement details in the various specimens. As indicated in the model identification code summary in Table 2.3, six major designations denote the principal variables:

1.   Type of structure — All specimens in this phase were cantilever overhang specimens with the external geometry shown in Figure 2.2

2.   Flexural design philosophy — A major difference between specimens was the basic flexural design philosophy used. Major categories were:

      a)   Reinforced concrete (no prestressing) in which the normal AASHTO provisions for flexure were used in which ultimate strength governs the amount of flexural reinforcement with serviceability checks such as the

Table 2. 3   Model Identification Code

Model ID	Description
CO	Type of structure: Cantilever overhang
RU-PS-PU	Design philosophy: RU - Reinforced concrete with ultimate strength governing PS - Prestressed concrete with service conditions governing PU - Prestressed with ultimate strength concrete governing
0S-54S-74S-100S	Percentage of reinforcement nominal tensile strength which is prestressed and type of steel: X% prestressing, with strands
NA-OR-TH	Type of anchorage for non-prestressed flexural reinforcement: NA - Not applicable OR - Conventional anchorage TH - T-heads
N-V-I-M	Type of strut-and-tie model used for shear: N - None V - Vertical tie I - Inclined tie M - Modified to include concrete contribution **M1 for $v_c = 1\sqrt{f'_c}$** **M1.7 for $v_c = 1.7\sqrt{f'_c}$**
SF - SM	Design of side face reinforcement: SF - Based on Frantz SM - TxDOT Minimum
Example	CO-PU-54S-TH-V-SM

Z factor to determine the number of bars that must be used.

   b)   Prestressed concrete with the normal AASHTO provisions for service load stress limits govern the amount of prestressing that must be provided at the effective prestress level after losses taken here as 160 ksi (1120 MPa). Such specimens will generally have an ultimate capacity greater than required for factored load design.

   c)   Prestressed concrete with ultimate strength calculations governing the amount of prestressed and non-prestressed reinforcement provided in order to satisfy the ultimate capacity required for factored load design. Service load tensile stress limits in AASHTO are not satisfied but various percentages of tensile force may be supplied as non-prestressed reinforcement to ensure proper crack control and fatigue stress ranges. Determination of the proper values of such distribution between prestressed and non-prestressed reinforcement is a major goal of this study. Mixed reinforcement (prestressed and non-prestressed) are referred to as Structural Concrete in Table 2.4.

3. Percentage of the total tensile force of flexural reinforcement at ultimate which is provided by the prestressed reinforcement — Determined as the total area of prestressing strand times its calculated stress at nominal strength are determined by AASHTO equations divided by the sum of that ultimate prestressing reinforcement force and the product of the area of non-prestressed flexural reinforcement times its yield strength. This percentage of tensile force sets the area of prestressing steel and the service level prestressing force and hence service level stress conditions. They need not satisfy current AASHTO limits as this is the purpose of the investigation to investigate the effect of such a condition.

4. Type of anchorages of non-prestressed flexural reinforcement — half of the specimens used normal development length or had hooks for flexural bar anchorage. The other half used T-headed bars.

5. Shear design philosophy — another major difference between specimens was the basic shear design philosophy used. Major categories were:

   a)   No strut-and-tie model but shear reinforcement determined by the empirical equations and conditions of the conventional AASHTO approach.

   b)   Strut-and-tie model using vertical ties

   c)   Strut-and-tie model with vertical tie but supplemented by a concrete shear capacity contribution v_c of $1\sqrt{f_c'}$ or $1.7\sqrt{f_c'}$. In the latter case, only normal AASHTO minimum stirrups are required.

Table 2. 4   Summary of Specimen Variables

Specimen		Overhang Designation	Flexural Design	Percentage of Tensile Force Provided by Prestressing Strand	Flexural Reinforcement Anchorage	Shear Design Philosophy*	Side Face Steel	Bearing Pads
1	A	CO-RU-0S-OR-N-SF	Reinforced concrete AASHTO strength	0	Conventional	Conventional AASHTO and shear friction	Frantz	elastomeric
	B	CO-RU-0S-OR-N-SF	Reinforced concrete AASHTO strength	0	Conventional	Conventional AASHTO and shear friction	Frantz	elastomeric
2	A	CO-PS-100S-NA-N-SM	Prestressed concrete AASHTO service	100	No rebar	Conventional AASHTO and shear friction	Prototype #8@12″	steel
	B	CO-PS-100S-NA-N-SM	Prestressed concrete AASHTO service	100	No rebar	Conventional AASHTO and shear friction	Prototype #8@12″	steel
3	A	CO-PU-100S-NA-V-SM	Prestressed concrete AASHTO strength	100	No rebar	STM vertical ties	Prototype #8@12″	steel
	B	CO-PU-100S-NA-I-SM	Prestressed concrete AASHTO strength	100	No rebar	STM inclined ties	Prototype #8@12″	steel
4	A	CO-PU-74S-OR-V-SM	Structural concrete strength	74	Conventional	STM vertical ties	Prototype #8@12″	steel
	B	CO-PU-74S-OR-I-SM	Structural concrete strength	74	Conventional	STM inclined ties	Prototype #8@12″	steel
5	A	CO-PU-54S-TH-V-SF	Structural concrete strength	54	T-head	STM vertical ties	Frantz	elastomeric
	B	CO-PU-54S-TH-I-SM	Structural concrete strength	54	T-head	STM inclined ties	Prototype #8@18″	elastomeric
6	A	CO-Pu-74S-TH-V-SM	Structural concrete strength	74	T-head	STM vertical ties	Prototype #8@18″	steel
	B	CO-PU-74S-TH-I-SM	Structural concrete strength	74	T-head	STM inclined ties	Prototype #8@12″	steel
7	A	CO-PU-100S-TH-V-SF	Structural concrete strength	100	Several supplementary T-head bars for construction	STM vertical ties	Frantz	elastomeric
	B	CO-PU-100S-TH-I-SM	Structural concrete strength	100	Several supplementary T-head bars for construction	STM inclined ties	Prototype #8@18″	elastomeric
8	A	CO-RU-0S-TH-M1-SM	Reinforced concrete AASHTO strength	0	T-head	STM vertical tie but $V_c = 1.7\sqrt{f_c'}$	Prototype #8@18″	elastomeric
	B	CO-RU-0S-TH-M1.7-SM	Reinforced concrete AASHTO strength	0	T-head	STM vertical tie but $V_c = 1.7\sqrt{f_c'}$	Prototype #8@12″	elastomeric

*STM = Strut-and-Tie Model

d)   Strut-and-tie model using inclined ties (while inclined ties were used in the strut-and-tie modeling - example Figure 2.27- the actual reinforcement provided was orthogonal satisfying the vertical and the horizontal components of the inclined tie force - example Figures 2.19 and 2.21).

6.   Side face or skin reinforcement design — Because these members are very deep, they must have supplementary side face or skin reinforcement distributed along their side faces to ensure that cracking away from the level of the main tensile reinforcement is controlled. Two general levels of skin reinforcement were provided. One is based on the recommendations of Frantz and Breen (5) which is used in AASHTO, while the other is an arbitrary minimum reinforcement used by TxDOT in the San Antonio "Y" structures that corresponds in full-scale to #8 bars at 12-in. (305-mm) in reinforced concrete or 18-in. (457 mm) in post-tensioned designs.

2.3.3 Test Specimens

The sixteen cantilever overhangs tested in this phase are summarized in Table 2.4. To simplify reference to the overhangs in this section, they will be designated 1A, 1B, 2A, ..., 8B as shown in Table 2.4.

The major overall variable in the study is the design philosophy for flexural reinforcement and flexural crack control. Major secondary variables are the strut-and-tie model (STM) pattern for shear loads and the flexural reinforcement end anchorage. Fairly direct comparison of behaviors are given by contrasting behavior of groups of overhangs as shown in Table 2.5. The experiments were planned so that pertinent direct comparisons could be made with the limited number of tests feasible under time, man-power, and budgetary constraints.

2.4 MODEL DESIGN PROCEDURES

A brief summary of the design procedures used for each specimen are presented herein along with sample calculations for several specimens to illustrate the details of the procedures. More complete calculations are available in Refs. 7 and 8.

2.4.1 Introduction

Design procedures used to determine the reinforcement pattern for typical overhangs, columns, and anchorage zones are provided in this section. All designs were based on an assumed concrete compressive strength of 5000 psi (35 MPa). The actual yieldstrength was used to determine the required areas of steel for the #2 reinforcing bars and 7- and 9-gauge wires except for Specimen 8 (CO-RU-0S-TH-M-SM) where the nominal yield strength of 60 ksi (430 MPa) was assumed for all reinforcement.

Table 2. 5   Major Variable Comparisons

Design Philosophy	Ordinary Anchorage				T-Head Anchorage			
	AASHTO Shear	STM V-Ties	STM I-Ties	STM w/v_c	AASHTO Shear	STM V-Ties	STM I-Ties	STM w/v_c
Wholly reinforced concrete designed for AAASHTO ultimate	1A 1B							8A 8B
Wholly prestressed concrete designed for AASHTO service	2A 2B							
Wholly prestressed concrete designed for AASHTO ultimate		3A	3B					
Structural concrete with 54% prestressed steel						5A	5B	
Structural concrete with 74% prestressed steel		4A	4B			6A	6B	
Structural concrete with 100% prestressed steel		7A	7B					

A nominal yield strength of 60 ksi (420 MPa) was assumed for the #3 reinforcing bars and 10-gauge wire, and all strand was assumed to be Grade 270. All designs included the use of AASHTO strength reduction factors, Φ, of 0.9 for flexure and 0.85 for shear.

2.4.2 CO-RU-0S-OR-N-SF (Specimen #1A and #1B)

Both overhangs were design as reinforced concrete in accordance with the provisions of AASHTO. The reinforcing details are shown in Figure 2.4.

The primary moment reinforcement was determined from AASHTO Equation (8-15):

$$M_u \leq \Phi M_n = \Phi \left[A_s f_y d \left(1 - 0.6 \frac{\rho f_y}{f_c'} \right) \right] \qquad (2.7)$$

where M_u was the moment at the face of the column from the factored flexure load case. The number of bars was slightly increased to satisfy AASHTO Equation (8-61):

$$f_s = \frac{z}{(d_c A)^{1/3}} \leq 0.6 f_y \qquad (2.8)$$

The shear stirrup design was based on a 45° truss model implicit in AASHTO (see Figure 2.5). The quantity of vertical stirrups was determined from AASHTO Equations (8-46) and (8-47):

$$V_u \leq \Phi V_n = \Phi(V_c + V_s), \qquad (2.9)$$

Equation (8-49):

$$V_c = 2\sqrt{f_c'} \, b_w \, d , \qquad (2.10)$$

and Equation (8-53)

$$V_s = \frac{A_v f_y d}{s} . \qquad (2.11)$$

V_u was taken as the sum of the outside reaction from the factored flexure load case and the factored weight of the outside 27.17-in. (690 mm) of the overhang. The effective depth of the overhang at Section a-a in Figure 2.5 was used to determine V_c and V_s.

The side face bars were designed according to the recommendations of Frantz and Breen (5) for deep flexural members:

Side View

Section at Column Face
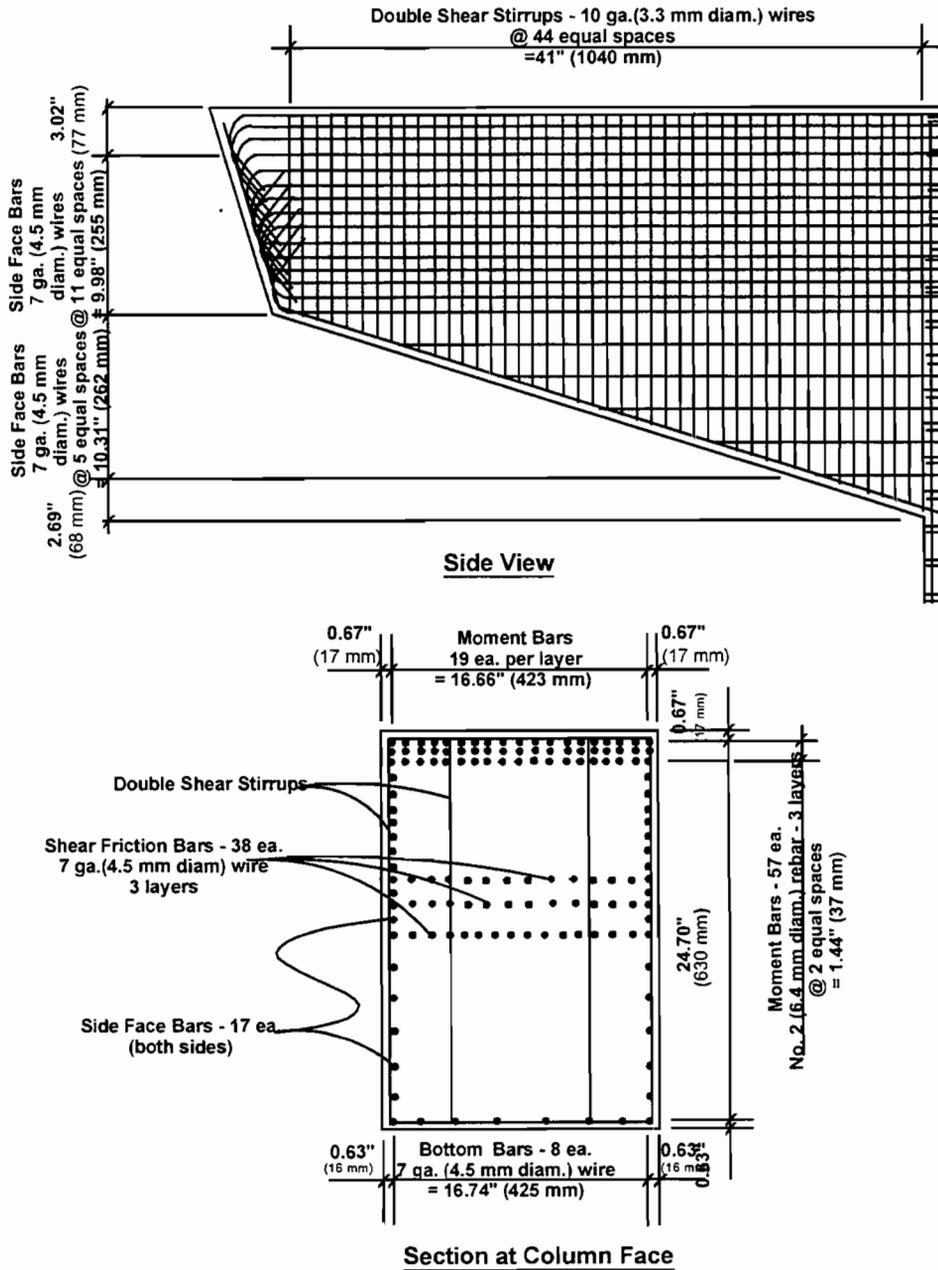
Figure 2. 4   Reinforcing details for the CO-RU-0S-OR-N-SF overhangs

23
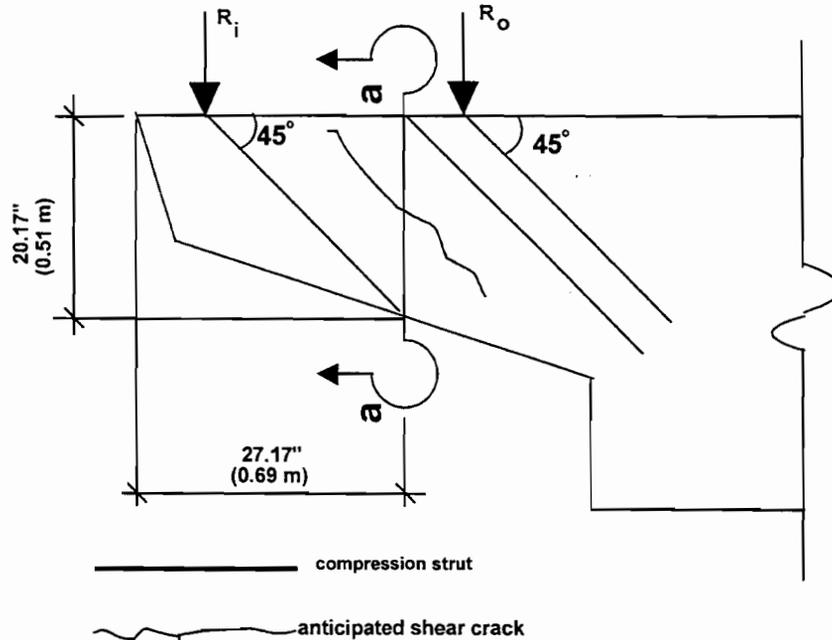
Figure 2. 5   Forty-five-degree compression strut implicit in AASHTO shear provisions

For d > 100 in. (2.54 m) (prototype dimension),

$$\rho_{sk} \geq 0.011 + 0.000058d \qquad (2.12)$$

and

$$\rho_{sk} = \frac{A_{sk}}{2[d/2 \cdot 2d_c]} \qquad (2.13)$$

The corbel provisions of AASHTO were used to determine the shear-friction steel requirement. V_u was taken from the factored shear loading case for the maximum shear at the face of column. The corbel provisions require the primary moment reinforcement, A_f, be made greater than the larger of A_s, as determined by Equation (2.7), and

$$\frac{2A_{vf}}{3} \qquad (2.14)$$

where A_{vf} is determined from AASHTO Equation (8-56):

24

$$\Phi V_n = A_{vf} f_y \mu \qquad (2.15)$$

A$_s$ from Equation (2.7) was found to control.

The corbel provisions further require that longitudinal steel with an area equal to ½ A$_f$ be distributed within 2/3 of the depth of the section adjacent to A$_s$, The side face bars within this region were counted toward partially fulfilling this requirement.

2.4.3 CO-PS-100S-NA-N-SM (Specimen #2A and 2B

Both overhangs were designed as fully post-tensioned concrete in accordance with the conventional AASHTO provisions. The reinforcing details are shown in Figure 2.6.

The quantity of primary moment reinforcement was determined by solving Equation (2.16), which limits the tensile stresses in the extreme fiber of an uncracked section to $3\sqrt{f_c'}$, with service flexure loads applied.

$$\text{Extreme Fiber Tensile Stress } = 3\sqrt{f_c'} = -\frac{P}{A} + \frac{Pey}{I} + \frac{M_{serv\,flex}\, y}{I} \qquad (2.16)$$

where
- P = the effective prestressing force = $A_{ps} \cdot f_{se}$,
- A = the cross-sectional area at the face of column,
- c = the post-tensioning eccentricity,
- y = the distance from the centroid of the section to the extreme fiber,
- I = the moment of inertia at the section, and
- M$_{serv\,flex}$ = the moment due to unfactored self weight and service flexure live loading

The effective prestress level, f$_{se}$, was assumed to be equal to 160 ksi (1120 MPa).

The shear stirrup design was identical to that of Specimen #1, as this was the typical manner for determining the vertical stirrup requirement in the fully post-tensioned piers in San Antonio.

The side face reinforcement consisted of 7-gauge wires at a spacing of 2.07 in. (52 mm) along both faces of the cap. This spacing corresponded to #8 bars at 12-in. (305 mm) in the typical full-scale post-tensioned design.

The corbel provisions of AASHTO were used to determine the shear-friction requirement, but a slightly different procedure was followed than for Specimen #1. It was recognized that the post-tensioning provided was governed by service load stress requirements and was substantially more than was required for factored flexural strength. This was used to advantage in determining the quantity of shear-friction steel. The ultimate post-tensioning force was converted to an equivalent area of 82.2 ksi (575 MPa) steel (82.2 ksi (575 MPa) is the yield strength of the 7-gauge wire which was used for the shear-friction steel).

Anchorage Zone Hoops - 15 ea.
10 ga.(3.3 mm diam.) wire

Double Shear Stirrups - 10 ga. (3.3 mm diam.) wire
@ 44 equal spaces
= 41" (1040 mm)

7.5"
(190 mm)

Side Face Bars
7 ga. (4.5 mm diam.) wire
@ 8 equal spaces
= 16.56" (420 mm)

1.94"
(50 mm)

Side View

Top Bars
2 ea. No. 2 (6.4 mm diam.)
reinforcing bar (corners),
3 ea. 7 ga. (4.5 mm diam.)
wire (middle)= 16.66" (423 mm)

0.67"
(17 mm)

0.67"
(17 mm)

0.67"
(17 mm)

Double Shear Stirrups

Side Face Bars - 9 ea.
(both sides)

Shear Friction Bars - 24 ea.
7 ga.(4.5 mm diam.) wire
2 layers

0.67"
(17 mm)

10 ea. Bottom Bar
No. 2 (6.4 mm diam.) reinf. bar
= 16.66" (423 mm)

0.67"
(17 mm)

Section at Column Face

2-5/8"
(67)

4-1/4"
(108mm)

4-1/4"
(108mm)

2-5/8"
(67)

○T1   ○T2   ○T3   ○T4

○T5   ○*   ○T6

3-1/2"   5-1/2"   5-1/2"   3-1/2"
(89mm) (140 mm) (140 mm) (89mm)

Post Tensioning Strand Arrangement
T1 ---- 0.6" (15mm) dia. strand
T2 ---- 3/8" (9.5 mm) dia. strand
T3 ---- 3/8" (9.5 mm) dia. strand
T4 ---- 0.6" (15 mm) dia. strand
T5 ---- 0.6" (15 mm) dia. strand
T6 ---- 0.6" (15 mm) dia. strand
* ---- empty duct

Left End View

Figure 2. 6   Reinforcing details for the CO-PS-100S-NA-N-SM overhangs

26

Then the area of 82.2 ksi (575 MPa) steel required for flexural strength was determined and subtracted from the equivalent area provided by the post-tensioning. The remaining area was considered to be available to partially fulfill the shear-friction steel requirement in the upper 1/3 of the beam. The remainder was provided by two #2 bars and three 7-gauge wires used for the top layer of steel in the overhang. Eight side face bars were counted towards partially fulfilling the requirement for the middle 1/3.

Ten #2 bars were provided along the bottom of the cap which is equivalent to the typical amount of steel used in the full-scale post-tensioned pier caps.

2.4.4 CO-PU-100S-NA-V-SM (Specimen #3A)

This overhang was designed with 100% of the primary moment reinforcement consisting of post-tensioning strand, but the quantity of strand was determined ignoring AASHTO service load concrete stress limits and was totally based on an ultimate strength design philosophy. Strut-and-tie modeling was used in the shear design. The reinforcing details for this overhang are shown in Figure 2.7.

The primary moment reinforcement was determined from AASHTO Equations (9-13):

$$M_u \leq \Phi M_n = \Phi \left[A_s^* \, f_{su}^* \, d \left(1 - 0.6 \frac{\rho^* \, f_{su}^*}{f_c'} \right) \right], \tag{2.17}$$

and (9-17):

$$f_{su}^* = f_s' \left(1 - 0.5 \frac{\rho \, f_s'}{f_c'} \right), \tag{2.18}$$

where f_{su}^* =   the average stress in prestressing steel at ultimate load,

ρ^* =   the ratio of prestressing, and

f_s' =   the ultimate strength of the prestressing steel.

The shear reinforcement consisted of vertical stirrups only and was designed using a strut-and-tie model incorporating the horizontal compressive stress block from Equation (2.17). This strut-and-tie model is shown in Figure 2.8. This model is one representation of the flow of forces in the overhang.

It is very important to recognize that there are generally no unique strut-and-tie models (STM) for a given problem. General guidance for STM applications are given in Ref. 4 and Ref. 2. The STM is a lower bound plasticity solution. The designer is free to develop a pattern of load distribution that approximates the natural load path and satisfies equilibrium. A pattern somewhat similar to the general elastic analysis

Side View

Double Shear Stirrups - 10 ga.(3.3 mm diam.) wire = 41"(1040 mm)

@ 6 equal spaces = 23.87"(606 mm)

@ 12 equal spaces = 8"(203 mm)

@ 3 equal spaces = 9.13"(231 mm)

Anchorage Zone Hoops - 15 ea. 10 ga.(3.3 mm diam.) wire

3.72" (94 mm)

Side Face Bars 7 ga. (4.5 mm diam.) wire @ 6 equal spaces = 18.56" (470 mm)

3.72" (94 mm)

Section at Column Face

0.63" (16 mm)

Top Bars - 5 ea. 7 ga. (4.5 mm diam.) wire = 16.74" (425 mm)

0.63" (16 mm)

0.63" (16)

Double Shear Stirrups

24.74" (630 mm)

Side Face Bars - 7 ea. (both sides)

0.63" (16 mm)

Bottom Bars - 5 ea. 7 ga. (4.5 mm diam.) wire =16.74"(425 mm)

0.63" (16)

Post Tensioning Strand Arrangement

3-1/2" (89) 5-1/2" (140 mm) 5-1/2" (140 mm) 3-1/2" (89)

2.22" (56 mm)

3" (76 mm)

T3   T2   T1

T6   T5   T4

T1 ---- 1/2" (13 mm) strand
T2 ---- 1/2" (13 mm) strand
T3 ---- 1/2" (13 mm) strand
T4 ---- 1/2" (13 mm) strand
T5 ---- 3/8" (9.5 mm) strand
T6 ---- 1/2" (13 mm) strand

Right End View

Figure 2. 7   Reinforcing details for the CO-PU-100S-NA-V-SM overhangs

28

pattern is usually best for also satisfying cracking limitations although obviously the elastic tensile stress distribution is invalid once cracking begins. Since this specimen is the first to discuss implementation of STM in this series, more detailed explanation will be given than for other specimens.

When strut-and-tie modeling is not familiar to the designer or when unusual structural applications are encountered in which the load paths are not immediately obvious, the designer may find a finite element analysis useful in visualizing general force paths.

Development of the model began with a finite element analysis of the overhang under the effect of factored flexure loads and the effective post-tensioning force. The finite element analysis program used was ANSYS. The effective post-tensioning force was based on an assumed stress in the strand of 160 ksi (1120 MPa).

Plots of the principal compressive and tensile stress vectors, shown in Figures 2.9 and 2.10, were generated to obtain a visual image of the elastic stress distribution under factored loads. The orientation of the struts and ties for the model were chosen to resemble the orientation of the stress vectors. However, struts C2, C_{sw}, C5 and C6 were forced to converge at the center of the horizontal compressive stress block, and the inclined tensile stresses in the middle of the web were approximated with a vertical tie T4.

C_{sw} is the compressive strut resisting the overhang self-weight. In the case of the model, the self-weight is small and is distributed at a single point. In a full-size overhang, the dead load of the overhang (self-weight) may be more substantial and might be distributed at three points.

Strut C2 runs directly from the level of the main longitudinal reinforcement (ties T1 and T2) immediately under Reaction R_i (the center of the inner bearing) to the centroid of the compression block at the column face. From the geometry of the strut (shown in Figure 2.8) the effective angle with the tension tie is Tan^{-1} ((320+213)/330)=58°. This lies well within the limits of 26.5°≤ ϕ ≤ 63.5° suggested in CTR Report 1127-3F (Ref. 4) where the redistribution of internal forces should be attainable without special detailing.

On the other hand, if a compressive strut runs directly from the longitudinal reinforcement layer directly below the outer Reaction R_o to the centroid of the compression block at the column face, the effective angle would be Tan^{-1} ((320+231)/991)=28°. This is allowable but right at the margins. Arbitrarily, to be more conservative, the designer decides to begin the strut at an inclination Tan^{-1} (213/283)=37° which is more favorable. This means that a tensile tie T4 must be added. One can think of this tie as "lifting" a good part of the load R_o back up to the top chord. It is then sent down the compressive strut C5 which has a more favorable inclination from the horizontal Tan^{-1} ((320+213)/(378+330))=54°.

The force in tie T4 (Figure 2.8) was determined from nodal equilibrium with factored flexure loads applied to the model. The number of stirrups used for tie T4 was
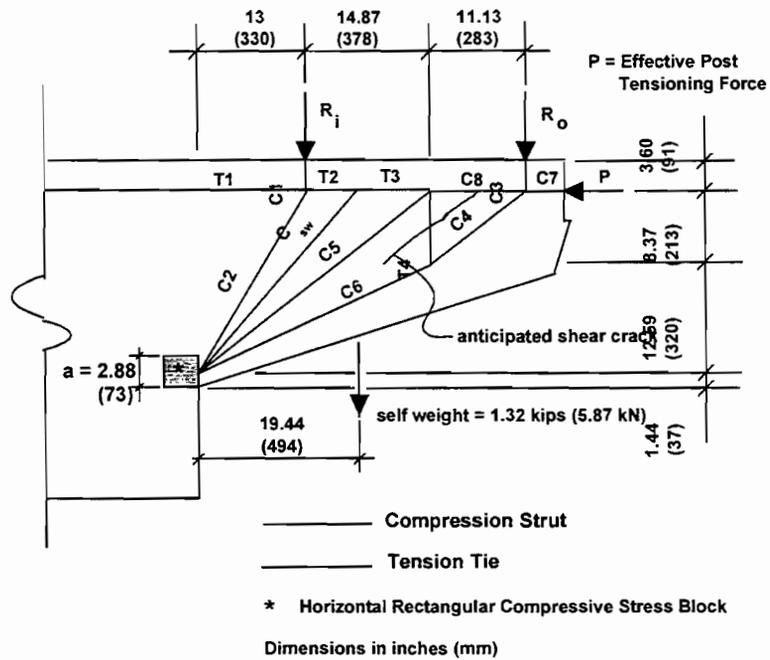
Figure 2. 8   Strut-and-tie model for the CO-PU-100S-NA-V-SM
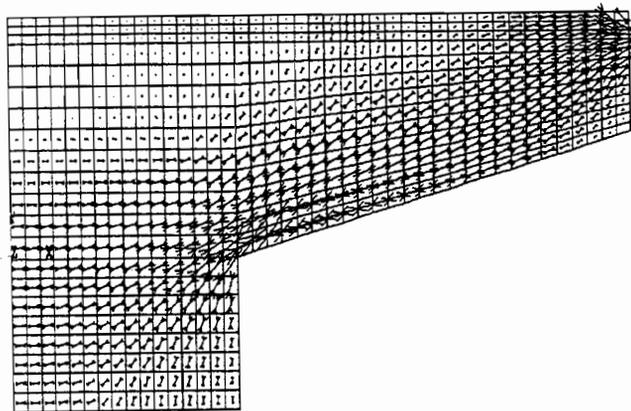
Figure 2. 9   Principal compressive stress vectors for the CO-PU-100S-NA-V&I-SM   overhangs   with factored flexure loads applied

Figure 2. 10 Principal tensile stress vectors for the CO-PU-100S-NA-V&I-SM overhangs with factored flexure loads applied

Figure 2. 11 Magnitude of principal tensile stresses for the CO-PU-100S-NA-V&I-SM overhangs with service flexure loads applied

determined from this force divided by a Φ-factor of 0.85. The width over which to distribute the vertical stirrups of tie T4 was determined from another finite element analysis with service flexure loads and the effective post-tensioning force applied to the overhang. Figure 2.11 shows the results of this analysis where each number represents the magnitude of the principal tensile stress in terms of multiples of $\sqrt{f_c'}$. The stirrups were placed at a minimum spacing of $\frac{1}{2}$-in. (13 mm). This was determined from 1.5 times the maximum coarse aggregate size. This resulted in an 8-in. (203 mm) tie width between centers of the outside bars. Stirrups were placed at a maximum spacing of 4.36-in. (111 mm) throughout all other regions along the overhang. This spacing corresponds with 24-in. (610 mm) in the full scale.

Minimum skin steel was used on the sides, top and bottom faces of the cap. The maximum spacing of this steel was 3.27-in. (83 mm) which corresponds to 18-in. (457 mm) in the full scale.

The final pattern of reinforcement shown in Figure 2.7 agrees with the STM of Figure 2.8 but is considerably different from traditional reinforced concrete shear design. As will be shown subsequently in the report, shear behavior of this model was quite acceptable. A flexural failure occurred (see Figures 3.3 and 3.14) and shear in no way governed. The absence of shear friction reinforcement typically used in the prototypes caused no problems. This illustrates the validity of STM procedure for this type of structural application.

2.4.5 CO-PU-100S-NA-I-SM (Specimen #3B)

The primary moment, side face, top and bottom reinforcement were the same as in CO-PU-100S-NA-V-SM. The shear reinforcement was determined from strut-and-tie modeling, but it consisted of both vertical and horizontal steel. The reinforcing details are shown in Figure 2.12.

The shear reinforcement was designed using the strut-and-tie model shown in Figure 2.13. This strut-and-tie model is similar to the one used for the CO-PU-100S-NA-V-SM overhang in that it incorporates the compressive stress block from the flexural design. However, this model uses inclined ties in the web. The inclined ties more closely match the orientation of principal tensile stress vectors shown in Figure 2.10.

Vertical stirrups were provided for the vertical component of each tie. The stirrups for tie T5 (Figure 2.13) were spaced evenly over the horizontal length of the tie. The stirrups for tie T6 were placed at the maximum spacing of $\frac{1}{2}$-in (13 mm) and centered on the horizontal center of the tie. This led to a band of stirrup[s that was 6.7-in. (170 mm) between the centers of the outside bars.

The horizontal steel was distributed over three levels at the same height as the side face bars. Tie T6 required more horizontal steel than tie T5. As a matter of good detailing, the steel required for T6 was extended through the cap to provide an equal area of steel for T5. This steel was further extended into the column. Six of the side face bars were used to partially fulfill the horizontal shear steel requirement.

Anchorage Zone Hoops - 15 ea
10 ga. (3.3 mm diam.) wire

Double Shear Stirrups - 10 ga. (3.3 mm diam.) wire
= 41 " (1040 mm)

@ 3 equal spaces
= 9.78" (248 mm)

@ 10 equal
spaces=6.7'
(170 mm)

@ 4 equal spaces
=14.64" (371 mm)

@ 4 equal spaces
=9.88" (251 mm)

3.72"
(94 mm)

Side Face Bars
7 ga. (4.5 mm) wire
@ 6 equal spaces
= 18.56" (470 mm)

3.72"
(94 mm)

Side View

0.63"
(16 mm)

Top Bars - 5 ea.
7 ga. (4.5 mm diam.) wire
= 16.74" (425 mm)

0.63"
16 mm)

Double Shear Stirrups

Horiz. Shear Bars - 9 ea.
7 ga. (4.5 mm diam.) wire
3 layers

Side Face Bars - 7 ea.
(both sides)

24.74"
(630 mm)

0.63"
(16 mm)

Bottom Bars - 5 ea.
7 ga. (4.5 mm diam.) wire
= 16.74" (425 mm)

0.63"
(16 mm)

Section at Column Face

3-1/2"
(89)

5-1/2"
(140 mm)

5-1/2"
(140 mm)

3-1/2"
(89)

O T1   O T2   O T3

2.22"
(56 mm)
3"
(76 mm)

O T4   O T5   O T6

Post Tensioning Strand Arrangement
T1 ---- 1/2" (13 mm) strand
T2 ---- 1/2" (13 mm) strand
T3 ---- 1/2" (13 mm) strand
T4 ---- 1/2" (13 mm) strand
T5 ---- 3/8" (9.5 mm) strand
T6 ---- 1/2" (13 mm) strand

Left End View

Figure 2. 12   Reinforcing details for the CO-PU-100S-NA-I-SM overhang

33

Figure 2. 13 Strut-and-tie model for the CO-PU-100S-NA-I-SM overhangs

2.4.6 CO-PU-74S-OR-V-SM (Specimen #4A)

This overhang was designed as a structural concrete member using a combination of non-prestressed and prestressed reinforcement based on an ultimate strength design approach. Seventy-four percent of the primary moment flexural tension force at ultimate was provided by post-tensioning strand and the remaining twenty-six percent was provided by mild reinforcement. The shear reinforcement was identical to that used in CO-PU-100S-NA-V-SM. The reinforcing details for this overhang are shown in Figure 2.14.

Finite element analysis of the overhang under factored and service loads with the reduced effective post-tensioning force were performed. The magnitude and orientation of the principal stresses did not change appreciably from what was determined for Specimen #3 with the higher post-tensioning force, so the shear reinforcement was not changed.

34

2.4.7 CO-PU-74S-OR-I-SM (Specimen #4B)

The primary moment, side face, top and bottom bars were identical to that used for CO-PU-74S-OR-V-SM. The shear reinforcement was the same as for CO-PU-100S-NA-I-SM, except that the horizontal shear steel requirement was not partially fulfilled by the side face bars. The reinforcing details for this overhang are shown in Figure 2.15.

2.4.8 Prestressed Overhangs with T-Headed Reinforcement

The six overhangs (Specimens 5A, 5B, 6A, 6B, 7A and 7B), with T-headed reinforcing bars, were designed using the strength design approach for flexure and strut-and-tie modeling design for shear. T-heads were used on all #2 bars used for flexure. The T-head dimensions will be given in a later section. Standard hooks were used with all 7-gauge flexural wires. The overall dimensions and reinforcing steel layouts are shown in Figures 2.16 through 2.21 for each of the six prestressed concrete T-head reinforcement overhangs.

2.4.8.1 Flexural Design

AASHTO standard provisions for ultimate strength, including a strength reduction (ϕ) factor of 0.9, were used to determine the quantity of post-tensioning steel at maximum effective stress needed to achieve 100 percent of the required ultimate capacity of the structure. Mixed reinforcement structures were designed for flexure by taking the desired percentage of that quantity of prestressing steel needed to achieve 100 percent of the required ultimate capacity (for prestressing steel at its calculated ultimate stress) to provide the amount of ultimate tensile force contributed by the prestressed reinforcement. Then the proper number of #2 bars, fy = 75.1 ksi (518 MPa), was added as non-prestressed reinforcement to provide the required balance of the moment capacity. Finally, the service level post-tensioning force was determined based on the area of prestressing steel times the effective post-tensioning stress.

Prestressing steel was designed with an eccentricity of 9.4 in. (239 mm). For models CO-PU-54S-TH (V and I), the post-tensioning steel consisted of a single row of three ½-in. (13 mm) diameter, grade 270 (1860 MPa), low relaxation strands, located as indicated in Figure 2.16 and 2.17. Model CO-PU-74S-TH (V and I) post-tensioning steel consisted two rows. There were two ½-in. (13 mm) diameter strands in the top row. The bottom row had one ½-in. (13 mm) strand in the middle, and two 3/8-in. (9.5 mm) diameter strands on the outside as indicated in Figures 2.18 and 2.19. Models CO-PU-100S-TH (V and I) were post-tensioned with the use of two rows of strands. The top row had three ½-in. (13 mm) strands. The bottom row had two ½-in. (13 mm) strands at the sides and one 3/8-in. (9.5 mm) strand in the middle, as shown in Figures 2.20 and 2.21.

Side View

Section at Column Face

Post Tensioning Strand Arrangement
T1 ---- 1/2" (13 mm) strand
T2 ---- 1/2" (13 mm) strand
T3 ---- 3/8" (9.5 mm) strand
T4 ---- 1/2" (13 mm) strand
T5 ---- 3/8" (9.5 mm) strand
* ---- empty duct

Right End View

Figure 2. 14 Reinforcing details for the CO-PU-74S-OR-V-SM overhangs

Side View

Anchorage Zone Hoops - 15 ea.
10 ga. (3.3 mm diam.) wire

Double Shear Stirrups - 10 ga.(3.3mm diam.) wire
= 41" (1040 mm)

@ 3 equal spaces
= 9.78" (248 mm)

@ 10 equal
spaces =
.7" (170 mm)

@ 4 equal spaces
=14.64" (371 mm)

@ 4 equal spaces
= 9.88" (251 mm)

3.76"
(95 mm)

Side Face Bars
=18.52" (470 mm)

No. 2 (6.4 mm) reinf. bar

3.09" wire

@ 2 equal
spaces =
6.18" (157 mm)

7 ga. (4.5 mm
diam.) wire
@ 3 equal
spaces =
9.27" (235 mm)

3.72"
(94 mm)

Section at Column Face

0.67"
(17 mm)

Top Bars - 7 ea.
No. 2 (6.4 mm) rebar
= 16.66" (423 mm)

0.67"
(17 mm)

0.67"
(17)

Double Shear Stirrups

24.70"
(630 mm)

Side Face Bars - 7 ea.
(both sides)

0.63"
(16 mm)

Bottom Bars - 5 ea.
7 ga. (4.5 mm diam.) wire
= 16.74" (425 mm)

0.63"
(16 mm)

Left End View

3-1/2"
(89)

5-1/2"
(140 mm)

5-1/2"
(140 mm)

3-1/2"
(89)

T1   O*   T2

2.07"
(52 mm)

3"
(76 mm)

T3   T4   T5

Post Tensioning Strand Arrangement

T1 ---- 1/2" (13 mm) strand
T2 ---- 1/2" (13 mm) strand
T3 ---- 3/8" (9.5 mm) strand
T4 ---- 1/2" (13 mm) strand
T5 ---- 3/8" (9.5 mm) strand
* ---- empty duct

Figure 2. 15   Reinforcing details for the CO-PU-74S-OR-I-SM
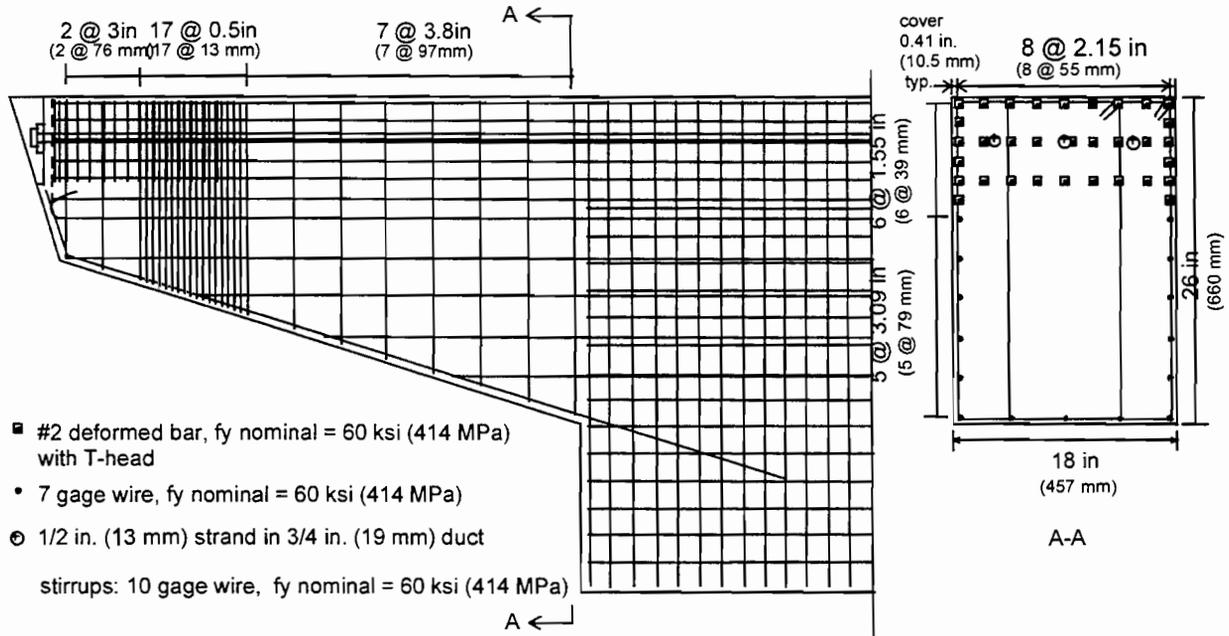
Figure 2. 16   Reinforcing cage for Model CO-PU-54S-TH-V-SF
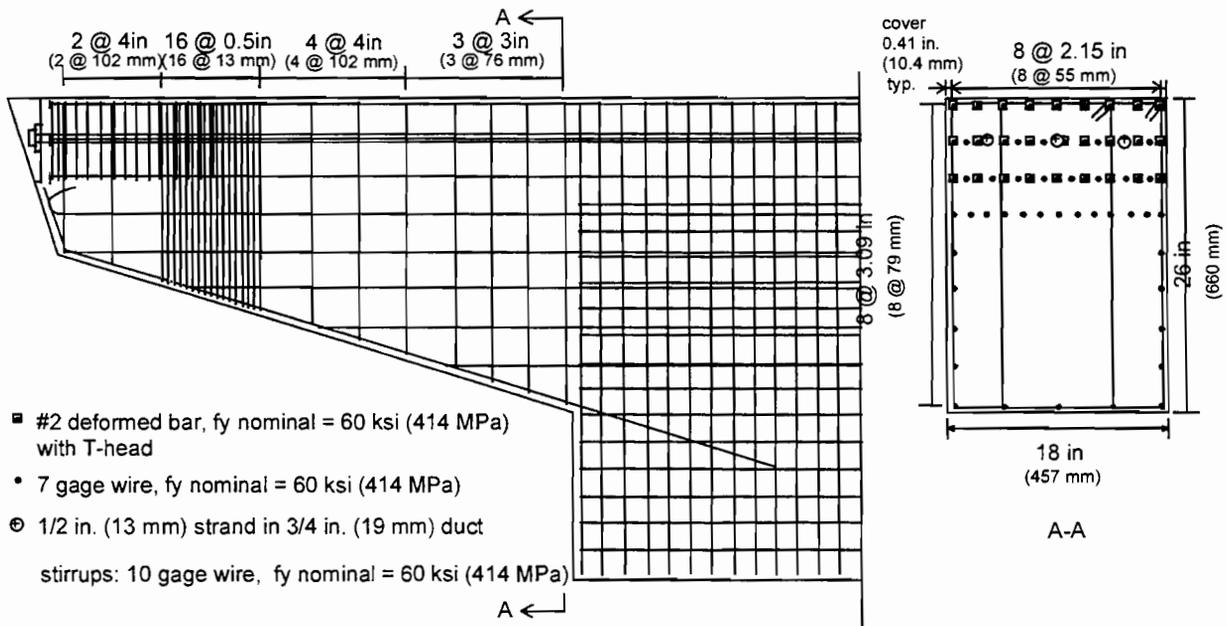
Figure 2. 17   Reinforcing cage for Model CO-PU-54S-TH-I-SM

38

3 @ 3.04in 12 @ 0.67in   6 @ 3.98in
(3 @ 77 mm) (12 @ 17 mm)   (6 @ 101 mm)

cover
0.41 in.   4.09 in   9 in   4.09 in
(10.4mm)(104 mm) (229 mm)(104 mm)
typ.

8 @ 3.09 in
(8 @ 79 mm)

26 in
(660 mm)

18 in
(457 mm)

A-A

■ #2 deformed bar, fy nominal = 60 ksi (414 MPa)
   with T-head
• 7 gage wire, fy nominal = 60 ksi (414 MPa)
⊕ 1/2 in. (13 mm) diam. strand in 3/4 in. (19 mm) duct
⊗ 3/8 in. (9.5 mm) diam. strand in 3/4 in. (19 mm) duct
○ open 3/4 in. (19 mm) diam. duct
   stirrups: 10 gage wire, fy nominal = 60 ksi (414 MPa)
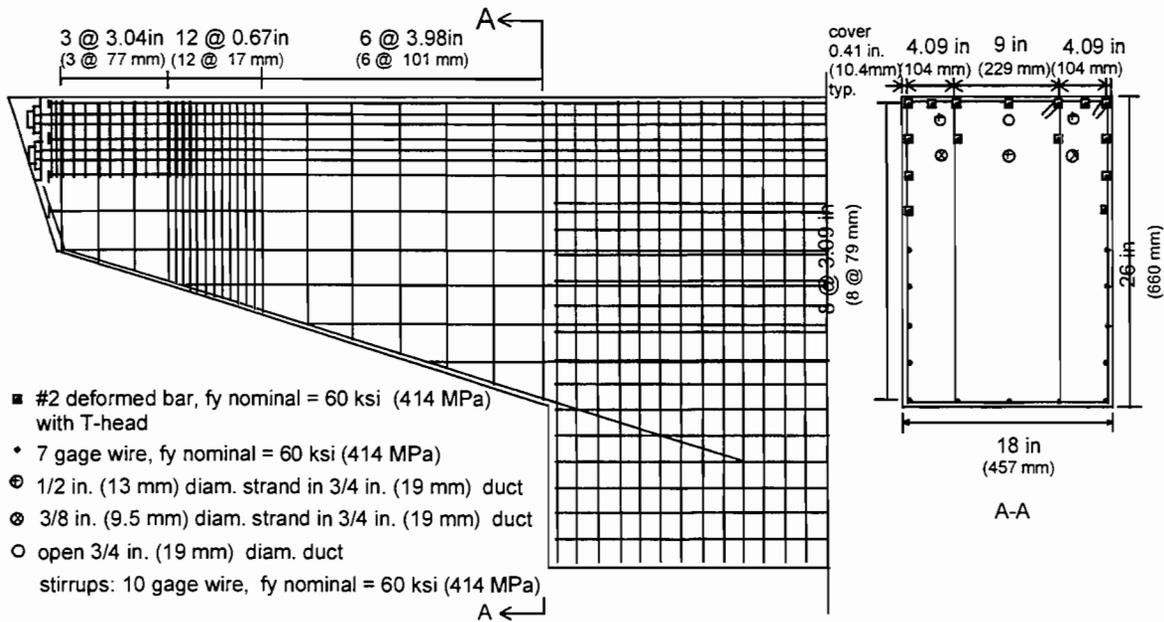
Figure 2. 18   Reinforcing cage for Model CO-PU-74S-TH-V-SM

3 @ 3.04in 12 @ 0.67in   6 @ 3.98in
(3 @ 77 mm) (12 @ 17 mm)   (6 @ 101 mm)

cover
0.41 in.   4.09 in   9 in   4.09 in
(10.4mm)(104 mm) (229 mm)(104 mm)
typ.

8 @ 3.09 in
(8 @ 79 mm)

26 in
(660 mm)

18 in
(457 mm)

A-A

■ #2 deformed bar, fy nominal = 60 ksi (414 MPa)
   with T-head
• 7 gage wire, fy nominal = 60 ksi (414 MPa)
⊕ 1/2 in. (13 mm) diam. strand in 3/4 in. (19 mm) duct
⊗ 3/8 in. (9.5 mm) diam. strand in 3/4 in. (19 mm) duct
○ open 3/4 in. (19 mm) diam. duct
   stirrups: 10 gage wire, fy nominal = 60 ksi (414 MPa)
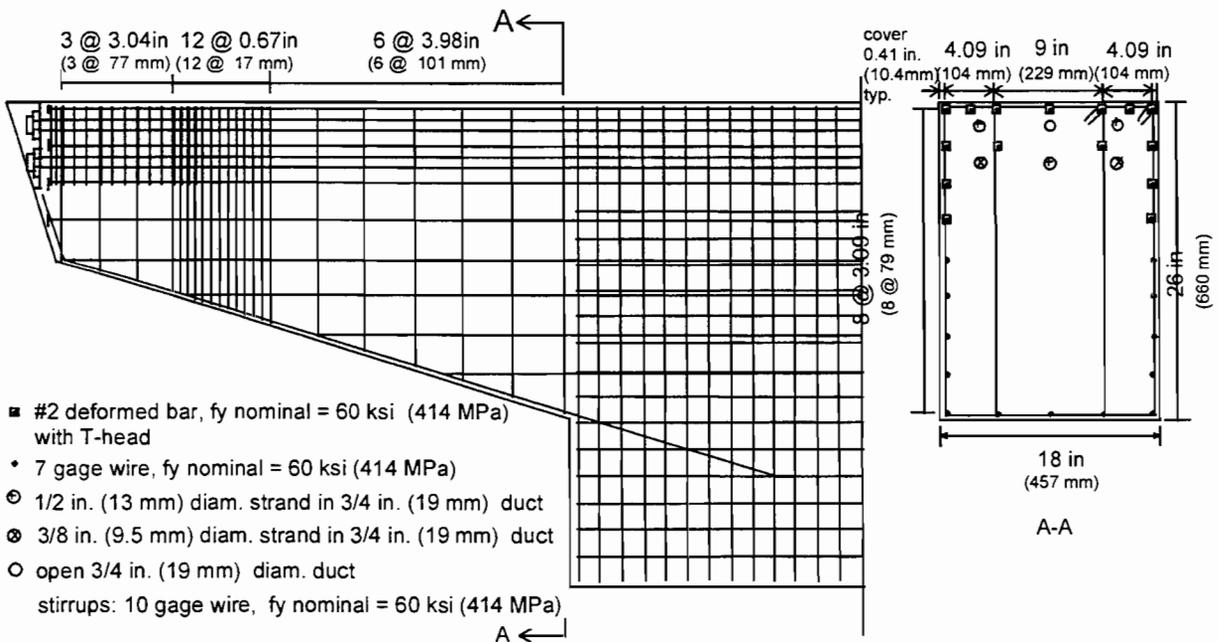
Figure 2. 19   Reinforcing cage for Model CO-PU-74S-TH-I-SM

39

3 @ 3.04in 12 @ 0.67in   6 @ 3.98in   A ←
(3 @ 77 mm) (12 @ 17 mm)   (6 @ 101 mm)

cover
0.41 in.   4.09 in   9 in   4.09 in
(10.4 mm)(104 mm) (229 mm) (104 mm)
typ.

6 @ 1.55 in
(6 @ 39 mm)

5 @ 3.09 in
(5 @ 79 mm)

26 in
(660 mm)

18 in
(457 mm)

A-A

- ▪ #2 deformed bar, fy nominal = 60 ksi (414 MPa)
  with T-head
- • 7 gage wire, fy nominal = 60 ksi (414 MPa)
- ⊕ 1/2 in. (13 mm) diam. strand in 3/4 in. (19 mm) duct
- ⊗ 3/8 in. (9.5 mm) diam. strand in 3/4 in. (19 mm) duct
  stirrups: 10 gage wire, fy nominal = 60 ksi (414 MPa)

A ←
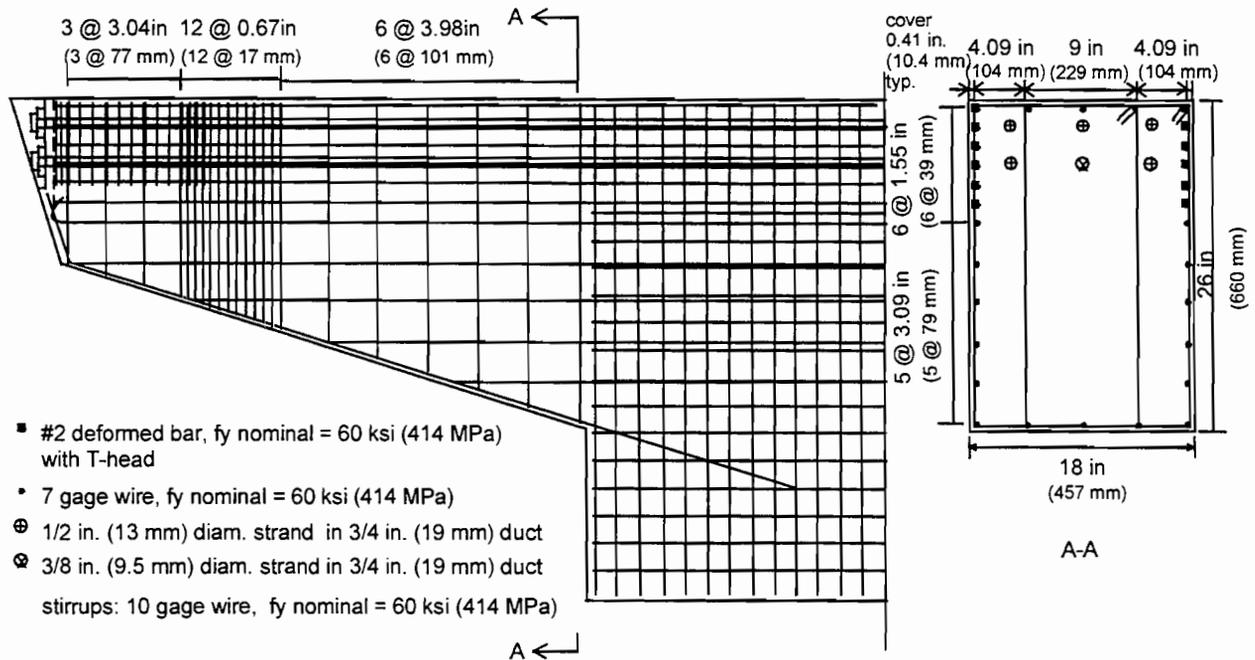
Figure 2. 20 Reinforcing cage for Model CO-PU-100S-TH-V-SF

A ←

3 @ 3.3in 10 @ 0.70in 4 @ 3.60in 4 @ 2.5in
(3 @ 84 mm) (10 @ 18 mm) (4 @ 91 mm) (4 @ 64 mm)

cover
0.41 in.   4.09 in   9 in   4.09 in
(10.4 mm)(104 mm)(229 mm)(104 mm)
typ.

8 @ 3.09 in
(8 @ 79 mm)

26 in
(660 mm)

18 in
(457 mm)

A-A

- ▪ #2 deformed bar, fy nominal = 60 ksi (414 MPa)
  with T-head
- • 7 gage wire, fy nominal = 60 ksi (414 MPa)
- ⊕ 1/2 in. (13 mm) diam. strand in 3/4 in. (19 mm) duct
- ⊗ 3/8 in. (9.5 mm) diam. strand in 3/4 in. (19 mm) duct
  stirrups: 10 gage wire, fy nominal = 60 ksi (414 MPa)

A ←

Figure 2. 21 Reinforcing cage for Model CO-PU-100S-TH-I-SM

2.4.8.2 Shear Design / Strut and Tie Models

Shear reinforcement was designed with the aid of strut-and-tie models developed using force flow paths determined from elastic finite element analyses. Principal stresses were plotted for all models under both service and factored load levels for both shear and flexure loads (see Figures 2.22 and 2.23 for typical examples). These analyses were performed using 8-node isoparametric elements and nominal concrete properties.

Based on these plots and on strut-and-tie model theory (2, 4), two different models were developed: one with inclined ties and another with a single vertical tie. Both models would be acceptable from a strength basis. However, the aim of the research project was to evaluate their performance with the different percentages of prestressing steel, as shown in Table 2.5, and to compare results.

Additional horizontal steel required in those overhangs with inclined tie models was provided with 7-guage wire.

The particular strut-and-tie models selected are shown in Figure 2.24 through 2.27. The strut-and-tie forces are given in Ref. 8.

It is important to mention that any shear contribution provided by concrete was not taken into account when proportioning the tie steel. In addition, tie forces were divided by a ϕ factor of 0.85 as in a typical ultimate strength design approach. For this reason it was anticipated that these shear models would provide a very conservative design (lower bound solution).

2.4.8.3 Skin Reinforcement

Cantilever overhangs CO-PU-54S-TH-V-SF and CO-PU-100S-TH-V-SF were designed with an area of skin reinforcement of 0.59 in.^{2} (380 mm^2), as per Frantz and Breen (5). Calculation of the area of skin reinforcement based on that report includes all the face steel that is to be distributed over ½ of the effective depth of the member nearest the principal reinforcement. For the bottom half, supplementary steel (7-gauge wire) was arbitrarily provided at a spacing of 2.09 in. (79 mm) as minimum reinforcement for shrinkage and temperature.

Face steel in models CO-PU-54S-TH-I-SM and CO-PU-74S-TH (V and I)- SM was not the result of a direct design, but rather was the computation of the reinforcement in this area after the distribution of the main flexural steel (#2 reinforcing bars) in the top of the cage at a spacing of 3.09 in. (79 mm), and the addition of supplementary steel (7-gauge wire) at the same spacing until reaching the bottom of the cage. The spacing corresponded to 18 in. (457 mm) in the prototype structure. By referring to Figure 2.17 and 2.19, and using the same criteria as described above, this gives an area of skin reinforcement of 0.29 in.^{2} (187 mm^2) for the CO-PU-54S-TH-I-SM model, and 0.34 in.^{2} (219 mm^2) for the CO-PU-74S-TH (V and I)-SM models.

\
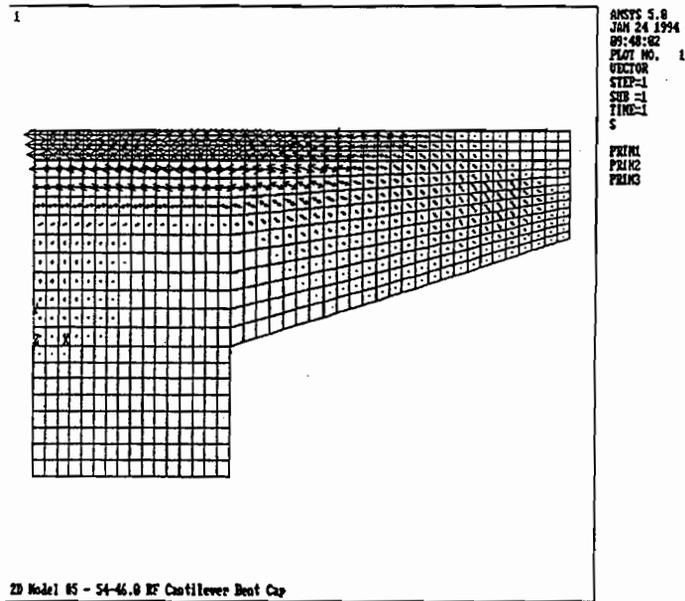
Figure 2. 22   Principal tensile stresses for Specimen CO-PU-54S-TH under flexure service loads
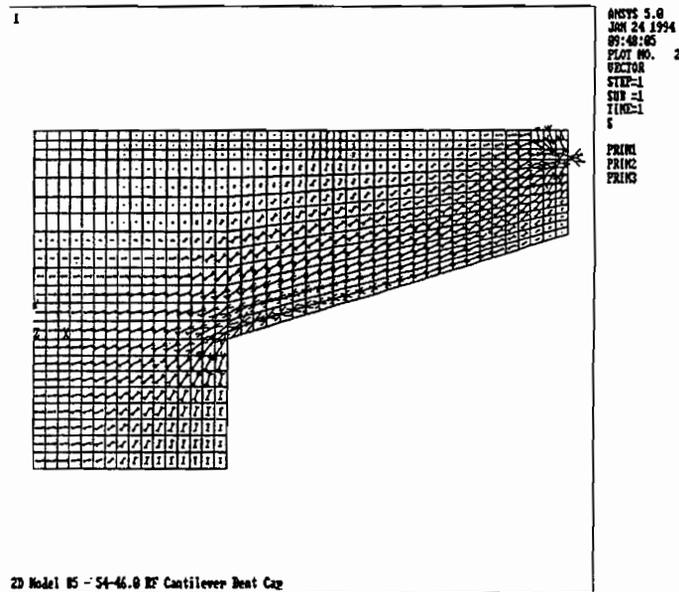
Figure 2. 23   Principal compressive stresses for Specimen CO-PU-54S-TH under flexure service loads
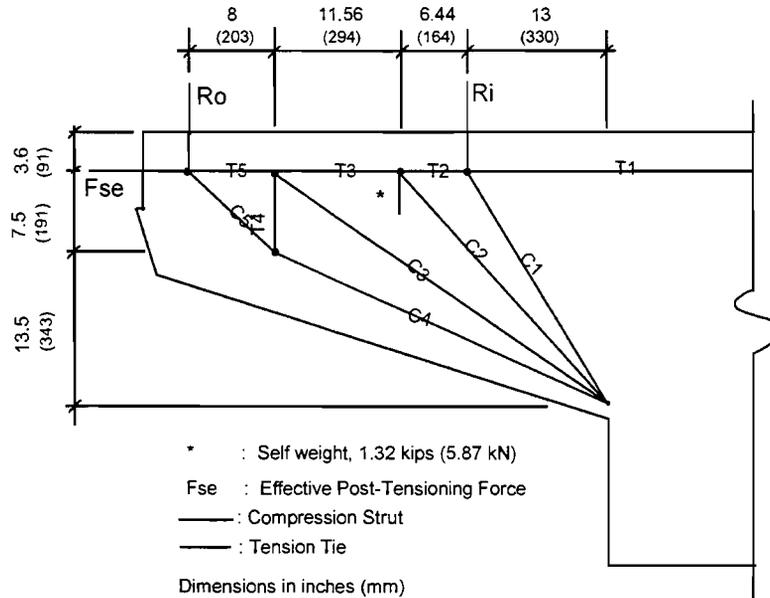
Figure 2. 24   Strut-and-tie model for overhang CO-PU-54S-TH-V-SF
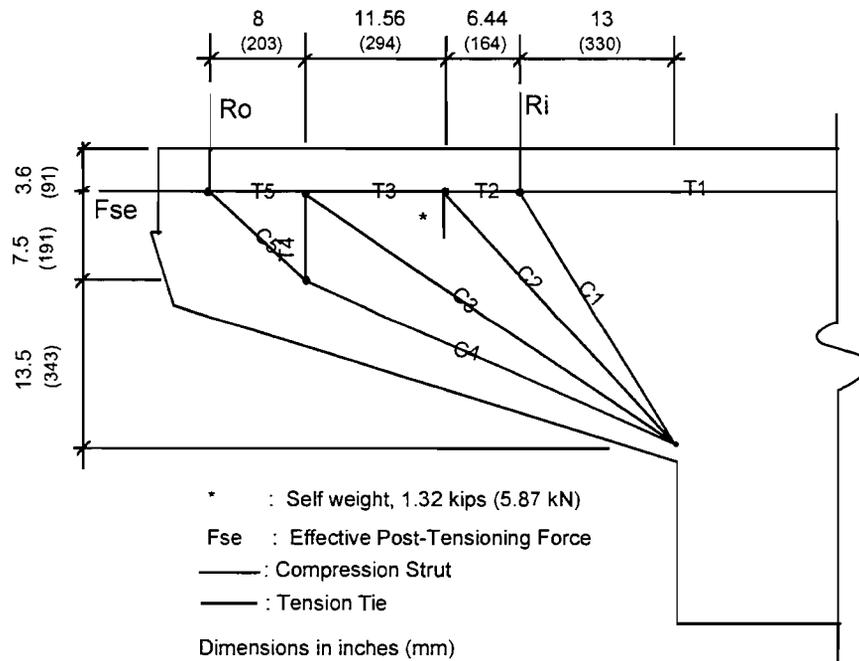
Figure 2. 25   Strut-and-tie model for overhang CO-PU-54S-TH-I-SM
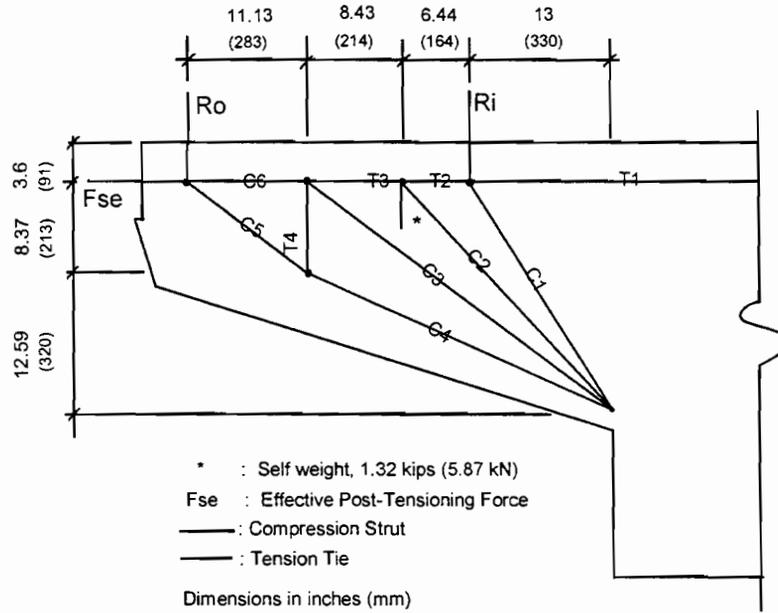
Figure 2. 26 Strut-and-tie model for overhangs CO-PU-74S-TH-V-SM and CO-PU-100S-TH-V-SF
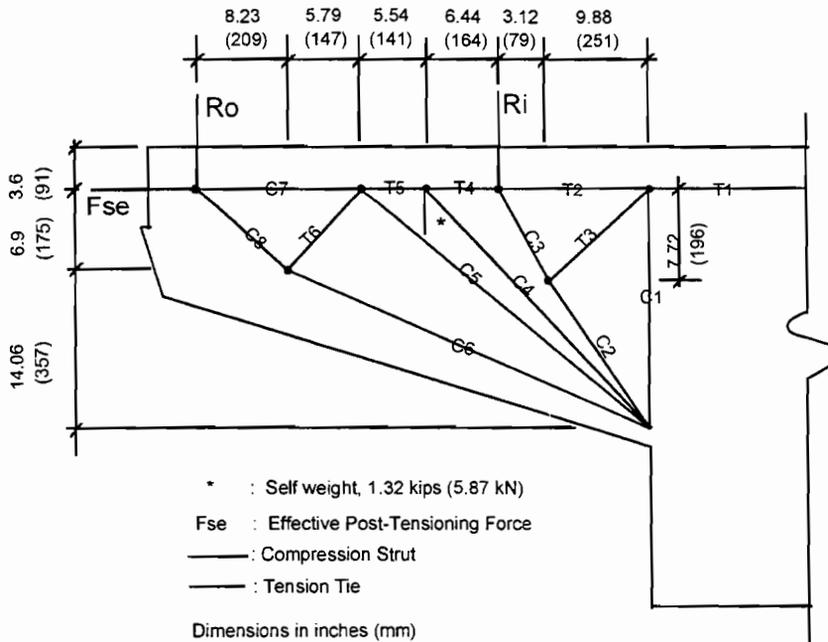
Figure 2. 27 Strut-and-tie model for overhangs CO-PU-74S-TH-I-SM and CO-PU-100S-TH-I-SM

For the CO-PU-100S-TH-I-SM overhang, even when it was not necessary for strength, some non-prestressed reinforcement was included in the detailing process for construction purposes. Minimum corner bars, as well as minimum face steel, were included in the design at a spacing of 3.09 in. (79 mm) with the purpose of providing a working frame for the adequate placement and support of the stirrups and to facilitate handling of the cage. Spacing of the bars was selected arbitrarily as 2.09 in. (79 mm) to be consistent with the other specimens. Based on this, and referring to Figure 2.21, the area of skin reinforcement in this model was calculated as 0.29 in.² (187 mm²).

2.4.8.4 *Post-Tensioning Anchorage Zone Reinforcement*

Prior to this series, a mock-up test was performed to define the adequate reinforcement that had to be provided in the post-tensioning anchorage zone. The mock-up test structure was a simply supported rectangular concrete beam, 44-in. x 18-in. x 13-in. (1118 mm x 457 mm x 330 mm), with minimum shear and flexural steel, and without bursting reinforcement in one end and with bursting reinforcement in the other end designed according to the NCHRP 10-29 proposed provisions (9). During the test, some spalling was observed on the side without bursting reinforcement, while the other end remained undamaged. As a result, bursting steel, as shown in Figure 2.28, was used in all prestressed models.

2.4.8.5 *CO-RU-0S-TH-M1-SM (Specimen 8A)*

This specimen was designed on a somewhat different basis than its companion Specimen 1A and 1B. While the flexural design was based on ultimate requirements, the quantity of primary flexural reinforcement was determined based on the nominal yield strength of 60 ksi (420 MPa) rather than the known reinforcement yield strength of 75 ksi (525 MPa). Thus, the reinforcement quantity was approximately 25 percent more than in a specimen designed with the known reinforcement strength. This would be similar to the normal design process where the engineer does not know actual strength at time of design but rather must use the nominal or minimum allowable strength. The ultimate capacity of the resulting specimen was expected to be much greater than the factored design loads, but the evaluation of the serviceability conditions and crack width conditions should be in closer agreement with a full-scale prototype.

The amount of primary reinforcement was determined from Eq. 2.7 and the spacing and number of bars was chosen to satisfy Eq. 2.8.

The amount of shear reinforcement was based on the strut-and-tie model hanger force T4 from the models shown in Figure 2.29. The tests of the previous specimens had shown that the amount of reinforcement provided to satisfy the full hanger force was excessive because some force was provided by tensile concrete or aggregate interlock. In this specimen, the force T4 was considered to be shared by the reinforcement and a concrete contribution. In this overhang a $1\sqrt{f_c'}$ concrete tensile stress was assumed at the cross section where the vertical tension tie was located. The reinforcement
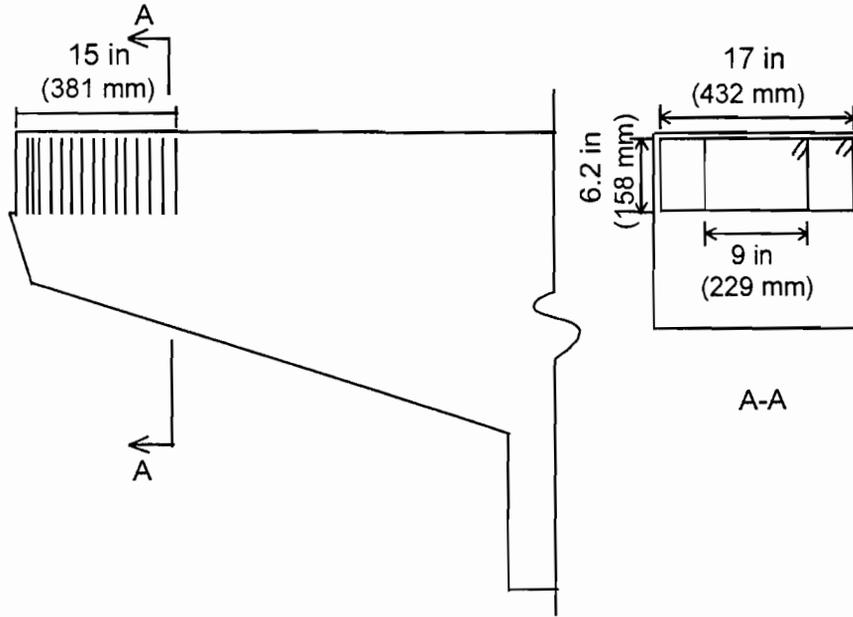
Figure 2. 28 Detail of confinement reinforcement in bearing area of post-tensioning anchorage
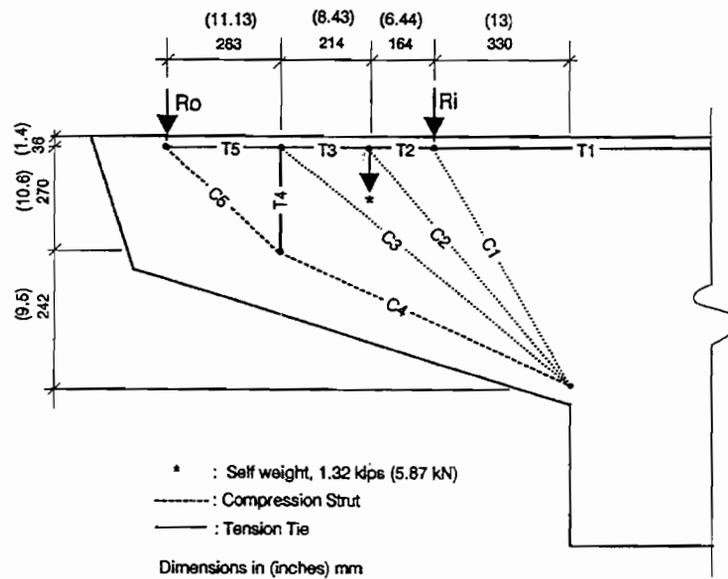
Figure 2. 29 Strut-and-tie model for overhangs CO-RU-0S-TH-I-M1-SM and CO-RU-0S-TH-M1.7-SM

46
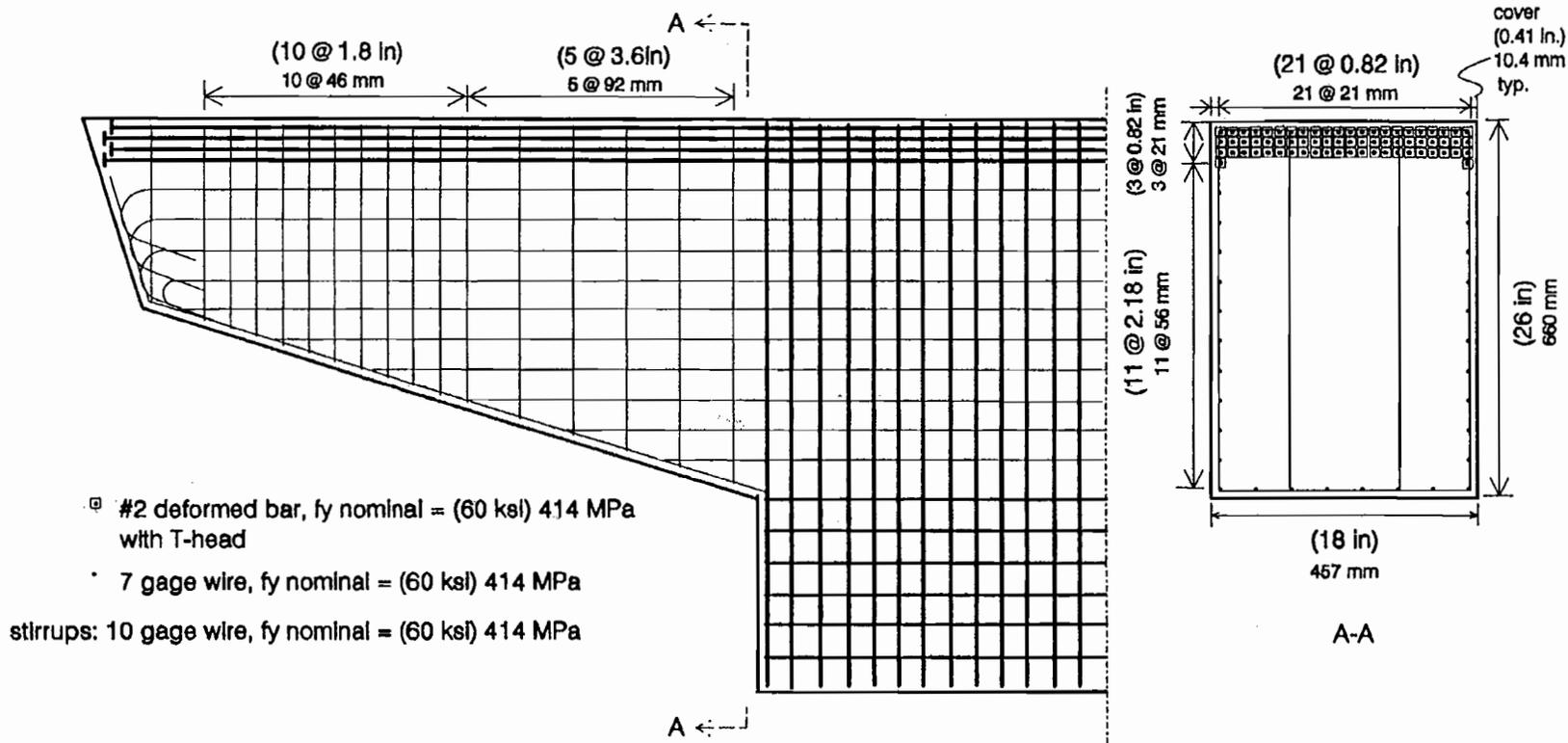
Figure 2. 30 Reinforcing cage for Model CO-RU-0S-TH-M1-SM

47

48
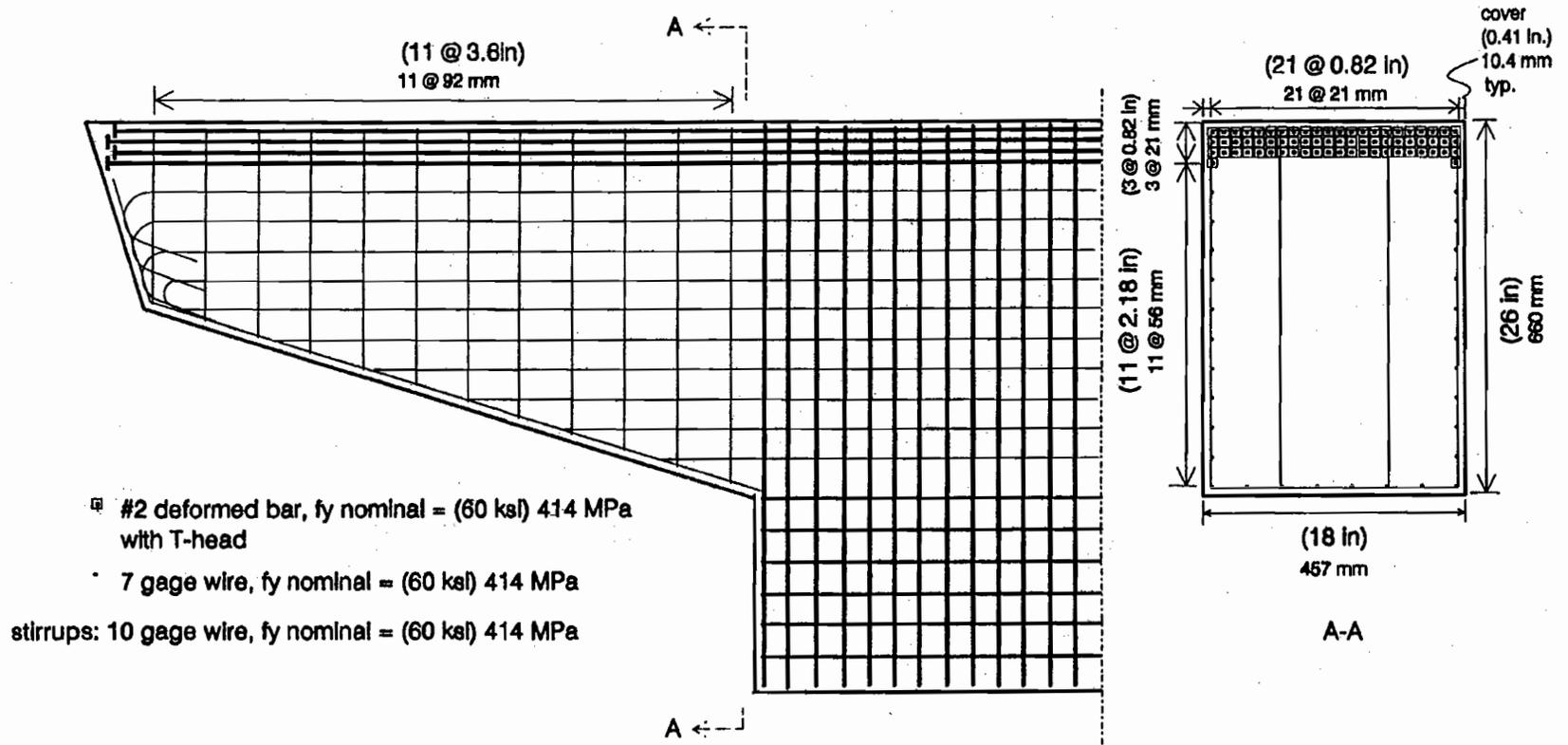
Figure 2. 31 Reinforcing cage for Model CO-RU-0S-TH-M1.7-SM

quantity was then determined by reducing T4 by the quantity $1\sqrt{f_c'}\,b\,d$ as an indicator of the shear carrying capacity of the concrete not attributed to reinforcement. The stirrups were equally distributed over a distance d/2 on each side of the assumed tension tie T4. Minimum shear reinforcement was used throughout the remainder of the overhang. The skin reinforcement was based on the minimum temperature and shrinkage quantity used in the prototype.

The actual reinforcement distribution used is shown in Figure 2.30. Note that the number of primary flexural reinforcing bars (#2 size) is increased to 68 where it was 57 in the earlier CO-RU specimens of Figure 2.4. This reflects the use of the nominal fy. In contrast to CO-RU-0S-OR-N-SF overhangs, the large quantity of shear-friction steel shown in Figure 2.4 was omitted.

2.4.8.6 *CO-RU-0S-TH-M1.7-SM*

This overhang was designed on the same basis as CO-RU-0S-TH-M1-SM except that minimum shear reinforcement was used over the entire length of the overhang. This corresponds to assuming a concrete contribution of $1.7\sqrt{f_c'}\,b\,d$ to supplement the tension tie T4. The actual reinforcement distribution used is shown in Figure 2.31. Again, the shear-friction steel shown in Figure 2.4 was omitted.

2.4.8.7 *Columns*

The column portion of all specimens was identical. Vertical reinforcement and ties were placed in amounts that were direct scaled models of details typically observed in the full-scale piers constructed in San Antonio. Reinforcing details for the column are shown in Figure 2.32.

2.4.8.8 *Anchorage Zone Stirrups*

The anchorage zone hoops were designed according to the provisions of NCHRP Report No. 356 (10). The required number of hoops were determined for the post-tensioning force of Specimen #2 and the same number of hoops was used for all other models.

2.4.8.9 *Fatigue Considerations*

Steel stress ranges (between full dead load and full dead load plus live load with impact) and maximum steel stresses under service loads were of major concern during the design of the models. Table 2.6 shows the results of these calculations for every case. Under no circumstance was a stress allowed in excess of 0.70 of the specified tensile strength of the prestressing tendons or yield of the non-prestressed steel when full service loads were applied. Specimens CO-PU-74S-TH-V-SM and CO-PU-74S-OR-V-SM substantially exceeded the 15 ksi tendon stress range proposed by Wollmann et.al. (11) while Specimen CO-PU-74S-TH-I-SM was marginally above this stress range.
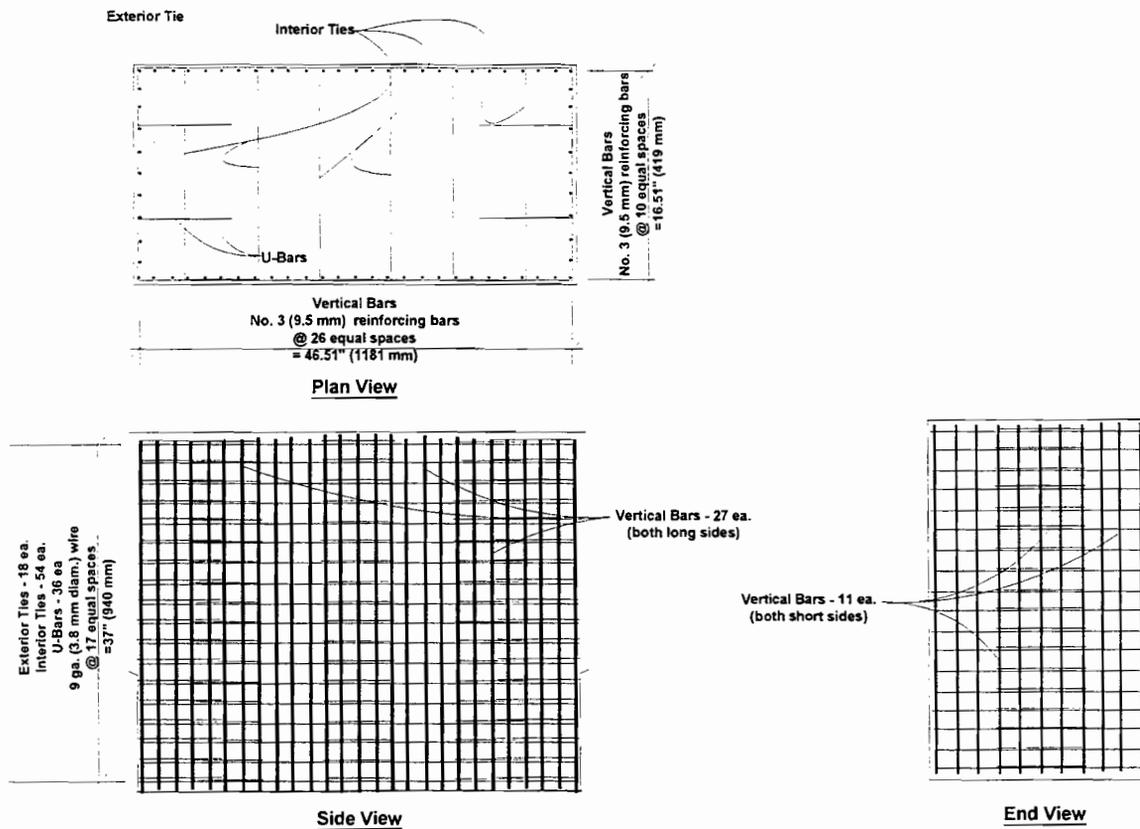
Figure 2. 32   Reinforcing details for columns

Table 2. 6   Stress Ranges at Service Loads and Strand Stresses at Full Service Loads

Specimen		Overhang Designation	Stress Range		f_{pt}/f_{pu}*
			ksi	MPa	
1	A	CO-RU-0S-OR-N-SF	8	56	--
	B	CO-RU-0S-OR-N-SF	8	56	-
2	A	CO-PS-100S-NA-N-SM	2	14	0.60
	B	CO-PS-100S-NA-N-SM	2	14	0.60
3	A	CO-PU-100S-NA-V-SM	10	70	0.63
	B	CO-PU-100S-NA-I-SM	9	63	0.63
4	A	CO-PU-74S-OR-V-SM	18	126	0.70
	B	CO-PU-74S-OR-I-SM	15	105	0.69
5	A	CO-PU-54S-TH-V-SF	13	91	0.70
	B	CO-PU-54S-TH-I-SM	12	84	0.70
6	A	CO-PU-74S-TH-V-SM	18	126	0.70
	B	CO-PU-74S-TH-I-SM	16	112	0.69
7	A	CO-PU-100S-TH-V-SF	8	56	0.62
	B	CO-PU-100S-TH-I-SM	8	56	0.63
8	A	CO-RU-0S-TH-M1-SM	8	56	--
	B	CO-RU-0S-TH-M1.7-SM	8	56	--
			*	f_{pt}: stress in strand at full service loads f_{pu}: ultimate tensile stress of strand	

50

2.5 MATERIALS

2.5.1 Concrete

The concrete strength typically used for the TxDOT post-tensioned pier cap design is 4000 psi (28 MPa) at time of prestressing and 5000 psi (35 MPa) at 28 days. Based on this, 5000 psi (35 MPa) at 28 days was selected for the test specimens and ordered from a local concrete supplier. Maximum aggregate size was 3/8 in. (9.5 mm) to allow the material to fit within the 0.41in. (10.4 mm) cover and for adequate placement of the mix in the congested areas of the cage. To delay initial set and improve workability, the mix included a retarder agent (Pozz. R) and a superplasticizer (Rheobuild). The design mix used, per cubic yard, is shown in Table 2.7.

Table 2. 7   Concrete Mix Proportions

Description	Quantity*	
Type II Cement, lb. (N)	564	(2509)
Aggregate - 3/8 in. (9.5 mm), lb. (N)	1463	(6507)
Sand, lb. (N)	1631	(7255)
Water, lb. (N)	200	(890)
Retarder additive, oz. (ml)	25	(750)
Superplasticizer, oz. (ml)	45	(1350)
W/C ratio	0.35	(0.35)

*Quantities per cubic yard (0.76 cubic meters)

Consistency of the mix was determined by the use of slump tests. A great variability was found between mixes. The water-cement (W/C) ratio was calculated based on the mix component weights from the concrete supplier taking into account any extra water that the driver estimated to have added while transporting the mix. Water-cement ratios varied from 0.27 to 0.45. Comparing results from the initial slump test and the W/C ratio, it was difficult to rely on the water and cement quantities said to be in the mix. This was recognized during casting operations. As a result, it was decided upon arrival of the concrete to add the water necessary to achieve a slump in the range of 3.5 in. (90 mm) to 5.5 in. (140 mm). In addition, superplasticizer [in excess of the initial 45 oz. (1350 ml)] was then added to obtain a slump of approximately 8 in. (200 mm). The superplasticizer was added to improve workability.

In spite of the great variability of apparent water content found between mixes, very similar concrete strengths were obtained. Table 2.8 summarizes the average cylinder compressive strengths at the day of testing. The cylinders tested were 6 in. (150 mm) by 12 in. (300 mm), and were loaded using neoprene pads. The results on each day are the average of two cylinder tests, consecutively. A third cylinder was tested when very different strengths were obtained from the first two tests.

2.5.2 Passive Reinforcement

Reinforcement used in all test specimens for the overhang section was #2 deformed Swedish bars and 7-gauge heat-treated wire as longitudinal steel, and 10-gauge heat-treated wire as vertical steel. For construction of the column cage, #3 deformed bars were used for the vertical steel while 9-gauge annealed wires were used for the stirrups.

Bars and wires used in the eight specimens were taken from the same lot. Number 10 and 9 wires were received in coils which had to be uncoiled, straightened, and cut to length.

Figures 2.33 and 2.34 show the stress-strain curves for #2 reinforcing bars and 7-gauge wire.

2.5.3 Active Reinforcement

Prestressing steel consisted of 3/8 in. (9.5 mm) and ½ in. (13 mm) diameter, Grade 270 (1860 MPa), low relaxation 7-wire strands. The size utilized in a given model depended on the post-tensioning force requirements. Each size strand was taken from a single spool. Figure 2.35 and 2.36 show the stress-strain curves for the strands.

2.5.4 Ducts and Prestressing Hardware

Ducts consisted of ¾-in. (19 mm) semi-rigid galvanized steel conduit. Grout tubes were made of ½-in. (13 mm) diameter flexible hoses secured to the ducts with silicone caulk.

The anchorage hardware consisted of single steel bearing plates, 4-1/4 in. x 3 in. x 7/8 in. to 1 in. thick (108 mm x 76 mm x 22 mm to 25 mm) for each strand. Strands were anchored with commercial wedges and chucks. Threaded chucks with nuts that were prepared in the laboratory were used to minimize seating losses (see Figure 2.37).

2.5.5 Grout

Grout mix proportions were selected to allow an expansion of 2-4% and a W/C ratio of 0.44 to 0.49 to comply with AASHTO [Division II, Sec. 10.6.4 (2)]. For a typical 0.42 ft^3 (0.0126 m^3) batch the mix included 34.33 pounds (15.45 kg) of Type I Portland cement, 1.8 gallons of water (0.00684 m^3) and 0.31 pounds (0.14 kg) of Interplast N,

Table 2. 8   Concrete Compressive Strengths

Specimen		Overhang Designation	Concrete Cylinder Strength, f'_c	
			psi	MPa
1	A	CO-RU-0S-OR-N-SF	5620	38.7
	B	CO-RU-0S-OR-N-SF	5620	38.7
2	A	CO-PS-100S-NA-N-SM	6270	39.3
	B	CO-PS-100S-NA-N-SM	6270	39.3
3	A	CO-PU-100S-NA-V-SM	7350	50.6
	B	CO-PU-100S-NA-I-SM	7350	50.6
4	A	CO-PU-74S-OR-V-SM	5440	37.5
	B	CO-PU-74S-OR-I-SM	5440	37.5
5	A	CO-PU-54S-TH-V-SF	6350	43.8
	B	CO-PU-54S-TH-I-SM	6350	43.8
6	A	CO-PU-74S-TH-V-SM	6400	44.1
	B	CO-PU-74S-TH-I-SM	6400	44.1
7	A	CO-PU-100S-TH-V-SF	6450	44.5
	B	CO-PU-100S-TH-I-SM	6450	44.5
8	A	CO-RU-0S-TH-M1-SM	6450	44.5
	B	CO-RU-0S-TH-M1.7-SM	6450	44.5
		$\overline{X}$	6290	43
		σ	580	4
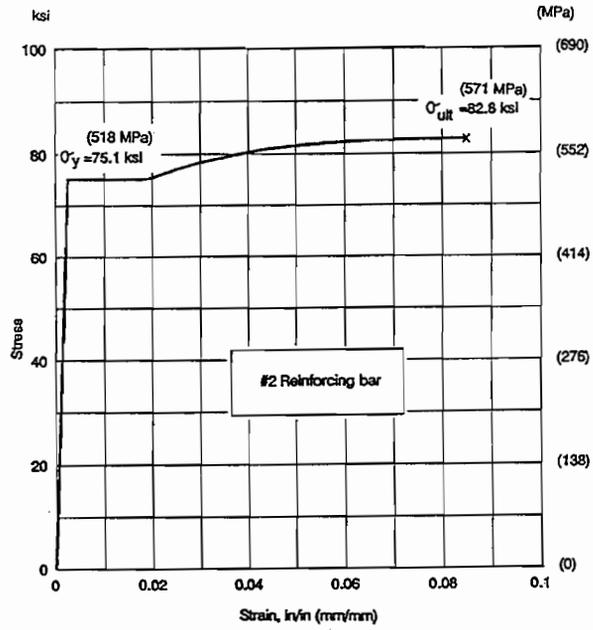
Figure 2. 33   Stress-strain curve for #2 reinforcing bar (7)
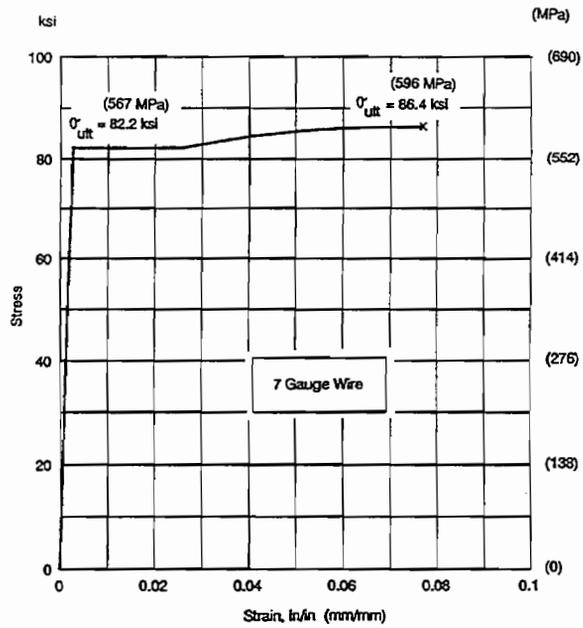
Figure 2. 34   Stress-strain curve for 7-gauge wire (7)

54
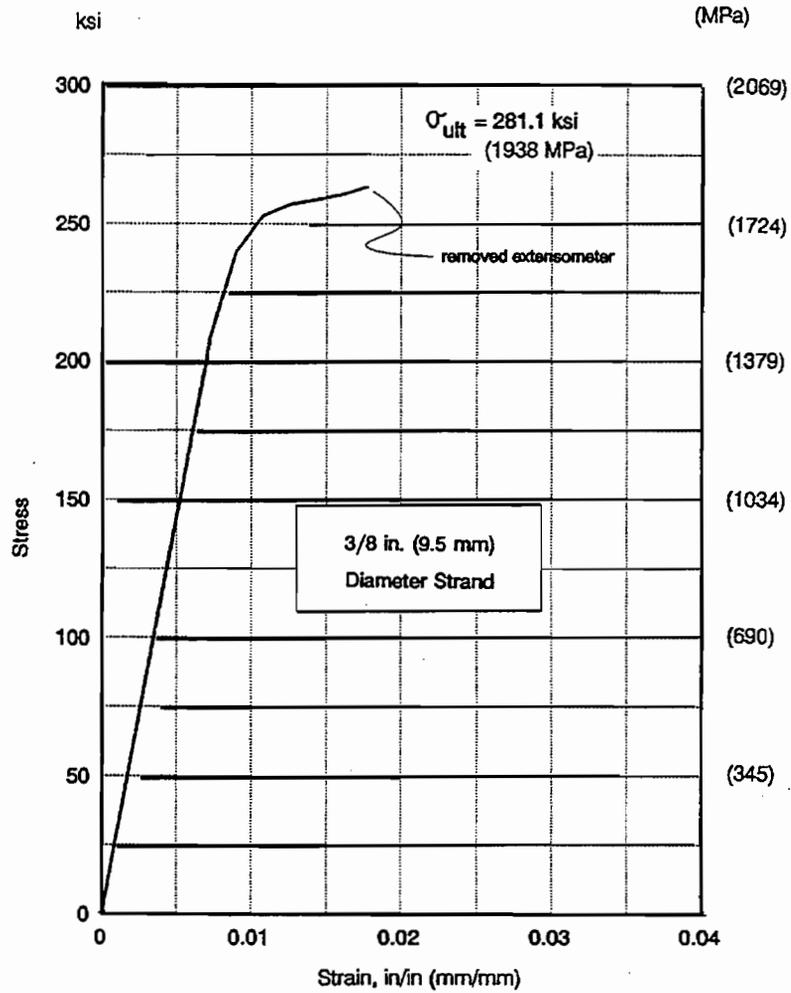
Figure 2. 35   Stress-strain curve for 3/8-in. (9.5 mm) strand
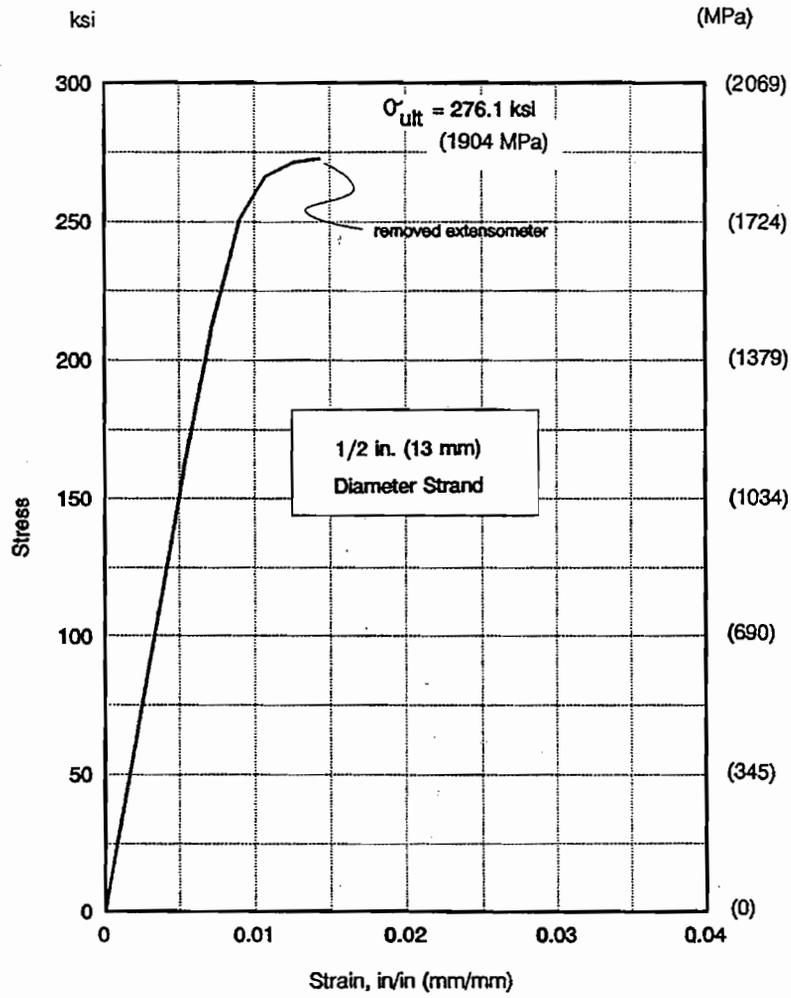
Figure 2. 36 Stress-strain curve for ½-in. (13 mm) strand (5)
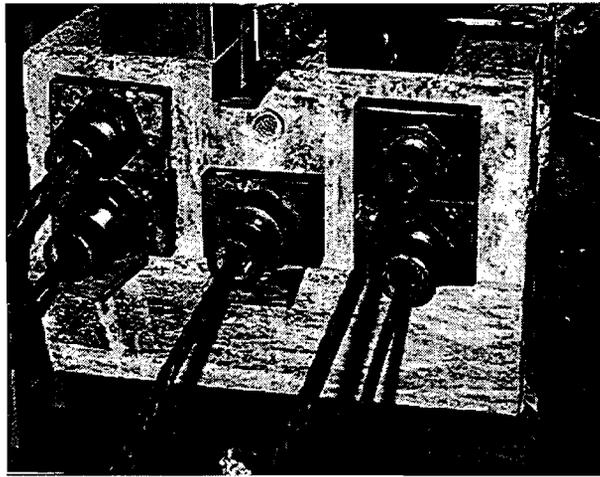
*Figure 2. 37 Prestressing hardware for
Models CO-PU-74S-TH-(V&I)-SM*

approximately 0.91 percent by weight of cement, as the expansive additive. The expansive agent was added to prevent shrinkage and minimize bleeding. One batch was used for grouting of three strands, approximately 11 feet long (3.35 m) each.

2.5.6 T-heads

T-headed reinforcing bars or HR-bars (headed reinforcing bars) were used for all #2 flexural reinforcement in specimens designated TH. The design was based on recommendations from Norwegian Contractors (13, 14, 15) based on their experience in using T-headed reinforcing bars in highly congested cages in offshore concrete structures, especially as shear reinforcement.

In general, experience suggests the use of T-heads with six to ten times the cross-sectional area of the reinforcement bar (4) and a thickness of approximately 8/10 of the diameter of the bar. Heads may be square or circular. There are different ways of attaching them to the bars. The most commonly used is by friction welding where the head is rotated, forced onto the bar and heat is generated between the surfaces. "The weld is completed by the application of a forge force after the cessation of the rotation" (3). Fatigue tests, as well as pull-out tests, have been performed and reported (3).

For this study, square heads were used on all #2 deformed bars with an approximate area of 0.50 in.^{2} (323 mm^2) and a thickness of ¼-in. (6.4 mm), as shown in Figure 2.38. Fillet welding, 1/8-in. (3.2 mm) thick, using an E70 electrode, was used between heads and bars. Special care was taken to check that every T-headed bar had at least the same cross-sectional area in the weld region as in the bar itself. Figure 2.39 shows the use of T-headed reinforcing bars in Model CO-PU-74S-TH-V-SM.
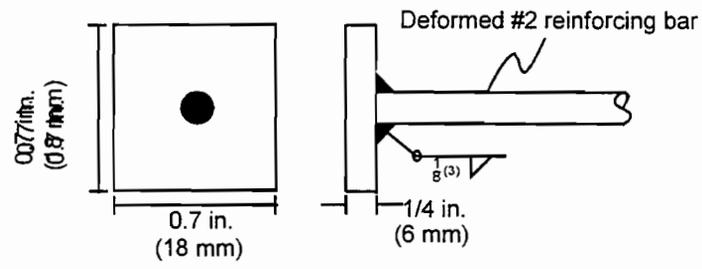
Figure 2. 38   T-head dimensions
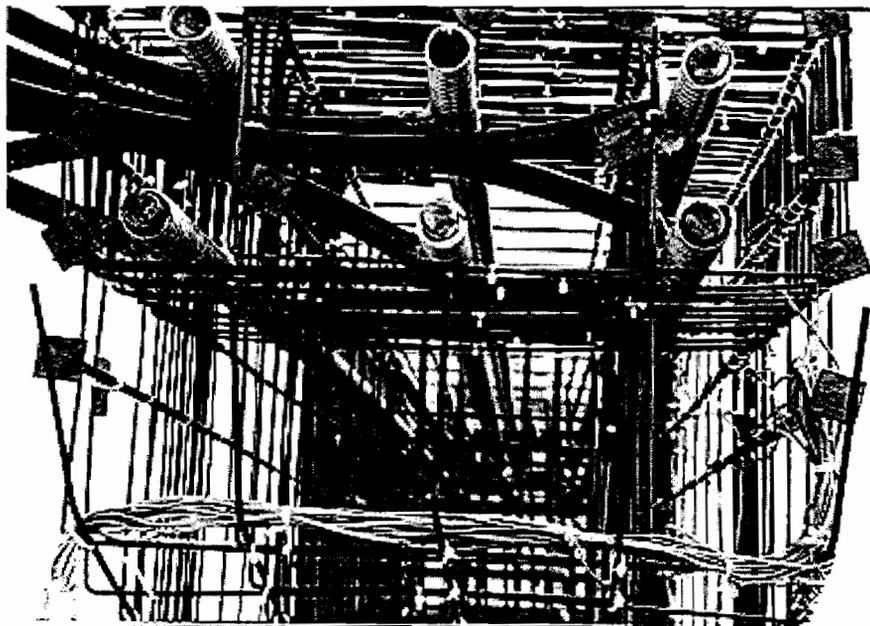
Figure 2. 39   T-headed reinforcement in Model CO-PU-74S-TH-V-SM

Four pull-out tests (elongation tests conducted by pulling in air with the bars anchored by the T-heads) were performed and results are summarized in Table 2.10. All T-headed bars developed yield stresses of at least 95% of the average of the original #2 reinforcing bar and achieved ultimate stresses of at least 96% of the average of the original bars. One of the four tests resulted in breaking of the bar itself at a point far from the T-head. The other three tests resulted in failure of the weld material between the head and bar. Elongations were substantially reduced.

2.6 FABRICATION

As mentioned before, fabrication of all models was carried out at the Ferguson Structural Engineering Laboratory.
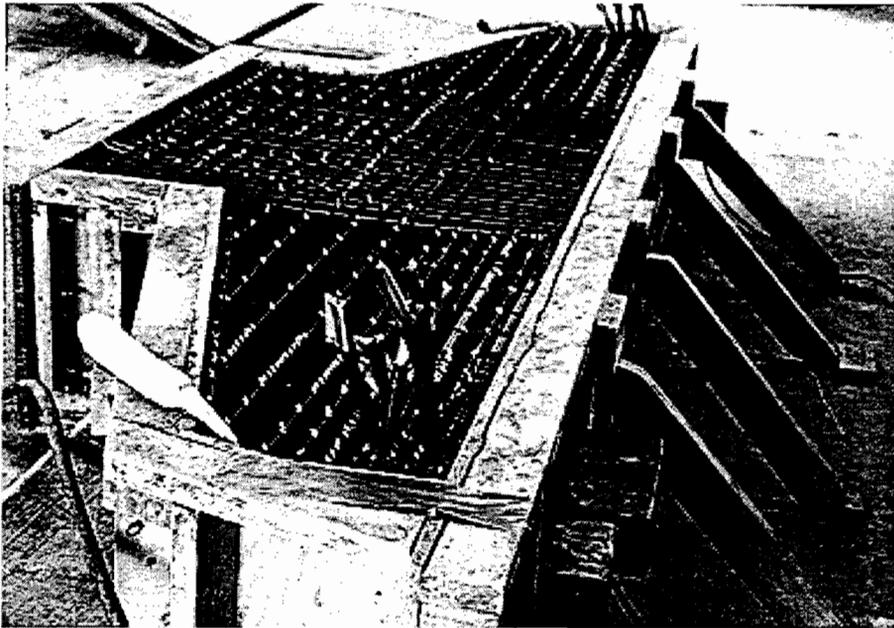
Figure 2. 40 Formwork

2.6.1 Formwork

Forms were made so that the models could be cast on their side (see Figure 2.40). This was done to facilitate and control placement of the reinforcing cage, and casting and consolidation of the concrete mix. Reusable ¾-in. (19 mm) plywood and 2-in. (50.8 mm) x 4-in. (101.6 mm) ribs were used. The formwork was cleaned and lacquered with several layers of varnish before casting.

2.6.2 Reinforcing Cage

All bars and wires were cut and bent at the laboratory except for all #3 deformed bars used in the column cages; these were ordered from a local fabricator and were received with reasonable tolerance of approximately 3/8-in. (9.5 mm). Reinforcing bar and wires used for flexure, shear-friction and horizontal shear had hooks on their ends. Nylon and wire ties, 4 in. (101.6 mm) in length, were used to secure the cages.

The column cage was constructed first, followed by the placement of ducts. Rods were placed into the ducts to keep them straight while constructing the cage and during casting. This construction was followed by the placement of flexural steel, shear stirrups, anchorage reinforcement and additional horizontal steel. Ducts were then secured to the cage by the use of wire ties in various locations. In all cases the main longitudinal steel passed inside the vertical column bars. Stirrups were all closed and anchored at the top around a longitudinal bar. Plastic spacers, 0.41 in. thick (10.4 mm), were used on reinforcing bars parallel to the edges of the specimen to ensure adequate cover on all sides (see Figures 2.41 and 2.42).

2.6.3 Casting of Concrete

Concrete conforming with the mix described in Section 2.5.1 was ordered for all models that were cast on different days. After receipt of the mix, the concrete slump was measured according to the ASTM C-143 procedure. Water and superplasticizer were added to achieve the desired slump of 8 to 10 in. (203 to 254 mm). Every model was cast in three layers with the use of a one-cubic-yard (0.76 m³) bucket hoisted by the overhead crane. Vibration was provided internally with flexible shaft vibrators, and externally with form vibrators to achieve good consolidation. Figure 2.43 shows casting of the CO-PU-54S-TH (V and I)-SM overhangs. Adequate curing was provided by covering the models with wet burlap and plastic, maintaining adequate humidity and heat during the curing process. Twenty 6-in. (152 mm) x 12 in. (305 mm) cylinders per model were also cast in plastic molds according to ASTM C-31. They were also covered with burlap and plastic and maintained wet for approximately three to five days until forms were removed from the model.

No honeycombing was found in any of the specimens after stripping the forms.

2.6.4 Prestressing Procedure

The stressing operations varied according to the characteristics of each model. In general the prestressing hardware and set-up for post-tensioning of the single strands consisted of a steel chair bearing on the corners of the bearing plate, a 30-ton (294 kN) hydraulic ram positioned at the end of the chair and centered over the strand, and a temporary anchor plate and wedges placed at the end of the ram. The ram force was applied in increments of approximately five percent of ultimate until the desired prestress was obtained.
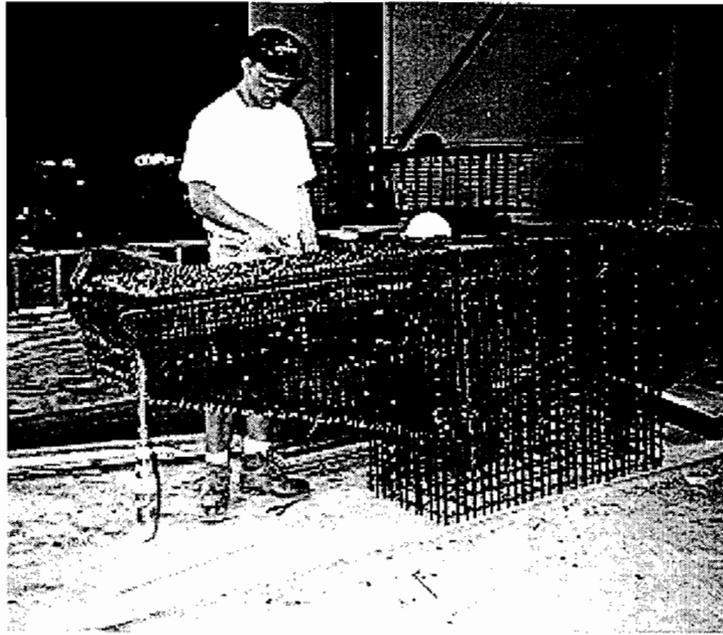
Figure 2. 41   Assembly of reinforcing cage
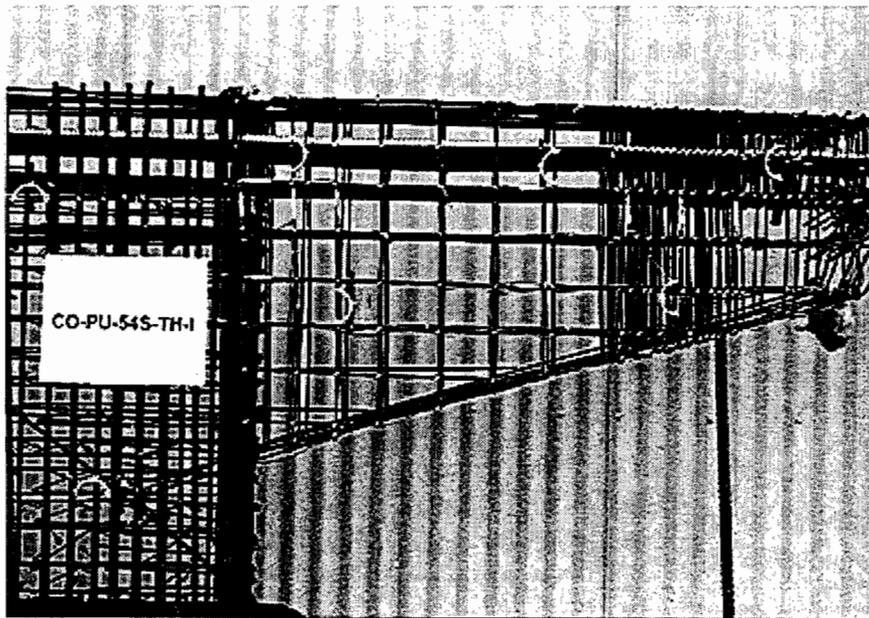
Figure 2. 42   Reinforcement cage for Model CO-PU-54S-TH-I-SM
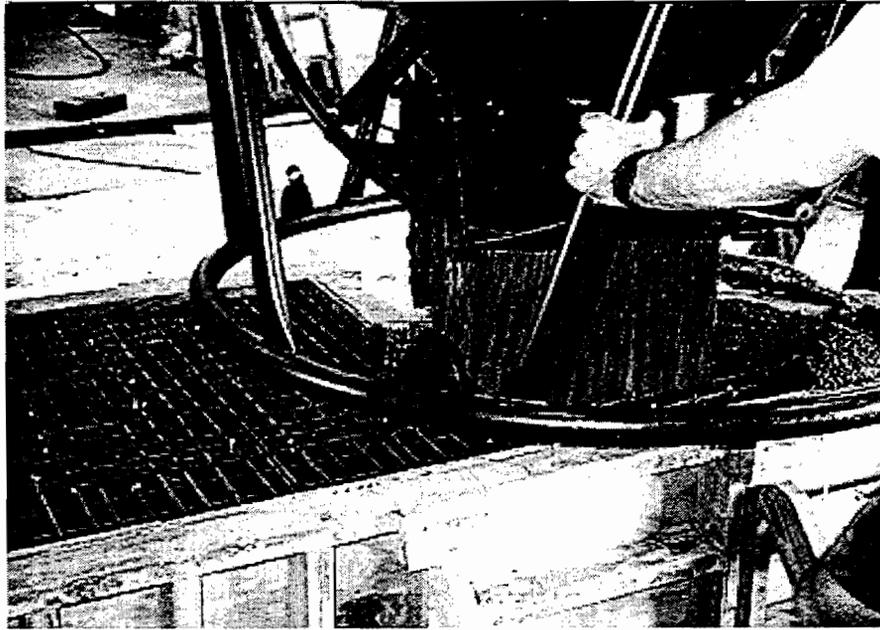
Figure 2. 43   Casting of Specimen CO-PU-54S-TH

It was kept reasonably constant by adjusting the nut on the chuck to the desired position to overcome seating losses. The prestressing force was gradually released onto the anchorage system by reversing the ram direction, to ensure adequate seating of the wedges. All prestressing operations took place at one end (the "live end" or north end) of the models. Stressing sequences were varied to ensure that tensile stresses never exceeded $3\sqrt{f_c'}$.

The force in the strands was checked and controlled to an acceptable degree by following a lift-off procedure and restressing as necessary. This operation was performed after all strands were initially stressed.

As stress level of 160 ksi (1100 MPa) was chosen to correspond with the stress level that would be expected in the strand after all long-term losses. This stress is equal to 59% of F_{pu} for grade 270 (1860 MPa) strand. The specimens were tested from two to four days after the post-tensioning operation.

The lift-off operation can be better described by referring to Figure 2.44. A linear potentiometer attached to the ram was used to measure the elongation I the strand while the load was measured by an electronic pressure transducer. Both were plotted continuously. The plot showed an initial linear relationship between load and elongation, which prior to lift-off reflected only elongation in the portion of strand that was located between the anchorage wedges ("live load") and the temporary wedges located behind the ram. When the stress in this portion of strand equaled the stress in the strand inside the specimen, the force in the ram started pulling out the entire strand length ("dead end" to the temporary wedges) producing a change in the slope of the curve. The stress at which this break point occurred represented the actual
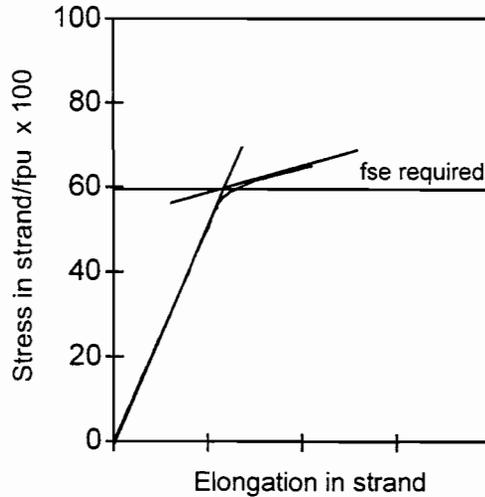
Figure 2. 44   *Example of plot obtained in a lift-off operation of a typical strand*

stress in the tendon. Depending on the difference between this stress and the desired value, the nut in the anchorage system had to be adjusted, and the procedure was repeated (usually two to three times) until the desired stress was obtained. At no time was the stress in the strand allowed to exceed 75 percent of its ultimate tensile strength.

All specimens were grouted immediately after doing the lift-offs. Grout proportions are presented in Section 2.5.5. Water was added first, then the cement and finally the expensive agent. The materials were mixed for approximately four minutes. The grout was forced into the ducts, through the grout tubes, with the aid of a manual pump. The grout was allowed to flow for a short period of time to eliminate any entrapped air in the conduit.

The exit grout tube was plugged first and additional grout was pumped into the duct before plugging the access side. Grout cubes were cast for every grout batch. Results are shown in Table 2.9.

Screw jacks were placed between the model and the hydraulic loading rams to avoid any undesirable upward deflections due to possible losses in the hydraulic rams which applied the simulated dead load. Further details on prestressing sequences are given in References 7 and 8.

63

Table 2. 9   Grout Compressive Strengths

Specimen		Overhang Designation	Grout Strength	
			f'_{cube} psi	MPa
1	A	CO-RU-0S-OR-N-SF	--	--
	B	CO-RU-0S-OR-N-SF	--	--
2	A	CO-PS-100S-NA-N-SM	1650	11.4
	B	CO-PS-100S-NA-N-SM	1650	11.4
3	A	CO-PU-100S-NA-V-SM	1670, 2330	11.5, 16.0
	B	CO-PU-100S-NA-I-SM	1670, 2330	11.5, 16.0
4	A	CO-PU-74S-OR-V-SM	1910	13.2
	B	CO-PU-74S-OR-I-SM	1910	13.2
5	A	CO-PU-54S-TH-V-SF	3200	22.1
	B	CO-PU-54S-TH-I-SM	3200	22.1
6	A	CO-PU-74S-TH-V-SM	2290	15.8
	B	CO-PU-74S-TH-I-SM	2290	15.8
7	A	CO-PU-100S-TH-V-SF	2940	20.2
	B	CO-PU-100S-TH-I-SM	2940	20.2
8	A	CO-RU-0S-TH-M1-SM	--	--
	B	CO-RU-0S-TH-M1.7-SM	--	--

Table 2. 10   Results from Tests of T-Headed Bars

Test No.	Yield Stress ksi (MPa)		Ultimate Stress ksi (MPa)		Strain at Ultimate in/in (mm/mm)	Comments
1	73.57	(507.27)	85.64	(590.49)	0.068	failed in bar
2	74.14	(511.20)	81.58	(562.49)	0.027	broke in weld area
3	71.56	(493.41)	NA		NA	broke in weld area
4	72.42	(499.34)	80.15	(552.63)	0.017	broke in weld area
Average results from elongation tests of #2 bars without heads	75.1	(517.81)	82.8	(570.91)	0.085	

2.7 SPECIMEN INSTRUMENTATION AND DATA MEASUREMENT

2.7.1 Post-Tensioning and Loading Rams

Ram loads were controlled by measuring the pressure on the calibrated hydraulic system. The load was considered to be equal to the product of the ram piston area and the hydraulic pressure.

The pressure on each set of rams was measured using hydraulic pressure transducers. Each pressure transducer had a 10,000 psi capacity and 10 mv/v output. The output voltage from the transducer was displayed on a voltmeter located next to each pump which allowed the pump operator to control the amount of pressure applied to the system. Each pump was additionally fitted with a hydraulic dial gauge which was used to verify the pressure given by the transducers.

2.7.2 Deflections

Overhang deflections were measured with linear potentiometers connected to the data acquisition system. Tip deflection measurements were backed up with the use of digital gauges. In addition, dial gauges were placed at the column base, as shown in Figure 2.45, with the purpose of monitoring the behavior of the model at this level and recording any important deflections that had to be subtracted from the top measurements.
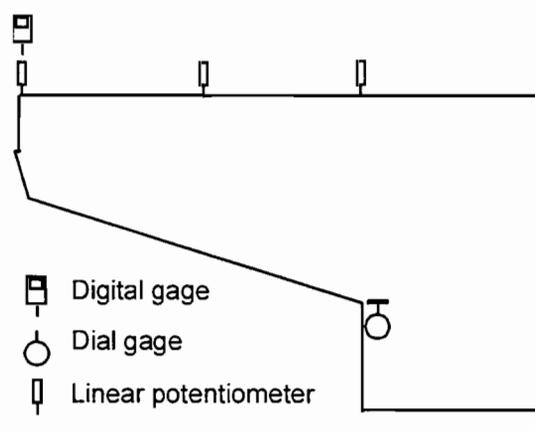
Figure 2. 45 Location of linear potentiometers, digital gages and dial gages

2.7.3 Strains

Several strain gauges were used to monitor the stresses in reinforcing steel. Typically, 0.2 in. (5 mm) strain gauges were used on all longitudinal steel and 0.08 in. (2 mm) strain gauges on all shear reinforcement. Figure 2.46 shows typical locations of these gauges in the models. Locations of strain gauges will be shown in Chapter 3 when results are given.

2.7.4 Crack Widths

Crack widths were measured at key grid points, shown in Figure 2.47, using an optical crack comparator. The accuracy of the crack comparator was ± 0.0005 inches (0.013 mm). Crack readings were taken when first cracking occurred and at every major loading stage above that level. Above service load levels only minimum crack widths were recorded.

CO-PU-54S-TH-V-SF
((East)

CO-PU-54S-TH-V-SM
((East)

All strain gages in east side face of cage
unless noted:

sh : 2 mm strain gage in shear stirrup (10 gage wire)
sk: 5 mm strain gage in skin reinforcement (7 gage wire)
fx: 5 mm strain gage in flexural reinforcement (#2 reinforcing bar)
sh*: an additional strain gage was placed in interior stirrup
    at same height.
fx*: an additional strain gage was placed in interior middle
    flexural bar at same distance from column face.

Figure 2. 46   Location of strain gages for Models CO-PU-54S-TH (V & I)

Figure 2. 47 Crack reference grid

2.8 TEST SETUP

Two different test setups were utilized in the course of the project. Specimen #1 was tested in the setup shown in Figure 2.48. The frame consisted of structural steel elements bolted together. The frame was bolted to the floor of the testing laboratory. This setup required the use of a 2-foot high concrete pedestal to bring the specimen up to the level of the loading rams.

Specimens #2, #3, and #4 were all tested in the second setup. This setup, shown in Figures 2.49 and 2.50, used vertical tension rods connected to the laboratory floor and structural steel elements. Note that in Specimens 5, 7 and 8 that elastomeric pads were inserted below the steel loading plates to release horizontal restraint forces at large deflections.

The specimens were loaded using 100-ton (981 kN) hydraulic rams. The exterior rams (RO loads) were controlled together and independently from the interior rams (RI loads), which also acted together. Each group was operated with a manual pump, and the load was recorded with the use of a pressure transducer connected to a data acquisition system and to a voltmeter.

2.9 TESTING PROCEDURE

2.9.1 Loading

Loading was applied in discrete increments. The "RO" loads were the outer loads applied to the overhang, at 39 inches (991 mm) from the column face, and the "RI" loads were the inner loads, at 13 inches (330 mm) from the column face. Loads required to increase model density based on scale relations were applied as additional dead load (load step 1) using the same loading rams.
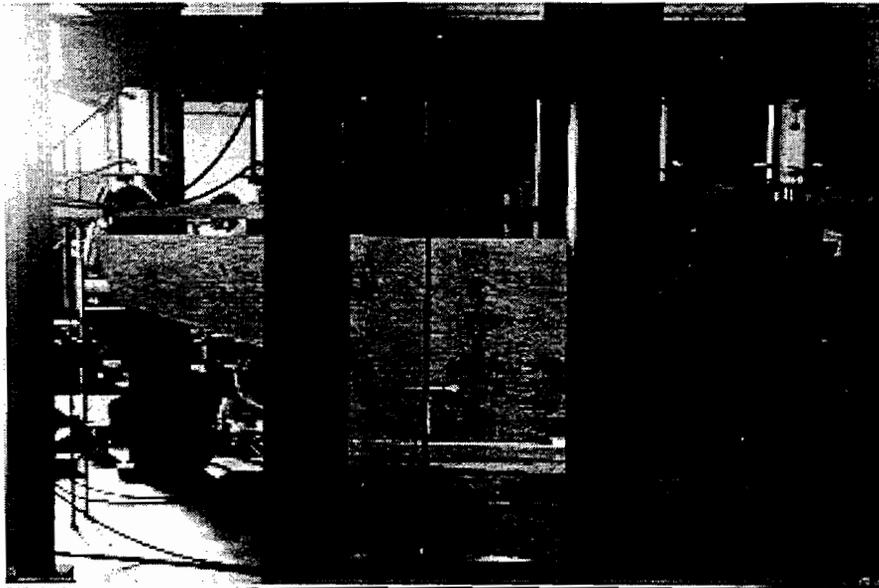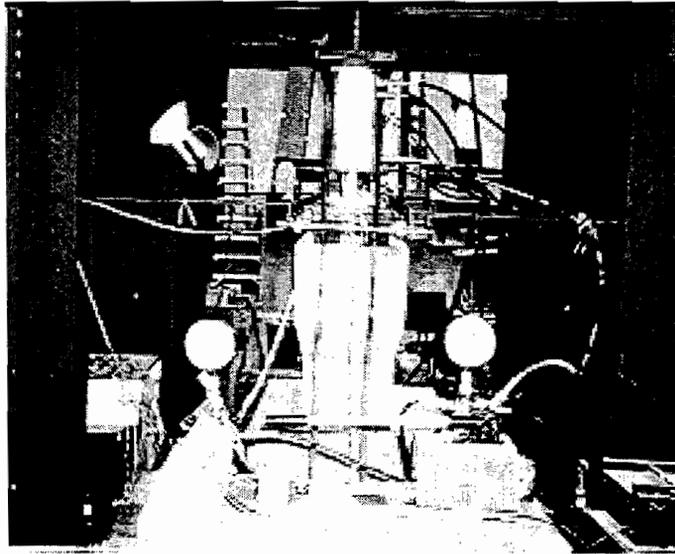
Figure 2. 48   Test setup for Specimen #1
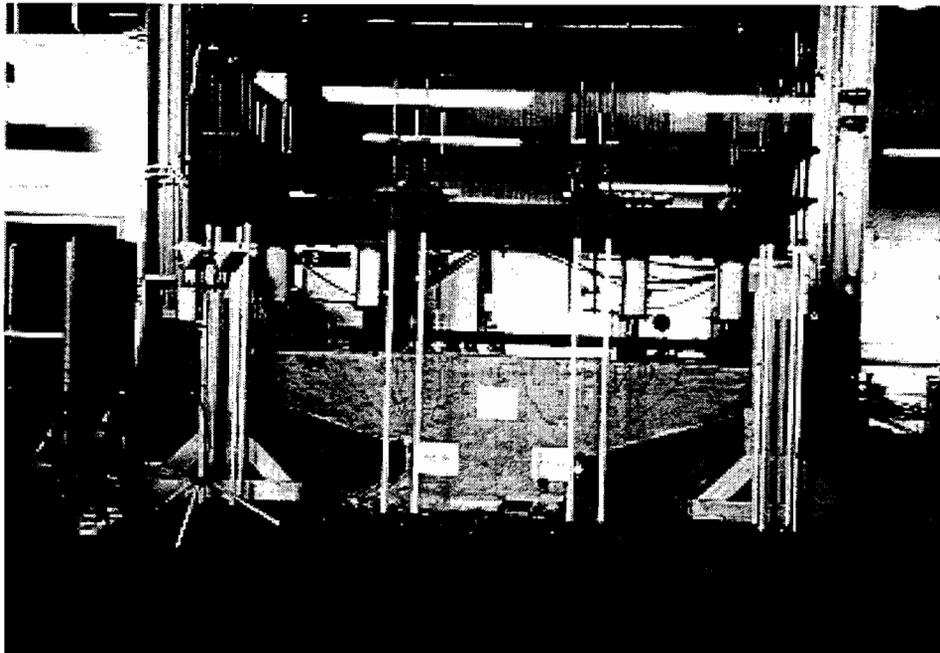
Figure 2. 49 Test setup for Specimens #2 through #8

W12x120

8x12x2 in.
(203 x 305 x
51 mm)
steel plate

Elastomeric pad used in
54 and 100 percent
prestressed models,
7 x 9 1/4 x 2 1/2 in.
(178 x 235 x 63.5 mm)

7 1/2 x 9 1/4 x 1 in.
(191 x 235 x
25 mm)
steel plate

100 Ton
(980.6 kN)
capac.
hidraulic ram

1 in.(25.4 mm)
diam. threaded
rod anchored to
reaction floor

4x4x8 in.
(102 x 102 x
203 mm)
steel blocks

Elevation view

Side view
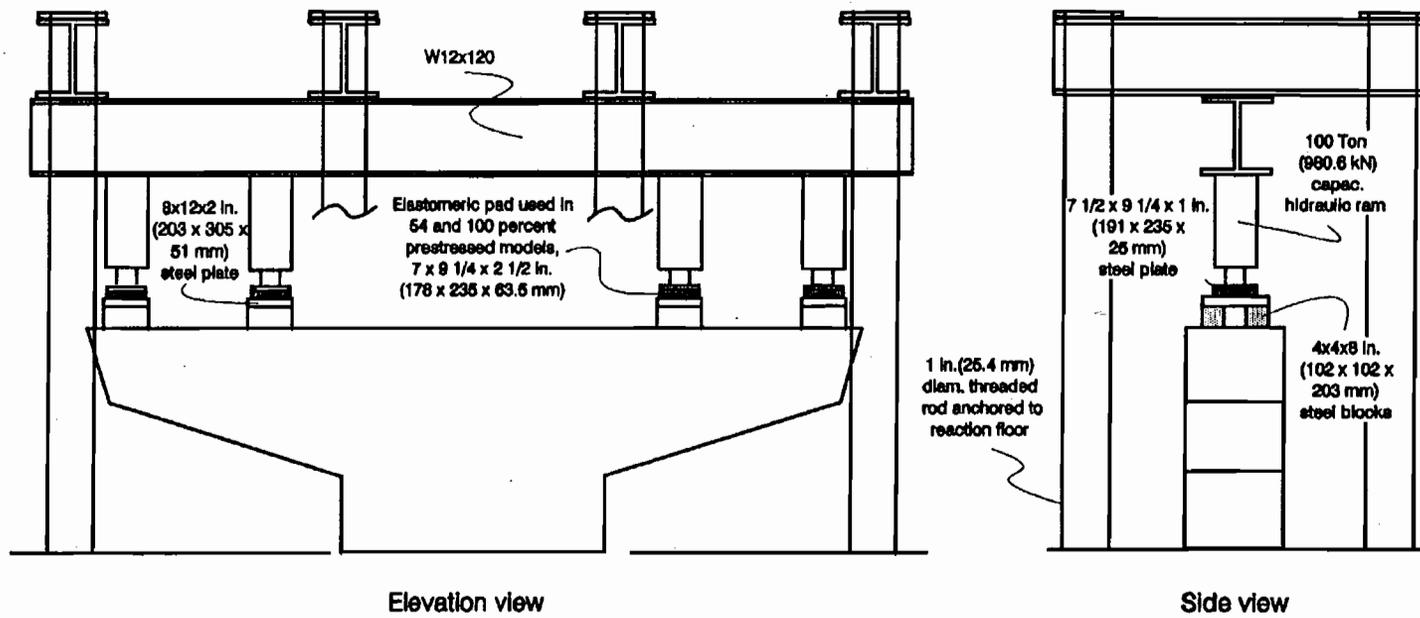
Figure 2. 50   Test setup

70

The loading sequence included various cycles. A typical sequence consisted of:

a) Loading from dead load to service flexure load (three outside lanes loaded), then unloading to dead load;

b) Loading from dead load to service shear load (4 lanes loaded), then unloading to dead load;

c) Loading from dead load to service flexure load, continuing to factored flexure load, then unloading to dead load;

d) Loading from dead load to service shear load, continuing to factored shear load, then unloading to dead load;

e) Loading from dead load to service flexure load, then to factored flexure load and continuing to ultimate flexure load.

Detailed load step sequences are given in References 7 and 8.

For the models CO-PU-100S-TH (V and I), due to the fact that no cracking was observed while following steps a) and b) above, additional cycles were performed to evaluate the behavior of existing cracks at service level. To do this, the steps that are presented below were followed between steps b) and c) above:

b') Loading from dead load to service flexure load, continuing to first crack, and then unloading to dead load.

b") Loading from dead load to service flexure load, continuing until cracks were observed in both overhangs and both sides, and then unloading to dead load.

2.9.2 Data Collection

All electronic instrumentation was read at each load step. Data from pressure transducers, strain gages, and linear potentiometers was collected and stored using a data acquisition system. The system consisted of a Hewlett Packard 3497A scanner driven by an in-house computer program (HPDAS2) operating on an IBM XT personal computer. Mechanical gages were read at each load stage. Crack widths were measured at initiation and at every following load stage up to and including factored shear load. The cracks were numbered sequentially in the order of appearance within each of the six regions shown on Figure 2.47.

CHAPTER THREE

TEST RESULTS

Eight concrete specimens with sixteen overhang structures with various combinations of reinforcement were tested under static loading. The specimens four non-prestressed specimens included overhangs (six 100 percent prestressed overhangs, four overhangs) with 74 percent of the main flexural reinforcement prestressed and two overhangs with 54 percent of the main flexural reinforcement prestressed. One overhang in each specimen was tested to failure.

The same loading sequence was used for all models except for the 100 percent prestressed overhangs where two additional service load cycles were included to determine cracking loads.

All models were oriented in the test set-up such that overhangs designed using "inclined ties," in the strut and tie modeling, were always located at the north end, corresponding to the "live end" for prestressing.

Testing was performed over several days for each overhang. Between days of testing, applied loads were released and only dead loads were maintained overnight. Typically the first day of testing included load cycles in the service range, while the second and third days included testing to factored loads and then to failure.

Scans of data using Data Acquisition System, including strain readings from strain gages, deflections from liner potentiometers and loading from pressure transducers, were taken at every load step until failure. Tip deflections from digital gages precision of 0.0001 in. (0.0025 mm), as well as column settlement from dial gages having a precision of 0.0005 in. (0.013 mm), were recorded with the same frequency. Documentation of crack widths and crack patterns was performed at every major load step as described later. In addition, several photographs were taken at every major load level (service shear, service flexure, etc.).

Specimens 2, 3, 4 and 6 of Table 2.4 were tested without elastomeric pads between the loading rams and steel plates. This presented a problem for loads higher than factored loads since some friction forces were developed, limiting the deflection of the overhang and providing an additional moment at the column face which acted opposite to that from applied loads. As will be discussed in Chapter 4, this was considered one of the causes of the additional capacity observed in these overhangs. The other models were tested with the 2-1/2 in. (63.5 mm) thick reinforced elastomeric bearing pads shown in Figure 2.50. This eliminated the restraint problem for these specimens.

In the following sections the response of all overhang structures to the applied loads is discussed in detail in terms of load versus deflection, cracking, and failure modes.

3.1 LOAD VERSUS DEFLECTION RESPONSE

Linear potentiometers and digital gages were mounted on a steel reference frame. This frame was supported independently of the test specimens and loading system.

Figures 3.1 to 3.8 show the individual applied moment-deflection responses for all models. Particular deflections and loads have been indicated in these figures for all major load levels. Plots for one overhang in each figure with the smaller ultimate deflection do not represent the behavior of such overhangs to complete failure since these models could be loaded only to the level of ultimate load of the other overhang for each specimen. The scales for the graphs were intentionally held constant for comparative purposes. In Figures 3.2, 3.4 and 3.6, discontinuities in the plot above factored loads levels were mainly due to the lack of elastomeric pads, as explained before. In this case, built-up friction forces between rams and steel plates were suddenly relieved (whether in part or in whole is unknown) at certain load steps due to the horizontal movement of the overhang. These restraining forces were a function of the rigidity of the loading frame and the lack of shear deformation capacity of the bearing system. The modified loading system for the other models, where elastomeric pads were used, greatly relieved these restraining forces. Figure 3.9 shows the horizontal deformation of the elastomeric pad in model CO-PU-100S-TH-V.

In all cases the initial deflection measurements were made before prestressing operations. No corrections of the tip deflection were made based on column settlement or deflections at the top of the overhang at the column face, since deflections at these locations were negligible. In addition, no normalization of results based on concrete strength were performed since all models were tested at very similar cylinder compressive strengths. Tip deflections used in the moment-deflection plots were taken in all cases from linear potentiometer data since there was a perfect correlation with the results from digital gages. The dead load level corresponds to a column face moment of 2168 k-in. (245 kN-m). The service flexure load level for moment at the face of the column was 2749 k-in (310 kN-m) and the factoral flexure load moment was 4078 k-in. (461 kN-m). The nominal capacity (M_u /ϕ) corresponding to those levels are 3054 k-in. (345 kN-m) and 4530 k-in. (512 kN-m), respectively.

3.1.1 CO-RU-0S-OR-N-SF

Figure 3.1 shows a classic under-reinforced moment-deflection curve for the south overhang. There is an initial linear stage noticeable decrease in stiffness after cracking, which occurs well under service load levels and, in fact, well below dead load level., and a rapid decrease in stiffness above 7000 in-k (791 kN-m) where first yielding probably occurred. There was minor unloading after ultimate was reached until crushing of concrete occurred in the compression zone at the juncture of the bottom of the overhang and the column. The actual capacity was substantially above the required nominal moment capacity ($M_u.\phi$) if 4530 k-in. (512 kN-m). Since fabric pads were used in the loading system, there were no signs of binding in these curves.

3.1.2 CO-PS-100S-NA-N-SM

Figure 3.2 shows considerable evidence in binding in the loading system with slippage occurring (accompanied by distinct banging noises) near ultimate. First cracking occurs well above the service live load level, indicating that this specimen designed for full prestressing at service load levels would be uncracked at that stage. When cracking does occur, the specimen loses stiffness but much more slowly than the non-prestressed overhangs. Maximum deflections are only 60 percent of the non-prestressed Specimen 1. These occur at about 18 percent more load than the non-prestressed Specimen 1 and substantially above the factored moment since all design was governed by service conditions.

3.1.3 CO-PU-100S-NA-I&V-SM

Figure 3.3 shows little evidence of binding release although no fabric pads were provided. Cracking load was around service live load and substantial softening was evidenced. The ultimate load was considerably below the CO-PS Specimen 2 since selection of strand was based upon ultimate. Ultimate deflection was about 90 percent of CO-PS Specimen 2.

3.1.4 CO-PU-74S-OR-I&V-SM

Figure 3.4 shows distinct evidence of release of binding in the loading system and distinct release noises were heard. First cracking was above dead load but below service load. The provision of a portion (26 percent) of the tensile flexural force through non-prestressed reinforcement resulted in ultimate deflection about 90 percent of the CO-RU non-prestressed specimen.

3.1.5 CO-PU-54S-TH(V&I)-(SF&SM)

Figure 3.5 shows this lightly prestressed specimen experienced first cracking slightly below dead load levels, showed no sign of loading restraint (it was tested with elastomeric pads), developed one ultimate moment well above factored load levels, but had a maximum tip deflection no larger than the fully prestressed specimens.

From Figure 3.5 it can be observed that the behavior was basically linear until cracking occurred. After this load stage, gradual non-linear behavior began with some plastic behavior seen near the peak load. A clear point of onset of yielding in the main flexural reinforcement was observed approximately at an applied moment of 5000 k-in. (565 kN-m), 23 percent above factored flexure load level. Crushing was extensive at failure loads which did not allow for large plastic deformations. A post-mortem investigation found evidence of one #2 reinforcing bar broken in the top layer of the main flexural reinforcement and signs of yielding in all other #2 reinforcing bars.

kip-inches CO - RU - 0S - OR - N - SF (north) (kN-m)

Ultimate Loads R_i = 60.0 kips, R_o= 170.1 kips
R_i = (267 kN)R_o = (756 kN)

Moment at Column Face

Service Flexure Loads, δ_{tip} = 0.118 in. (3.0 mm)
Service Shear Loads, δ_{tip} = 0.118 in. (3.0 mm)
Dead Load, δ_{tip} = 0.081 in. (2.1 mm)
Cracking Loads, R_i = 28.47 kips, R_o = 25.59 kips
R_i = (128 kN), R_o = (114 kN)

Tip Deflection

kip-inches CO - RU - 0S - OR - N - SF (south) (kN-m)

Ultimate Loads R_i = 60.0 kips, R_o= 170.1 kips
R_i = (267 kN)R_o = (756 kN)

Moment at Column Face

Service Flexure Loads, δ_{tip} = 0.101 in. (2.6 mm)
Service Shear Loads, δ_{tip} = 0.092 in. (2.3 mm)
Dead Load, δ_{tip} = 0.063 in. (1.6 mm)
Cracking Loads, R_i = 28.47 kips, R_o = 25.59 kips
R_i = (127 kN), R_o = (114 kN)

Tip Deflection

Figure 3. 1   Moment-deflection curves for the CO-RU-0S-OR-N-SF overhangs (north and south)

76

Figure 3. 2   *Moment-deflection curves for the CO-PS-100S-NA-N-SM overhangs (north and south)*

Figure 3. 3   Moment-deflection curves for the CO-PU-100S-NA-I-SM and CO-PU-100S-NA-V-SM overhangs

78

CO-PU-74S-OR-I-SM (north)

kip-inches

Moment at Column Face

Maximum Loads, R_i = 56.8 kips, R_o = 143.6 kips
R_i = (253 kN), R_o = (639 kN)

slippage in loading assembly plates

Service Flexure Loads, δ_{tip} = 0.017 in. (0.4 mm)

Service Shear Loads, δ_{tip} = 0.020 in. (0.5 mm)

Cracking Loads, R_i = 41.29 kips, R_o = 49.66 kips
R_i = (184 kN), R_o = (221 kN)

Dead Load, δ_{tip} = -0.002 in. (-0.05 mm)

Tip Deflection

(kN-m)

CO-PU-74S-OR-V-SM (south)

kip-inches

Moment at Column Face

Ultimate Loads, R_i = 56.8 kips, R_o = 143.6 kips
R_i = (253 kN), R_o = (639 kN)

slippage in loading assembly plates

Service Flexure Loads, δ_{tip} = 0.031 in. (0.8 mm)

Service Shear Loads, δ_{tip} = 0.028 in. (0.7 mm)

Cracking Loads, R_i = 41.29 kips, R_o = 49.66 kips
R_i = (184 kN), R_o = (221 kN)

Dead Load, δ_{tip} = 0.012 in. (0.3 mm)

Tip Deflection

(kN-m)

Figure 3. 4   Moment-deflection curves for the CO-PU-74S-OR-I-SM and
CO-PU-74S-OR-V-SM overhangs

79

CO-PU-54S-TH-I-SM

Factored Flexure Load, δtip = 0.169 in. (4.3 mm)
Factored Shear Load, δtip = 0.138 in. (3.5 mm)
Service Flexure Load, δtip = 0.060 in. (1.5 mm)
Service Flexure Load, δtip = 0.046 in. (1.2 mm)
Dead Load, δtip = 0.029 in. (0.7 mm)
Cracking Loads, Ri = 40.48 kips (180 kN)
Ro = 37.46 kips (167 kN)

Tip Deflection

CO-PU-54S-TH-V-SF

Ultimate Loads, Ri = 54.4 kips, Ro = 136.9 kips
Ri = (242 kN), Ro = (609 kN)

Factored Flexure Loads, δtip = 0.181 in. (4.6 mm)
Factored Shear Loads, δtip = 0.154 in. (3.9 mm)
Service Flexure Loads, δtip = 0.068 in. (1.7 mm)
Service Shear Loads, δtip = 0.065 in. (1.7 mm)
Dead Load, δtip = 0.043 in. (1.1 mm)
Cracking Loads, Ri = 40.48 kips, Ro = 37.46 kips
Ri = (180 kN), Ro = (167 kN)

Tip Deflection

Figure 3. 5   Moment-deflection response for models CO-PU-54S-TH (V & I)

80

Figure 3. 6   Moment-deflection response for models CO-PU-74S-TH (V & I)

81

CO-PU-100S-TH-I-SM

kip-inches (kN-m)

Moment at Column Face

Ultimate Loads, Ri = 54.9 kips, Ro = 141.5 kips
Ri = (244 kN), Ro = (629 kN)

Factored Flexure Loads, δtip = 0.145 in. (3.7 mm)
Factored Shear Loads, δtip = 0.118 in. (3.0 mm)
Cracking Loads, Ri = 38.68 kips, Ro = 57.46 kips
Ri = (172 kN), Ro = (256 kN)
Service Flexure Loads, δtip = 0.045 in. (1.1 mm)
Service Shear Loads, δtip = 0.039 in. (1.0 mm)
Dead Load, δtip = 0.026 in. (0.7 mm)

Tip Deflection

CO-PU-100S-TH-V-SF

kip-inches (kN-m)

Moment at Column Face

Factored Flexure Loads, δtip = 0.127 in. (3.2 mm)
Factored Shear Loads, δtip = 0.115 in. (2.9 mm)
Cracking Loads, Ri = 40.22 kips, Ro = 65.46 kips
Ri = (179 kN), Ro = (291 kN)
Service Flexure Loads, δtip = 0.042 in. (1.1 mm)
Service Shear Loads, δtip = 0.041 in. (1.0 mm)
Dead Load, δtip = 0.026 in. (0.7 mm)

Tip Deflection

Figure 3. 7   Moment-deflection response for models CO-PU-100S-TH (V & I)

82

CO-RU-0S-TH-M1-SM

(kip-inches) / kN-m

Moment at Column Face

Factored Flexure Loads, δtip = (0.1959 in.) 4.98 mm
Factored Shear Loads, δtip = (0.170 in.) 4.33 mm
Service Flexure Loads, δtip = (0.093 in.) 2.35 mm
Service Shear Loads, δtip = (0.081 in.) 2.06 mm
Dead Load, δtip = (0.057 in) 1.46 mm

Tip Deflection

CO-RU-0S-TH-M1.7-SM

(kip-inches) / kN-m

Moment at Column Face

Ultimate Loads, Ri =(57.6 kips), Ro =(155.5 kips)
Ri = 242 kN,   Ro = 609 kN

Factored Flexure Loads, δtip = (0.170 in.) 4.32 mm
Factored Shear Loads, δtip = (0.146 in.) 3.71 mm
Service Flexure Loads, δtip = (0.082 in.) 2.08 mm
Service Shear Loads, δtip = (0.071 in.) 1.81 mm
Dead Load, δtip = (0.046 in) 1.16 mm

Approx. cracking load

Tip Deflection

Figure 3. 8   Moment-deflection response for models CO-RU-0S-TH (M1 & M1.7)

83

*Figure 3. 9   Use of elastomeric pads in model CO-PU-100S-
TH-V-SF*

At ultimate loads, tip deflection was 0.914 inches (23 mm), corresponding to a ratio of tip deflection to overhang length of 0.020 (Δ = L/50). Failure occurred at a moment of 6046 k-in. (683 kN-m), at approximately 33 percent above factored flexure load level when a ϕ of 0.915 included.

3.1.6 CO-PU-74S-TH-(V&I)-SM

Figure 3.6 shows this more substantially prestressed specimen experienced first cracking slightly above dead load but below service flexural load, obviously had binding in the loading system which did not have fabric pads, and had a smaller ultimate deflection than its 74 percent companion shown in Figure 3.4 and developed only about 70 percent of the non-prestressed Specimen 1.

3.1.7 CO-PU-100S-TV-(V&I)-(SF&SM)

Figure 3.7 shows that this fully prestressed specimen again first cracked well above service load conditions and while it did not develop quite as high a moment as its 100 percent companion (Figure 3.3), it did develop almost 60 percent more deflection prior to failure. Since it had fabric pads where the companion did not, the larger deflection probably indicates the absence of such loading restraint.

3.1.8 CO-RU-0S-TH-(M1&M1.7)-SM

Figure 3.8 shows that this non-prestressed specimen had very early cracking. The actual cracking load was not determined but when ½ dead load was applied, several small cracks were detected. The increased percentage of flexural reinforcement when compared to the other non-prestressed specimen (See Figure 3.1) resulted in a more brittle failure condition with only about 1/3 of the ultimate deflection at about the same moment capacity. Very large shear cracks formed in this specimen and a great deal of spalling was observed near the bottom of both overhangs. This high shear probably reduced the ultimate capacity, since this specimen was designed with reduced shear capacity by assuming concrete contributions to aid the strut-and-tie model. Again, as in all specimens, the ultimate load was well above the factored design load.

3.2 CRACKING MOMENTS

The cracking moments for each overhang are summarized in Table 3.1. The moments are for the inside and outside reactions that were applied when cracking of the overhang was first detected. The cracking moment includes the self weight of the overhangs.

The moment at the face of the column corresponding to superstructure plus overhang dead load is 2169 k-in. The moment corresponding to service flexure live loads plus impact is 580 k-in. The combination of these is the service flexure moment (DL + LL + I) which is 2749 k-in. The factored design moment determined using the AASHTO Load Factors and all dead load plus applied loads is M_u = 4078 k-in. (461 kN-m)

In the design of all flexural reinforcement, the basic AASHTO approach given by Equation (3.1) was used.

$$M_u \leq \phi \, M_n \qquad\qquad (3.1)$$

In these laboratory experiments with carefully controlled and measured dimensions and material properties, the use of ϕ values complicates interpretation when comparing test results ($M_{n\ test}$) to design values (M_u). For more consistent comparison, Equation (3.1) will be rearranged as

Table 3. 1   *Cracking and Failure Moments*

Specimen		Overhang Designation	Cracking Moments				Failure Moments		
			Moment, M_{cr}		M_{cr} / M_{dead}*	$M_{cr} / M_{serv\,flex}$**	Moment, M_n		$M_u/M_u/0.9$ ***
			kip-in	kN-m			kip-in	kN-m	
1	A	CO-RU-0S-OR-N-SF	1394	157	0.64	0.51	7440	840	1.64
	B	CO-RU-0S-OR-N-SF	1394	157	0.64	0.51	----	----	----
2	A	CO-PS-100S-NA-N-SM	3272	370	1.51	1.19	8734	986	1.93
	B	CO-PS-100S-NA-N-SM	----	---	----	----	----	---	----
3	A	CO-PU-100S-NA-V-SM	2923	330	1.35	1.06	7044	796	1.56
	B	CO-PU-100S-NA-I-SM	3087	349	1.42	1.12	----	----	----
4	A	CO-PU-74S-OR-V-SM	2222	251	1.02	0.81	6364	719	1.40
	B	CO-PU-74S-OR-I-SM	2499	282	1.15	0.91	----	----	----
5	A	CO-PU-54S-TH-V-SF	1987	224	0.92	0.72	6046	683	1.33
	B	CO-PU-54S=TH-I-SF	1987	224	0.92	0.72	----	----	----
6	A	CO-PU-74S-TH-V-SM	2322	262	1.07	0.84	6648	751	1.47
	B	CO-PU-74S-TH-I-SM	2465	278	1.14	0.90	----	----	----
7	A	CO-PU-100S-TH-V-SF	3076	348	1.42	1.12	----	----	----
	B	CO-PU-100S-TH-I-SM	2750	311	1.27	1.00	6232	704	1.37
8	A	CO-RU-0S-TH-M1-SM	<1035	<117	<0.48	<0.38	----	----	----
	B	CO-RU-0S-TH-M1.7-SM	<1035	<117	<0.48	<0.38	6813	769	1.50

*M_{dead} = 2169 k-in = 245 kN-m;   **$M_{serv\,flex}$ = 2749 k-in = 311 kN-m;   ***$M_u/0.9$ = 4530 k-in = 512 kN-m: Since desing of specimens used ϕ = 0.9, test results were compared to M_u/ϕ for consistency

$$\frac{M_u}{\phi} \leq M_n \qquad\qquad (3.1\text{a})$$

and the comparison of test results ($M_{n\,test}$) will be made to be required design moment, M_u/ϕ, equal to 4098 / 0.9 = 4530 k-in. These ratios are also included in Table 3.1.

The significance of the results and the discussion of the effects of variables will be given in Chapter 4.

3.3 CRACK PATTERNS AND WIDTHS

A major objective of this study was to determine the influence of major variables on crack distribution and crack sizes, particularly at service load conditions. Hence, very careful and detailed examinations of crack patterns and crack widths were made.

Cracking loads for each model are presented in Table 3.1. First cracking corresponds to the load step where cracking was first visually observed. However, this is somewhat subjective since cracks may not be immediately seen when they originate.

To identify cracks and document their location on the model faces, a 4-in. (100 mm) x 4-in. (100 mm) grid system was drawn on each side. In addition, a horizontal line was drawn at approximately one inch (25 mm) from the top of the specimens, at the approximate location of the top flexural reinforcing bar. Each line was identified by an alphabetical letter A through G from top to bottom, including A' for the additional horizontal line.

At specific load steps, cracks were detected with the unaided eye and marked. Cracks as small as 0.001 in. (0.025 mm) could be seen and documented. Crack measurements were made with a crack measurement device with an accuracy of ±0.0005 inches (0.013 mm). An attempt was made to measure each crack at the same location at every load stage.

Complete documentation of crack width measurements is given in Appendix A. For each overhang, figures indicate the crack identification number, location and pattern for each side face. Tables give the maximum crack width which occurred at each critical loading stage from initial cracking through factored flexure loading. In each table, shaded columns highlight the "major" cracks — those cracks which showed a maximum crack width for the particular side at the overhang at any given load step. Crack widths on the top face were always checked but top face crack widths never exceeded the side face values.

In Chapter 4 a complete discussion of maximum crack widths, cracking patterns, major crack envelopes and the relation to the major variables will be presented.
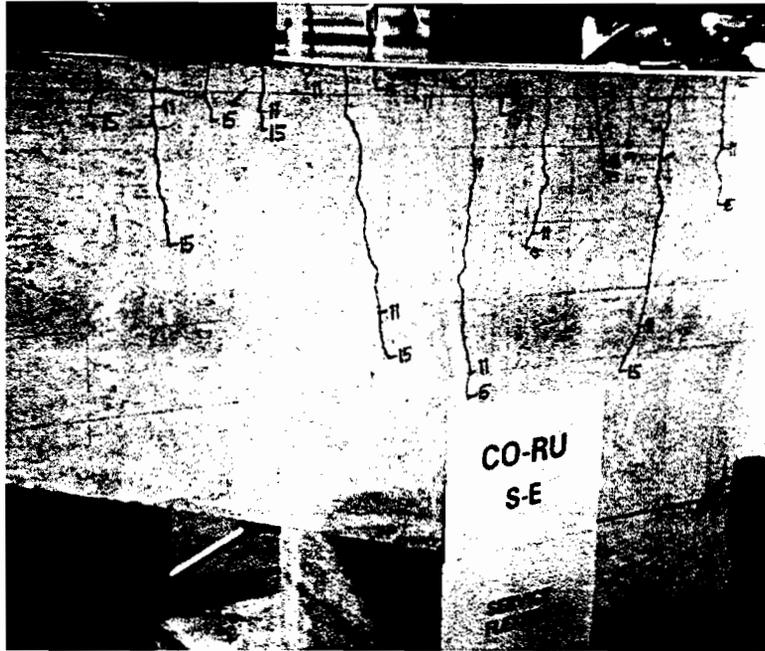
Figure 3. 10 Cracks on typical CO-RU-0S-OR-N-SF overhang at service flexure loads
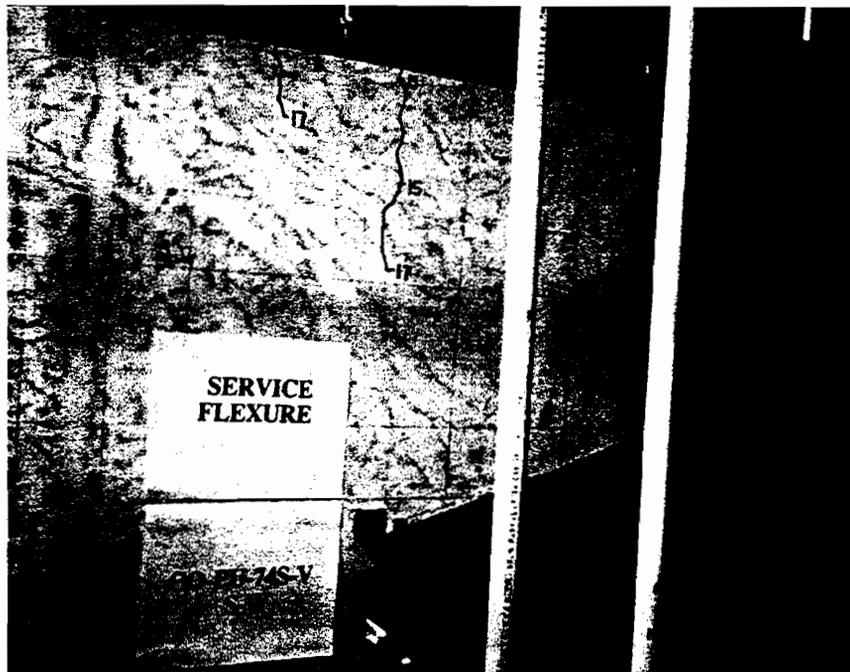
Figure 3. 11 Cracks on typical CO-PU-74S-OR-V-SM overhang at service flexure loads

The exceptions of CO-RU-0S-TH-M1&M1.7-Sm, the crack pattern for each overhang was indicative of typical flexural behavior. Cracks initiated perpendicular to the top fiber near the region of maximum moment at the face of this column. The first cracks propagated nearly vertically toward the compression zone at the juncture of the bottom of the overhang and the column. Subsequent cracks occurring outside the maximum moment region initiated perpendicular to the top fiber, but developed inclination toward the compression zone as they propagated, in the fashion of typical inclined-shear cracks.

In contrast, CO-RU-0S-TH-M1&M1.7-SM was designed utilizing concrete contributions to supplement the strut-and-tie model for carrying shear. As can be seen in Figures A-15 and A-16, very substantial inclined cracks developed from the top in towards the support. The opening of these inclined cracks governed the final shear type failure of this specimen.

All specimens with less than 100 percent prestress were cracked at the service load moment. These cracks were typical flexural cracks. Both specimens without prestress were much more heavily cracked at the service load level than those with 54 or 74 percent prestress. This can be seen in the typical specimen shown in Figures 3.10 and 3.11.

3.4 TIP DEFLECTIONS

Table 3.2 lists the tip deflections of each overhang at dead load, service load, factored load and ultimate load levels. The deflections are also expressed in terms of a Δ/ℓ ratio. Significance of these deflections and comparison between variables will be given in Chapter 4.

3.5 FAILURE MODES

Seven of the eight overhangs which failed experienced classic flexural-type failure as shown in Figures 3.12 through 3.21. This flexural-type failure was primarily controlled by very wide opening of major flexural cracks close to the column, frequent development of inclined cracks whose width remained controlled, yielding of the main flexural reinforcement when non-prestressed reinforcement was present, and final crushing of the lower flange concrete immediately adjacent to the column face (see typical close-ups of this region in Figures 3.17 and 3.19. Failure moments for all specimens are given in Table 3.1 and both the tip deflection at failure and the corresponding Δ/ℓ ratio are given in Table 3.2. The only specimen which did not experience a tip deflection ratio of 0.02 or better was CO-RU-0S-TH-M1.7-SM. This specimen had been designed with flexural reinforcement based on the nominal yield strength of $f_y = 60$ ksi (420 MPa) rather than the actual yield strength of $f_y = 75$ ksi (525 MPa)

In addition, shear reinforcement was essentially the conventional AASHTO minimum shear reinforcement which meant that a 45° truss STM was supplemented with a V_c

Table 3. 2   Tip Deflections at Important Load Levels

Specimen	Overhang Designation	Dead Load Tip Δ in.	mm	Δ/l	Service Shear Load Tip Δ in.	mm	Δ/l	Service Flexure Load Tip Δ in.	mm	Δ/l	Factored Shear Load Tip Δ in.	mm	Δ/l	Factored Flexure Load Tip Δ in.	mm	Δ/l	Ultimate Load Tip Δ in.	mm	Δ/l
1 A	CO-RU-OS-OR-N-SF	0.081	2.050	0.0018	0.116	2.99	0.0028	0.116	2.99	0.0028	0.190	4.83	0.0041	0.220	5.59	0.0048	----	----	----
B	CO-RU-OS-OR-N-SF	0.063	1.600	0.0014	0.092	2.34	0.0026	0.101	2.56	0.0022	0.170	4.32	0.0037	0.220	5.59	0.0048	1.780	45.200	0.0387
2 A	CO-PS-100S-NA-N-SM	0.010	0.250	0.0002	0.017	0.43	0.0003	0.020	0.51	0.0004	0.030	0.76	0.0006	0.035	0.84	0.0007	1.090	27.690	0.0237
B	CO-PS-100S-NA-N-SM	0.010	0.250	0.0003	0.016	0.41	0.0003	0.020	0.51	0.0004	0.030	0.76	0.0006	0.040	1.02	0.0009	----	----	----
3 A	CO-PU-100S-NA-V-SM	0.001	0.020	0.0000	0.007	0.018	0.0004	0.011	0.28	0.0003	0.040	1.02	0.0009	0.080	2,03	0.0017	0.980	24.880	0.0213
B	CO-PU-100S-NA-I-SM	0.030	0.760	0.0006	0.036	0.91	0.0008	0.041	1.04	0.0009	0.040	1.02	0.0009	0.080	2.03	0.0017	----	----	---
4 A	CO-PU-74S-OR-V-SM	0.012	0.300	0.0003	0.028	0.71	0.0006	0.031	0.79	0.0007	0.105	2.67	0.0032	0.125	3.18	0.0023	1.620	41.150	0.3520
B	CO-PU-74S-OR-I-SM	-0.002	-0.050	0.0000	0.020	0.51	0.0004	0.017	0.43	0.0004	0.090	2.29	0.0019	0.105	2.67	0.0023	----	----	---
5 A	CO-PU-54S-TH-V-SF	0.043	1.090	0.0009	0.065	1.65	0.0014	0.680	1.73	0.0015	0.154	3.91	0.0033	0.181	4.60	0.0039	0.914	23.220	0.1990
B	CO-PU-54S-TH-I-SF	0.029	0.740	0.0006	0.046	1.17	0.0010	0.060	1.52	0.0013	0.138	3.51	0.0030	0.169	4.29	0.0037	----	----	---
6 A	CO-PU-74S-TH-V-SM	0.016	0.410	0.0003	0.036	0.91	0.0008	0.036	0.91	0.0008	0.109	2.77	0.0024	0.126	3.20	0.0027	0.990	25.150	0.0215
B	CO-PU-74S-TH-I-SM	-0.003	-0.060	0.0001	0.007	0.18	0.0002	0.014	0.36	0.0003	0.071	1.81	0.0016	0.065	2.17	0.0019	----	---	---
7 A	CO-PU-100S-TH-V-SF	0.026	0.660	0.0006	0.041	1.04	0.0009	0.042	1.07	0.0009	0.115	2.92	0.0025	0.127	3.23	0.0028	----	----	----
B	CO-PU-100S-TH-I-SM	0.026	0.660	0.0006	0.039	0.99	0.0008	0.045	0.14	0.001	0.118	3	0.0026	0.145	3.68	0.0032	1.110	28.190	0.2410
8 A	CO-RU-OS-TH-M1-SM	0.057	1.460	0.0012	0.081	2.06	0.0018	0.093	2.35	0.0022	0.170	4.33	0.0037	0.196	4.98	0.043	----	----	---
B	CO-RU-OS-TH-M1.7-SM	0.046	1.160	0.0010	0.071	1.01	0.0015	0.082	2.08	0.0018	0.146	3.71	0.0032	0.170	4.32	0.0037	0.620	15.750	0.0134

90
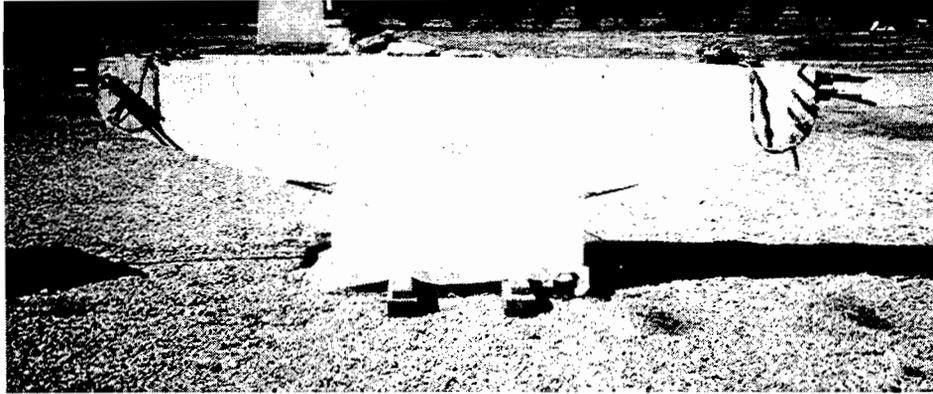
Figure 3. 12 CO-RU-0S-OR-N-SF overhangs after testing
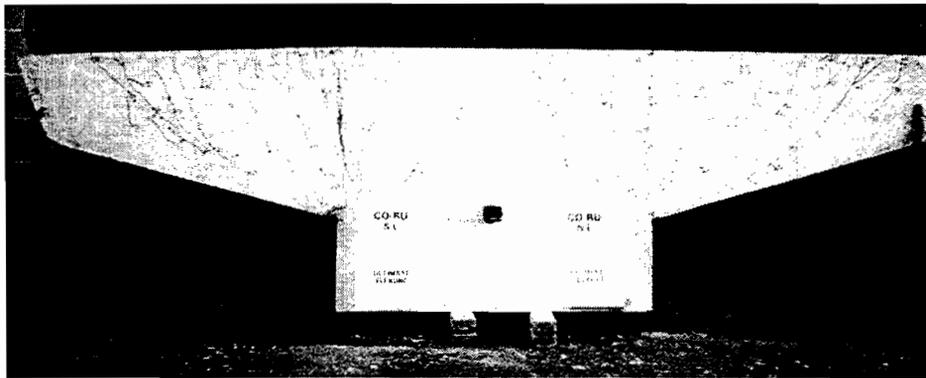
Figure 3. 13 CO-PS-100S-NA-N-SM overhangs after testing
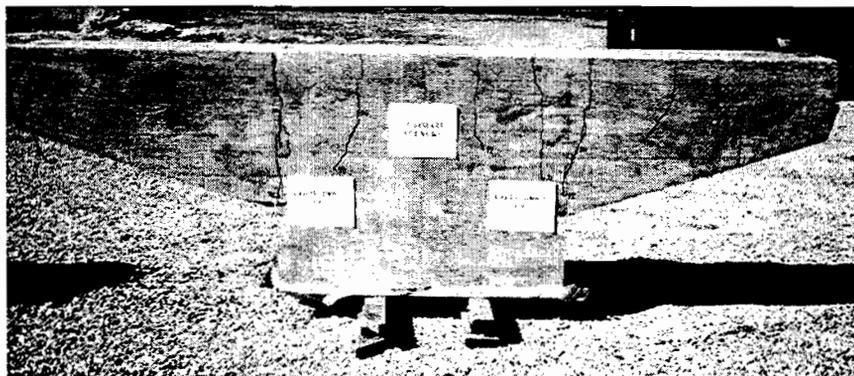
Figure 3. 14 CO-PU-100S-NA-I-SM and CO-PU-100S-N-V-SM overhangs after testing
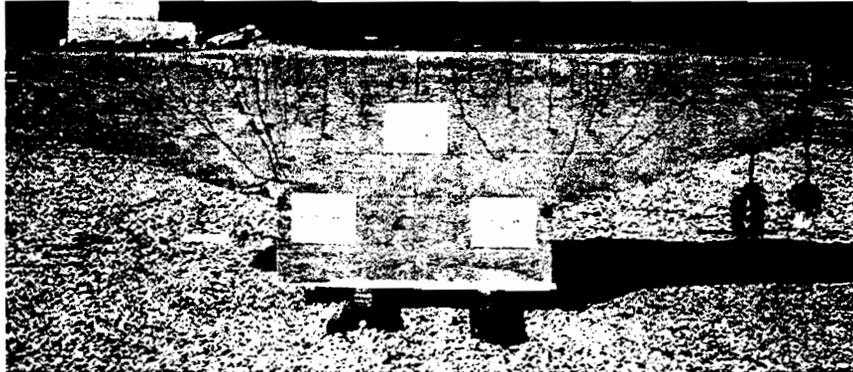
Figure 3. 15 CO-PU-74S-OR-I-SM and CO-PU-74S-OR-V-SM overhangs after testing

Figure 3. 16 Crack distribution in Model CO-PU-54S-TH-V-SF after failure

Figure 3. 17   Crushing in Model CO-PU-54S-TH-V-SF
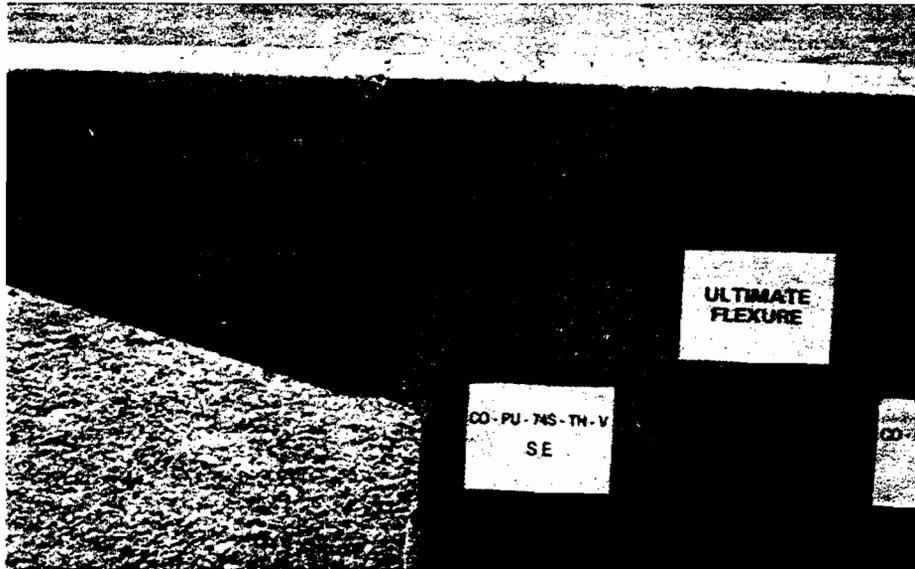
Figure 3. 18   Crack distribution in Model CO-PU-74S-TH-V-SM after failure
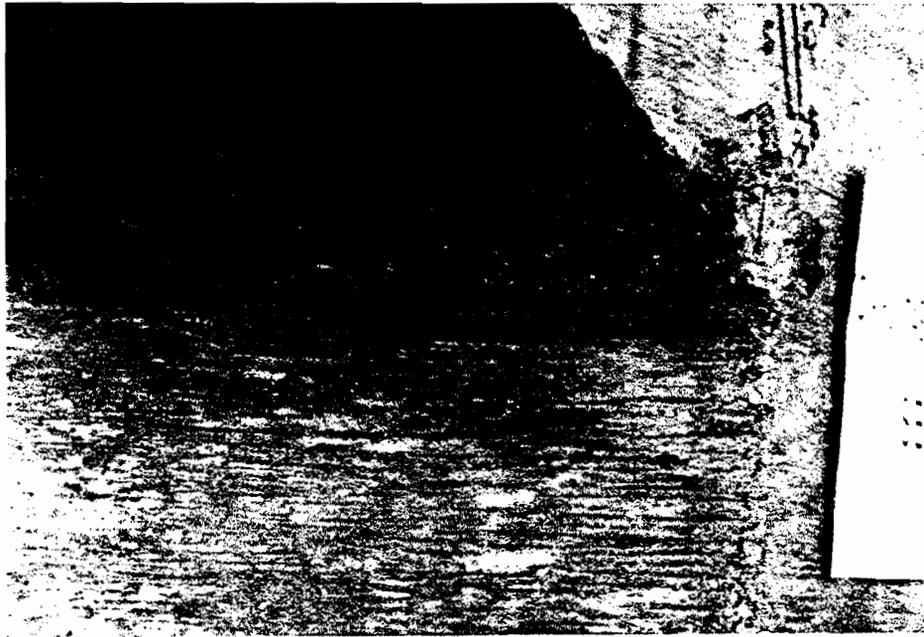
Figure 3. 19   Crushing in Model CO-PU-74S-TH-V-SM

ULTIMATE
FLEXURE

CO-PU-100S-TH-I

NE
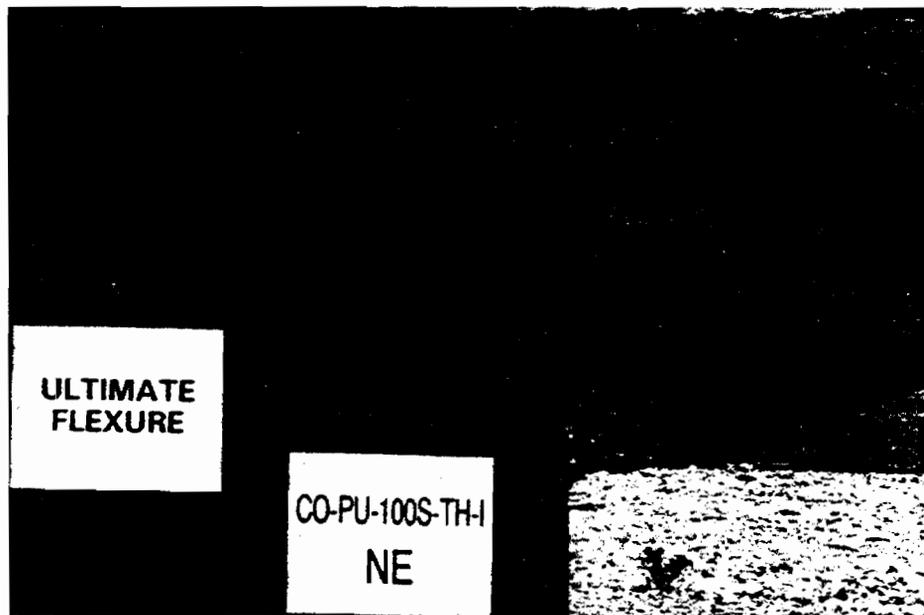
Figure 3. 20   Crack distribution in Model CO-PU-100S-TH-I-SM after failure

Figure 3. 21 Crushing in Model CO-PU-100S-TH-I-SM
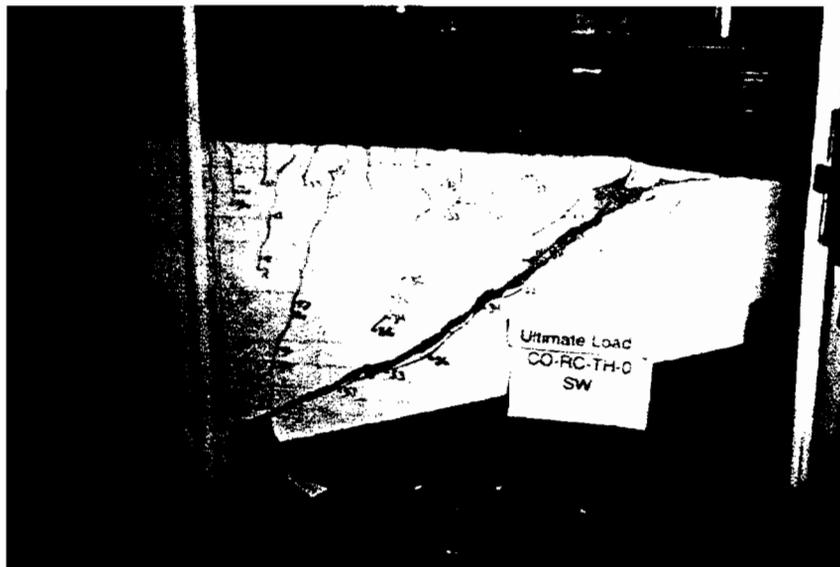
Figure 3. 22 Crack distribution in Model CO-RU-0S-TH-M1.7-SM
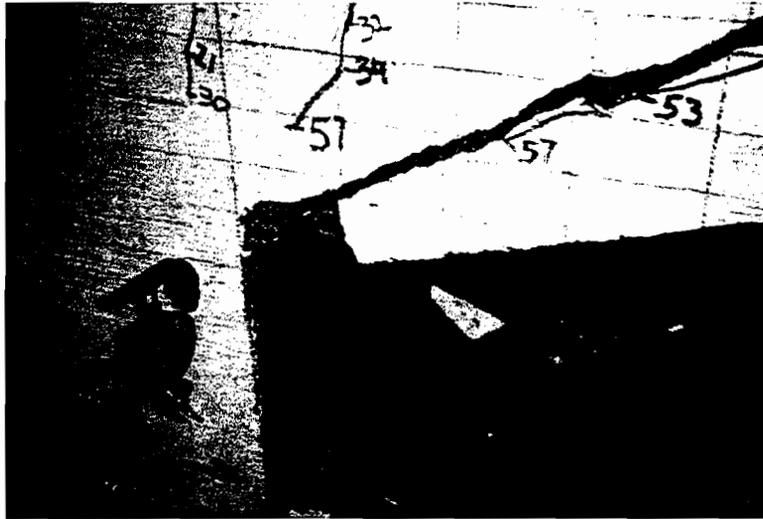
Figure 3. 23 Crushing in Model CO-RU-0S-TH-M1.7-SM

term of $1.7\sqrt{f'_c}\, b_w d$. This resulted in a specimen stronger in flexure and weaker in shear than the other fourteen overhangs. As can be seen in Figures 3.22 and 3.23, an inclined crack extending from just inside the tip loading point to the column face opened widely and complete crushing of the zone at the column face occurred. This shear controlled failure occurred with a tip deflection ratio of 0.0134 which was only 35 percent of the value for CO-RU-0S-OR-N-SF, the other non-prestressed specimen taken to failure. This lack of ductility is typical in shear controlled specimens.

Comparison of the actual failure load to the factored design load for all specimens will be given in Chapter 4.

3.6 REINFORCEMENT STRAINS

A very large number of strain gages were attached to reinforcing bars and wires in each specimen. Figure 2.47 showed a typical instrumentation layout. Generally speaking, many gages showed little strain since they were not in the vicinity of a crack. In many specimens the gages which showed strains less than about 270 microstrain (around 10 percent of the yield strain of the reinforcing bars and wires) were not plotted in the figures to improve clarity. The low strains for a few specimens are shown to give a full picture.

In general, the results of strain gages on the horizontal reinforcement are presented as plots of the steel strain versus the moment in the overhang from applied loads at the location of the gage. Results from the strain gages on the vertical shear stirrups are plots of the steel strain versus the shear in the overhang from applied loads at the location of the gage. All plots are for the full range of test loading. No plots are

included for strains on the post-tensioning strand as none of these strain gages were operating after post-tensioning was completed.

It is important to keep in mind that maximum strains in the reinforcement will occur where cracks cross the reinforcement. The gage only measures the strain in the reinforcement at the location of the gage which may or may not coincide with the location of cracks, so the recorded strains may not be the maximum strain experienced by the reinforcement.

3.6.1 CO-RU-0S-OR-N-SF Overhang

Strain gages were used on the reinforcement in both the north and south CO-RU overhangs, but most gages were located in the north overhang. Only a few gages were used in the south overhang and these gages were placed in identical locations to gages in the north overhang. The gages in the south overhang were only used to verify that the straining of the reinforcement in each overhang was the same, as it should have been since the reinforcing designs were identical and the loading was symmetrical. Examination of the data from gages on both overhangs revealed that the straining of the steel on each overhang was in fact essentially the same. Therefore, only results from the strain gages on the north overhang will be presented.

Figures 3.24 through 3.26 show results of strain gages on the primary moment, shear-friction, and side face reinforcement. The plots show that at final failure all gages at the face of the column recorded strains in excess of the yield strain, even including the side face reinforcement (SK01B) located around mid-height. However, at factored load levels, none of the side face nor shear-friction reinforcement had yielded.

Figure 3.27 shows results of the strain gages on the vertical shear stirrups. These reveal that no yielding of the vertical shear reinforcement was recorded. The most significant straining on the vertical stirrups was recorded on gages ST08, ST09, ST10 and ST11. These gages were located in the vicinity of cracks which formed parallel to the compression strut from the outside reaction. I can also be observed that at factored loads, straining of all stirrups was quite small with the maximum strains limited to approximately 50 percent of yield strain.

3.6.2 CO-PS-100S-NA-N-SM Overhang

Gaging of the reinforcement in this overhang was similar to the previous overhang in that most of the gages were placed in only one overhang. In this overhang most of the gages were in the south overhang. Examination of gages in both overhangs revealed that steel strains were similar in both overhangs, so only results from the south overhang are presented.

Figure 3.28 and 3.29 shows results of the strain gages on the shear-friction and side face reinforcement. The figures show that this horizontal reinforcement was well below yield at factored loads but at final failure had yielded at the face of the column.
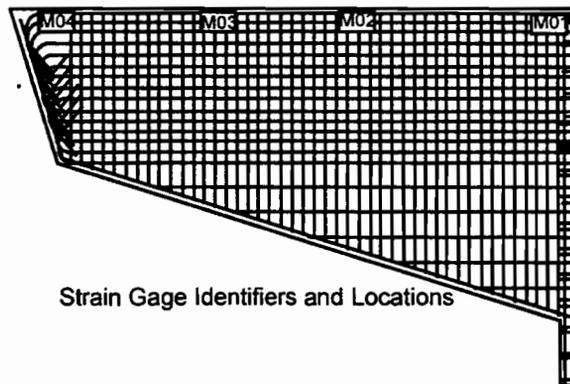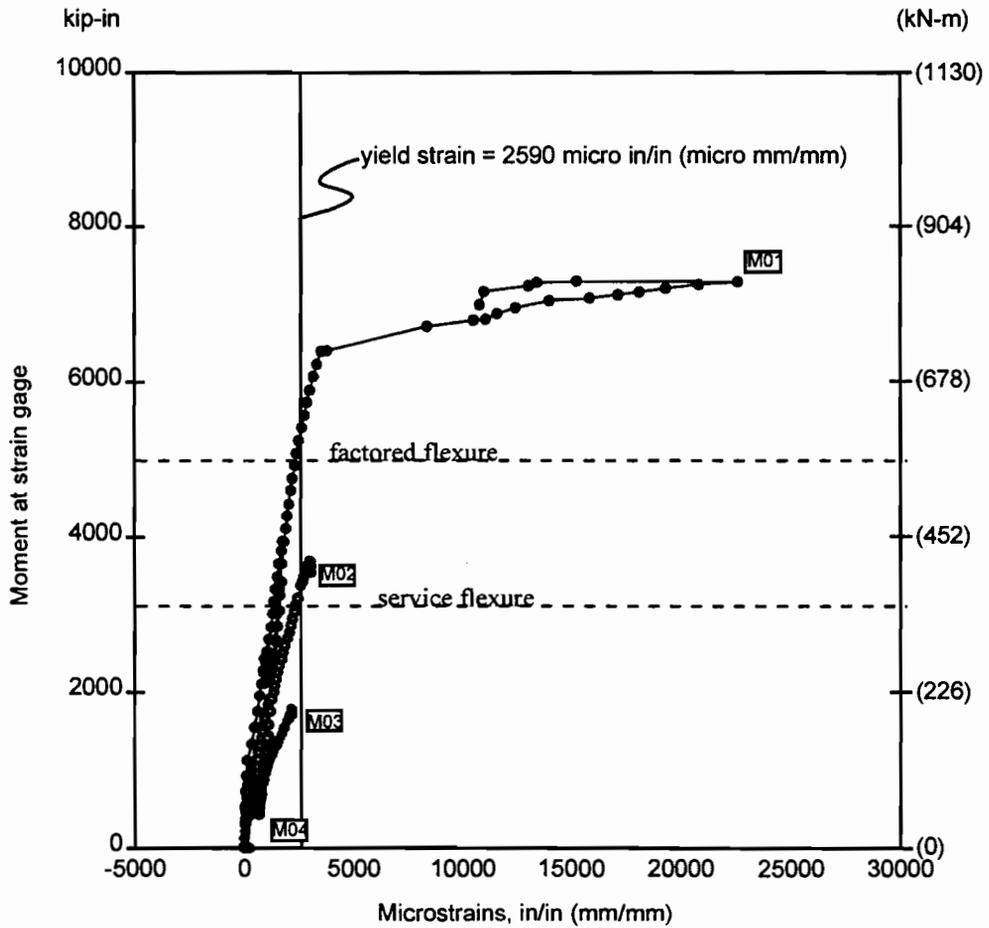
Figure 3. 24 Strain gages on the moment reinforcement in CO-RU-0S-OR-N-SF
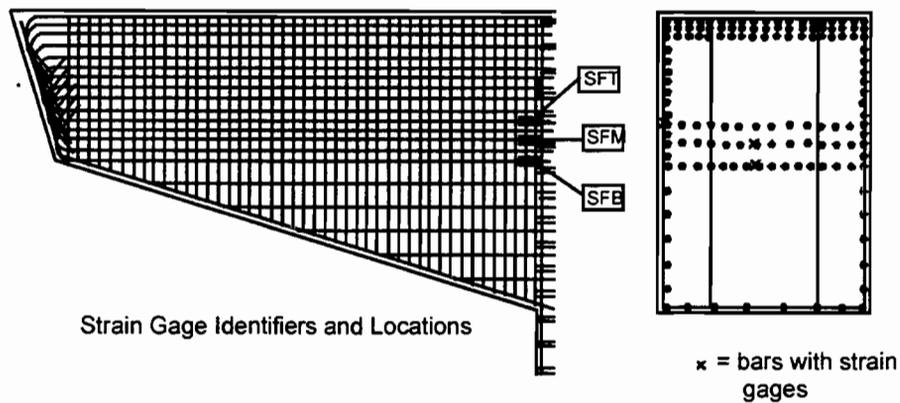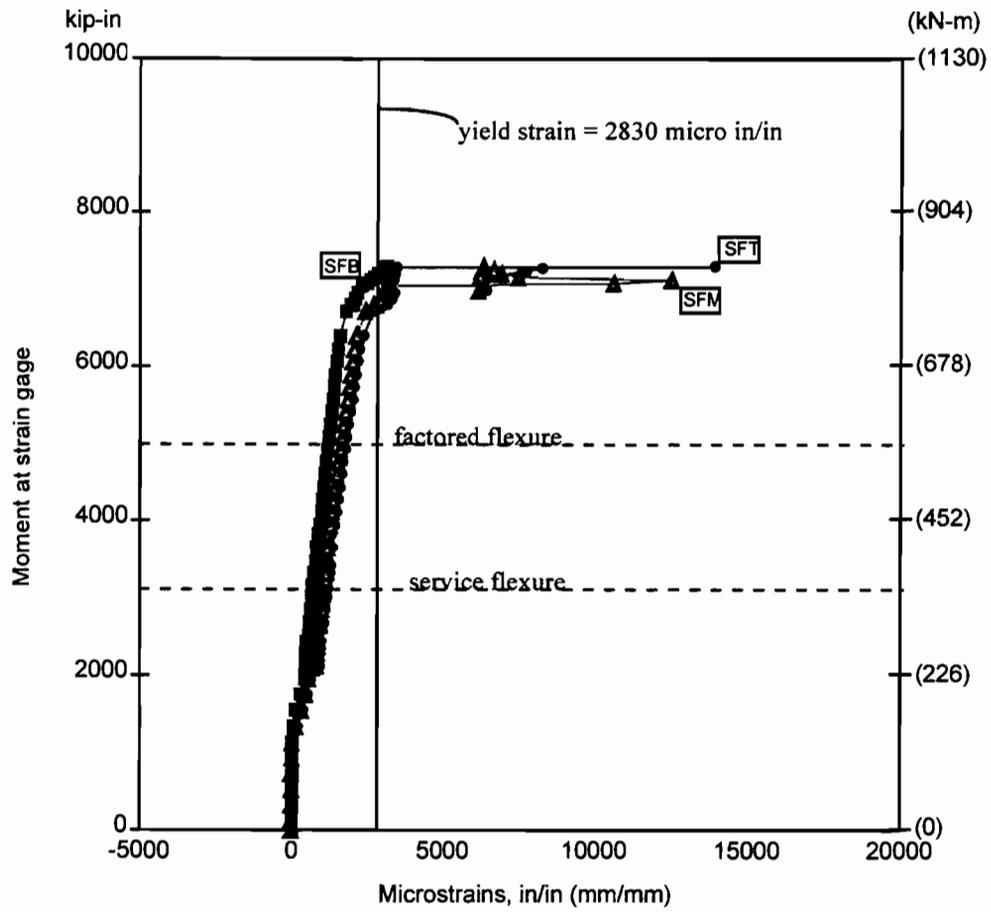
Figure 3. 25 Strain gages on the shear-friction reinforcement in CO-RU-0S-OR-N-SF (north) overhang
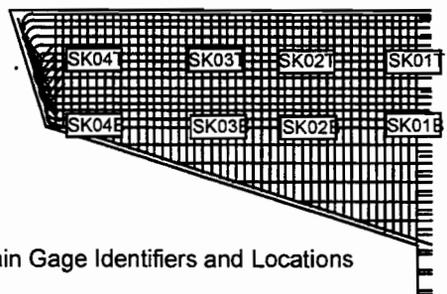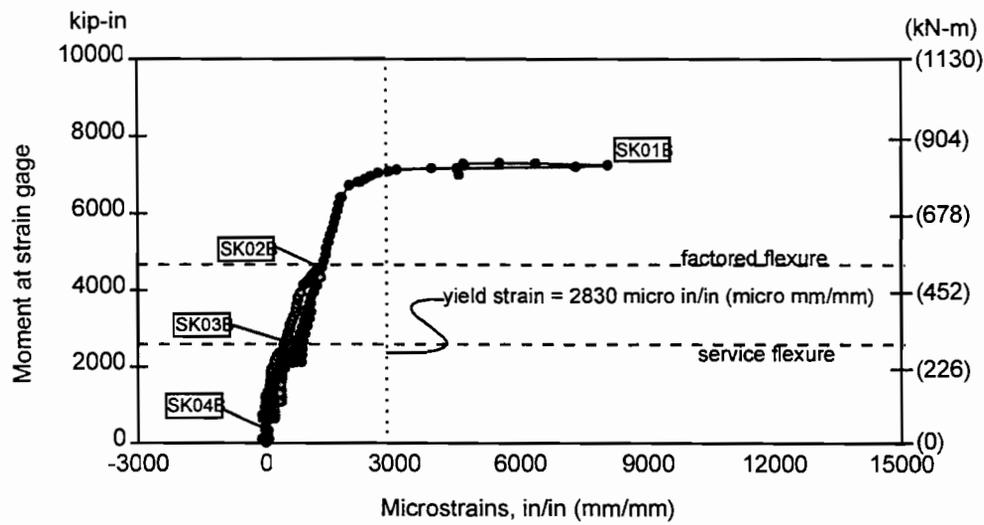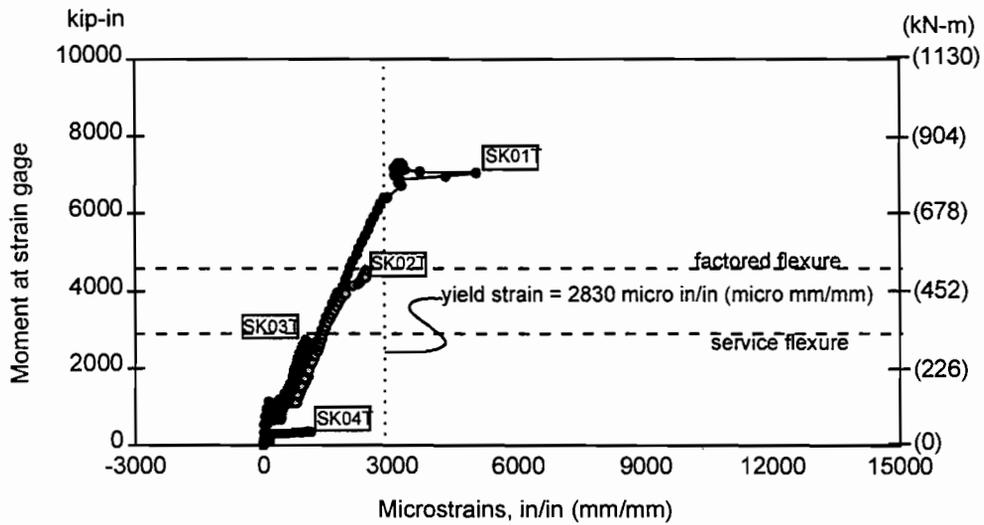
Figure 3. 26 Strain gages on side face reinforcement in CO-RU-0S-OR-N-SF (north) overhang

kips (kN)

yield strain = 2370 micro in/in (micro mm/mm)

Factored Shear = 132.5 kips (590 kN)
(gages ST01 - ST05)

Factored Shear = 88.0 kips (390 kN)
(gages ST06 - ST12)

Shear from applied loads at strain gage

Microstrains, in/in (mm/mm)

all gages 6.5" below top of overhang

Strain Gage Identifiers and Locations
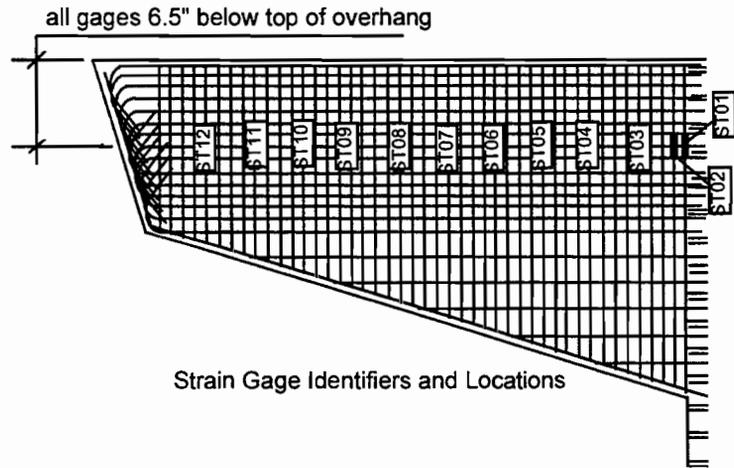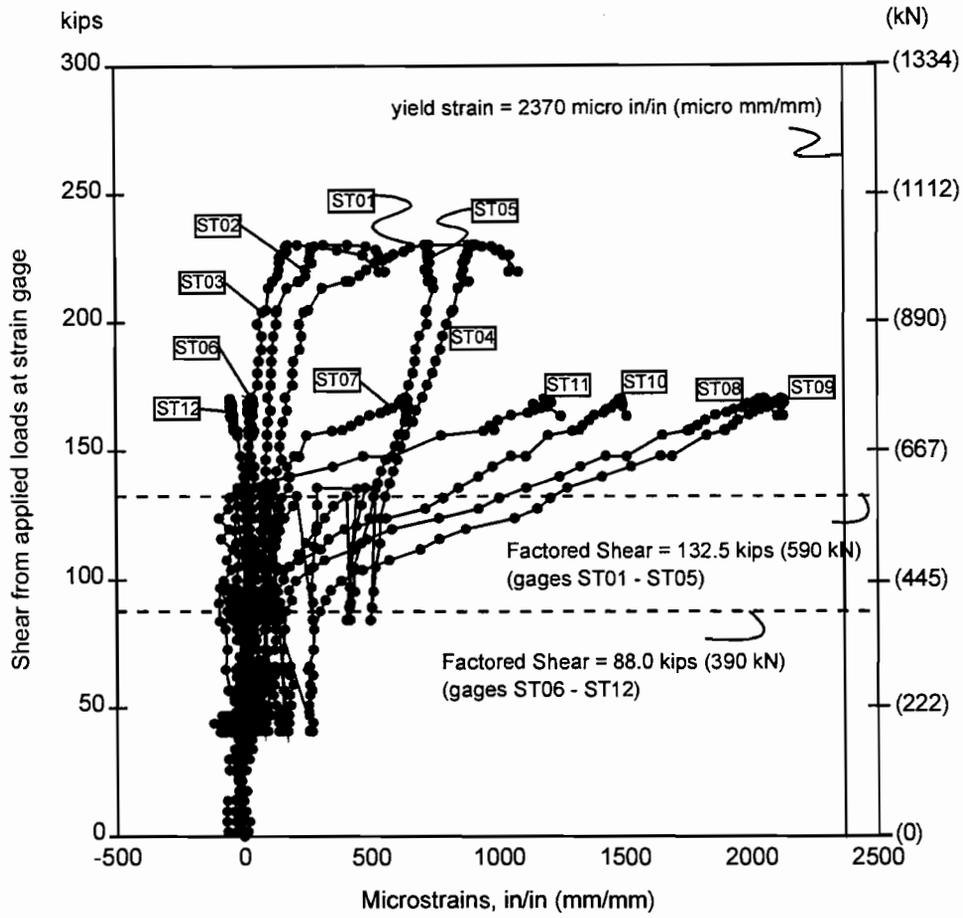
Figure 3. 27   Strain gages on shear stirrups in CO-RU-0S-OR-N-SF

101

kip-in   (kN-m)

yield strain = 2830 micro in/in (micro mm/mm)

factored shear

service shear

Microstrains, in/in (mm/mm)

Moment at strain gage

SFB

SFT

SFT

SFB

Strain Gage Identifiers and Locations   × = bars with strain gage
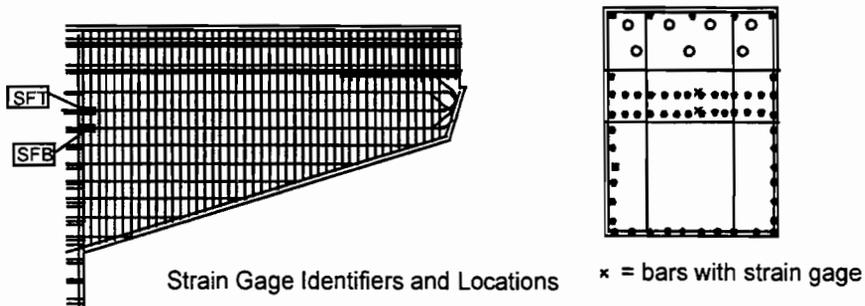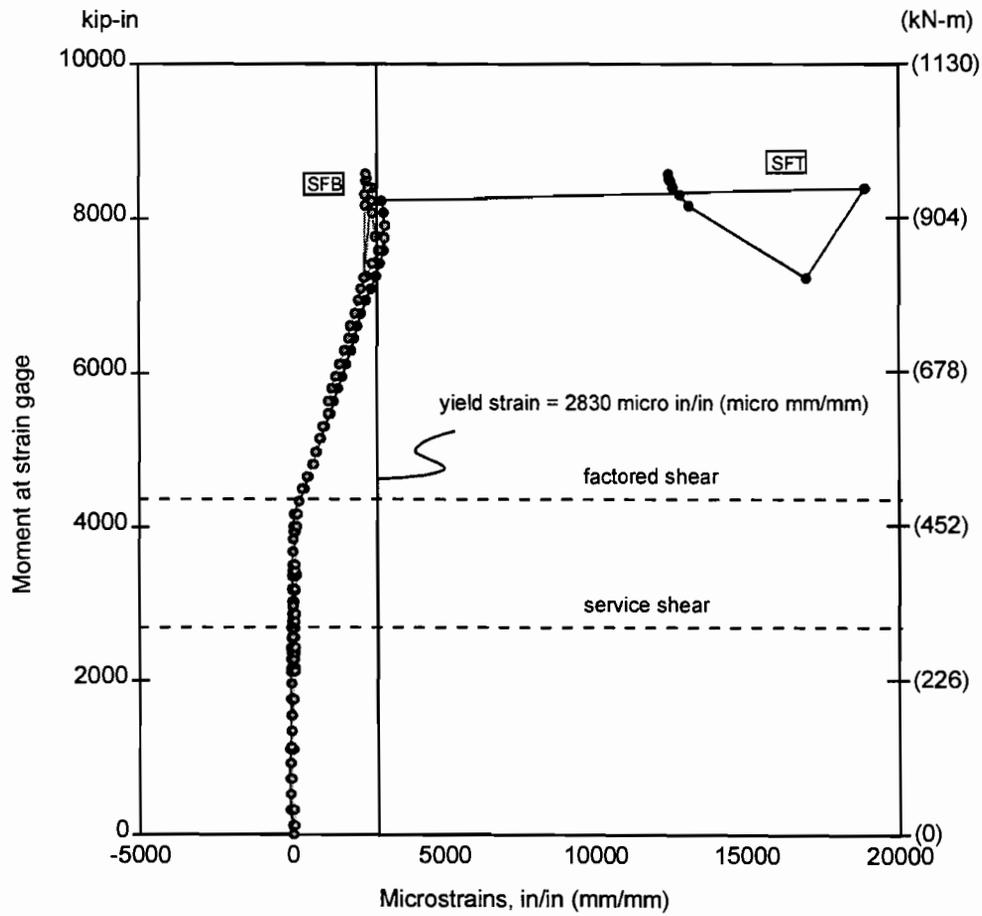
Figure 3. 28   Strain gages on shear-friction reinforcement in CO-PS-100S-NA-N-SM (south) overhang

102
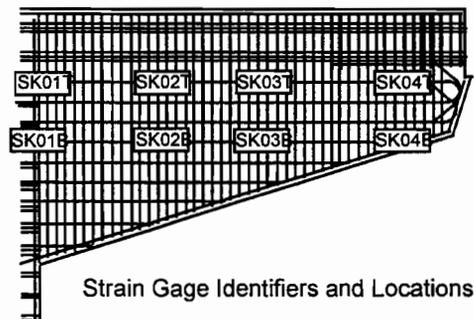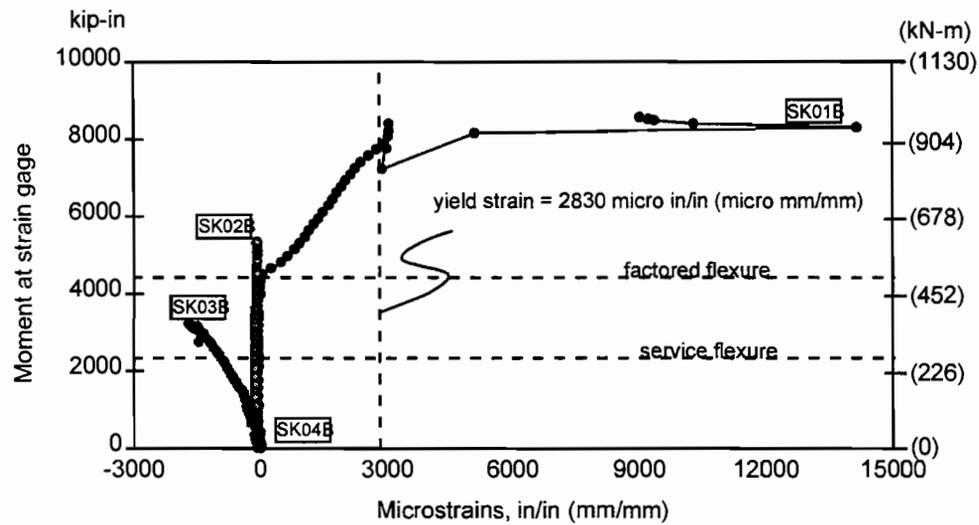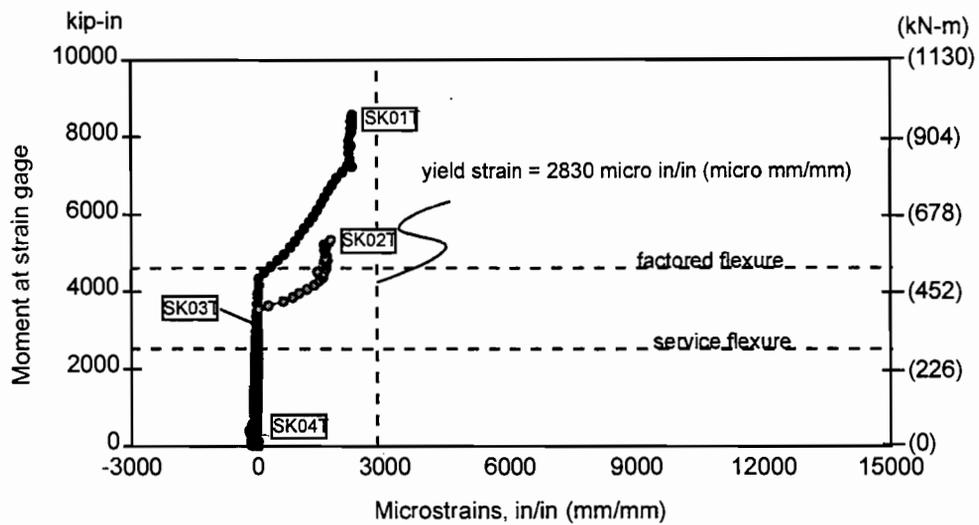
Figure 3. 29 Strain gages on side face reinforcement in CO-PS-100S-NA-N-SM

103

In this overhang, almost no strains were recorded on the vertical stirrups so no plots are shown for these gages. The vertical shear stirrups were the same for this overhang as the CO-RU-0S-OR-N-SR overhang and the same number and location of gages were used. The maximum strain in all gages was recorded on the second stirrups from the face of the column (see ST02 in Figure 3.27). The strain recorded by this gage was only 503 micro inches/inch at ultimate loads. The strain in this gage at factored flexure loads was only 104 micro inches/inch. This is not surprising since there was very little inclined cracking in this overhang, and no cracking in the outer region of the overhang in the vicinity of the compression strut from the outside reaction. It can be concluded from these observations that the shear capacity of the overhang would have been quite high even with a significant reduction in stirrups.

3.6.3 CO-PU-100S-NA-I-SM Overhang

Figure 3.30 and 3.31 show the results from the strain gages on the horizontal shear and side face reinforcement. These figures show that at maximum loads the horizontal shear reinforcement yielded at the face of the column even though this overhang was not loaded to failure. However, the side face crack control reinforcement (Figure 3.31) showed no significant strain until well above service load levels.

The locations of strain gages used on the vertical shear stirrups are shown in Figure 3.32. No plots are given for any of these gages because only minimal strains were recorded. The maximum strain was recorded on gage ST01 which was 1370 micro inches/inch at maximum test loads and 225 micro inches/inch at factored flexure loads. Gage ST02 recorded the next highest strains which were 800 micro inches/inch at maximum test loads and 135 micro inches/inch at factored flexure load. These strains are very low at factored loads. Furthermore, gages on stirrups located in the vicinity of the anticipated shear crack were even lower suggesting that the shear capacity of the overhang in this region would have been quite high even with significantly fewer stirrups.

3.6.4 CO-PU-100S-NA-V-SM

Figure 3.33 shows the results from the strain gages on the side face reinforcement. This figure shows that the side face reinforcement was well below yield at factored loads but by ultimate load had yielded at the face of the column.

The locations of strain gages used on the vertical shear stirrups are shown in Figure 3.34. The recorded strains on these gages were even lower than for the CO-PU-100S-NA-I-SM overhang. The maximum strain was recorded on gage ST20 which was 126 micro inches/inch at ultimate loads and 32 micro inches/inch at factored loads. Again, it can be said that the shear capacity of this overhang would have been quite high even with substantially fewer stirrups.
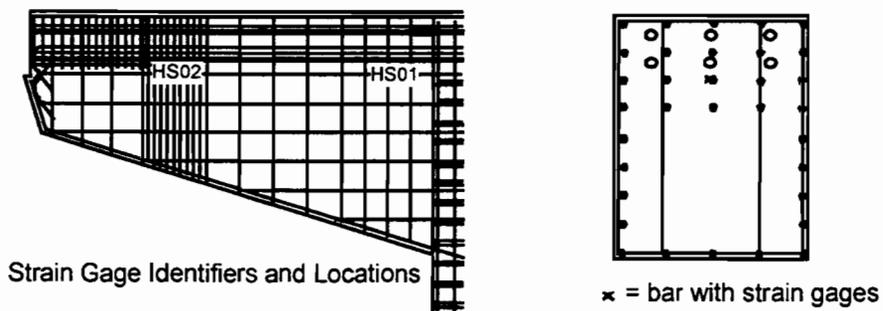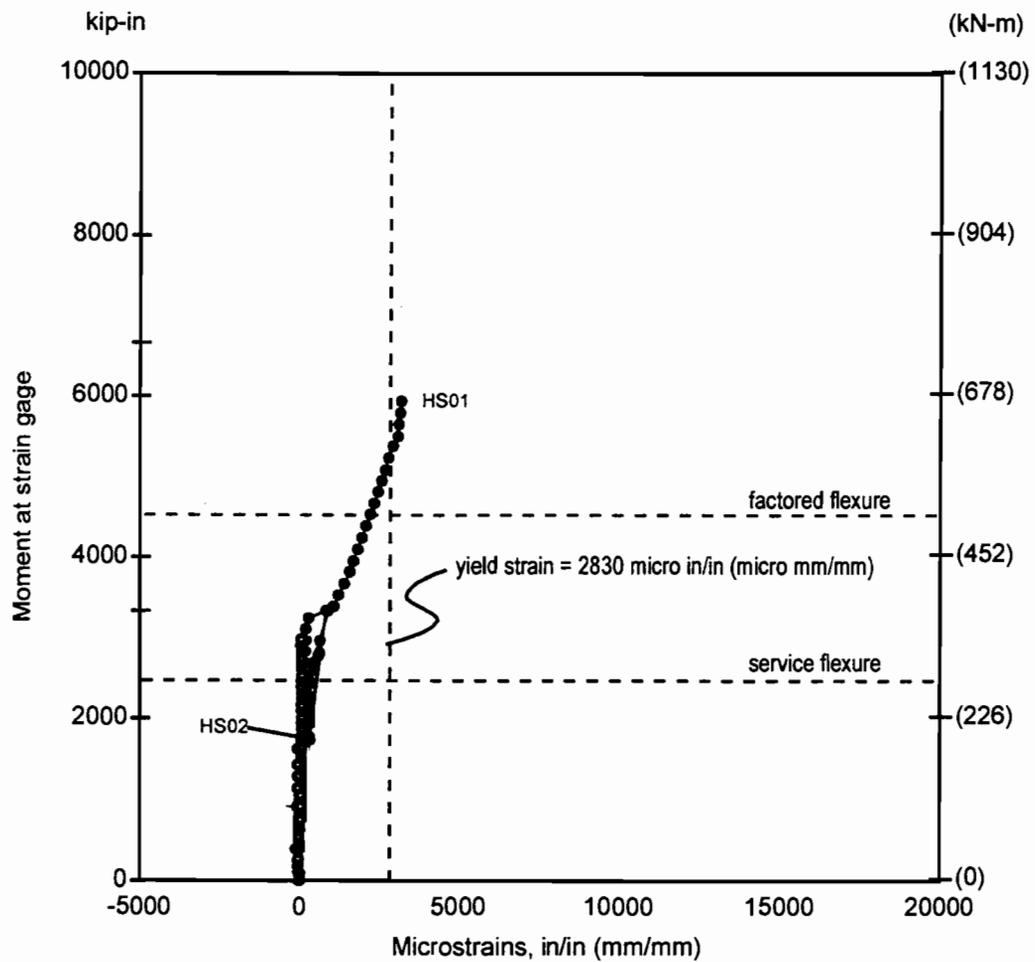
Figure 3. 30 Strain gages on horizontal shear reinforcement in CO-PU-100S-NA-I-SM overhang
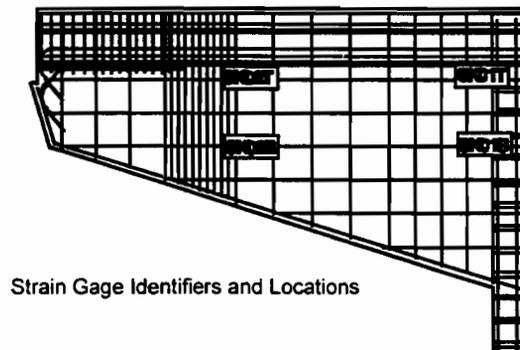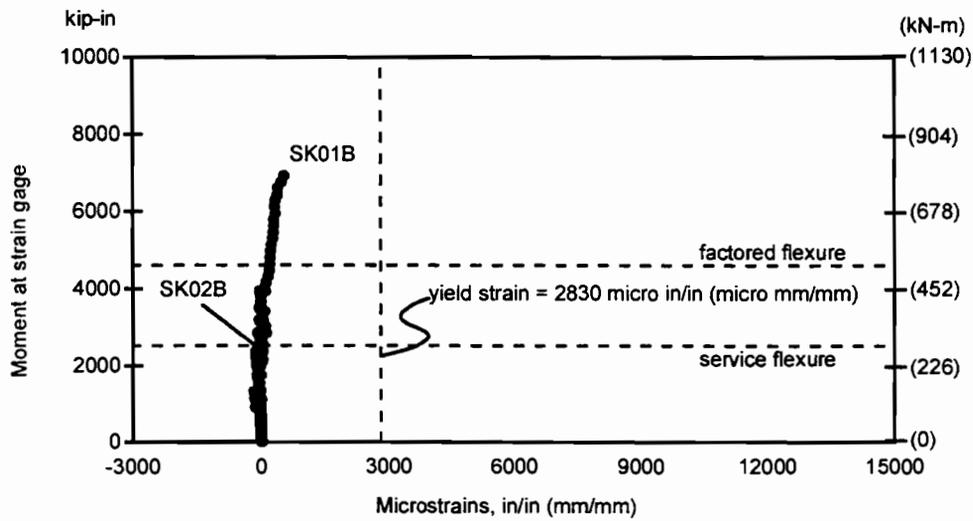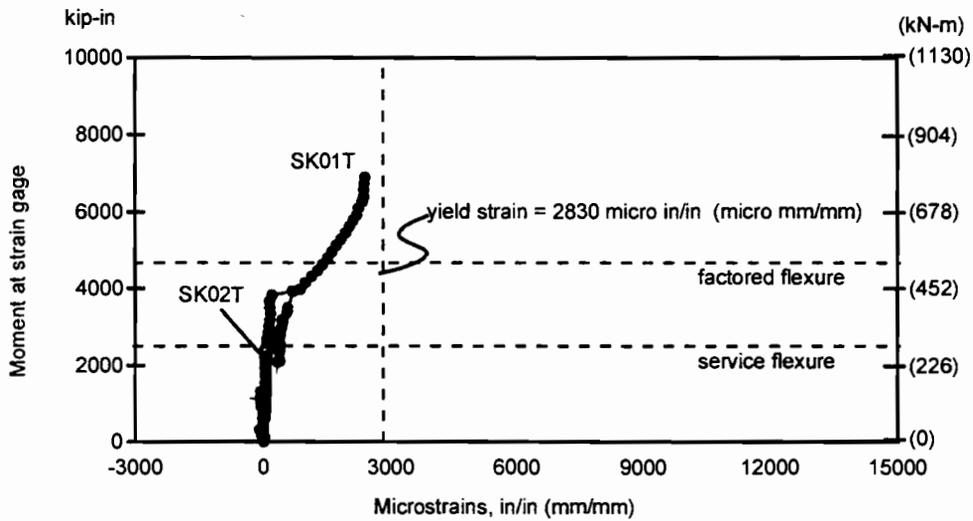
Figure 3. 31   Strain gages on side face reinforcement in CO-PU-100S-NA-I-SM overhang
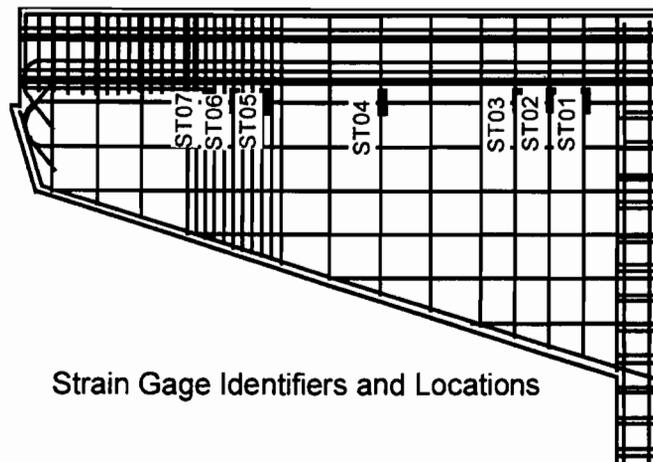
Figure 3. 32 Strain gages on shear stirrups in CO-PU-100S-NA-I-SM overhang

3.6.5 CO-PU-74S-OR-I-SM Overhang

Figures 3.35 through 3.37 show the results from the strain gages on the non-prestressed moment, horizontal shear, and side face reinforcement. These figures show that near factored loads the horizontal reinforcement yielded at the face of the column. The strain gage on the primary moment reinforcement at the face of the column (M01) was not working after the fabrication of the specimen so no results are shown for this gage.

Figure 3.38 shows the results of the strain gages on the vertical shear stirrups. Only a slight increase in stirrup strains can be observed over that of the vertical stirrups in the CO-PU-100S-OR-I-SM overhang. These strains are also quite low at both factored and maximum test loads. It can be concluded that the shear capacity of this overhang would have been substantial even with significantly few stirrups.

3.6.6 CO-PU-74S-OR-V-SM

Figure 3.39 and 3.40 show the results from the strain gages on the non-prestressed moment and side face reinforcement. These figures show that the main non-prestressed flexural horizontal reinforcement was yielded at the face of the column even below factored load level and stayed at yield strain as substantially higher load was applied. The side face skin steel began working around service load level and yielded by ultimate loads.

Figure 3.41 shows the results of the strain gages on the vertical shear stirrups. Again, it can be concluded that the shear capacity of this overhang would have been substantial even without any stirrups.
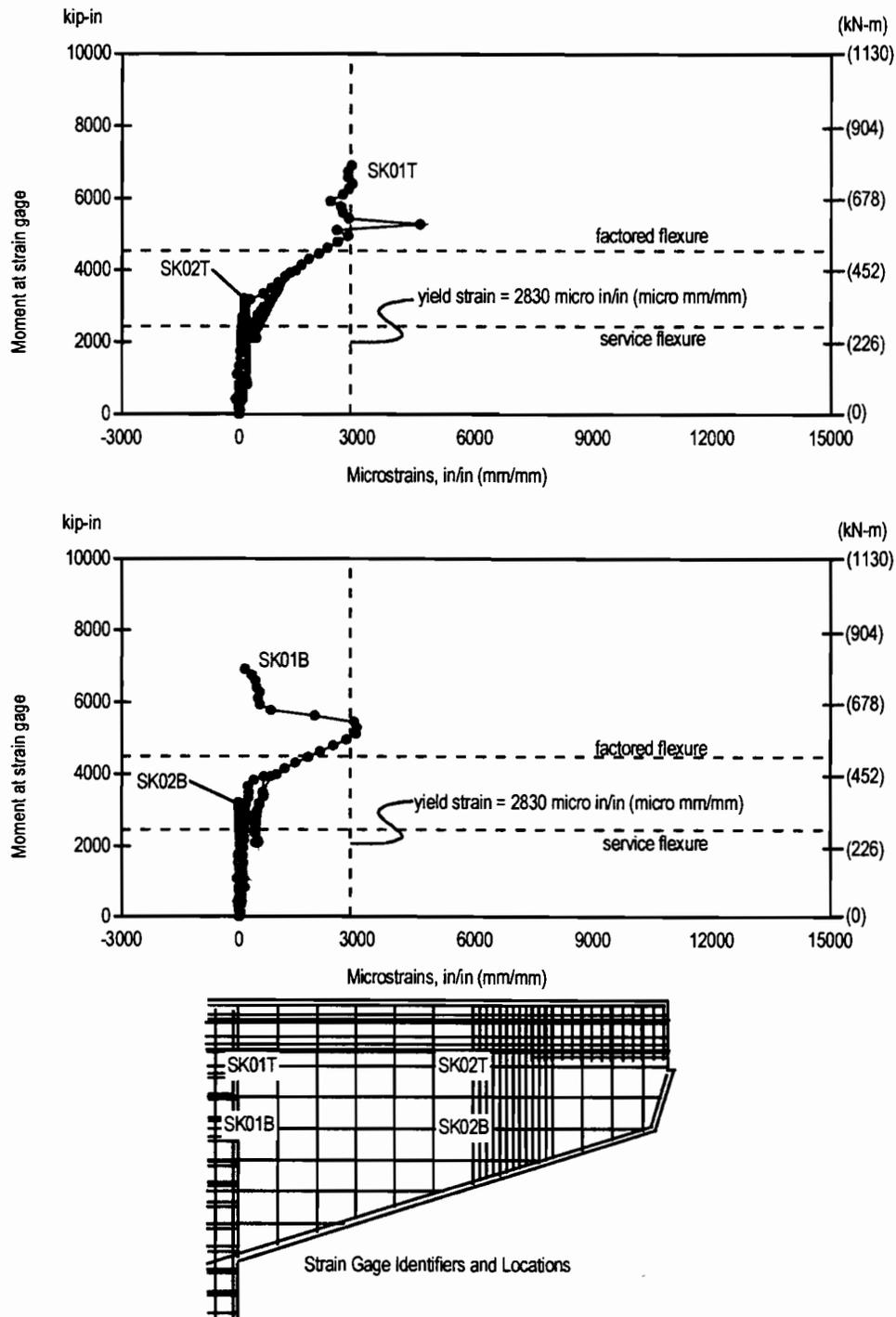
Figure 3. 33   Strain gages on side face reinforcement in CO-PU-100S-NA-V-SM overhang

Strain Gage Identifiers and Locations
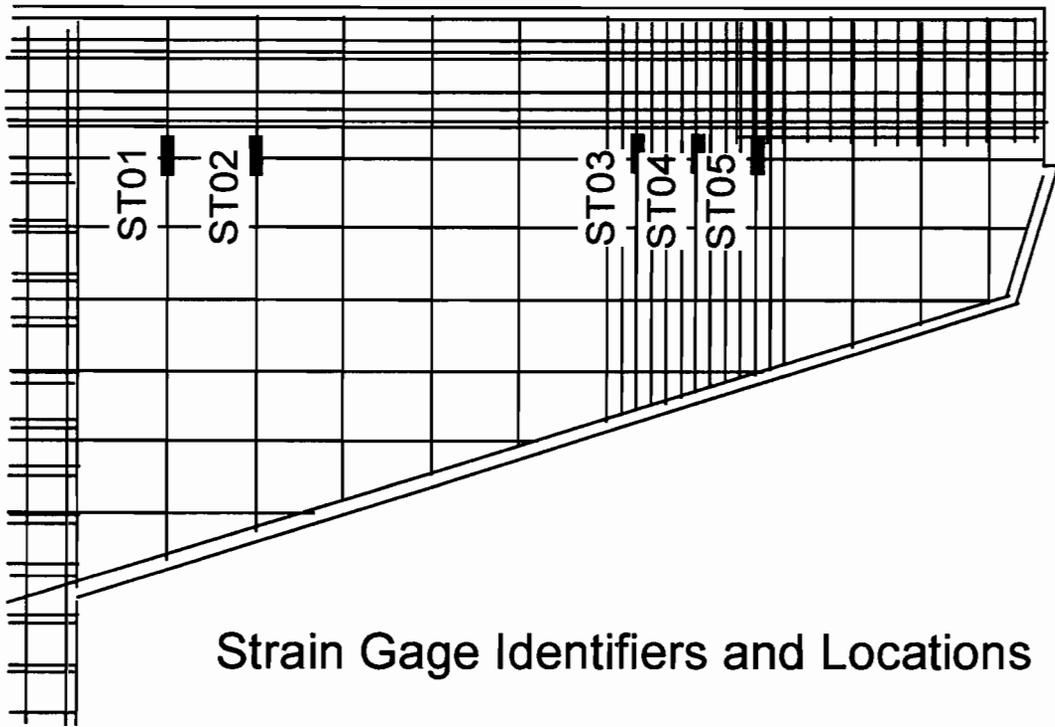
Figure 3. 34   Strain gages on shear stirrups in CO-PU-100S-NA-V-SM overhang

kip-in   (kN-m)

yield strain = 2590 micro in/in (micro mm/mm)

factored flexure

service flexure

M02

Microstrains, in/in (mm/mm)

Strain Gage Identifiers and Locations

x = bar with strain gage
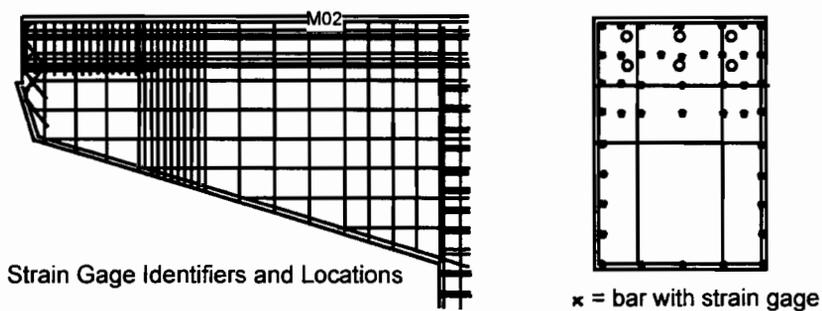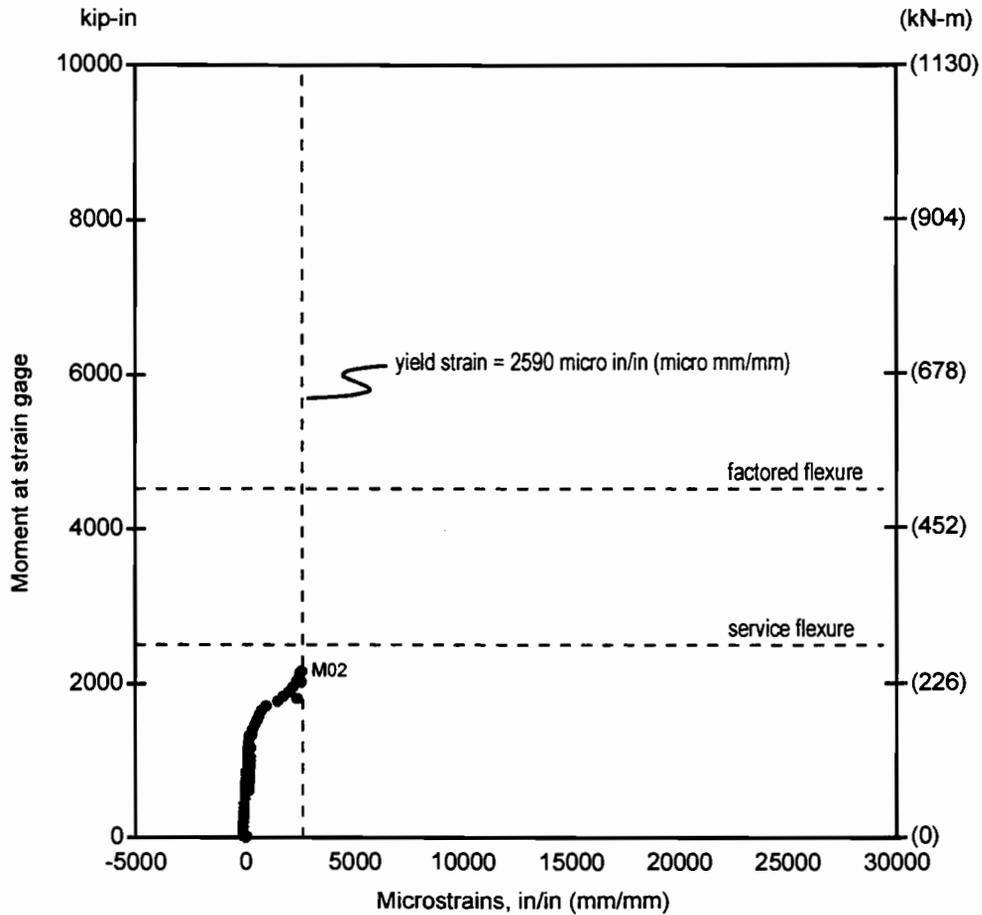
Figure 3. 35 Strain gages on non-prestressed moment reinforcement in CO-PU-74S-I overhang

110
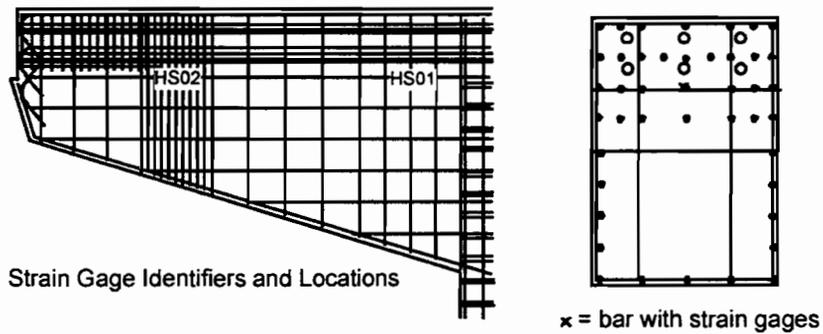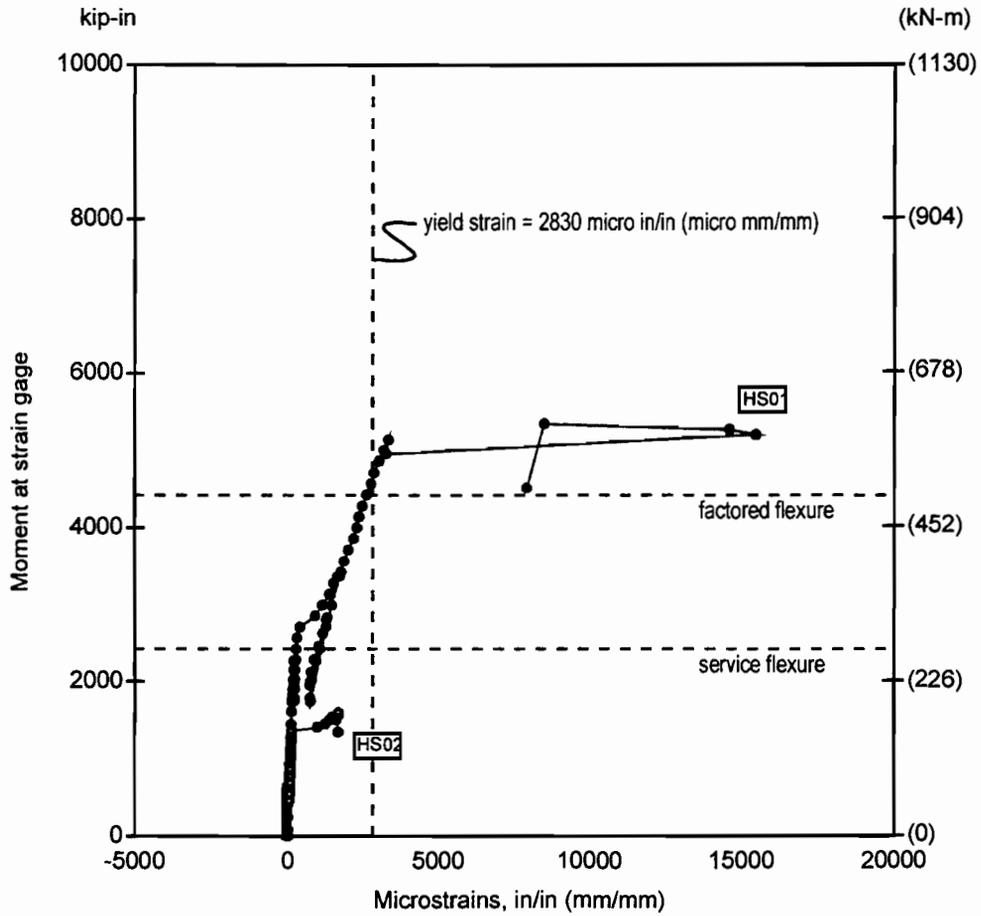
Figure 3. 36 Strain gages on horizontal sher reinforcement in CO-PU-
74S-I overhang

111
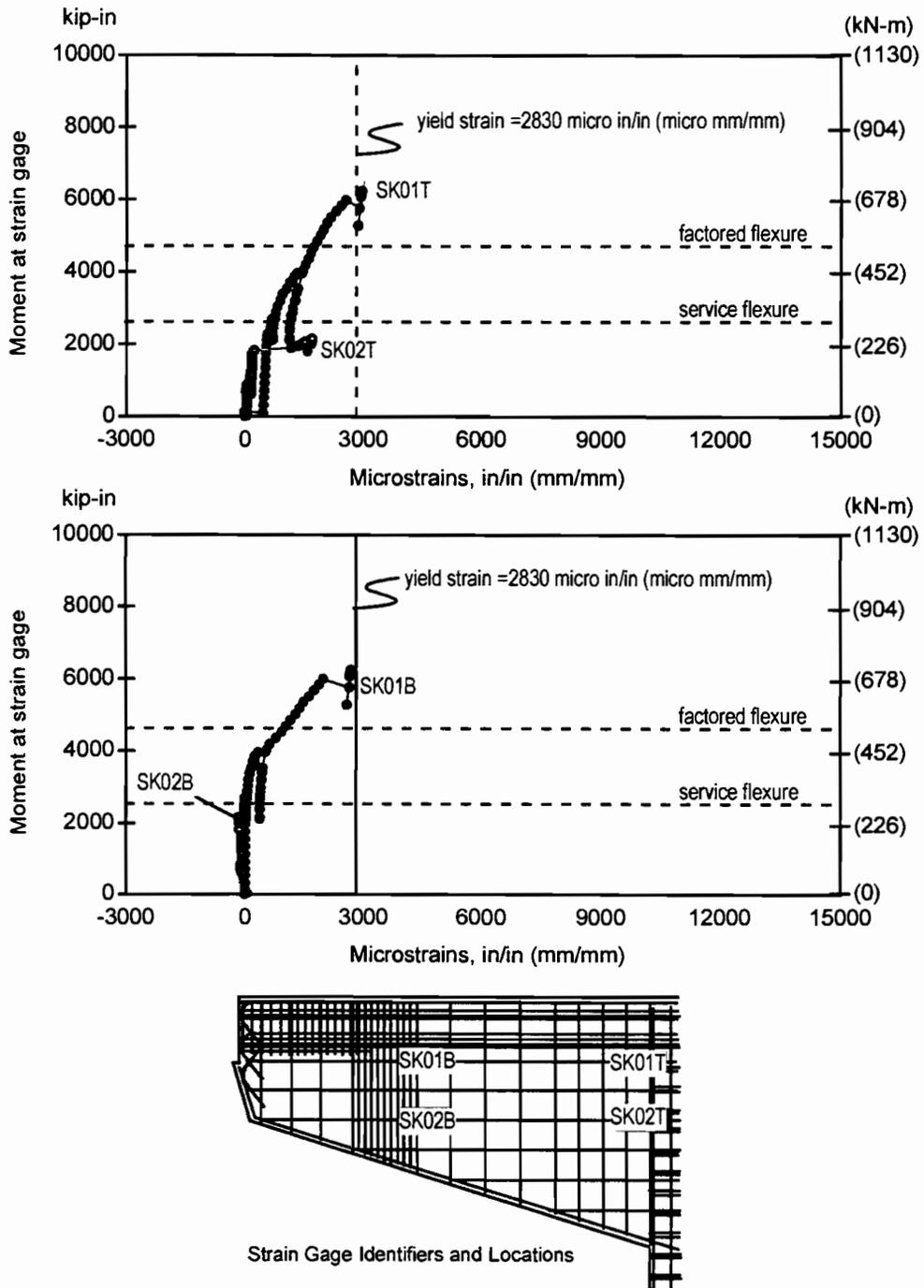
Figure 3. 37   Strain gages on side face reinforcement in CO-PU-74S-I
overhang

112
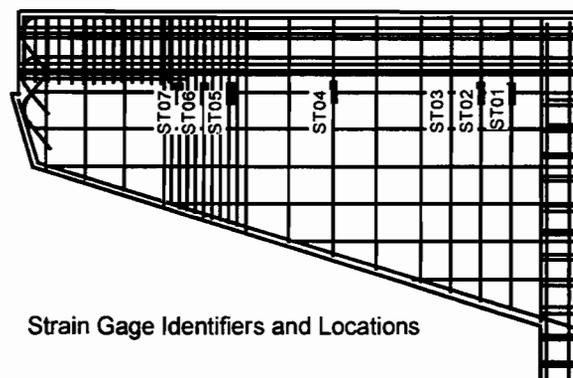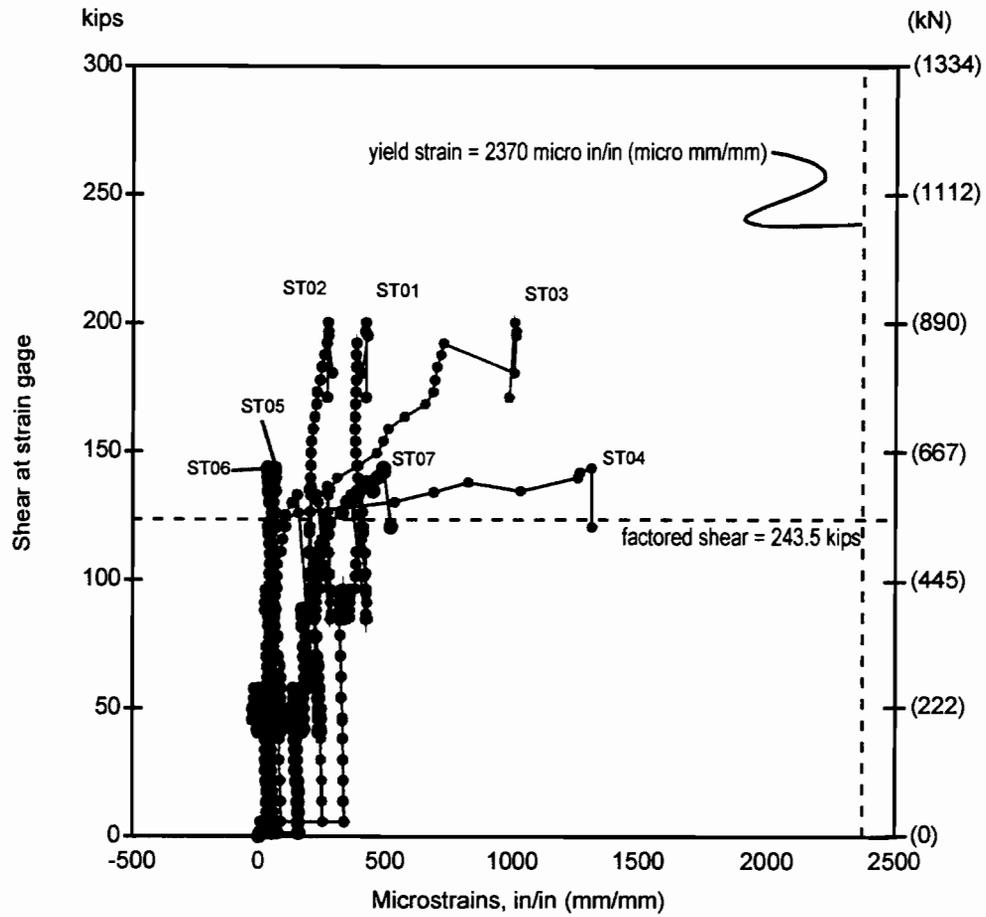
Figure 3. 38   Strain gages on shear stirrups in CO-PU-74S-I-overhang
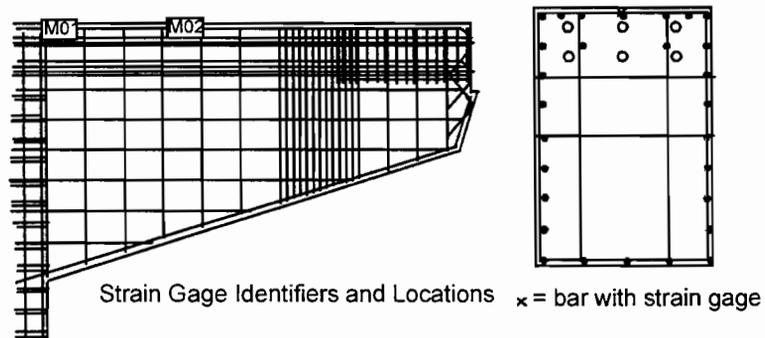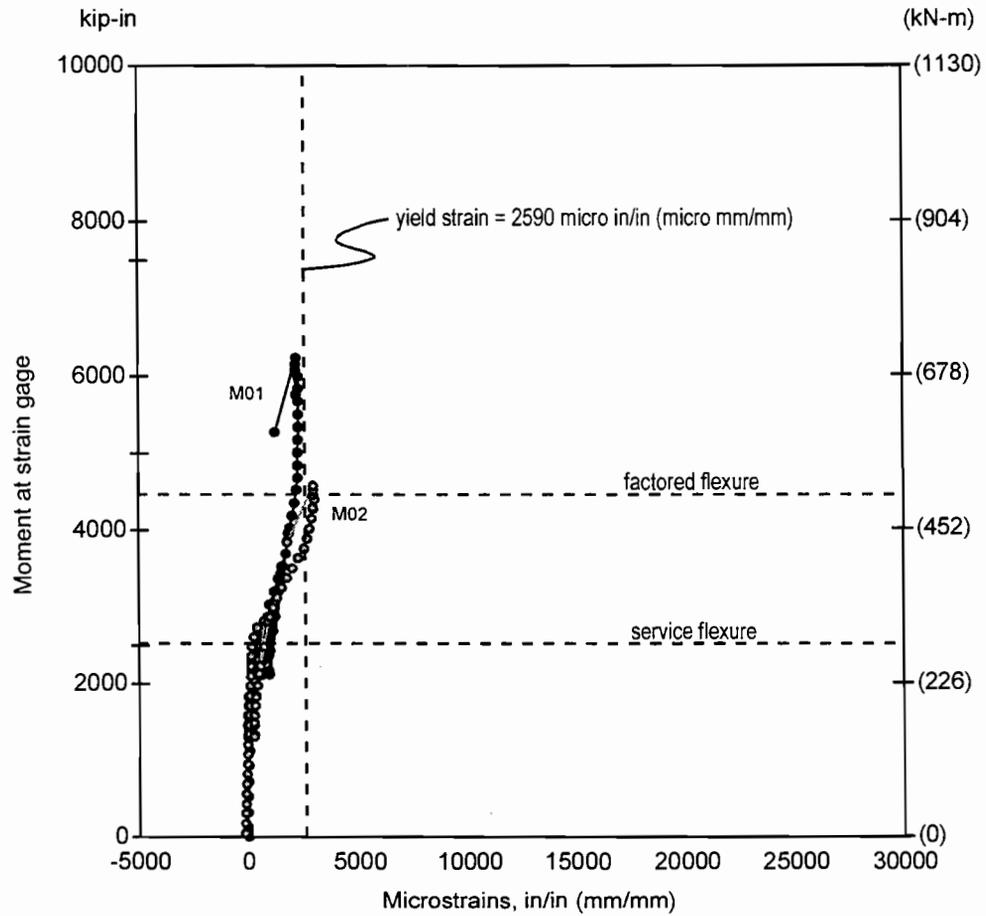
Figure 3. 39   Strain gages on non-prestressed moment reinforcement in CO-PU-74S-OR-V-SM overhang

114
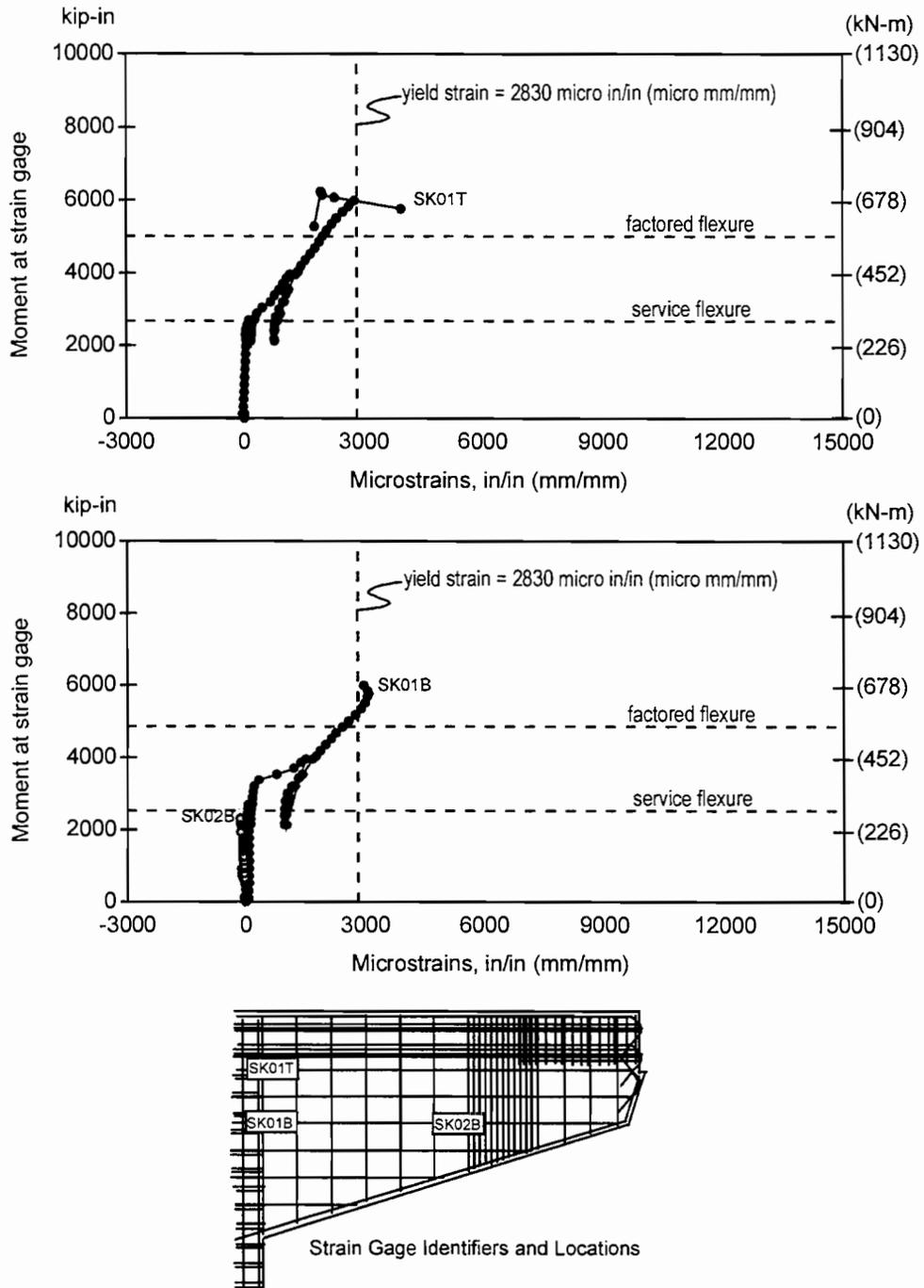
Figure 3. 40   Strain gages on side face reinforcement in CO-PU-74S-OR-
V-SM

115

kips

(kN)

Shear at strain gage

Microstrains, in/in (mm/mm)

yield strain = 2370 micro in/in (micro mm/mm)

ST01

ST02   ST03

factored shear - 132.5 kips

ST01

ST02 ST03

Strain Gage Identifiers and Locations
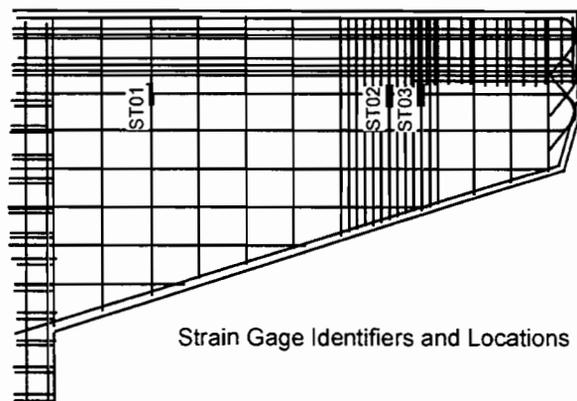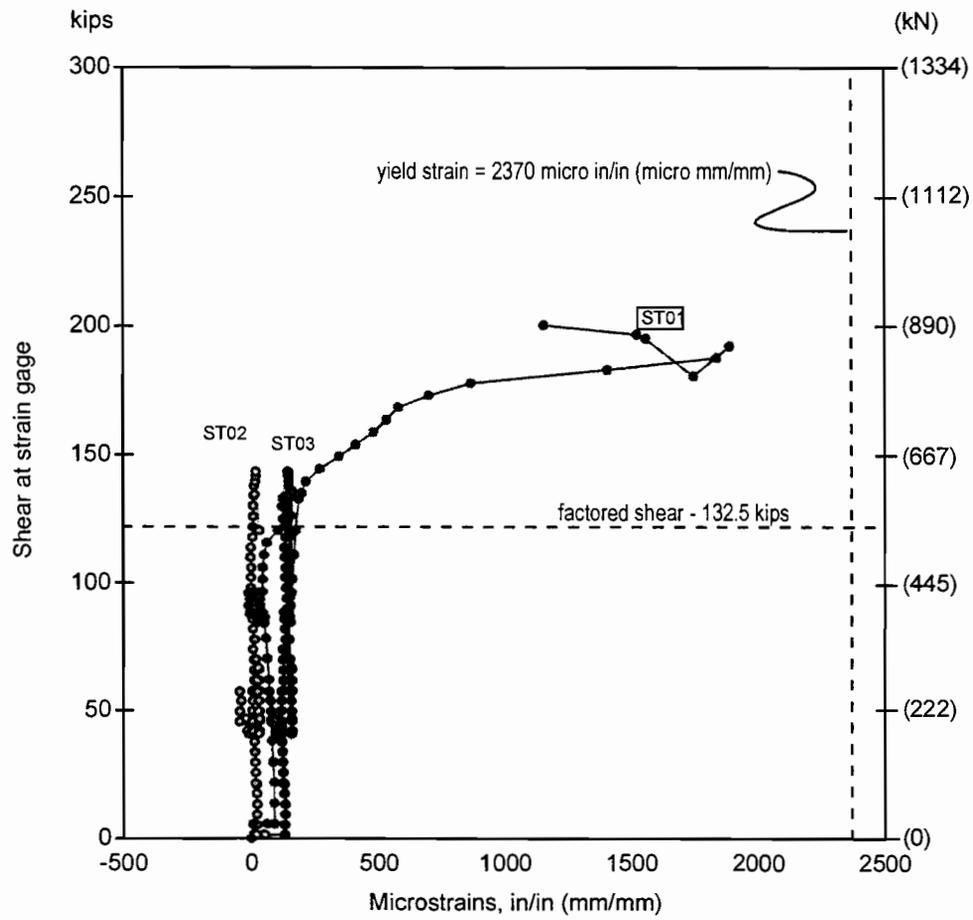
Figure 3. 41   Strain gages on shear stirrups in CO-PU-74S-OR-V-SM
overhang

116

3.6.7 CO-PU-54S-TH-V-SF

Figure 3.42 shows, with a circle, the location of reinforcement strain gages which achieved a strain of at least 270 microstrains, arbitrarily chosen as about 10 percent of yield strain. In these, and subsequently discussed overhangs, the term "effective strain gages" will indicate such gages for easy identification. This shows the location of gages with appreciable elastic or plastic deformations.

All strain gage data was set to zero strain at the beginning of the test, before prestressing operations. Any strains due to prior shrinkage and creep of concrete is not reflected in the strain gage results.

Effective strain gages have been classified in groups depending on their location in non-prestressed flexural reinforcement (#2 reinforcing bars, horizontal), skin reinforcement (7-gage wire, horizontal) and vertical steel (10 gage wire). Non-prestressed flexural reinforcement strain gage data has been plotted against the applied moment at the column face. Shear reinforcement strain gage data, depending on the location of the gages, has been plotted against the total applied loads (Ro and Ri) or against the outer load only (Ro).

Figure 3.43 shows that prior to failure, all layers of the main non-prestressed flexural reinforcement in CO-PU-54S-TH-V-SF were well past yield at the column face and even the top flexural reinforcement out near midspan on the overhang had yielded. Figure 3.44 shows that the skin steel near mid depth began to pick up strain at about the service load level and had reached yield well before ultimate although it was only at about ½ its yield strain at the factored flexural load level. Figures 3.45 and 3.46 indicate that the shear reinforcement had little strain even at factored shear level and was at less than half of its yield strain at ultimate.

3.6.8 CO-PU-54S-TH-I-SM

Even at failure load on the other overhang of the specimen, Figure 3.47 shows none of the non-prestressed main flexural reinforcement in this overhang had yet yielded. Appreciable strains exist at service load levels after load cycling. Figure 3.48 indicates that like its companion overhang, the skin reinforcement near mid-depth at the column face yielded at ultimate but was less than half yield strain at factored flexure. Strains in shear reinforcement shown in Figures 3.49 and 3.50 are very low at service and factored load levels and well below yield at ultimate load levels.

3.6.9 CO-PU-74S-TH-V-SM

Effective gages for the 74S specimen are shown on Figure 3.51. Figure 3.52 indicates that at factored flexural load the main non-prestressed flexural reinforcement was slightly below yield strain but had yielded and experienced large strains before failure. It actually began unloading near ultimate load levels. Figure 3.53 shows skin reinforcement near mid depths at the column face was at strain levels at service load, about half yield strain at factored flexure, but yielded before failure. Figure 3.54
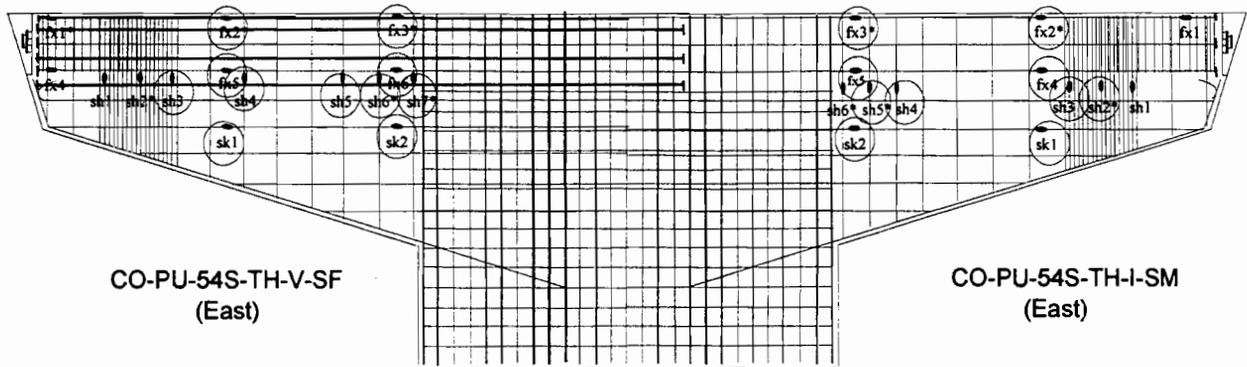
	Gages with negligible readings	Bad gages
CO-PU-54S-TH-V	sh1, sh2, fx1	fx4
CO-PU-54S-TH-I	sh1, sh6, fx1	

Figure 3. 42   Effective strain gages for Models CO-PU-54S-TH (V & I), (SF & SM)
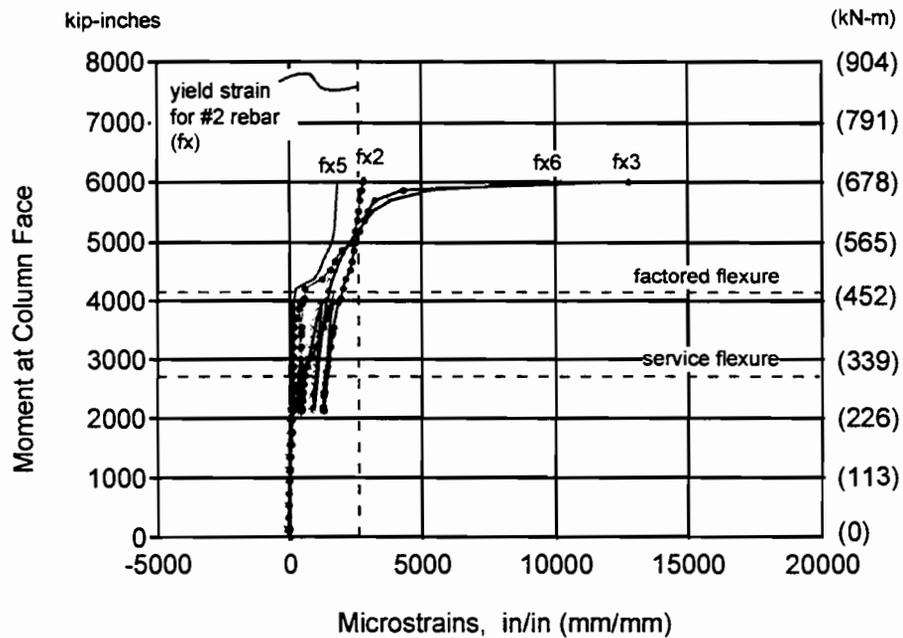
Figure 3. 43 Resultant moment vs. strain in effective strain gages in flexural bars for Model CO-PU-54S-TH-V-SF
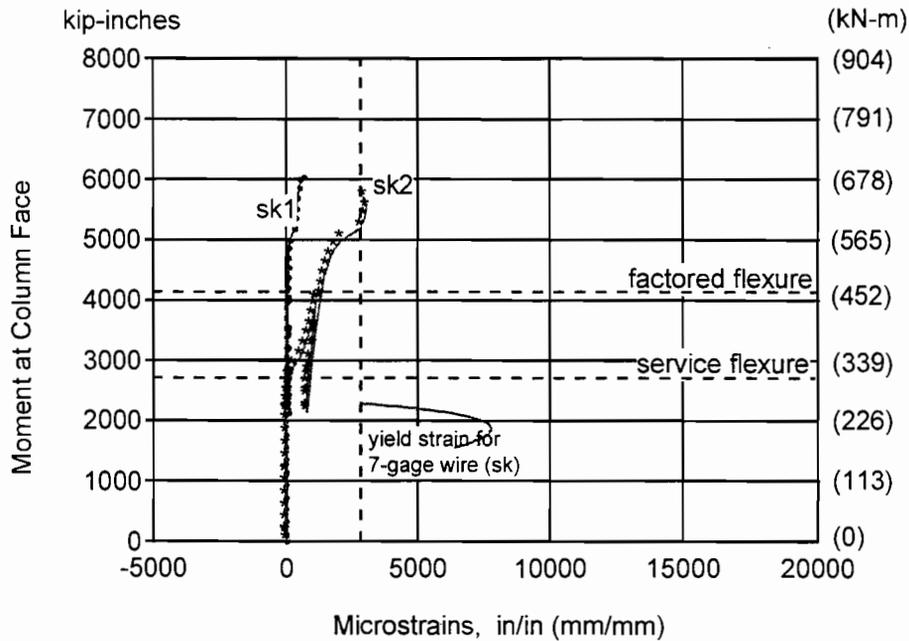
Figure 3. 44   Resultant moment vs. strain in effective strain gages in skin reinforcement for Model CO-PU-54S-TH-V-SF
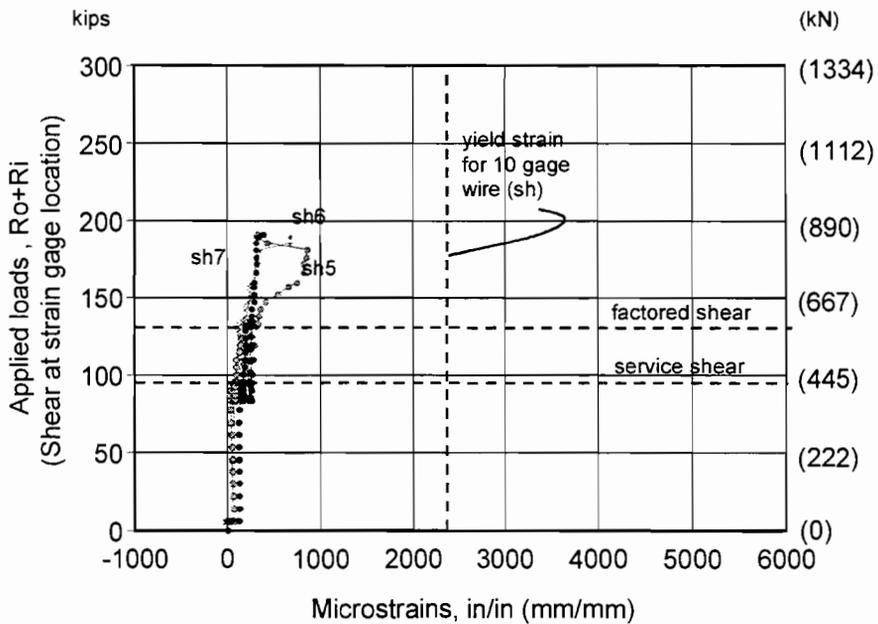
Figure 3. 45   Resultant load vs. strain in effective strain gages in shear reinforcement for Mode CO-PU-54S-TH-V-SF

119
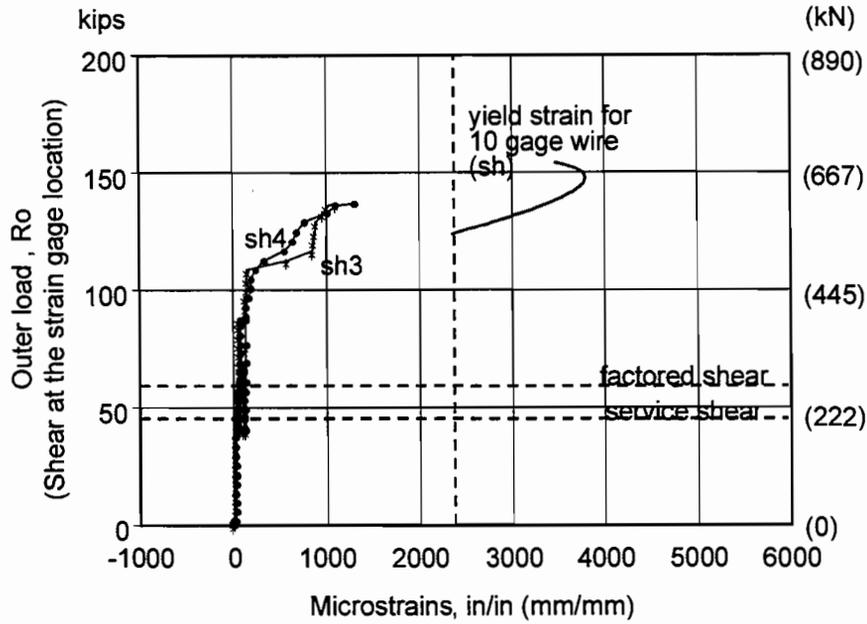
Figure 3. 46 Resultant load vs. strain in effective strain gages in shear reinforcement for Model CO-PU-54S-TH-V-SF
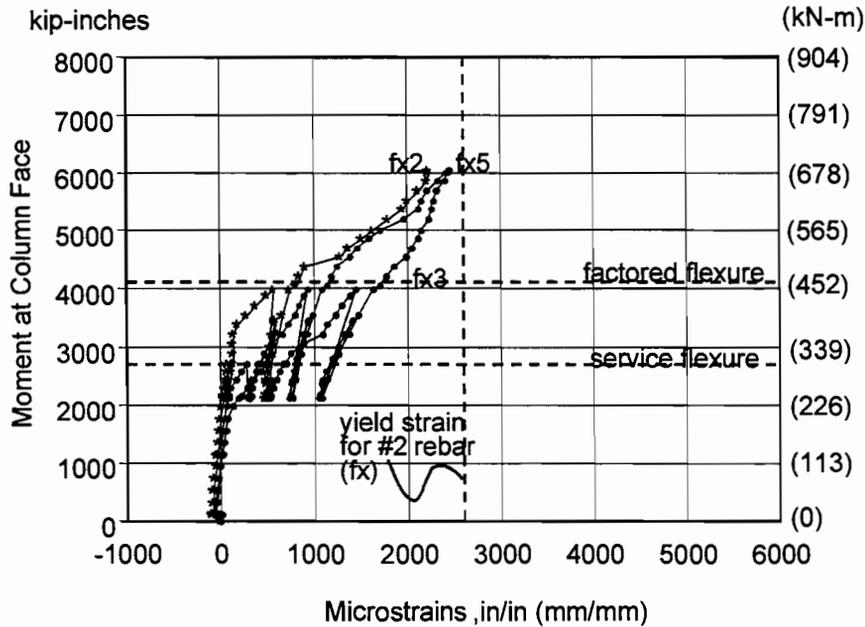
Figure 3. 47 Resultant moment vs. strain in effective strain gages in flexural bars for Model CO-PU-54S-TH-I-SM

120
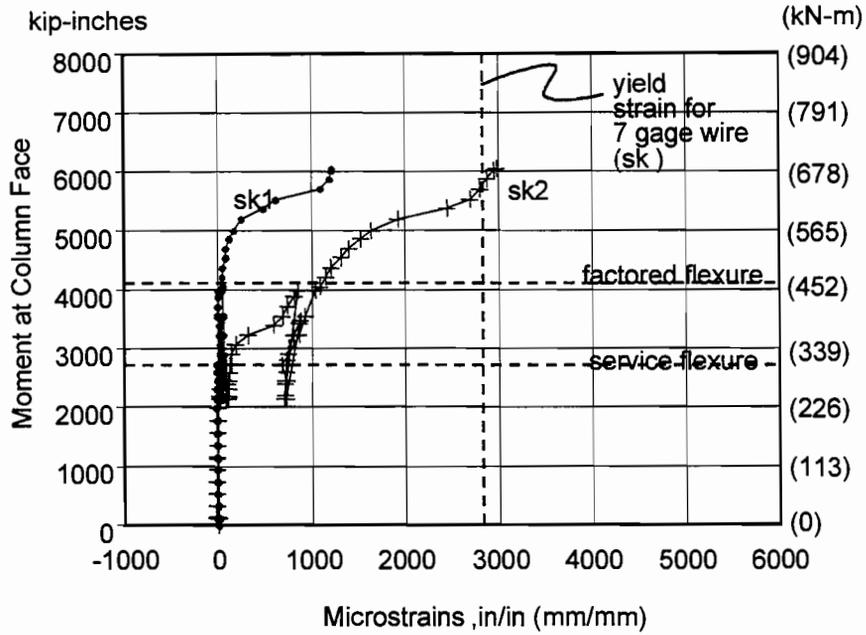
Figure 3. 48 *Resultant moment vs. strain in effective strain gages in skin reinforcement for Model CO-PU-54S-TH-I-SM*
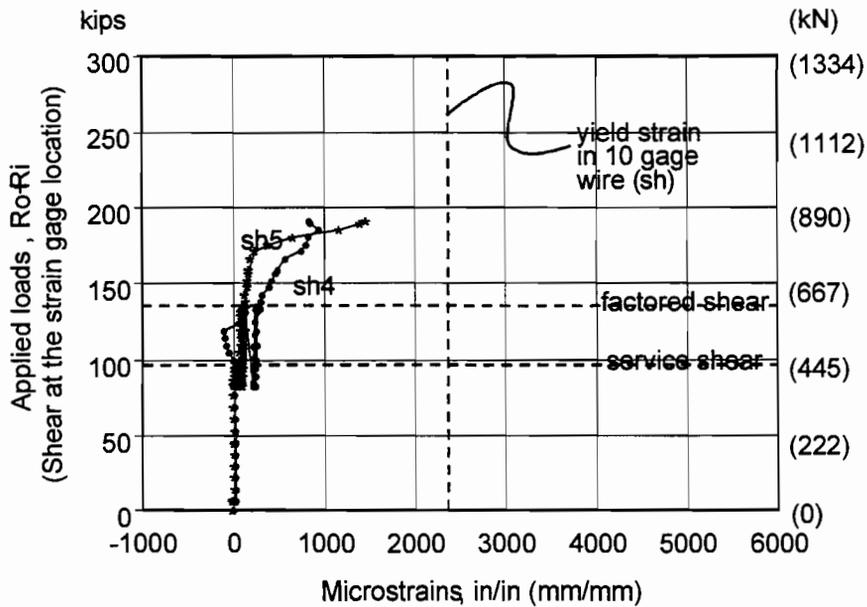
Figure 3. 49 *Resultant load vs. strain in effective strain gages in shear reinforcement for Model CO-PU-54S-TH-I-SM*
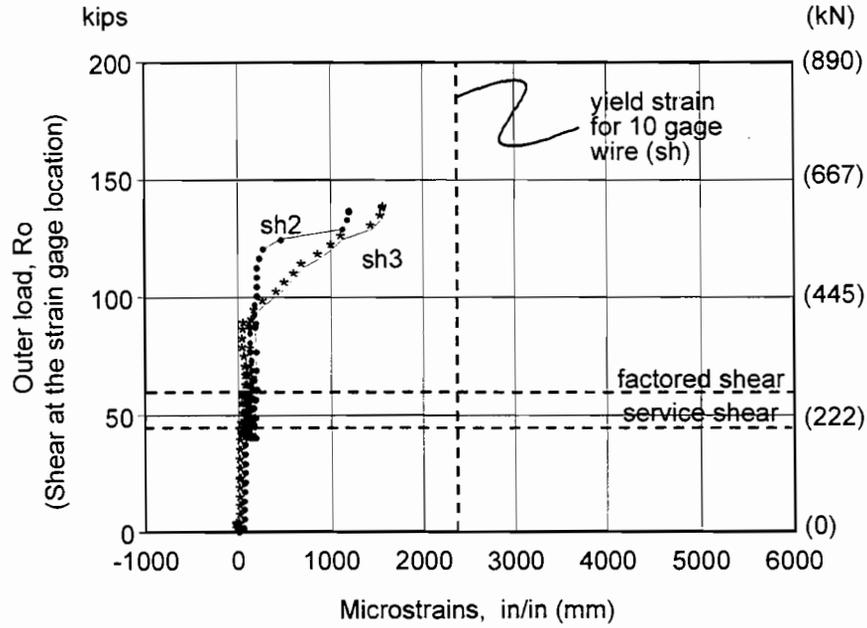
Figure 3. 50 Resultant load vs. strain in effective strain gages in shear reinforcement for Model CO-PU-54S-TH-I-SM

Gages with negligible readings   Bad gages

CO-PU-74S-TH-V: sh1,sh2,sh3,sh5,fx1,fx2,fx4,fx5,sk1   ---
CO-PU-74S-TH-I: sh1,sh2,sh3,sh6,sh7,fx1,fx4,sk1   ---
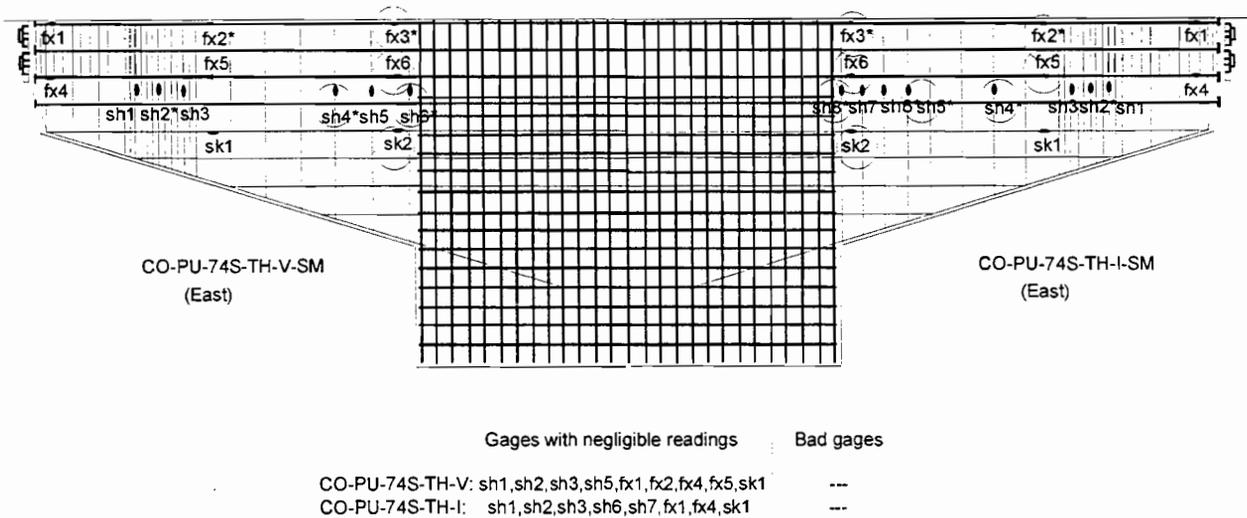
Figure 3. 51 Effective strain gages for Models CO-PU-74S-TH-(V & I)-SM
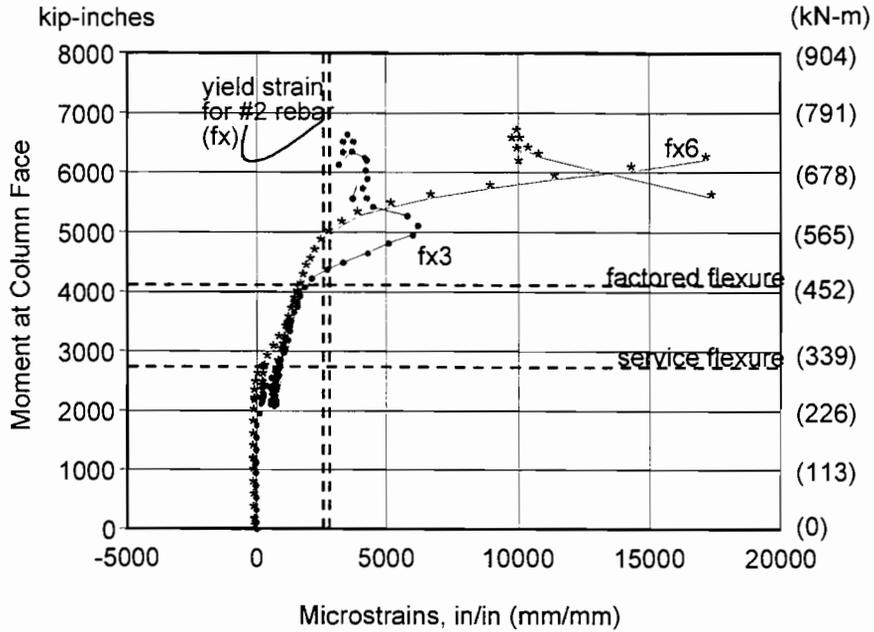
Figure 3. 52 Resultant moment vs. strain in effective strain gages in flexural bars for Model CO-PU-74S-TH-V-SM
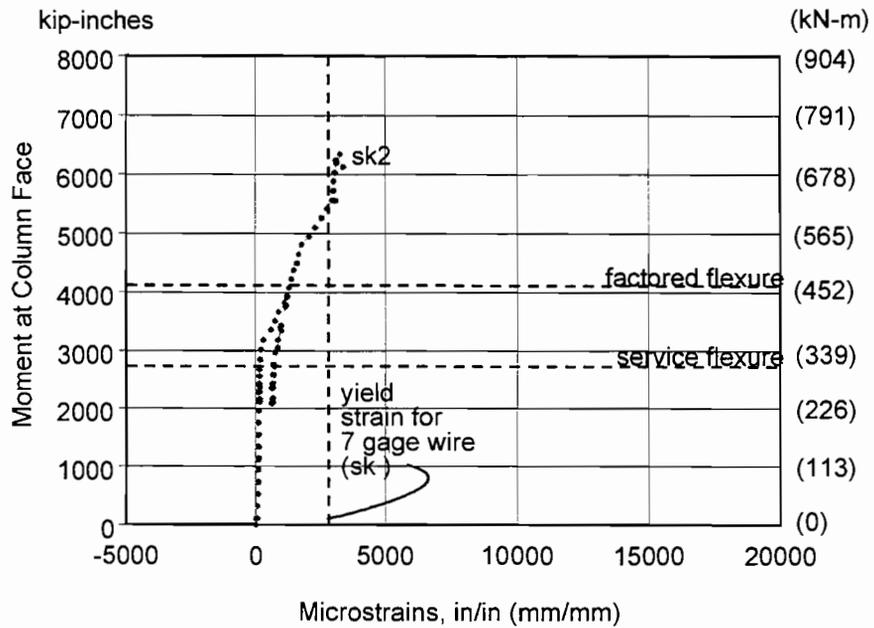
Figure 3. 53 Resultant moment vs. strain in effective strain gages in skin reinforcement for Model CO-PU-74S-TH-V-SM
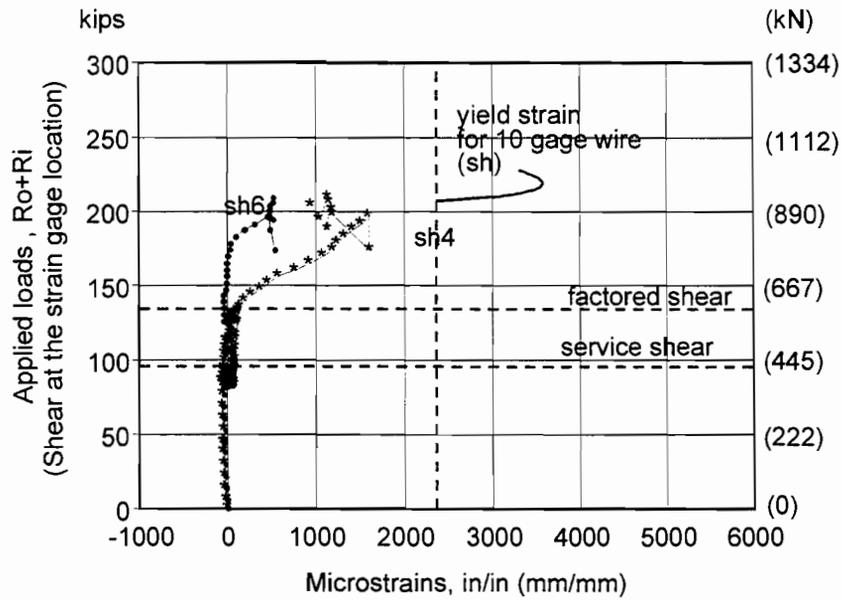
Figure 3. 54 Resultant load vs. strain in effective strain gages in shear reinforcement for Model CO-PU-74S-TH-V-SM
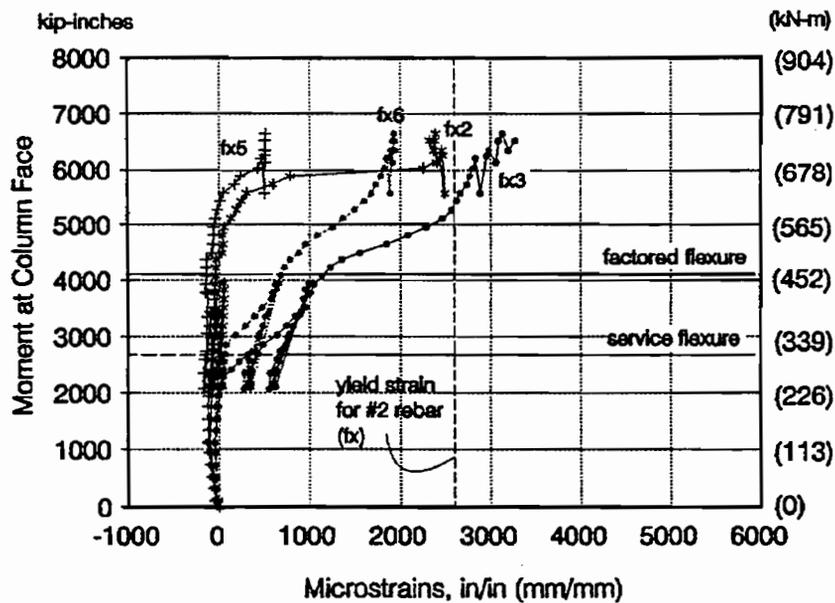
Figure 3. 55 Resultant moment vs. strain in effective strain gages in flexural bars for Model CO-PU-74S-

indicates shear reinforcement had negligible strains at factored shear loads and had larger strains but less than yield even at ultimate level.

3.6.10 CO-PU-74S-TH-I-SM

Figure 3.55 shows yielding on non-prestressed flexural reinforcement barely occurred at ultimate level although Figure 3.56 shows mid-depth skin reinforcement yielding just at the ultimate level. Figures 3.57 and 3.58 show very small strains in shear reinforcement even at factored shear and less than half the yield strain in the shear reinforcement at ultimate.

3.6.11 CO-PU-100S-TH-V-SF

Figure 3.59 shows the location of the effective strain gages in the 100 percent prestressed specimens. Note that a few supplementary non-prestressed flexural bars were provided as cage steel and these were instrumented as shown. Figure 3.60 shows these bars had yielded at the column face prior to ultimate although their strains were only about 50 percent yield strain at factored flexure. Figure 3.61 shows the mid-depth skin reinforcement also yielded at ultimate but had low strains at service and factored load levels. Figure 3.62 shows low strain in shear reinforcement.

3.6.12 CO-PU-100S-TH-I-SM

Figure 3.63 shows low strain in non-prestressed flexural reinforcement at service load levels, but yielding occurring in the third level of non-prestressed bars at factored flexure load. All flexural bars yielded before ultimate. Figure 3.64 shows that skin reinforcement near mid-depth also yielded prior to ultimate. Figure 3.65 indicates that some of the shear reinforcement was very close to yielding at the time of ultimate.

3.6.13 CO-RU-0S-TH-M1.7-SM

Effective strain gage locations for these overhangs are shown in Figure 3.66. Figure 3.67 shows the main reinforcement clearly yielded prior to failure at the column face and Figure 3.68 shows it yielded at the critical rupture section several inches away from the column face. Thus, while the final failure was a massive inclined shear crack and crushing, the flexural reinforcement had yielded. Figure 3.69 shows even well out on the overhang the flexural reinforcement had yielded at ultimate. Side face skin reinforcement strains shown in Figure 3.70 were appreciable even out in the outer portion of the overhang at ultimate and, as shown in Figures 3.71 and 3.72, had fully yielded at the column face and near the column face by ultimate. Figures 3.73 and 3.74 show that many of the shear reinforcing bars yielded prior to failure although strains were very low at factored flexural load.
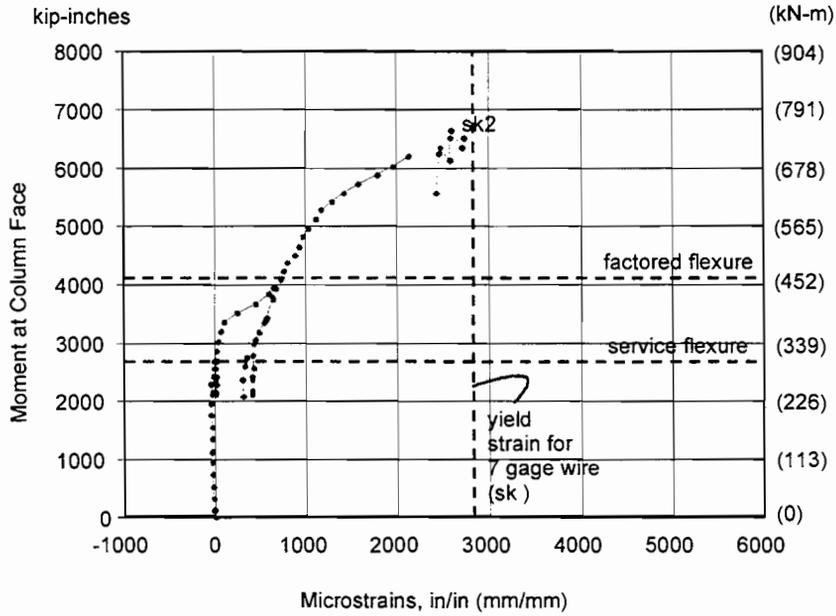
Figure 3. 56 Resultant moment vs. strain in effective strain gages in skin reinforcement for Model CO-PU-74S-TH-I-SM
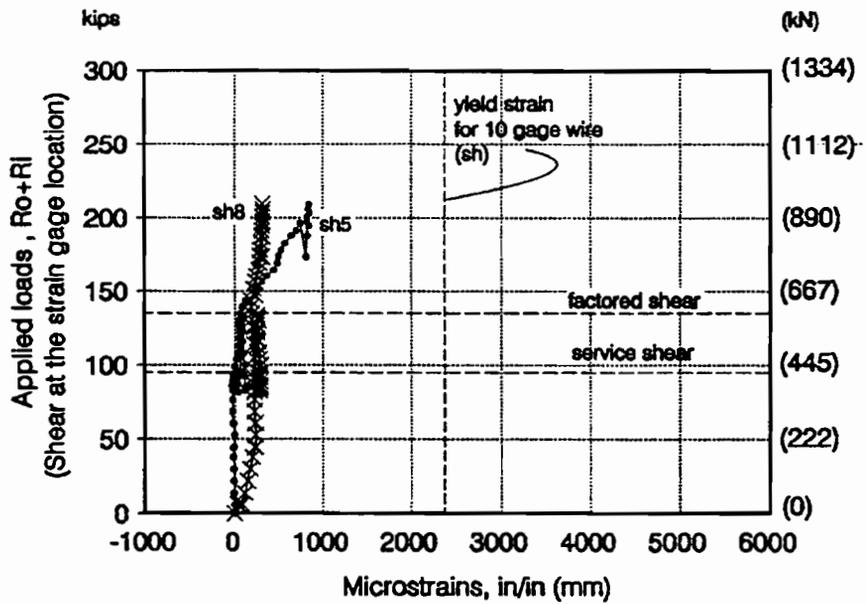
Figure 3. 57 Resultant load vs. strain in effective strain gages in shear reinforcement for Model CO-PU-74S-TH-I-SM

126
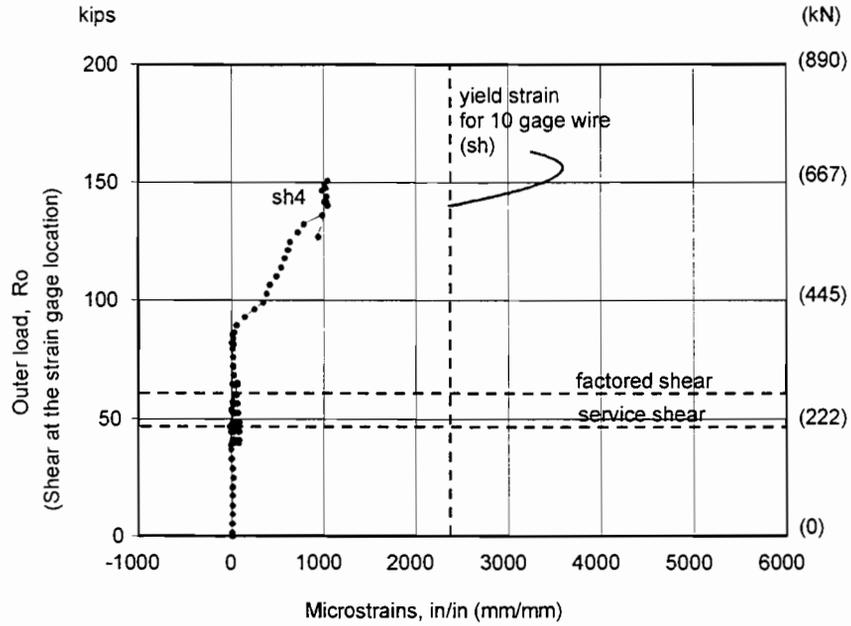
Figure 3. 58   Resultant load vs. strain in effective strain gages in shear reinforcement for Model CO-PU-74S-TH-I-SM

	Gages with negligible readings	Bad gages
CO-PU-100S-TH-V:	fx1,fx2,fx4,sh1,sh2,sh3,sk1	—
CO-PU-100S-TH-I:	fx2,sh1,sh2,sh3,sh4,sh7,sk1	—
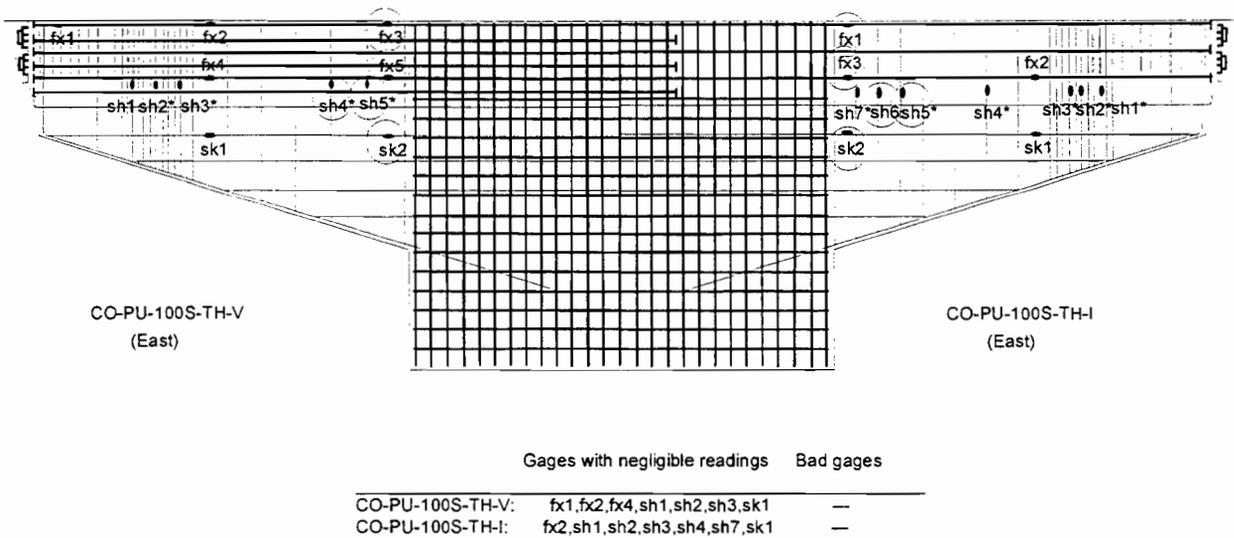
Figure 3. 59   Effective strain gages for Models CO-PU-100S-TH (V & I)

127
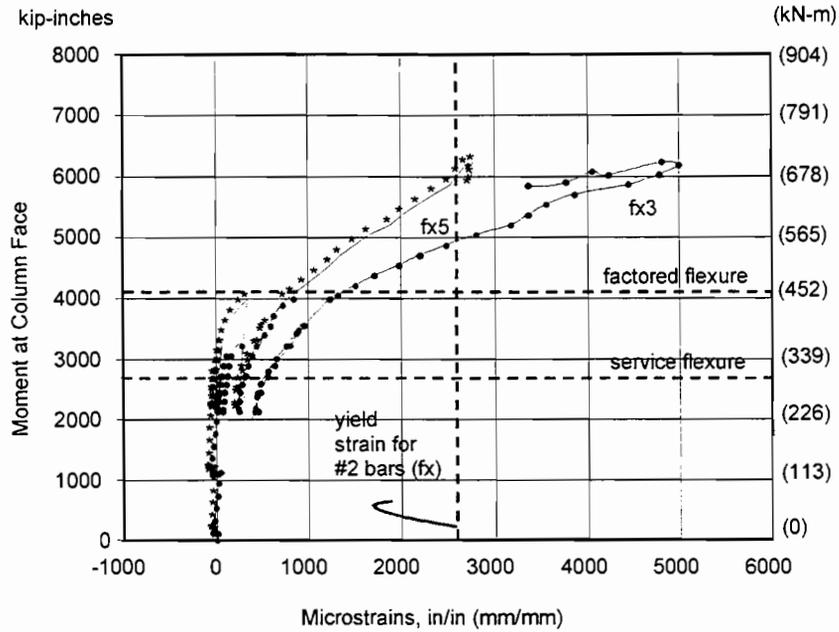
Figure 3. 60 Resultant moment vs. strain in effective strain gages in flexural bars for Model CO-PU-100S-TH-V-SF
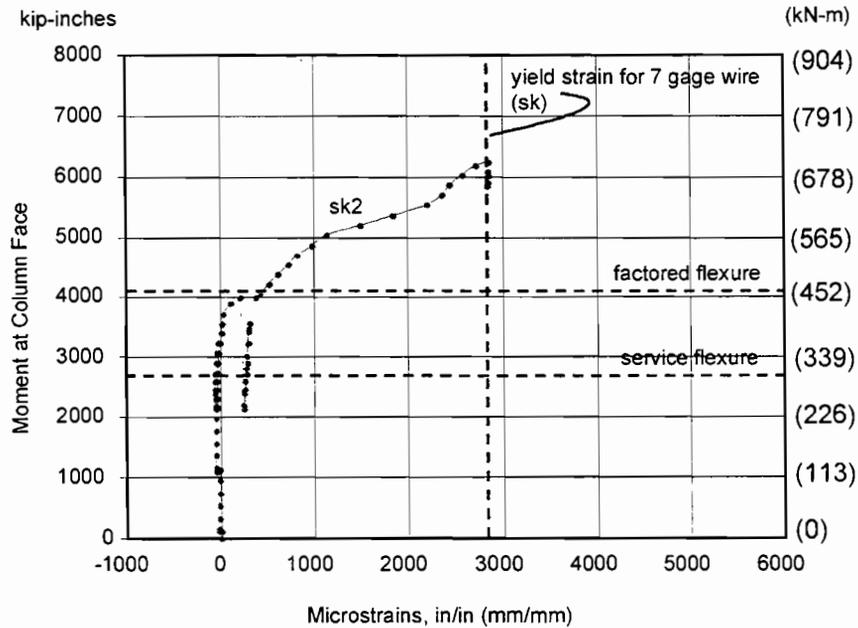
Figure 3. 61 Resultant moment vs. strain in effective strain gages in skin reinforcement for Model CO-PU-100S-TH-V-SF
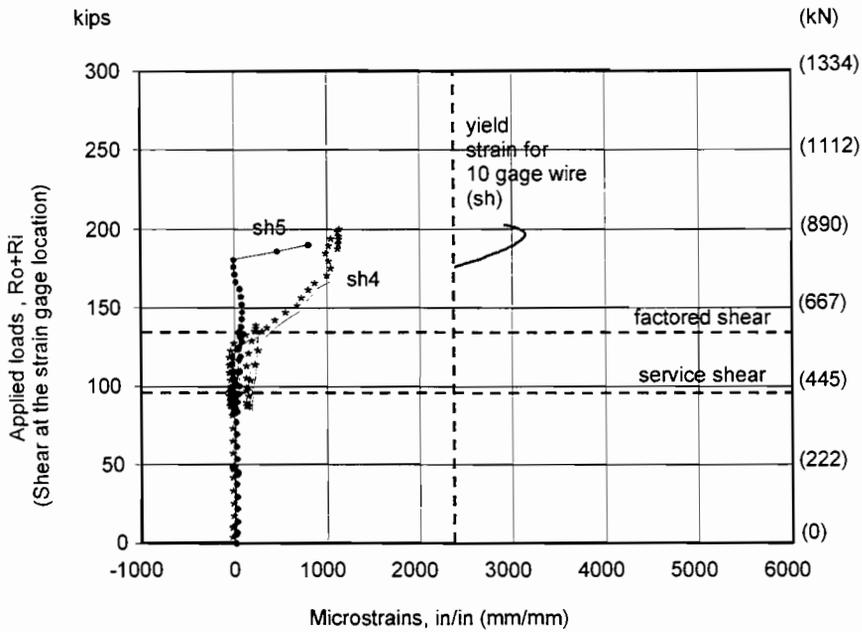
Figure 3. 62 Resultant load vs. strain in effective strain gages in shear reinforcement for Model CO-PU-100S-TH-V
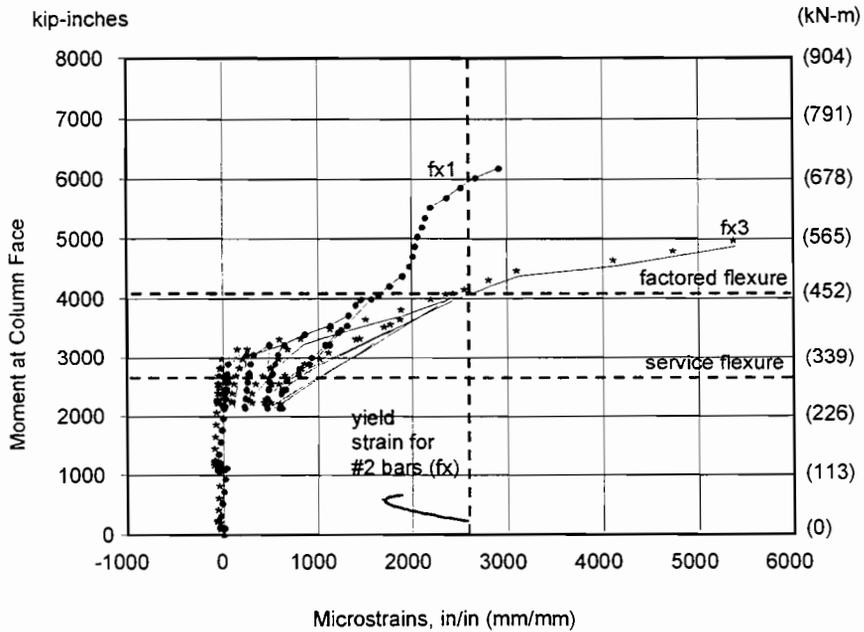
Figure 3. 63 Resultant moment vs. strain in effective strain gages in flexural bars for Model CO-PU-100S-TH-I-SM
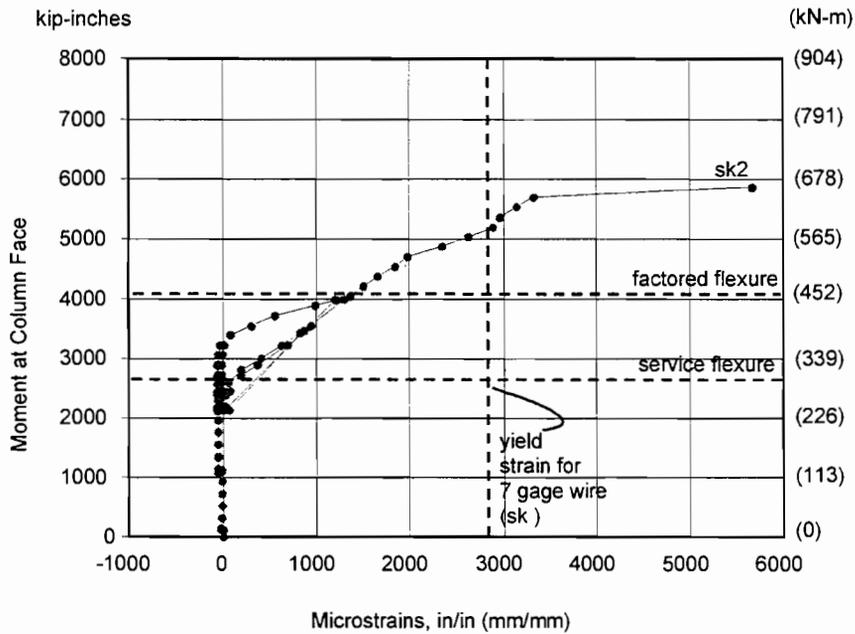
Figure 3. 64 Resultant moment vs. strain in effective strain gages in skin reinforcement for Model CO-PU-100S-TH-I-SM
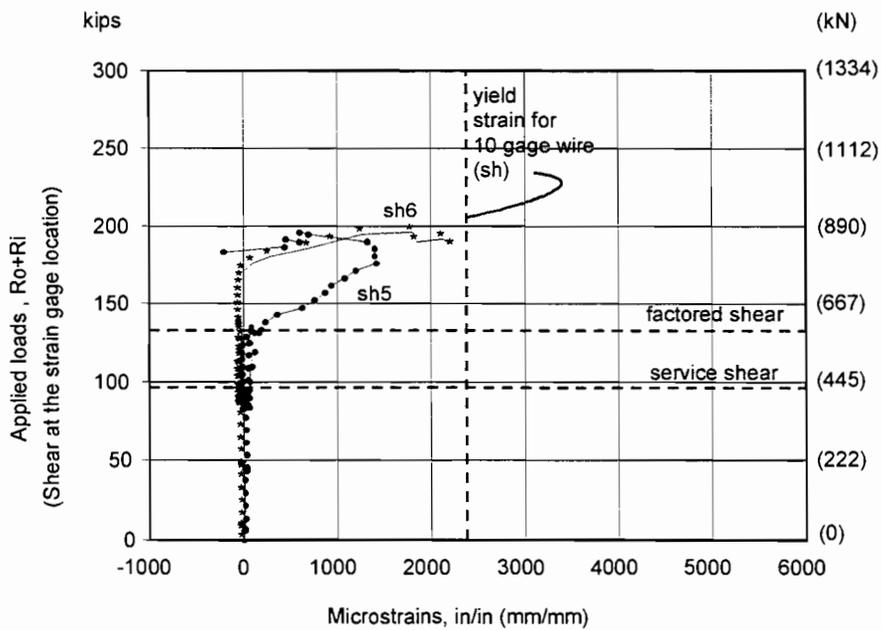
Figure 3. 65 Resultant load vs. strain in effective strain gages in shear reinforcement for Model CO-PU-100S-TH-I-SM

130
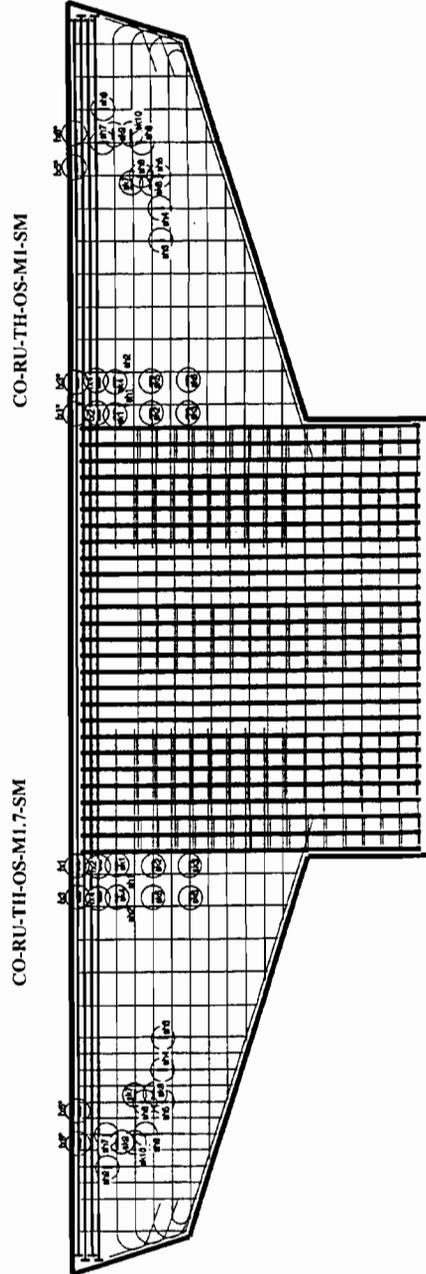
Figure 3. 66 Effective strain gage locations in CO-RU-0S-TH-(M1.7 and M1)-SM
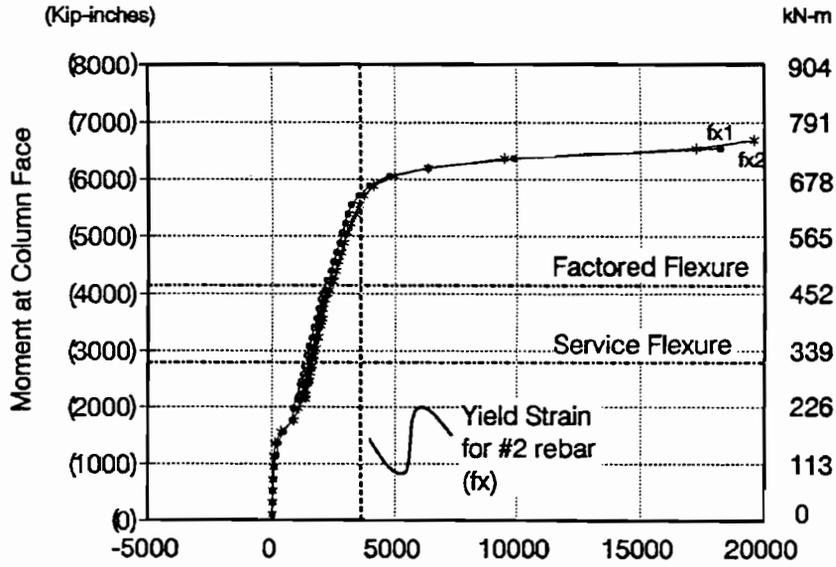
Figure 3. 67   Resultant moment vs. strain in effective strain gages on main flexural reinforcement <u>at column face</u> in CO-RU-0S-TH-M1.7-SM
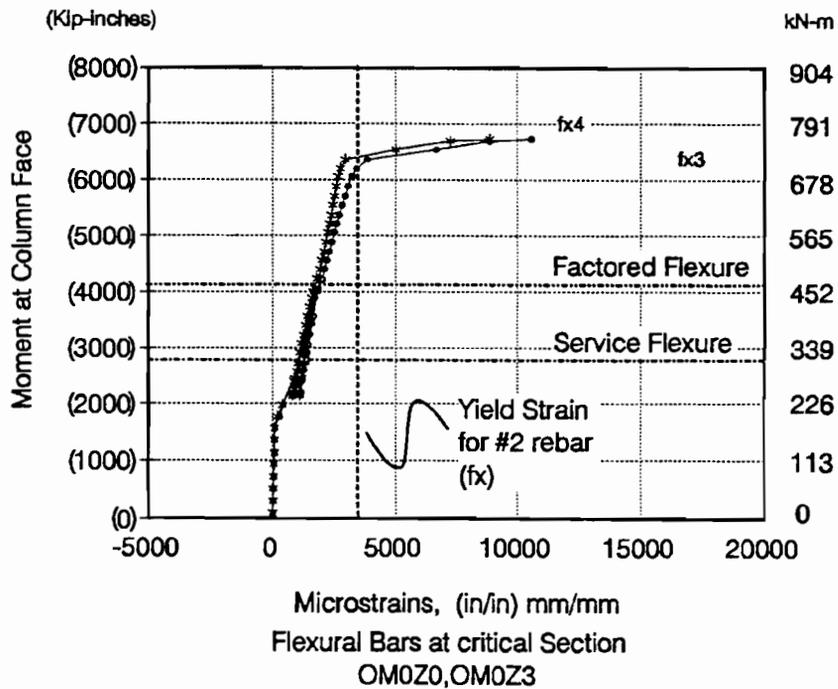
Figure 3. 68   Resultant moment vs. strain I effective strain gages on main flexural reinforcement <u>at rupture section adjacent to column face</u> in CO-RU-0S-TH-M1.7-SM

132
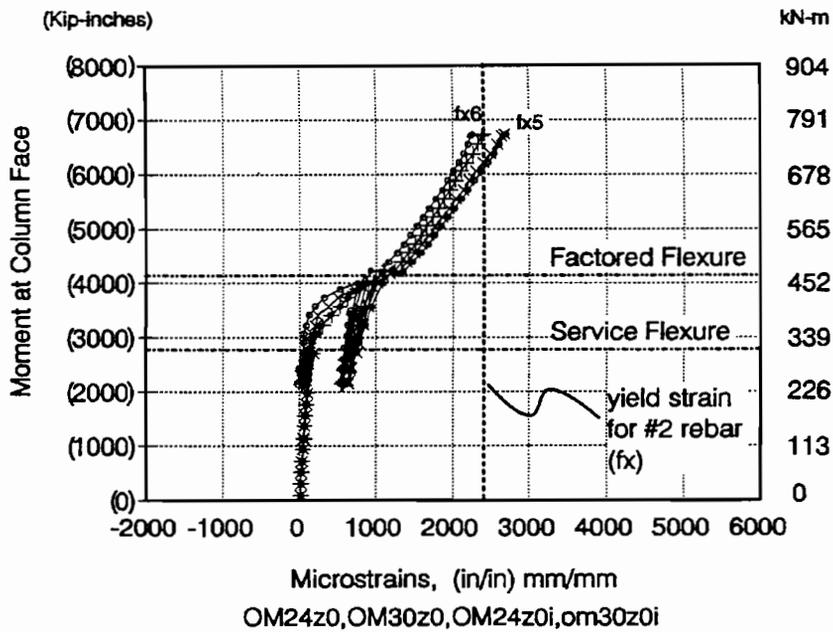
Figure 3. 69 Resultant moment vs. strain in effective strain gages on main flexural reinforcement in center region of overhanging CO-RU-0S-TH-M1.7-SM
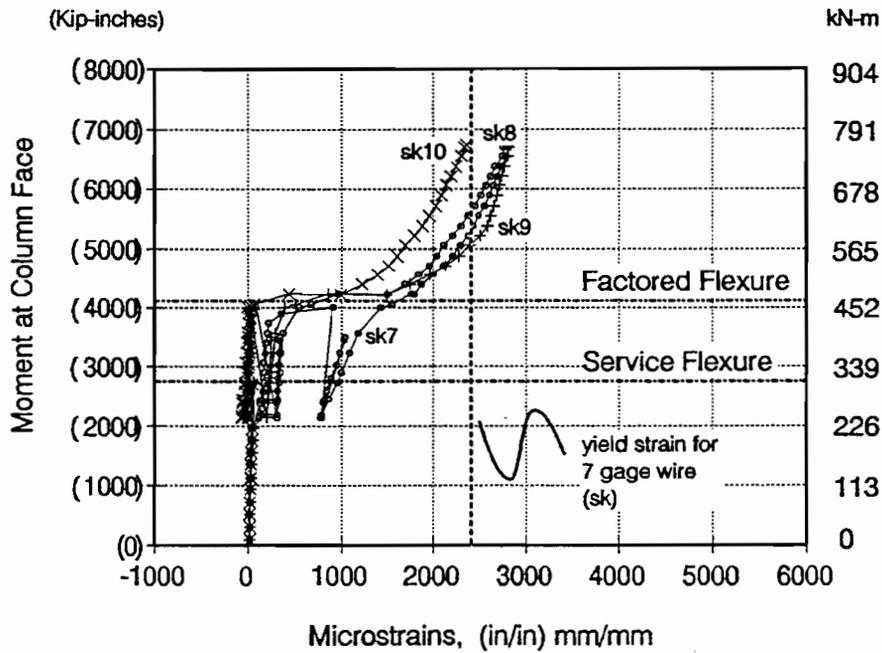
Figure 3. 70 Resultant moment vs. strain on side face skin reinforcement in CO-RU-0S-TH-M1.7-SM

133
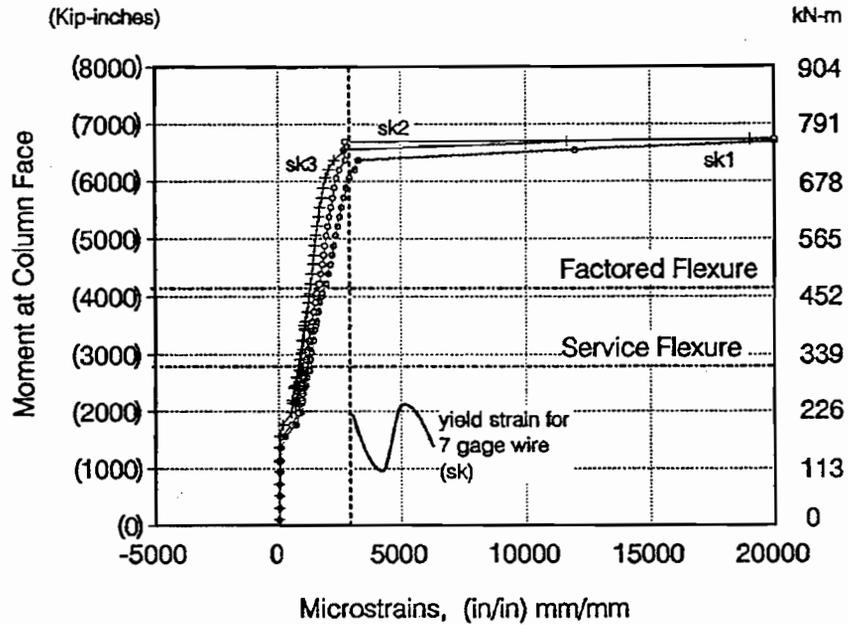
Figure 3. 71 Resultant moment vs. strain on side face skin reinforcement in CO-RU-0S-TH-M1.7-SM
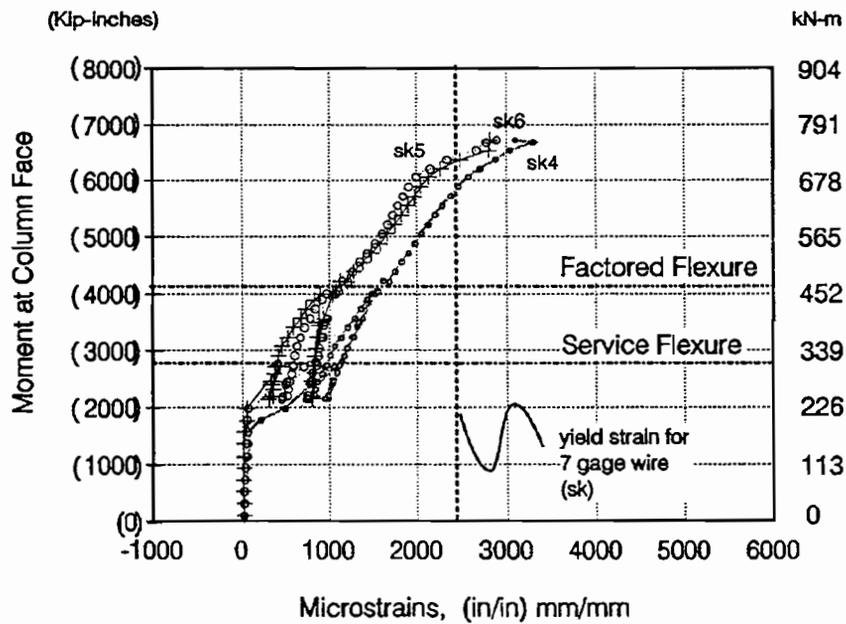
Figure 3. 72 Resultant moment vs. strain on side face skin reinforcement in CO-RU-0S-TH-M1.7-SM
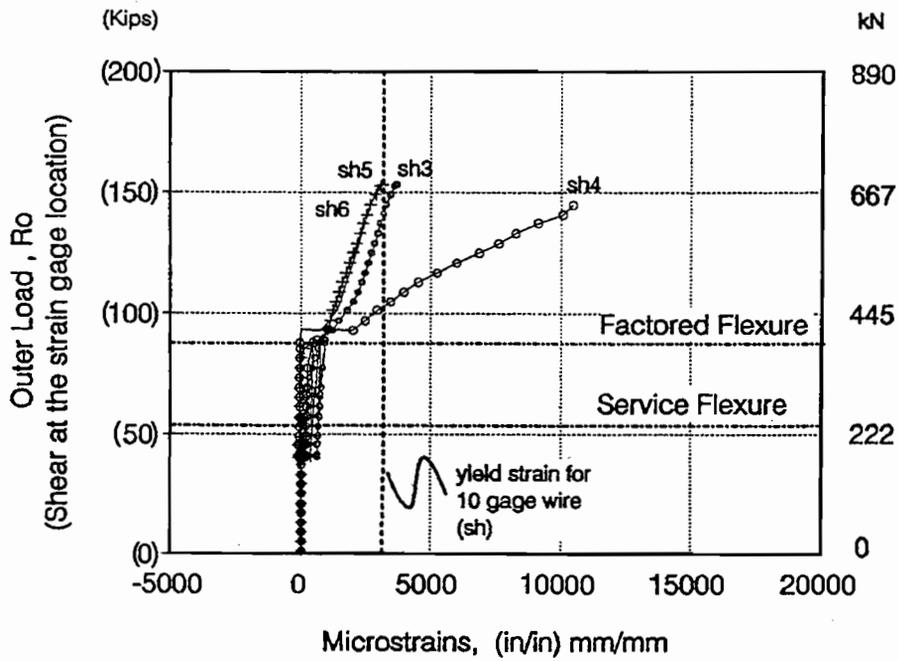
Figure 3. 73 Resultant load vs. strain in effective strain gages in shear reinforcement in CO-RU-0S-TH-M1.7-SM
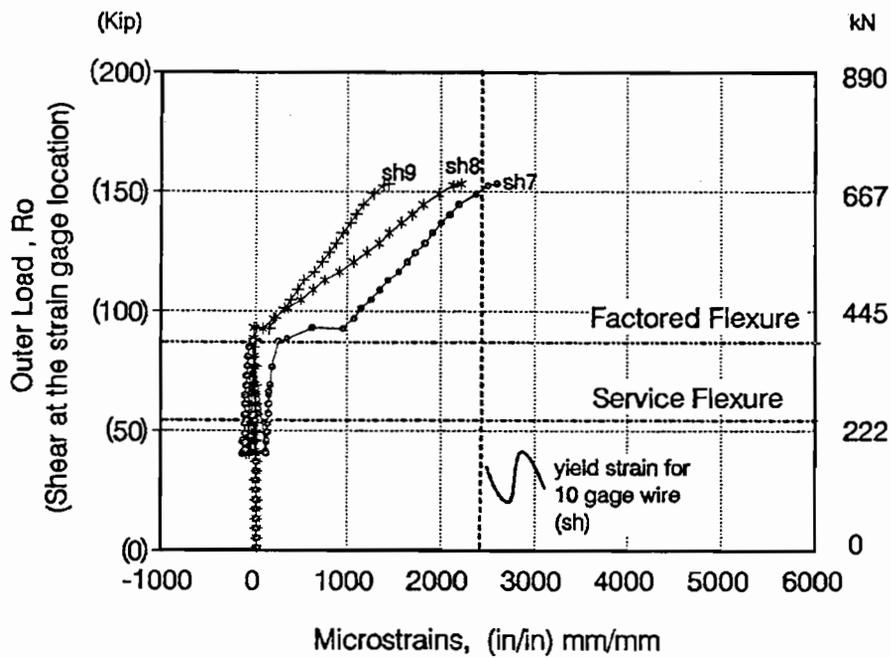
Figure 3. 74 Resultant load vs. strain in effective strain gages in shear reinforcement in CO-RU-0S-TH-M1.7-SM

135

3.6.14 CO-RU-0S-TH-M1-SM

Figures 3.75 and 3.77 show the main flexural reinforcement in this overhang to be almost identical to the other overhang shown in Figures 3.67 to 3.69. Similarly, the skin reinforcement (shown in Figures 3.78 to 3.80) is very like the other overhang. The main difference from the other overhang is in the shear reinforcement in which Figures 3.81 and 3.82 show even larger strains above yield strain developed prior to failure. These overhangs are the only ones in which the shear reinforcement was highly stressed.

3.7 POST-MORTEM INVESTIGATION

Each specimen was examined after completion of testing to determine the condition of the reinforcement. Concrete was removed from the maximum moment regions of each overhang using a jackhammer. All strands in the top level of each post-tensioned overhang were removed and the duct material and grout was opened to reveal the strands.

The extent of damage to reinforcement is given in Table 3.3. Typical fractures of reinforcement are shown in Figures 3.83 and 3.84. While main flexural reinforcing bars and some wires fractured in give of the eight overhangs taken to failure and severe necking down was noted in many bars, non of the post-tensioned strands fractured. The only stirrups to yield and fracture were in the last specimen which did not utilize a full strut-and-tie model design, but relied on a concrete V_c contribution.
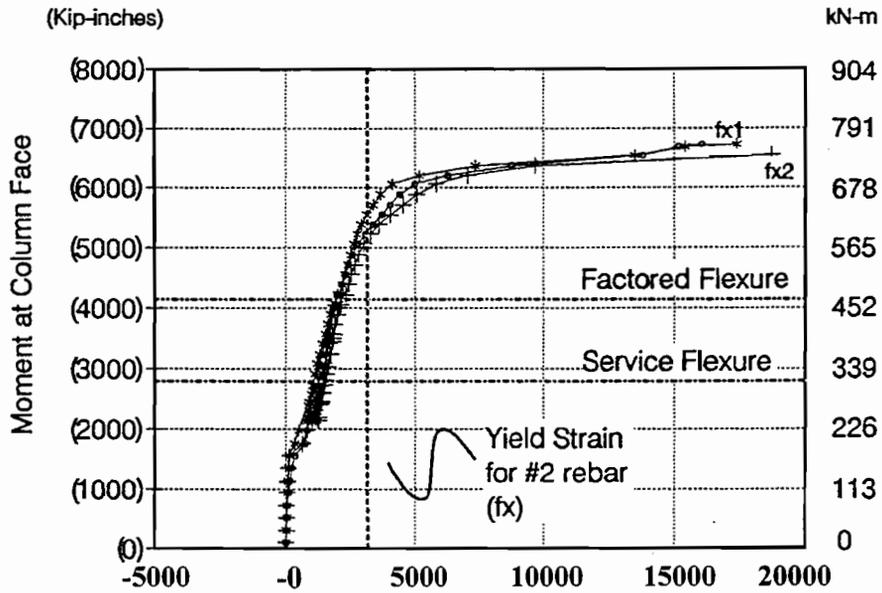
Figure 3. 75 Resultant moment vs. strain in effective strain gages on main flexural reinforcement at column face in CO-RU-0S-TH-M1-SM
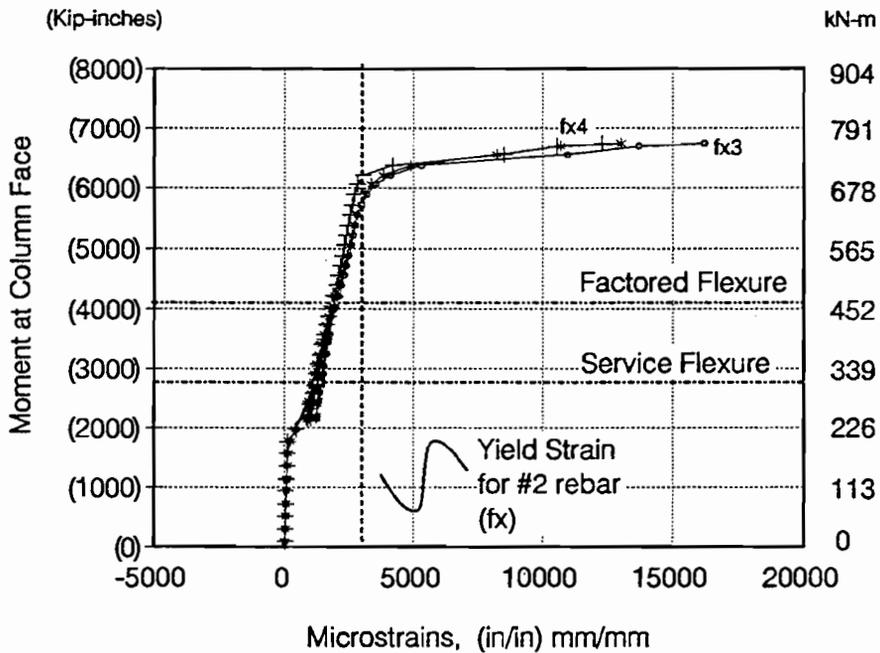
Figure 3. 76 Resultant moment vs. strain in effective strain gages at section adjacent to column face in CO-RU-0S-TH-M1-SM

137
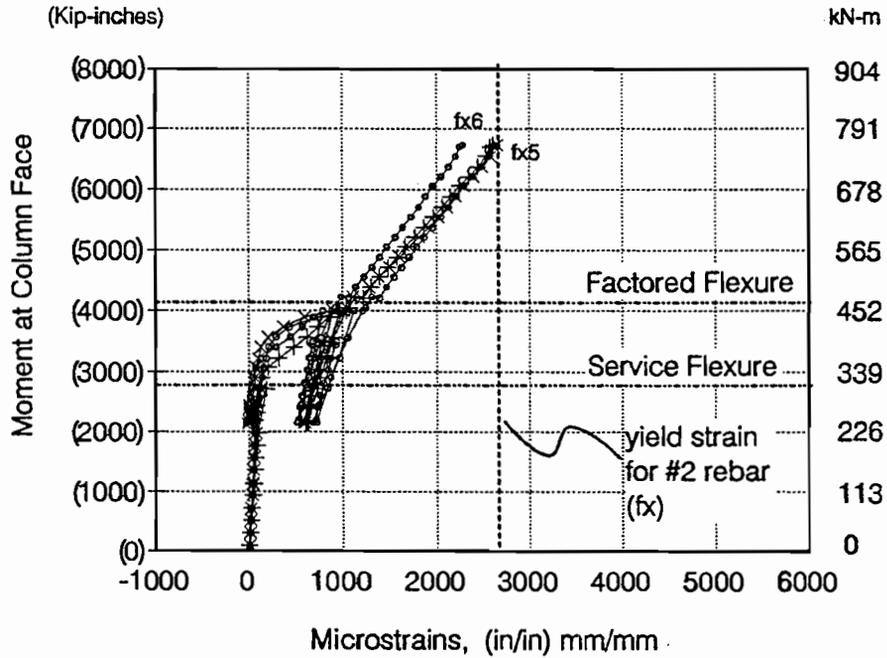
Figure 3. 77 Resultant moment vs. strain in effective strain gages on main flexural reinforcement in outer region of overhang in CO-RU-0S-TH-M1-SM
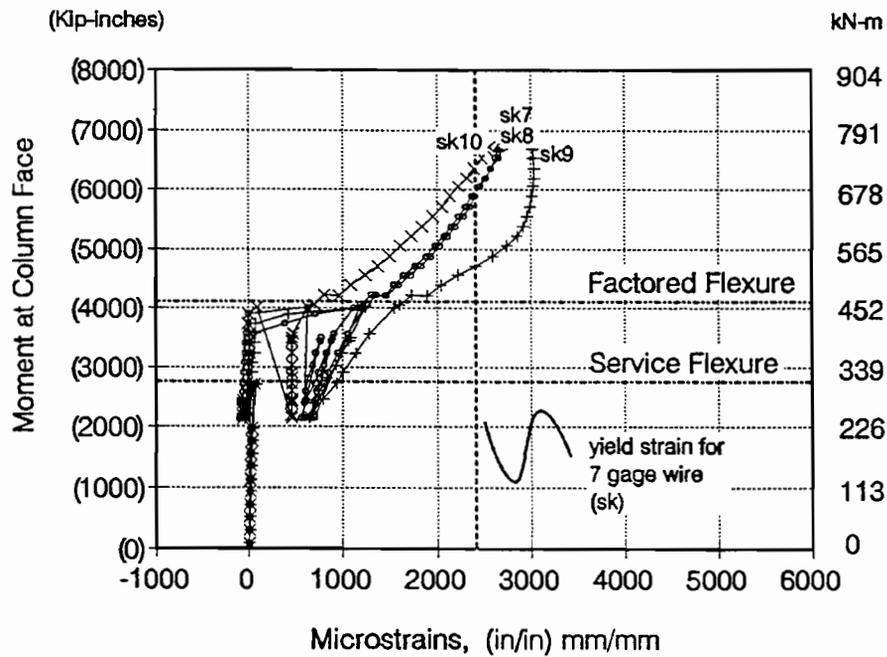
Figure 3. 78 Resultant moment vs strain on side face skin reinforcement in CO-RU-0S-TH-M1-SM
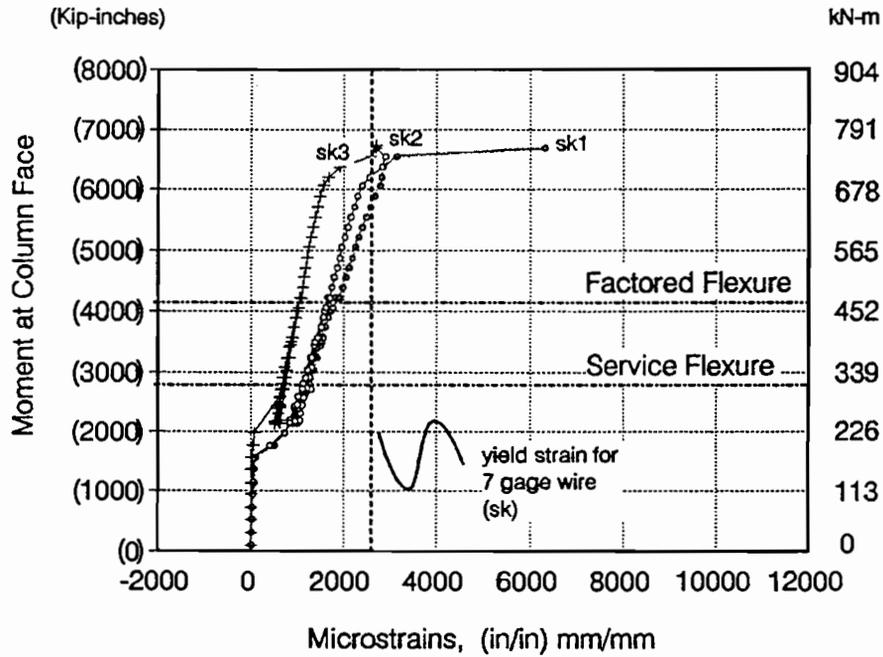
Figure 3. 79 Resultant moment vs strain on side face skin reinforcement in CO-RU-0S-TH-M1-SM
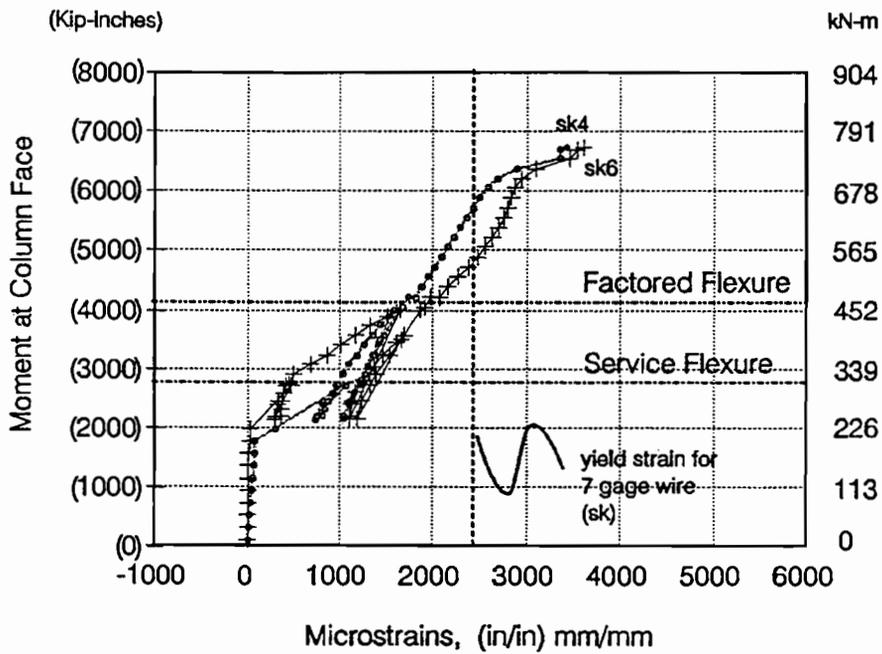
Figure 3. 80 Resultant moment vs strain on side face skin reinforcement in CO-RU-0S-TH-M1-SM

139
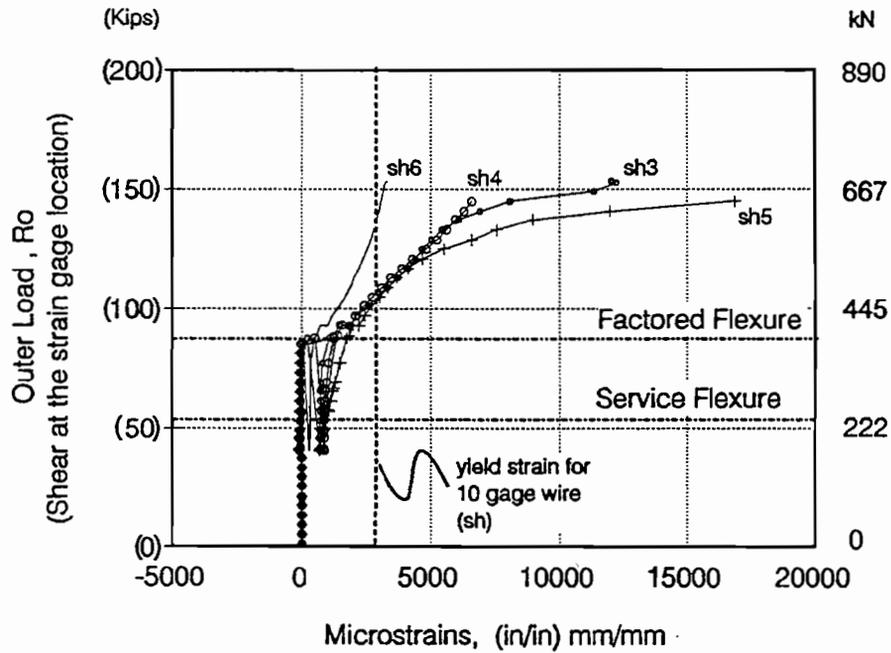
*Figure 3. 81   Resultant moment vs strain in effective strain gages
in shear reinforcement in CO-RU-0S-TH-M1-SM*
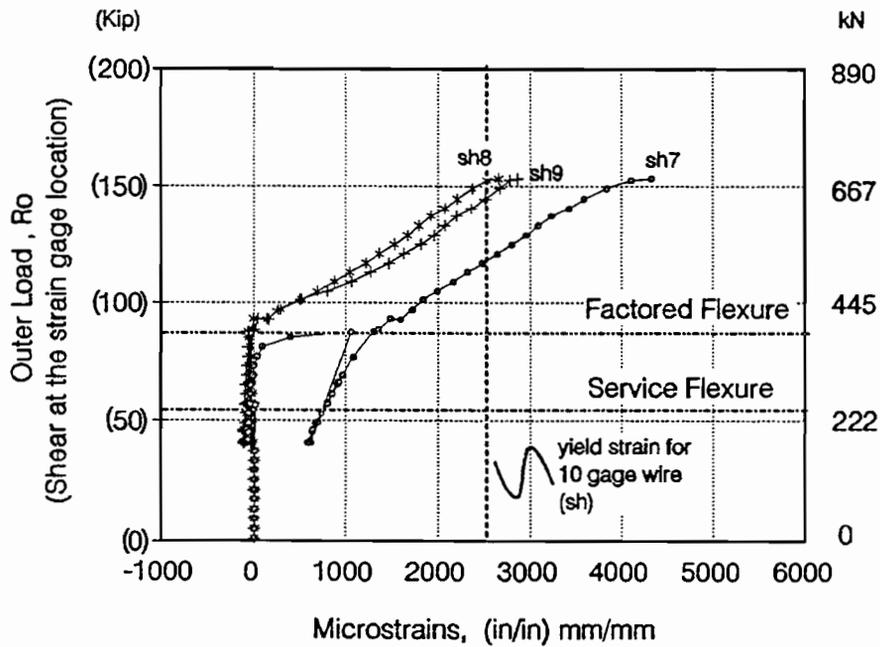
*Figure 3. 82   Resultant moment vs strain in effective strain gages
in shear reinforcement in CO-RU-0S-TH-M1-SM*

Table 3. 3   Post-Mortem Investigations

Specimen	Overhang Designation	Fractured Flexural Reinforcing Bars	Fractured Flexural Prestressing Strands	Fractured Stirrups
1 A	CO-RU-0S-OR-N-SF	None	----	None
B	CO-RU-0S-OR-N-SF	None	----	None
2 A	CO-PS-100S-NA-N-SM	Two No. 2 Bars and Two 7-ga. wires in outer	None	None
B	CO-PS-100S-NA-N-SM	----	----	----
3 A	CO-PU-100S-NA-V-SM	None	None	None
B	CO-PU-100S-NA-I-SM	None	None	None
4 A	CO-PU-74S-OR-V-SM	Eleven No. 2 Bars in outer layers	None	None
B	CO-PU-74S-OR-I-SM	----	----	----
5 A	CO-PU-54S-TH-V-SF	One No. 2 bar in outer layer	None	None
B	CO-PU-54S-TH-I-SF	----	----	----
6 A	CO-PU-74S-TH-V-SM	One No. 2 bar in outer layer; many necked	None	None
B	CO-PU-74S-TH-I-SM	----	----	----
7 A	CO-PU-100S-TH-V-SF	All No. 2 bars in outer three layers; two of three 7-ga wires in outer	None	None
B	CO-PU-100S-TH-I-SM	----	----	----
8 A	CO-RU-0S-TH-M1-SM	----	----	----
B	CO-RU-0S-TH-M1.7-SM	None	----	----

141
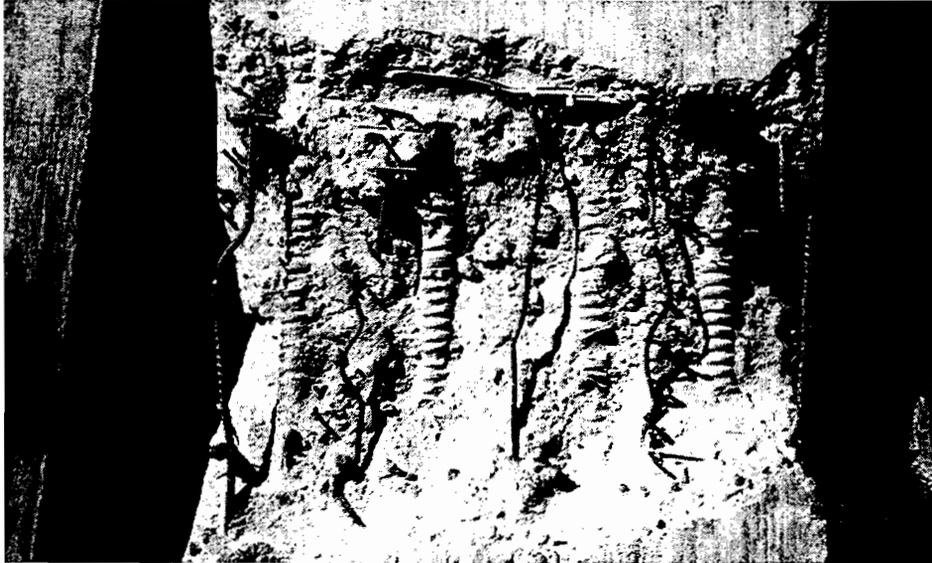
Figure 3. 83   Fractured tension reinforcement in north CO-PS-100S-NA-N-SM overhang
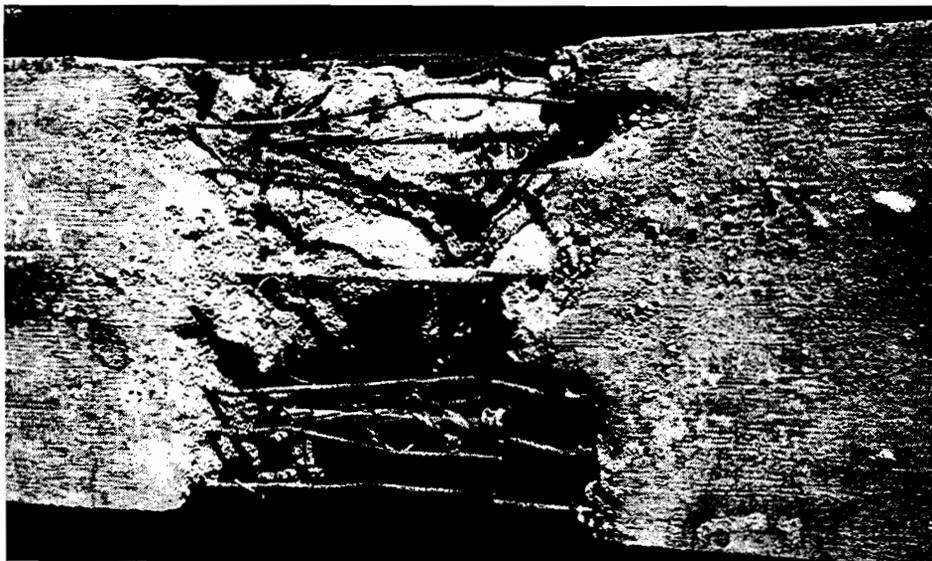
Figure 3. 84   Fractured tension reinforcement in CO-PU-74S-OR-V-SM overhang

CHAPTER FOUR

ANALYSIS OF RESULTS

In this chapter the results of the 16 overhangs tested will be compared. Major variables are the degree of prestressing, basic philosophy of design (service or ultimate), anchorage of reinforcement, shear capacity model and side face reinforcement design method. The effect of these variables will be discussed as appropriate and the basis laid for recommendations for future practice.

This chapter is organized along a limit state format, treating first the service limit state and then the strength limit state. Specific topics and comparisons include:

Service Limit State	Sec. 4.1 — Cracking Moment
	Sec. 4.2 — Crack Widths
	Sec. 4.3 — Crack Width Limits
	Sec. 4.4 — Skin Reinforcement
	Sec. 4.5 — Deflections
	Sec. 4.6 — Fatigue Stress Range
Strength Limit State	Sec. 4.7 — Deflection Response
	Sec. 4.8 — Ultimate Capacity
Special Variables	Sec. 4.9 — T-Headed Bars
	Sec. 4.10 — Strut-and-Tie Models

4.1 CRACKING MOMENT — SERVICE LIMIT STATE

Table 4.1 provides the actual test cracking moment and the predicted cracking moment. The predicted cracking moment was based on the moment required to produce an extreme fiber tensile stress of $7.5\sqrt{f_c'}$ considering the effect of prestressing force and eccentricity and with calculations based on the uncracked transformed section. Ratios are given for the actual cracking moment divided by the predicted value, the dead load moment, and the service load moment, respectively. Since there may have been some restraint in the loading system for specimens tested without elastomeric bearing pads, the type of baring pads are also given. The only direct comparison (between Specimens 3 and 7) does indicate a possible 12 to 20 percent increase with steel bearing pads. The data indicates cracking moments were all predicted ± 0 to 14 percent. Since the tensile strength of the concrete is only crudely estimated by $7.5\sqrt{f_c'}$ (others use $6\sqrt{f_c'}$), this type variation is not surprising.

Table 4. 1   Cracking Moments, M_{cr}

Specimen		Overhang Designation	Predicted		Actual		Actual/Predicted	Actual./M_{dead}*	Actual/$M_{service}$**	Bearing Pads
			kip-in (1)	kip-in (1a)	kip-in (2)	kip-in (2a)	(3)	(4)	(5)	
1	A	CO-RU-0S-OR-N-SF	1286	145	1394	157	1.08	0.64	0.51	elastomeric
	B	CO-RU-0S-OR-N-SF	1286	145	1394	157	1.08	0.64	0.51	elastomeric
2	A	CO-PS-100S-NA-N-SM	2857	323	3272	370	1.15	1.51	1.19	steel
	B	CO-PS-100S-NA-N-SM	2857	323	----	----	----	----	----	steel
3	A	CO-PU-100S-NA-V-SM	2611	294	2923	330	1.12	1.35	1.06	steel
	B	CO-PU-100S-NA-I-SM	2611	295	3087	349	1.18	1.42	1.12	steel
4	A	CO-PU-54S-OR-V-SM	2101	237	2222	251	1.18	1.02	0.81	steel
	B	CO-PU-74S-OR-I-SM	2102	237	2499	282	1.11	1.15	0.91	steel
5	A	CO-PU-54S-TH-V-SF	2221	257	1987	224	0.87	0.92	0.72	elastomeric
	B	CO-PU-54S-TH-I-SM	2221	257	1987	224	0.87	0.92	0.71	elastomeric
6	A	CO-PU-74S-TH-V-SM	2599	294	2322	262	0.89	1.07	0.84	steel
	B	CO-PU-74S-TH-I-SM	2599	214	2465	278	0.95	1.14	0.90	steel
7	A	CO-PU-100S-TH-V-SF	3089	349	3076	248	1.00	1.42	1.12	elastomeric
	B	CO-PU-100S-TH-I-SM	3089	349	2750	311	0.89	1.27	1.00	elastomeric
8	A	CO-RU-0S-TH-M1-SM	882	100	<1035	<117	<1.17	<0.48	<0.38	elastomeric
	B	CO-RU-0S-TH-M1.7-SM	88s	100	<1035	<117	<1.17	<0.48	<0.38	elastomeric

* M_{dead} = 2169 kip-in = 245 kip-in

** $M_{service}$ flexure = 2749 kip-in = 311 kN-m
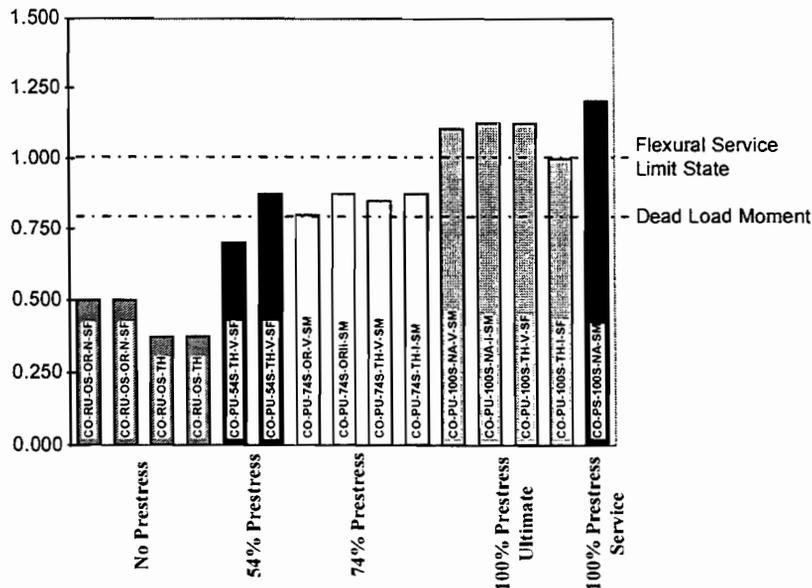
Figure 4. 1   Ratio of cracking moment to flexural service moment

The ratio of cracking moment to service flexural load level is shown in Figure 4.1. Also shown is the high proportion of service load that is provided by dead load.

The effect of prestressing degree is clearly shown in Figure 4.1. The non-prestressed specimens cracked well below dead load levels and at 40 to 50 percent of the service limit state moment. Thus, such non-prestressed members would be expected to be well cracked in service. The specimens with 54 percent of the tensile force provided by prestressing steel had low values of pre-compression which was overcome at both dead load and service limit state moments. Such members would also be expected to be well cracked at service levels. In contrast, the overhangs with 74 percent of the tensile capacity provided by the prestressing were not cracked at dead load, but would be lightly cracked at the service limit state. As would be expected, the fully prestressed member with design based on service level stresses was uncracked at both dead load and service limit state and had an almost 20 percent reserve above service limit state. Interestingly, the fully prestressed specimen with amount of strand based on ultimate conditions is also uncracked in three of the four overhangs at the service limit state and the cracking in the fourth overhang occurs only at full service load. Only minor cracking might be expected in such specimens at the service limit state. Many of the specimens had concrete strengths greater than 5000 psi (35 MPa) specified. Table 2.8 shows the mean concrete strength to be 6290 psi (43 MPa). Obviously, if actual concrete strengths were 5000 psi, cracking loads would have been lowered around 20 percent on the average. All specimens might then be cracked at full service limit state.

4.2 CRACK WIDTHS — SERVICE LIMIT STATE

Literally thousands of crack width measurements were made at the locations where cracks crossed grid lines at major loading levels on all specimens. Presentation of this data in a usable form is a major challenge. Tables of crack width measurements are given in Appendix A along with crack patterns for the major crack width readings.

4.2.1 Crack Width Envelopes

To evaluate the crack width performance of each overhang, curves were generated which give the relationship between the moment at the face of the column and the maximum measured crack width anywhere along the overhang. These curves are referred to as the "crack width envelopes" for each overhang.

The "crack width envelopes" were generated by first plotting the crack width readings of the "major" cracks on an overhang against the moment at the face of the column (see Figure 4.2). A "major" crack was defined to be any crack which had the greatest width of all cracks on the overhang at any single load stage. For those overhangs which were cracked before reaching service loads, multiple crack width readings were taken at the same load level because of the loading sequence (i.e. loading, unloading, and reloading between dead load, service flexure loads, and service shear loads). Curves were determined for each "major" crack by connecting the maximum measured crack with points at successively increasing load levels as shown in Figure 4.2. Each of these individual "major" crack curves were then overlaid onto an additional graph (see Figure 4.3) and the "crack width envelopes" shown by the heavy lines were determined by connecting the points of maximum crack width for each load

level from the "major" crack curves. For the CO-RU-0S-OR-N-SF specimen, this was done for both overhangs (see Figures 4.4 and 4.5). The north and south overhang envelopes were superimposed onto yet another graph and the combined envelope was determined (see Figure 4.6). This envelope represents the maximum crack width at every load stage anywhere on both overhangs. Some overhangs had only one "major" crack each, so the plot of this crack gave the "crack width envelope" directly. The "major" crack plots and "crack width envelopes" for all remaining overhangs are given in Figures A.1 and A.2 in Appendix A.

The "crack width envelopes" incorporate the readings from the "major" cracks only. Furthermore, crack width readings taken after reaching factored flexure loads are not included. For a number of specimens these "crack width envelopes" are also reported for "virgin loading" i.e. load stages where the different load levels had been reached for the first time. This eliminates crack widening due to repeated load sequencing.

A very local discontinuity exists when evaluating the crack widths in the immediate vicinity of the overhang - column intersections. As shown in Figure 2.32, the center to center dimensions of the corner vertical column bars were 46.51 in. (1181mm) or 16.51 in. (419mm). With allowance for the No. 3 (9.5mm) reinforcing bars and the 9 ga. (3.8mm) ties, this corresponds to clear side cover of 0.41 in (10.41mm). As can be seen from typical overhang reinforcing cage drawings (for example, see Figure 2.30), the same side clear cover was used on the horizontal reinforcing cages in the overhangs. Obviously, this would result in bars conflicting when the vertical and horizontal reinforcing intersect at the columns - overhang junction. As indicated in Section 2.6.2, at this intersection the main longitudinal steel was locally deviated laterally to pass inside the stiffer vertical column bars. This means that very locally at the overhang - column intersections the clear side cover over the longitudinal bars was substantially increased. Such decisions have to also be made in field construction or in reinforcing bar details.

Observed crack widths on the surface of a concrete member are generally larger than the crack widths at the level of the reinforcement. This increase in crack width is somewhat proportional to the concrete cover. While this has been shown true for bottom or top cover, it is also probably true but to a lesser degree for side cover. This is an enigma in service level design for concrete structures. Increased cover is generally desirable for increasing the corrosion protection of reinforcement in an uncracked concrete region. However, this increase in cover leads to larger surface crack widths for the same crack width at the level of the reinforcement. This may be unacceptable from a visual criteria although it is the crack width at the level of the reinforcement which is probably the key factor in exposing the bar to oxygen and moisture which are necessary for corrosion. This change in cover is important since the widest flexural cracking at service load flexural moment occurred at the region of side cover discontinuity in almost all specimens. However, it is typical of what would be expected in the field. The effect of the discontinuity in side cover cannot be quantified.
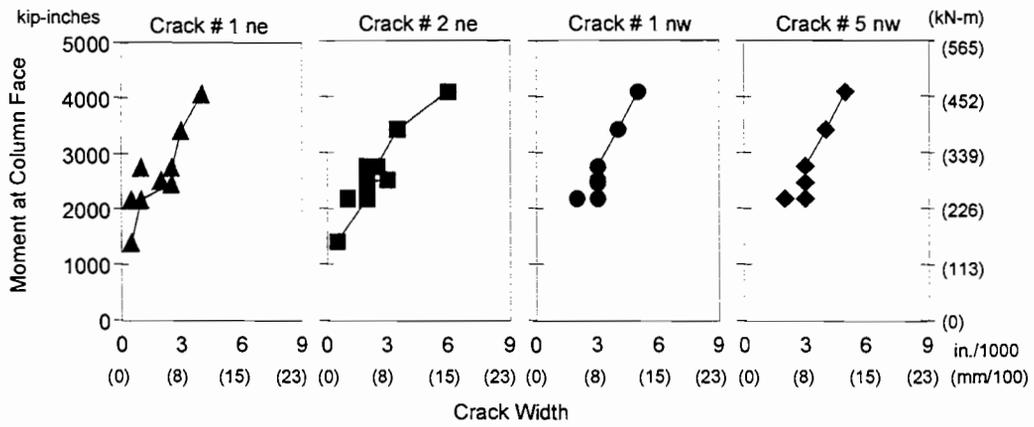
Figure 4. 2   "Major" crack plots for the north CO-RU-0S-OR-N-SF overhang
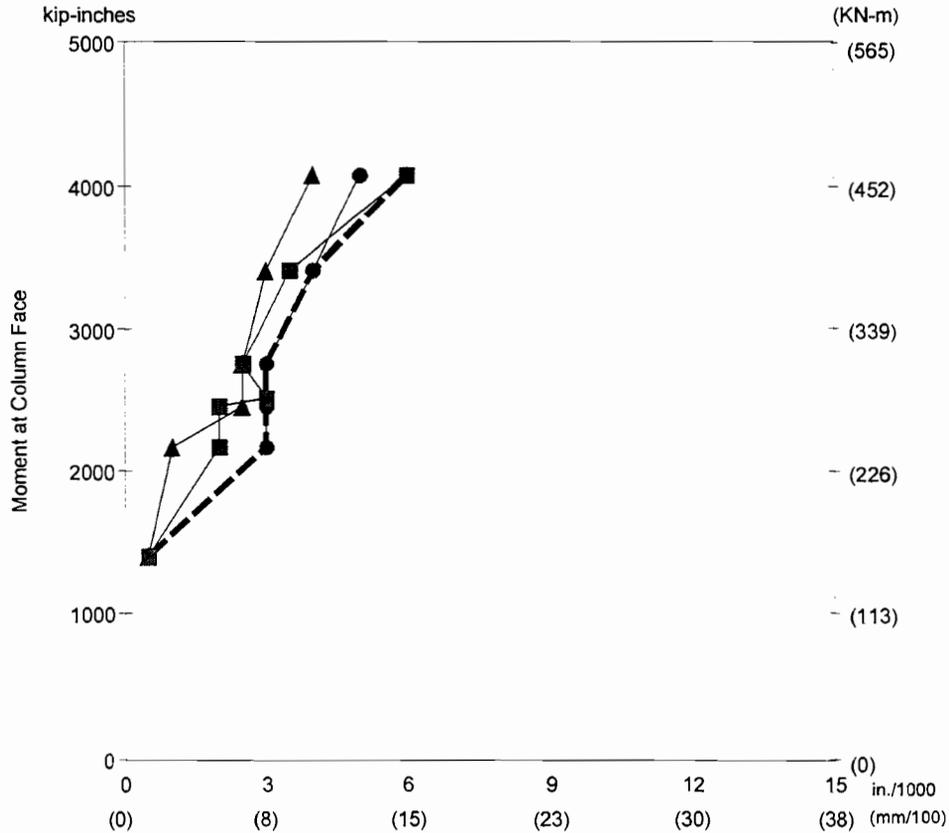
Figure 4. 3   "Crack Width Envelope" for the north CO-RU-0S-OR-N-SF overhang

147
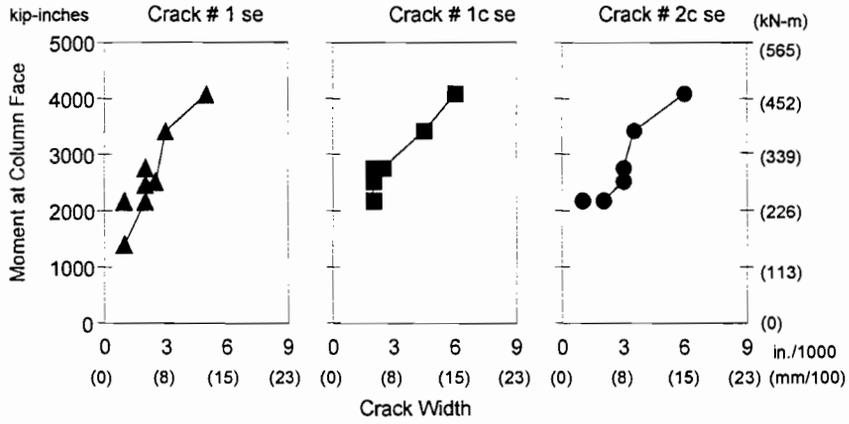
Figure 4. 4   "Major" crack plots for the south CO-RU-0S-OR-N-SF overhang
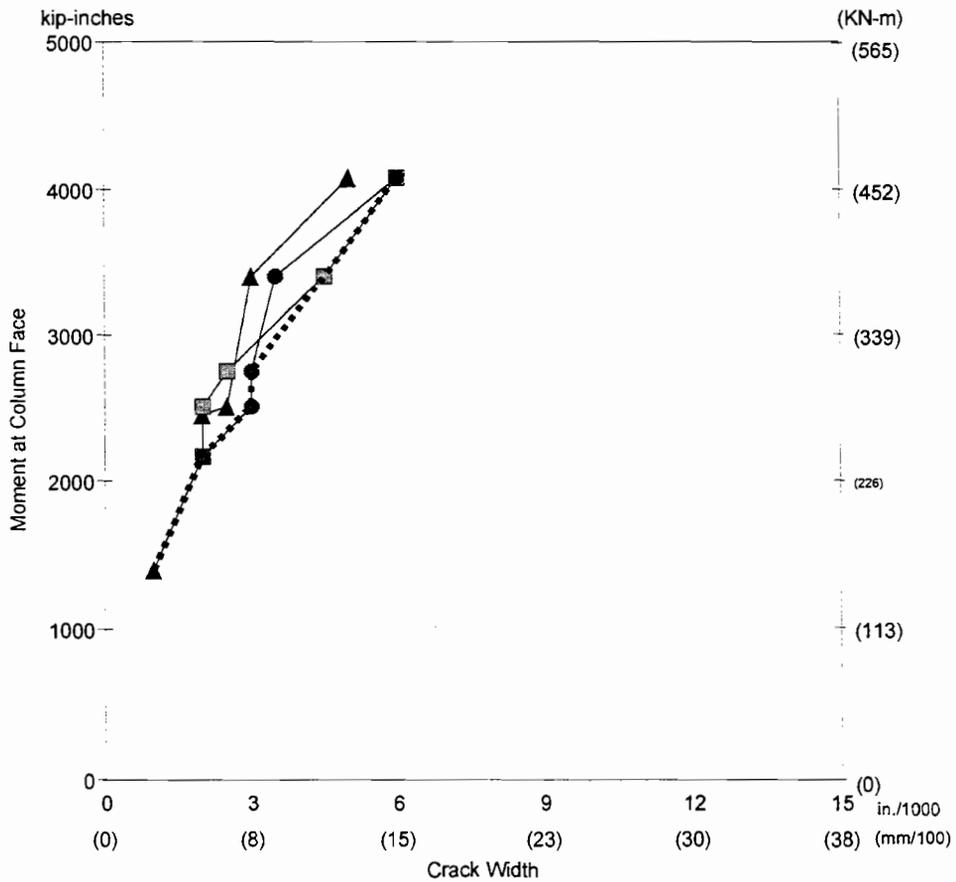
Figure 4. 5   "Crack Width Envelope" for the south CO-RU-0S-OR-N-SF
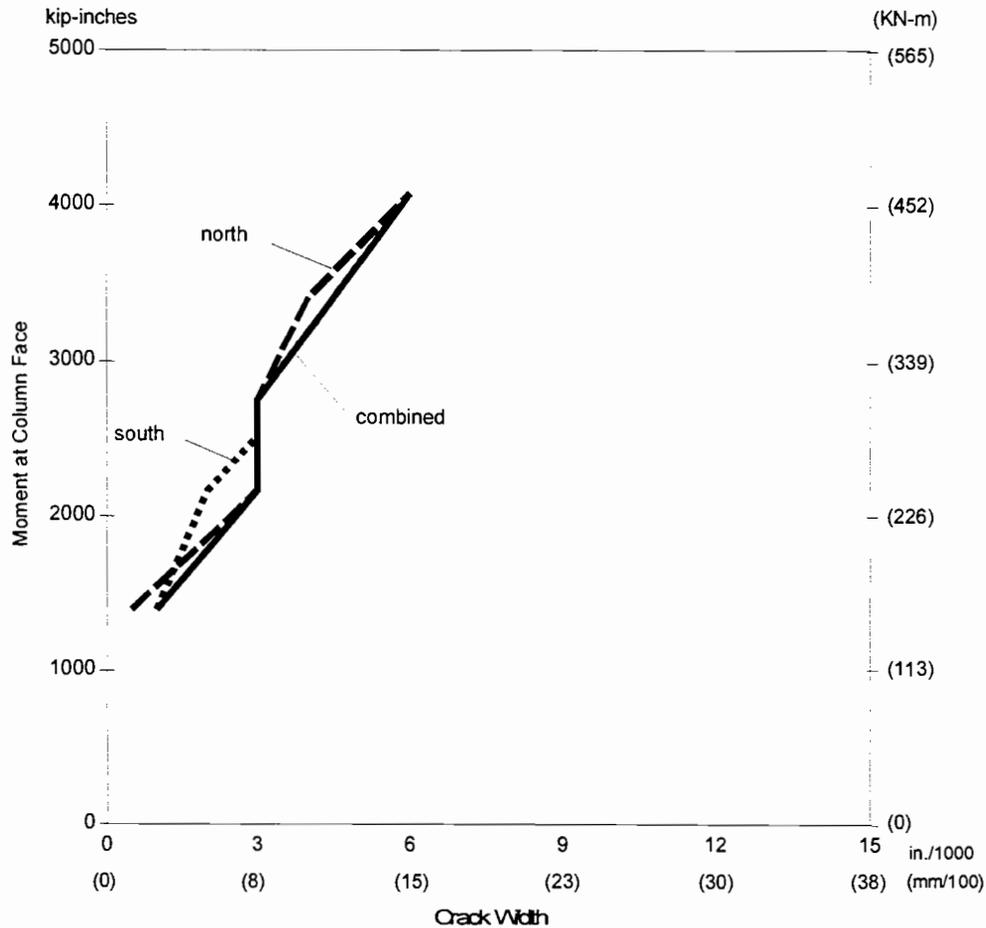
Figure 4. 6   Combined "Crack Width Envelope" for the north and south CO-RU-0S-OR-N-SF overhangs

Comparison of the overhang crack width envelopes based on virgin loading for some of the specimens of this series is shown in Figure 4.7. In this plot the level of service flexure moment, 2749 k-in (34 kN-m), and the acceptable AASHTO service load crack width for moderate exposure have been indicated. Any crack width envelope passing below the line of service flexure moment and right of the line of acceptable crack width is violating the limiting crack width, as set (indirectly by a z factor as discussed later) in the AASHTO provisions (16) for reinforced concrete structures under moderate exposure conditions. In viewing Figure 4.7 it must also be realized that since the level of accuracy of crack readings was 0.0005 in. (0.013 mm) the acceptable crack width of 0.0028 in. (0.071 mm) should be rounded to 0.003 in. (0.76 mm) when comparing with measurements. Thus, the crack width limit is shown as a shaded bar between the theoretical 0.0028 in. (0.071 mm) and the experimental equivalent 0.003 in. (0.076 mm).

It should be emphasized that there is still not a clear definition in the AASHTO Standard Specification (16) as to what should be an adequate limiting value for
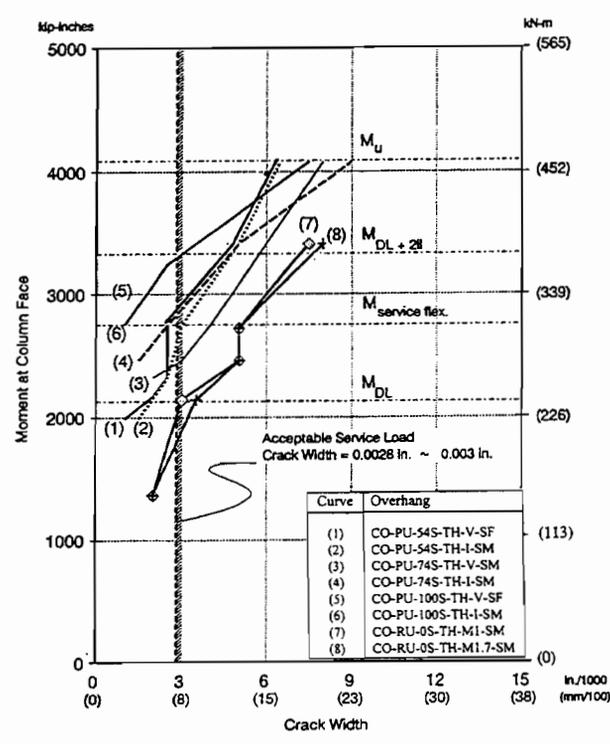
Figure 4. 7   Comparison of overhang "Crack Width Envelopes" based on "virgin" loading curves

maximum crack widths of concrete structures designed with a mixture of prestressed and non-prestressed reinforcement. A discussion in this sense, including comparison of provisions in different codes of practice, is presented in Section 4.2.3. In this section, results are compared only against current provisions of the AASHTO code for serviceability of reinforced concrete structures under service loads.

AASHTO provisions for reinforced concrete structures recommend for members in moderate exposure conditions that the factor "z' in Equation 4.1 should not exceed 170 k-in (29.8 kN-m).

$$z = f_s (d_c A)^{1/3} \qquad (4.1)$$

where:

z = quantity limiting distribution of flexural reinforcement
f_s = tensile stress in reinforcement at service loads $\sim 0.6\ f_y$
f_y = specified yield strength of reinforcement
A = average effective concrete area surrounding a reinforcing bar
d_c = thickness of concrete cover measured from extreme tension fiber to center of the closest bar or wire

150

Using the expression proposed by Gergely and Lutz (as included in the ACI-318-89 code, Section 10.6.4 (17), Equation 4.2, this value of z corresponds to a crack width of 0.0155 in. (0.397 mm) for the prototype structure and 0.0028 in. (0.071) mm) for the models at 1/5.5 scale.

$$w = 0.076 \, \beta \, f_s \, (d_c A)^{1/3} \qquad (4.2)$$

where:

$w =$ crack width in units of 0.001 in

$\beta =$ 1.2 for beams

A, f_s and $d_c =$ as defined above

Analyzing the data shown in Figure 4.7 it can be observed, considering an accuracy of ± 0.0005 in. (0.013 mm) in all crack width readings, that at service flexure load levels, the non-prestressed concrete overhangs (CO-RU-0S-TH-M1&M1.7-SM) greatly exceeded the crack limit at service load. Of the prestressed concrete overhangs, only the model CO-PU-74S-TH-V-SM exceeded the allowable value of 0.0028 in. $\approx$ 0.003 in. (0.07 mm) at service flexure load levels and even that model exceeded the quite arbitrary limit by only approximately 25 percent. Models CO-PU-54S-TH-V&I as well as model CO-PU-74S-TH-I performed well with values at the limit or close to the limit at service flexure loads. For models CO-PU-100S-TH (V&I), since they were uncracked at service flexure loads, their performance in terms of crack widths was obviously very good. After service loading, crack widths in these models were approximately 33 percent smaller than those from the other specimens at the same load levels. All models showed similar rates of increase of crack widths with respect to loading.

Comparison of all overhang crack width envelopes, based on "Complete Loading", is shown in Figures 4.8 and 4.9. T-head reinforcement specimens are separated for clarity. Examination of Figure 4.8, the eight overhangs without T-headed reinforcement, shows that the maximum crack widths (0.003 in., 0.07 mm) at service flexure loads for the CO-RU, CO-PU-74S-V, and CO-PU-74S-I overhangs, the only overhangs cracked at service loads are essentially equal to the acceptable width.

Figure 4.8 also reveals the variation in ability of each overhang to control crack widths at load above service loads. At factored loads, M_u, the maximum width occurred in the CO-PU-100S-V overhangs which had the least number of non-prestressed reinforcing bars of all of these overhangs. The CO-PU-100S-I and CO-PU-74S-V overhangs had the next largest width followed closely by the CO-PU-74S-I overhang. The improved ability of these overhangs to control crack widths at factored loads is due to the increased quantities of mild steel reinforcement. The CO-RU and CO-PS-100S overhangs had the smallest crack widths at factored loads, again because of the large amount of mild steel reinforcement in these overhangs. Crack width at factored loads is a fairly meaningless value in view of the very high dead load moments which are factored.
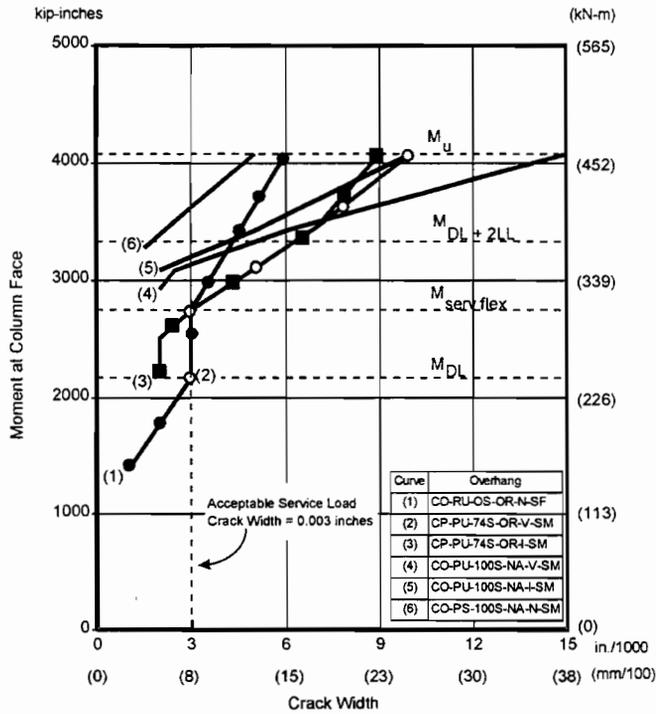
Figure 4. 8 "Crack Width Envelopes" for "complete" loading for all overhangs without T-head reinforcement
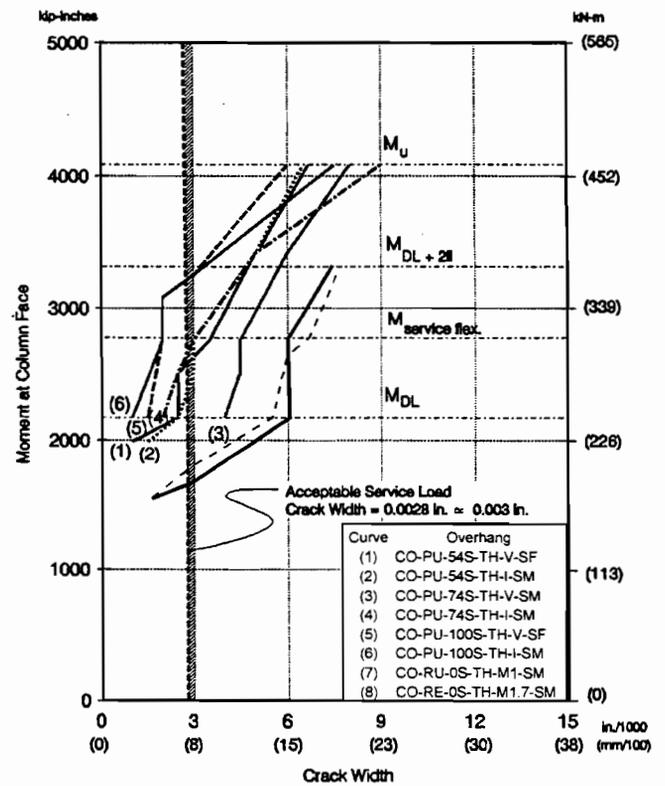
Figure 4. 9 "Crack Width Envelopes" for "complete" loading for all overhangs without T-head reinforcement

At less severe, and more feasible, overload conditions of dead load plus two times the service flexure live load, the CO-RU and CO-PU-100S overhangs performed about the same with crack widths about 150 percent of the AASHTO service level limit. The CO-PU-74S overhangs had crack widths about twice the AASHTO service level limits. Considering the elevated load levels these are quite well controlled. The CO-PS-100S overhang had the smallest widths being less than the AASHTO service level values under this overload.

Figure 4.9 shows the crack width envelopes for all overhangs with T-headed bars after various superimposed load cycles or "complete" loading. In contrast to the non-prestressed overhangs shown in Figure 4.8, Figure 4.9 indicates that the non-prestressed overhangs CO-RU-0S-TH-M1&M1.7-SM had crack widths twice as large as the AASHTO maximum at service load levels and, in fact, had very excessive crack widths even under dead load. Recall that this specimen was designed using the nominal yield strength rather than the actual yield strength. This resulted in approximately 20 percent more #2 bars in the T-headed specimens. In spite of this dramatic increase in the number of mild reinforcement bars, the crack widths were much wider at dead load, service load and moderate overload (DL + 2LL). This is because the maximum crack widths occurred not at the level of the main tensile reinforcement, but at approximately 1/3d from the top of the specimen at the column-beam interface. At that juncture the side face reinforcement was placed inside the column cage rather than outside the column cage. This increased the clear cover to 1.1 in. (28 mm) rather than the 0.4 in. (11 mm) which was the design value and the effective value away from the beam-column intersection. The next larger crack had only a 0.004 in. (.1 mm) value at service load. This indicates two weaknesses of the present crack width provisions. Increased cover protects the bar but results in *wider* surface cracks. The crack width approach using the "z" factor in AASHTO incorrectly addresses cover. The second problem is that the "z" approach is for the main flexural reinforcement and when the maximum crack occurs away from this steel, the skin reinforcement provisions do not include crack width. In this connection it is important to note that the non-prestressed specimen 1, which had side face reinforcement based on the Frantz criteria, was successful in controlling the maximum crack width at service levels even though it also had the side face reinforcement inside the column steel cage and hence greater effective cover (Figure 4.8, Curve 1). The non-prestressed specimen of Figure 4.9 (Curves 7-8), which had excessive width cracks, did not follow the Frantz criteria for side face reinforcement, but rather had the TxDOT minimum side face steel. This indicates the importance of proper side face reinforcement design. With the exception of CO-PU-74S-TH-V-SM, all prestressed specimens basically met the crack width criteria at service load levels and explicit control of cracking at service load levels does not seem to be a problem for the fully or partially prestressed specimens. An important observation when analyzing the results from all of these specimens is that the major cracks in the overhangs generally originated and propagated in the beam structure very close to the column face. In this region, because of the way the models were constructed (placing the overhang non-prestressed flexural bars inside of the column cage) a larger side cover existed, which corresponded to approximately double that assumed in design of 0.41 in. (10.4 mm). Since cover thickness is an important variable affecting crack widths, this factor was considered a contributory cause of the very large crack widths observed in that area.

4.2.2 Predictions Versus Test

Determination of the most probable maximum crack width on the tension face of the overhangs was carried out with the use of three equations. The first was introduced before as Equation 4.2 which is utilized indirectly in the ACI 318 Building Code (17). This equation was originally recommended by Gergely and Lutz (18), and was simplified for design purposes by ACI. The second equation, Equation 4.3, is actually the original equation suggested by Gergely and Lutz. The third equation, Equation 4.4, corresponds to an improved equation also suggested by those investigators (18).

As reported by Gergely and Lutz, Equation 4.4 is the preferred equation for the calculation of the most probable maximum crack width on the tension face of the beam. Equation 4.3 was suggested, and later utilized by ACI, because it was slightly simpler than Equation 4.4, recognizing that results may not be quite as good.

$$w = 0.076 \frac{h_2}{h_1} f_s \, (d_c A)^{1/3} \tag{4.3}$$

$$w = 0.091 \frac{h_2}{h_1} (f_s - 5)(d_c A)^{1/3} \tag{4.4}$$

where:

$\quad$ w = $\quad$ crack width in units of 0.001 in.

$\quad$ A = $\quad$ A_e/m: average effective concrete area around a reinforcing bar, in^2

$\quad$ A_e = $\quad$ 2b'(h-d): effective area of tension concrete surrounding tensile reinforcement, in^2

$\quad$ m = $\quad$ Number of tensile reinforcing bars

$\quad$ b' = $\quad$ width of beam at centroid of tensile reinforcement, in.

$\quad$ h = $\quad$ overall depth of beam, in.

$\quad$ d = $\quad$ effective depth of beam to centroid of tensile reinforcement, in.

$\quad$ d_c = $\quad$ thickness of concrete cover measured from extreme tension fiber to center of bar or wire located closest thereto, in.

$\quad$ f_s = $\quad$ steel stress in non-prestressed reinforcement calculated by elastic cracked section theory, ksi

$\quad$ h_2 = $\quad$ h - kd

$\quad$ h_1 = $\quad$ d - kd

$\quad$ k = $\quad$ distance from neutral axis to compression face divided by the effective depth of beam

Equations 4.2 to 4.4 were developed for reinforced concrete structures. To apply them to prestressed concrete structures some modifications had to be made. To this

end, variables involved were manipulated until acceptable predictions were obtained when compared to test results.

For the calculation of A (average effective concrete area surrounding a reinforcing bar), the factor m (number of bars) was calculated using three different methods:

a) Considering the actual number of all non-prestressed bars in the tension zone, independent of the size of those bars; and considering the post-tensioning tendon as if it were a non-prestressed bar of the largest size of non-prestressed reinforcement present.

b) Considering the total area of steel in the tension zone, including the area of all prestressed reinforcement (irrespective of the degree of prestress as recommended by Suri et. Al. (19) and all non-prestressed reinforcement, and dividing that total area of reinforcing steel by the area of the largest size non-prestressed reinforcement bar present, and

c) Considering the total area of non-prestressed reinforcement in the tension zone, adding an equivalent area for the post-tensioning tendons as if they were non-prestressed bars of the largest size non-prestressed reinforcement present, and dividing that total area of reinforcing steel by the area of the largest size non-prestressed reinforcement bar present.

This analysis was performed using test results from models with 54 and 74 percent of the tensile reinforcement prestressed. Models with 100 percent of the tensile reinforcement prestressed were not considered since these overhangs were uncracked at service load level. Table 4.2 shows the results after the comparison of the three options. To obtain these results all other variables involved in the crack width calculations were maintained constant. As can be noticed, options a) and b) gave, in general, the best predictions. The exception was observed when using option b) for model CO-PU-74S-TH-V-SM where the prediction differed considerably from test results. Considering that option a) was consistent and gave acceptable predictions which were mostly conservative, had an average ratio of 0.93 and is simple to use, this was the procedure recommended.

In addition to the above, two other variables were studied to adapt the Gergely and Lutz expressions to post-tensioned structures. These were the steel stress and the effective depth of beam. For these variables it was not necessary to test several options since the first trial gave very good results. The first, the steel stress, was taken as the steel stress in the non-prestressed reinforcement calculated by elastic cracked section theory, irrespective of the effective prestress in the tendons. The second, the effective depth, was calculated based on the location of the centroid of the primary flexural reinforcement (ignoring skin steel).

Based on the results shown in Table 4.2, it can be concluded that the use of any of the three expressions for the prediction of the most probable maximum crack widths can be applied with reasonable accuracy to structural concrete if the modifications are considered. It has to be recognized that scatter in crack widths is always very large even in ordinary reinforced concrete structures (18). In fact, in the derivation of

*Table 4. 2   Values of Test vs. Predicted Maximum Crack Widths Based on Three
Options to Account for Prestressed and Non-Prestressed Reinforcement*

Model	Ratio of Test to predicted Crack Width*		
	Option a)	Option b)	Option c)
CO-PU-74S-OR-V-SM	0.73	0.72	0.73
CO-PU-54S-TH-V-SF	0.89	0.92	0.89
CO-PU-54S-TH-I-SM	0.89	0.89	0.81
CO-PU-74S-OR-I-SM	0.97	0.94	0.97
CO-PU-74S-TH-V-SM	1.1	1.32	1.1
CO-PU-74S-TH-I-SM	0.93	0.97	0.90

*Test results based on complete loading.

the Gergely and Lutz expression (Equation 4.2) 10 percent of the data exceeded 1.5 times the crack width predicted by the equation, while two percent were less than 0.5 times the calculated with (18).

In summary, recommendations to apply the Gergely and Lutz expressions to structures with a mixture of prestressed and non-prestressed reinforcement are:

a) For the calculation of A, the effective area of concrete surrounding the tension reinforcement, it is recommended to use the actual number of non-prestressed bars present in the tension zone, and then add to that number an equivalent non-prestressed bar of the largest size present to account for each bonded prestressed strand.

b) The steel stress should be that for the non-prestressed reinforcement calculated by elastic cracked section theory.

c) The effective depth of beam should be calculated based on the primary flexural reinforcement (ignoring skin steel).

It has to be clear that results presented herein refer to models using single straight strands as tendons. It is not known at this stage if these results could be extrapolated to models with multi-strand tendons or with high strength bars instead of strands.

For the procedure above, steel stresses were determined using a program in the form of a spreadsheet. The program was developed by Bradley Wood specifically for the models in this series.

4.3 CRACK WIDTH LIMITS — SERVICE LIMIT STATE

The purpose of this section is to provide and compare provisions in different codes of practice with respect to crack width limits in structural concrete structures. No attempt is made to define, from basic performance characteristics such as corrosion protection, what should be an adequate limiting value for maximum crack widths in concrete structures designed with a mixture of prestressed and non-prestressed reinforcement. Such a study is outside the scope of the present study but is important and should be undertaken.

In the previous sections, test results were compared against the allowable maximum crack width at service load level based on current AASHTO Standard Specifications

for Highway Bridges (16) for the serviceability of ordinary reinforced concrete structures under moderate exposure conditions. This was done basically because TxDOT typically bases their bridge designs on the AASHTO Specifications and these do not yet provide provisions for concrete structures designed with a mixture of prestressed and non-prestressed reinforcement. The limiting value for the maximum crack width was calculated as 0.0155 in. (0.394 mm) for the prototype structure and 0.0028 in. (0.071 mm) for the models, assuming linear scaling of cracks as proposed by Borges and Lima (20).

When studying the serviceability requirements in the AASHTO Specifications, it is important to recognize that AASHTO also provides more strict limits for those structures which would be subjected to severe exposure conditions. In this case the AASHTO Specifications recommend that the value of "z", as shown in Equation 4.1 above, should not exceed 130 kips per inch (23 kN-mm), corresponding to a calculated crack width of 0.0119 in. (0.302 mm) for the prototype structure and 0.0022 in. $\sim$ 0.002 in. (0.055 mm) for the models.

In a like manner, provisions in the ACI-318 Building Code, in terms of crack width limits, are also expressed exclusively for the treatment of non-prestressed reinforced concrete structures. The ACI Code recommends maximum values of z of 175 kips per inch (31 kN-mm) for interior exposure and 145 kips per inch (25 kN-mm) for exterior exposure, which correspond to maximum crack widths of 0.016 in. (0.406 mm) and 0.013 in. (0.330 mm) for the prototype structure; and 0.0029 in. $\sim$ 0.003 in. (0.074 mm) and 0.0024 in. $\sim$ 0.0025 in. (0.060 mm) for the models, respectively.

To date, US bridge or building design codes have not specifically addressed limits for maximum crack widths in concrete structures using a mixture of prestressed and non-prestressed reinforcement for flexure, which have been designed using the ultimate strength approach. In fact, these structures are not yet explicitly allowed under those standards. It is clear, though, that crack widths in these structures should probably not exceed the limits for ordinary reinforced concrete structures. Moreover, it is anticipated that when considering the higher vulnerability of prestressed reinforcement to corrosion and the high level of risk that is involved, those limitations should possibly be more severe.

Looking at the Canadian Standards Association code (CSA Committee A23.3, Design of Concrete Structures for Buildings 1984 (21)), it is observed that this code already includes some provisions for structures designed with a mixture of prestressed and non-prestressed reinforcement. With respect to crack width limits, maximum values of z of 117 kips per inch (20 kN-mm) for interior exposure and 88 kips per inch (15 kN/mm) for exterior exposure are recommended. These values represent 67 percent and 60 percent, respectively, of those limits established by the CSA code and the ACI 318 code, since limits in both are the same for conventionally reinforced concrete structures. In terms of crack widths, these values correspond to 0.011 in. (0.270 mm) and 0.008 in. (0.200 mm) for the prototype structure and 0.002 in. (0.051 mm) and 0.0014 in. (0.37 mm) for the models.

In the same way, the current European Standard, CEB-FIP Model Code for Concrete Structures 1990 (22), developed by the Comité Euro-International du Béton, also establishes some limits on maximum crack widths for mixed reinforced concrete structures (Section 7.4). In this code instead of checking for full service load crack widths as in AASHTO, ACI, and CSA, checks are performed with respect to the "frequent load level," which includes the dead load plus the frequently occurring live load. Using recommendations for parking areas, since this code does not explicitly provide provisions for bridge structures, the frequent load combination corresponds to 70 percent of the characteristic live load (the latter is the value which is not likely to be exceeded during more than five percent of the projected life of the structure). Recommendations in the CEB code in terms of crack width limits for post-tensioned members are summarized in Table 4.3. It can be noticed that for a structure that is to be in a humid environment, this code recommends the same crack width limit as the CSA code of 0.008 in. (0.2 mm).

It has to be recognized that the CEB-FIP 1990 Code has not yet been adopted for actual operational codes in Europe. Instead, the CEB-FIP 1978 Code (23) is being used as the base for Eurocode 2. Table 4.4 summarizes the recommendations in that earlier version of the CEB-FIP Code. As can be observed in these tables, exposure conditions were modified in the latest version as well as the maximum crack width limits. For example, for a structure under usual exterior exposure conditions without frost or deicing agents, the CEB-FIP 78 provisions recommend a maximum crack width limit of 0.004 in. (0.1 mm). This is half the value that now is recommended for the same structure in the CEB-FIP-90 Code. Both sets are very stringent when compared to the AASHTO and ACI values.

Table 4. 3   *Summary of CEB-FIP-90 Crack Width Limits for Post-Tensioned Structures under Frequent Load Combinations*

Exposure class	Limiting crack width**	
	in.	(mm)
1. Dry environment	0.008*	(0.2)
2. Humid environment	0.008*	(0.2)
3. Humid environment with frost and de-icing agents. 4. Sea-Water environment	a) No tension is allowed within the section, or b) if tension is accepted, impermeable ducts or coating of the tendons should be applied; in this case wlim = 0.008 in. (0.2 mm)*	
5. Aggressive chemical environment	No tension is allowed within the section.	

* Corresponding limit in models at a 1/5.5 scale is 0.0014 in. (0.036 mm)
** For a cover equal to the minimum recommended by CEB.

158
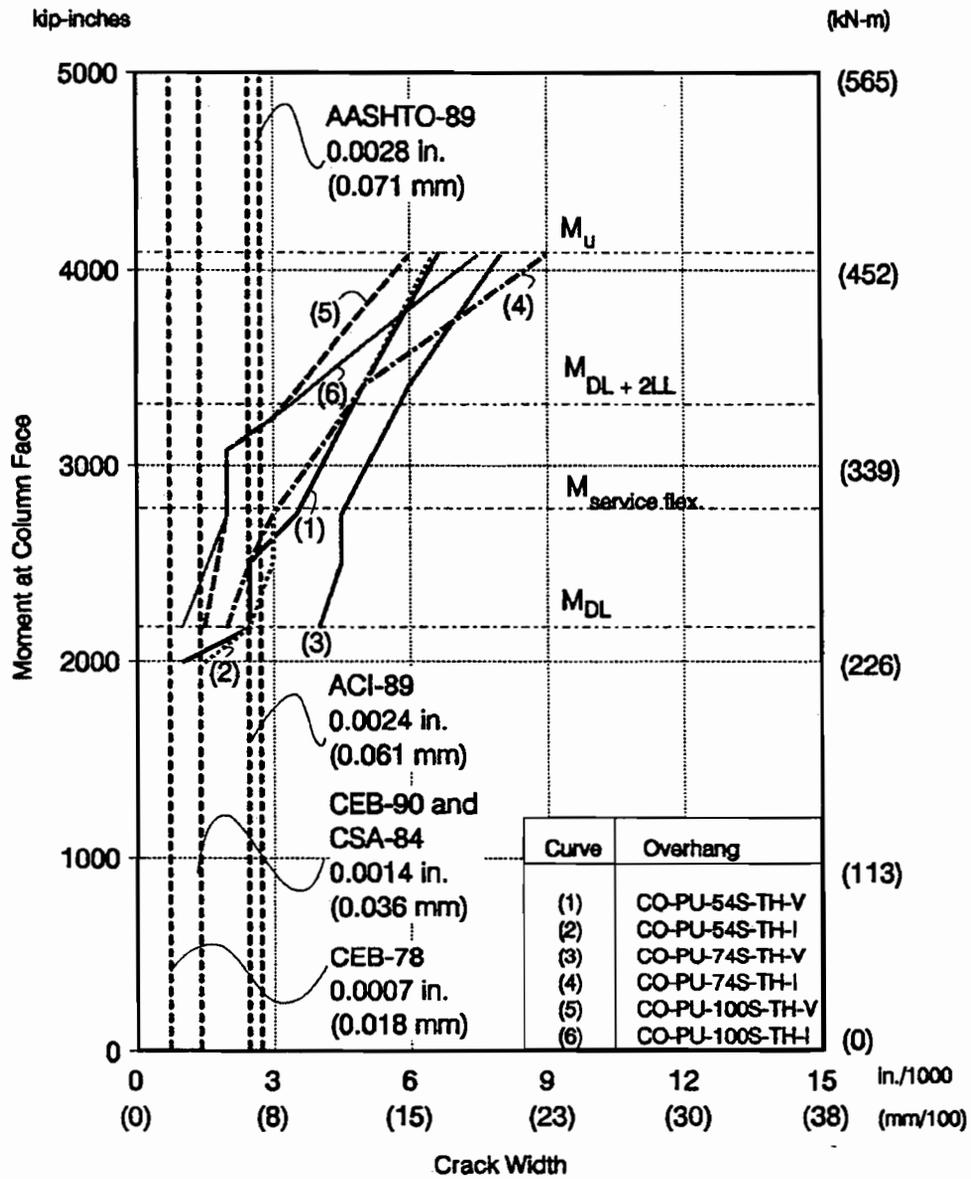
Figure 4. 10 "Crack Width Envelopes" for "complete" loading for all over-hangs without T-head reinforcement

To visualize how these crack width limits compare with test results, Figure 4.9 (which was presented before showing the comparison of overhang crack width envelopes for the T-head specimens based on complete loading curves) is reproduced in Figure 4.10. In this case controlling limits for maximum crack widths from each of the various standards are included. Controlling exposure conditions for the subject structures were selected corresponding to moderate exposure, exterior exposure, or dry or humid environment depending on the code.

Analyzing the results in this figure and applying the same limits to the non-T-head specimens shown in Figure 4.8 while considering an accuracy in the crack width readings of ± 0.0005 in. (0.013 mm), it can be observed that only the 100 percent prestressed overhangs met most of the codes, except for the CEB-FIP-78 where even the 100 percent T-head overhang models were marginally above the limit. Fifty-four and 74 percent prestressed models were approximately 200 to 300 percent above the limiting value set in CEB-FIP-90 and CSA.

As can be noticed, crack width limits as established by the CEB-FIP-90 and the CSA codes were the same for these structures (designed with a mixture of prestressed and non-prestressed reinforcement) and corresponded to approximately half of the limiting values set in AASHTO and ACI, which are provisions exclusively for reinforced concrete structures. CEB-FIP-78 code provisions were much more severe, corresponding, in this case, to a maximum crack width limit of half that proposed in the new CEB-FIP-90 and CSA codes. This plot clearly shows the concern in those foreign codes for the presence of cracks in structures with any amount of prestressed reinforcement.

When analyzing the results above, it has to be recognized that the CSA crack width limits for structures designed with a mixture of prestressed and non-prestressed reinforcement, which would be under exterior exposure conditions, could be influenced by the widespread use of salt due to the severe climate. In much of Texas, for example, those limits could possibly be much less severe.

4.4 PERFORMANCE OF SKIN REINFORCEMENT — SERVICE LIMIT STATE

Results from various models, which were designed and detailed using different amounts of skin reinforcement, were compared and evaluated to determine the differences that the various amounts of face steel made in controlling crack widths at service load levels, and in general to evaluate skin reinforcement performance on the overall behavior of the specimens.

Since skin reinforcement has as a main purpose the control of cracking on the side face of a deep member away from the level of the main reinforcement, it can be judged successful if the maximum crack width at service flexural limit state (α + LL) occurs in the top-most reinforcement layers, rather than closer to mid-height. If the overhang is uncracked at service load levels, one cannot determine the effectiveness of side face or skin reinforcement.

All specimens were designed with some skin reinforcement. Four overhangs had the higher amount of skin reinforcement recommended by Frantz and Breen (5) and

required by the ACI Building Code (7) and AASHTO (16). All other specimens had a lesser amount based on the TxDOT practice for design of large overhangs.

Table 4. 4   Summary of CEB-FIP-78 Crack Width Limits for Post-Tensioned Structures under Frequent Load Combinations [23]

Exposure Conditions		Limiting Crack Width***	
		in.	(mm)
I.	Mild Interior Exposure Low humidity exterior exposure	0.008*	(0.2)
II.	Moderate High humidity or slightly corrosive interior exposure Running water Ordinary soil exposure Usual exterior exposure	0.004**	(0.1)
III.	Severe Seawater exposure Deicing chemicals Corrosive gases and soils	No tension allowed in concrete	No tension allowed in concrete

*   Corresponding limit in models is 0.0014 in. (0.036 mm)
**   Corresponding limit in models is 0.0007 in. (0.018 mm)
***   For a cover equal to the minimum recommended by CEB

Based on Frantz	Based on TxDOT
CO-RU-0S-OR-N-SF	CO-PU-74S-OR-V-SM
CO-RU-0S-OR-N-SF	CO-PU-74S-OR-I-SM
CO-PU-54S-TH-V-SF	CO-PU-54S-TH-I-SM
	CO-PU-74S-TH-V-SM
	CO-RU-74S-TH-I-SM
	CO-RU-0S-TH-M1-SM
	CO-RU-0S-TH-M1.7-SM

The crack patterns for these 10 overhangs at service flexure loads are shown in Figure 4.11. Careful examination shows two trends. In the prestressed specimens (note the 100 percent prestressed specimens had no cracking at service load levels), the maximum crack width is at the top of the overhang regardless of whether the Frantz and Breen minimum or the TxDOT minimum was provided. This suggests that the skin reinforcement minimum need not be strictly applied to prestressed members. However, in the four non-prestressed overhangs, the maximum crack width is not at the top face. In the two overhangs with the TxDOT minimum bars (Figure 4.11 i and j), all four maximum crack openings are near mid-depth. In contrast, in the two non-prestressed overhangs with the Frantz and Breen amount of side face reinforcement (Figure 4.11 a and b), five of the seven maximum crack width locations were on the top face or immediately below the main reinforcement while the other two locations were around four inches closer to the main reinforcement than those shown in Figure 4.11, i and j, which used the smaller TxDOT reinforcement. This indicates that the

Frantz and Breen recommendation is generally effective and should be used for non-prestressed members.

A secondary purpose of the skin reinforcement is to control the side face cracking at higher load levels approaching full yield and failure and to ensure wide distribution of cracking (many small cracks rather than a few large cracks). Figure 4.12 shows the total number of cracks in each overhang at factored flexure load level, chosen so as to be an equal load on each specimen but certainly high enough to indicate cracking tendencies. Careful examination shows very little effect of side face reinforcement distribution (SF vs. SM). What is for more marked is the effect of the level of prestress. The higher the level of prestress, the lower the degree of cracking with the highest prestressing specimen (PS-100) having only single cracks in each overhang at factored flexural load levels.

A further direct comparison of the effect of skin reinforcement is available by comparing overhangs CO-PU-100S-TH-V-SF and CO-PU-100S-TH-I-SM. They are very much the same in main reinforcement but differ specifically in skin reinforcement.

As reported previously, these models first cracked above service flexure load level. For this reason it was obviously not possible to obtain any data with respect to the performance of skin reinforcement at service loads. In spite of that, an important contribution of the skin reinforcement, proportioned as per Frantz and Breen, was observed at high load levels up to ultimate loads. As shown in Figure 4.12, both models exhibited the same number of cracks at factored flexure load. At ultimate loads model CO-PU-100S-TH-V-SF showed approximately double the number of cracks. These results can be observed in Figure 4.13.

Based on the above discussion, it can be concluded that skin reinforcement for prestressed structures, designed as per Frantz and Breen, does not provide significant improvement for crack control at service and factored load levels. However, it provides a great deal of distribution of cracks above these loads up to ultimate. Considering that the distribution of cracks at these load levels is certainly beneficial and healthy (which provides a better distribution of the tensile forces in the horizontal steel and better overall ductility in the member), it is concluded that the minimum reinforcement suggested by Frantz and Breen should be used.

It is very important to recognize that recommendations by Frantz and Breen were actually developed for deep structure in which the maximum crack width would not occur in the extreme tensile fibers, as it did in the prestressed models tested as part of this series, but somewhere in the face of the structure between the locations of flexural reinforcement. In all prestressed models, the major crack width was at the level of the main flexural reinforcement. Thus, the skin steel provided in all models was sufficient to control side face cracking.
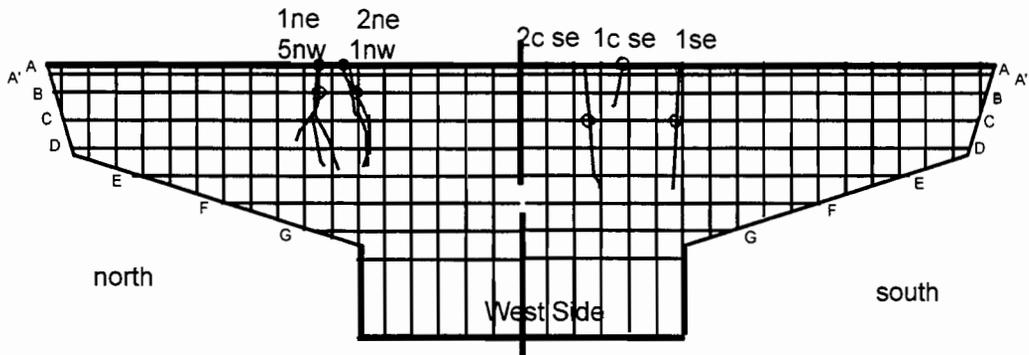
a) CO-RU-0S-OR-N-SF

b) CO-RU-0S-OR-N-SF
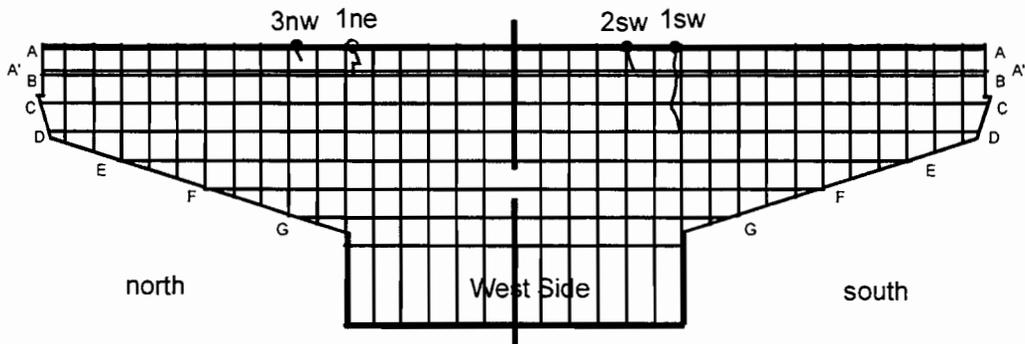
c) CO-PU-74S-OR-V-SM

d) CO-PU-74S-OR-i-SM

• location of maximum crack width on west side of specimen

○ location of maximum crack width on east side of specimen

Figure 4. 11 "Major" Cracks at Service Flexure Loads

163
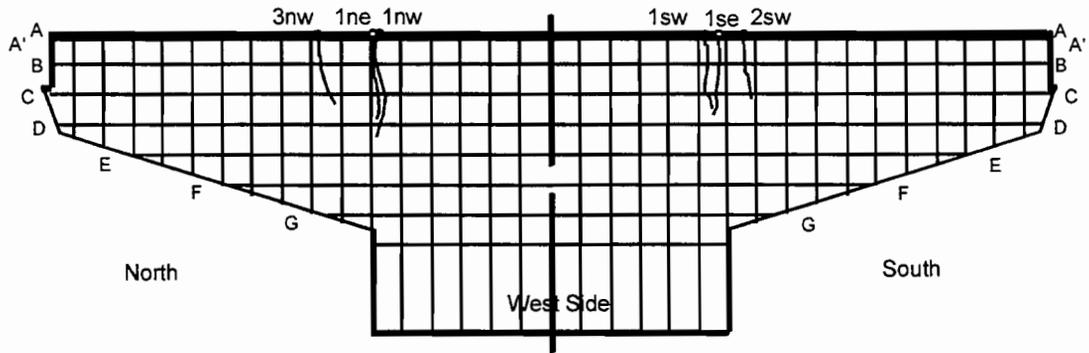
e) CO-PU-54S-TH-I-SM   f) CO-PU-54S-TH-V-SF
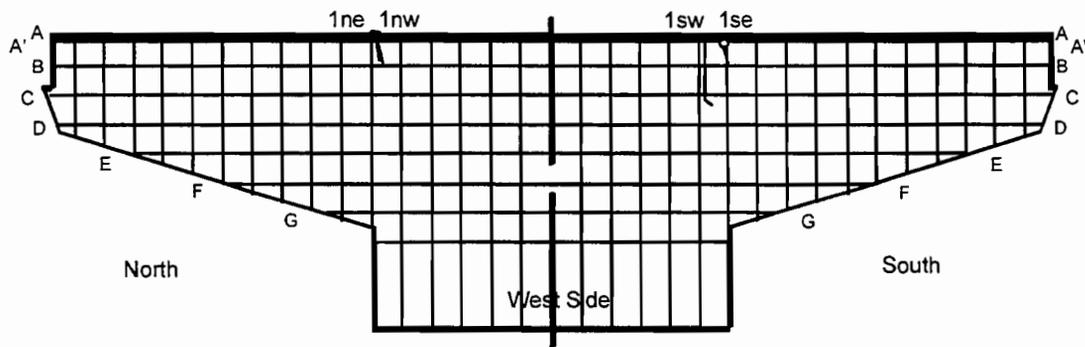
g) CO-PU-74S-TH-I-SM   h) CO-PU-74S-TH-V-SM

● location of medium crack width on west side of specimen

○ location of maximum crack width on east side of specimen

Figure 4. 11   "Major" Cracks at Service Flexure Loads (continued)
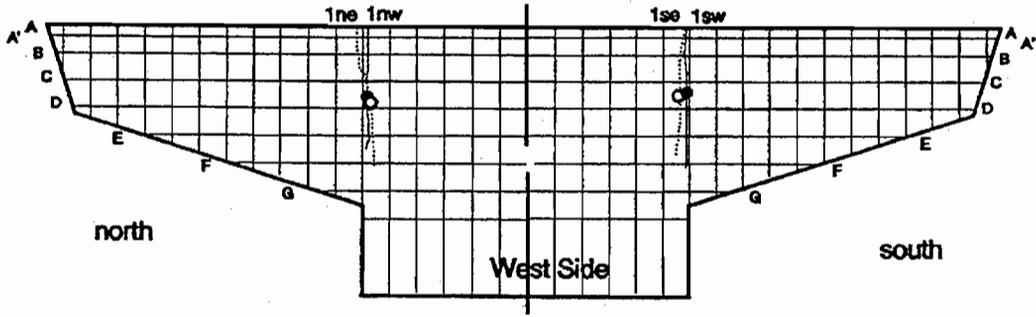
i) CO-PU-74S-TH-I   j) CO-PU-74S-TH-I

Figure 4. 11 "Major" Cracks at Service Flexure Loads (continued)
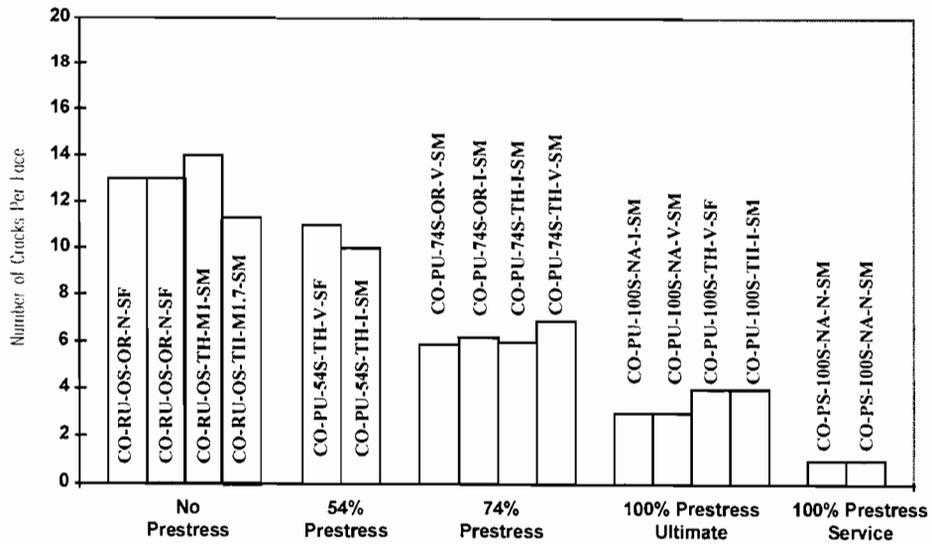
Figure 4. 12 Number of cracks at factored flexural load level
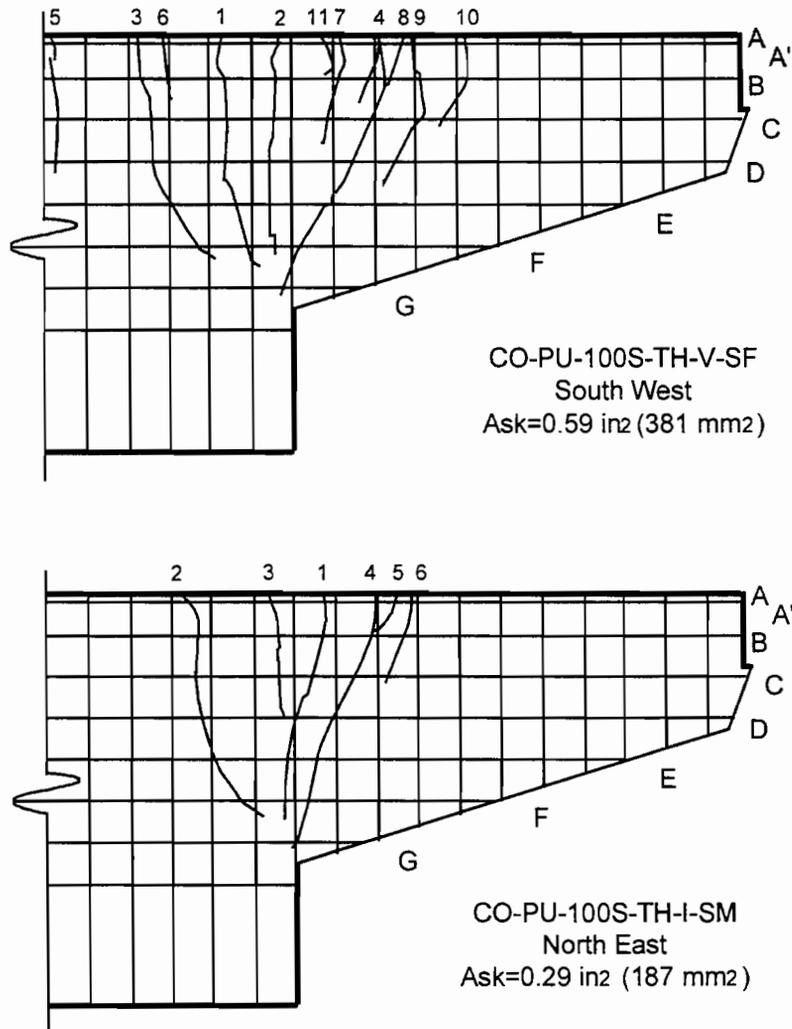
Figure 4. 13 Comparison of Crack Patterns in Models CO-PU-100S-TH-V-SF and CO-PU-100S-TH-I-SM at failure

4.5 DEFLECTIONS — SERVICE LIMIT STATE

Tip deflections for all overhangs at major load levels were summarized in Table 3.2. Deflection limits are assumed to be service load limit state values. Tabulated service load deflections were measured after several cycles of loading so that they include some cracking where appropriate. The comparison between the various overhangs and the effect of variables can be seen in Figure 4.14. Shaded areas are dead load deflections.

Allowable deflections, or more properly stated permissible deflections, at the service limit state for bridge structures have recently been suggested in the AASHTO LRFD Specifications (24). These apply to all concrete bridges and the suggested value for
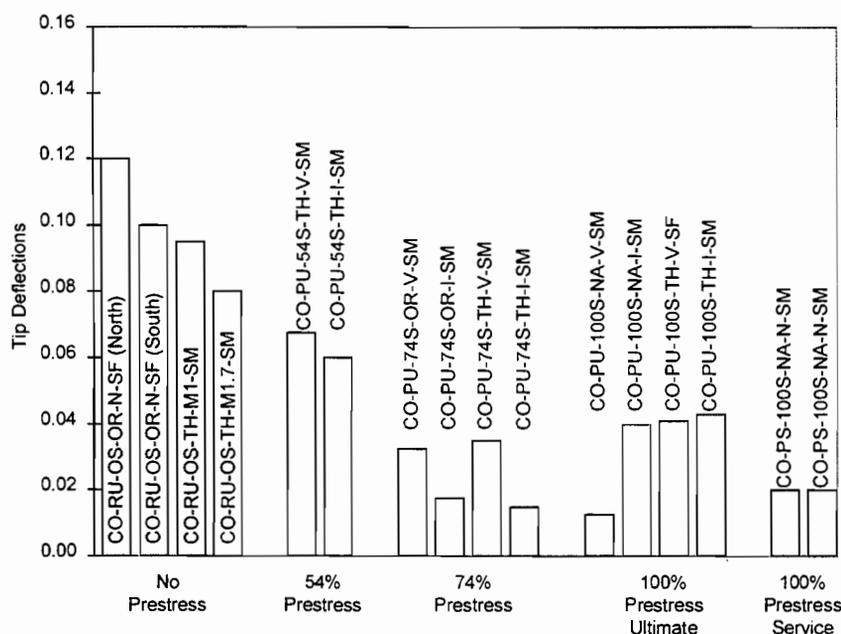
Figure 4. 14 Tip deflections at service flexure load level

live load or cantilever arms is $\ell/300$. Strictly speaking, this would be for superstructure girders but it is reasonable to expect stiffer substructure members. As one would expect, the non-prestressed overhangs have the largest service load deflection. The first two overhangs had f_y = 25 ksi and a reduced main reinforcement area compared to the next two overhangs which while using reinforcement with f_y = 25 ksi had the reinforcement quantity set by using the nominal values of f_y = 60 ksi. This resulted in over 20 percent more main flexural reinforcement which was stiffer when cracked. The average tip deflection of Specimen 1 is 125 percent that of Specimen 8 which is what would be expected. Note that Specimen 8 basically satisfies an $\ell/500$ criteria.

All of the prestressed concrete specimens have more stiffness and less deflection. The 54 percent prestress specimens are only somewhat better, being in the $\ell/750$ range. The 74 percent and 100 percent ultimate prestress specimens total live and dead load deflections easily meet the $\ell/1000$ value for live load only, while the traditional service stress fully prestressed specimen meet a $\ell/2000$ value. This is very stiff. If one looks at only the deflection due to live load, it is less than $\ell/1000$ for all non-prestressed specimens and less than $\ell/2000$ for all except one of the prestressed specimens. Deflections are thus no problem in these specimens.

4.6 FATIGUE STRESS RANGE — SERVICE LIMIT STATE

The values of change of tensile stressing the outermost layer of reinforcing bars or prestressing strains as the load is increased from the normal lower service value of dead load to the full service live load value are given in Table 4.5. For the non-prestressed overhangs the values are 8 ksi (55 - 58 MPa).

The acceptability of the stress ranges for the non-prestressed overhangs was evaluated on the basis of the current AASHTO criteria (16). AASHTO Equation (8-60) gives the maximum allowable stress range in customary units as

167

$$f_f = 21 - 0.33 f_{min} + 8(r/h) \qquad (4.5)$$

where

f_f =   stress range in ksi,

f_{min} =   algebraic minimum stress level = 31 ksi, and

r/h =   ratio of base radius to height of rolled on transverse deformations = 0.3.

From Equation 4.5 it was determined that the maximum allowable stress range, f_f, was equal to 13.2 ksi (91 MPa) which is greater than the calculated expected value of 8 ksi (55 MPa).

As shown in Table 4.5, the calculated stress ranges in the post-tensioning strand varied from a minimum of two ksi (14 MPa) in the CO-PS-100S overhang to a maximum of 18 ksi (124 MPa) in the CO-PU-74S-V overhangs. For post-tensioned strand in metal ducts, Wollmann et. Al. (11) have recommended a maximum stress range of 14.5 ksi (100 MPa) to ensure two million load cycles. The calculated stress ranges for all 54 or 100 percent prestressed overhangs were well below this value. However, the calculated stress ranges for the four CO-PU-74S overhangs were slightly to 25 percent above the recommended maximum level. The implication of this for design is that measures must be taken for these specimens to lower the expected stress range. This can be accomplished by adding additional mild reinforcement or by lowering the strand somewhat within the overhang. The latter would necessitate the use of a larger area of prestressed reinforcement. Since the 54 percent and 100 percent prestressed specimens met the criteria, a solution for the 74 percent case would be possible.

The maximum calculated service load stress level in the post-tensioning strand was 0.70 F_{pu} which occurred in four of the 54 and 74 percent overhangs. The current AASHTO specifications limit the maximum post-tensioning stress to 0.80 f_y^*. If f_y^* is taken as 0.90 F_{pu}, the maximum stress would be limited to 0.72 F_{pu}. On this basis, the maximum calculated stress level in the post-tensioning strand of all overhangs was acceptable.

4.7 DEFLECTION RESPONSE — STRENGTH LIMIT STATE

Comparisons of smoothed applied moment to tip deflection response for the eight overhangs taken to complete failure are given in Figure 4.15. For ease of reference the service limit state and the ultimate limit state moments are also indicated. The latter has been adjusted by dividing by ϕ = 0.90 since all dimensions and material properties are known for these laboratory specimens.

Table 4. 5 *Stress Ranges in Main Flexural Reinforcement at Service Load Levels and Strand Stresses at Full Service Load Level*

Specimen		Overhang Designation	Stress Range		f_{pt}/f_{pu} **
			ksi	MPa	
1	A	CO-RU-0S-OR-N-SF	8	55	----
	B	CO-RU-0S-OR-N-SF			
2	A	CO-PS-100S-NA-N-SM	2	14	0.60
	B	CO-PS-100S-NA-N-SM			
3	A	CO-PU-100S-NA-V-SM	10	69	0.63
	B	CO-PU-100S-NA-I-SM	9	62	0.63
4	A	CO-PU-54S-OR-V-SM	18	124	0.69
	B	CO-PU-74S-OR-I-SM	15	103	0.70
5	A	CO-PU-54S-TH-V-SF	13	88	0.70
	B	CO-PU-54S-TH-I-SM	12	84	0.70
6	A	CO-PU-74S-TH-V-SM	18	125	0.70
	B	CO-PU-74S-TH-I-SM	16	108	0.69
7	A	CO-PU-100S-TH-V-SF	8	54	0.62
	B	CO-PU-100S-TH-I-SM	8	58	0.63
8	A	CO-RU-0S-TH-M1-SM	8	56	----
	B	CO-RU-0S-TH-M1.7-SM	8	56	----

At service flexure load level, all specimens are quite stiff. Under combined dead plus live load, all have less than the $\ell/300$ deflection allowed for live load only under the AASHTO LFRD Provisions for superstructure cantilevers.

At the flexural factored load level, the two reinforced concrete specimens, the 54 percent prestressed and the 74 percent prestressed specimens, have around the same magnitude of tip deflection while the 100 percent prestressed specimens are stiffer. The 100 percent prestressed based on service load design is by far the stiffest.

A vivid contrast in ductility is indicated by the behavior of the two non-prestressed specimens at ultimate. CO-RU-0S-OR designed with some 25 percent less reinforcement than CO-RU-0S-TH-M1 actually develops a somewhat higher load and almost three times the deflection at failure of its heavier reinforced companion. The reason, of course, is that CO-RU-0S-OR had its shear design based on conservative strut and tie models while the companion counted on a concrete shear contribution to assist its lighter strut and tie reinforcement. This resulted in a premature shear failure in CO-RI-0S-TH-M1. All of the 54 percent, 74 percent and 100 percent (based on ultimate) specimens developed as much deformation at failure as the 100 percent prestressed (based on allowable stresses) specimen CO-PS-100S. Thus, their ductility is certainly acceptable since CO-PS-100S represents the type of specimen most likely to result from application of current AASHTO Specifications. Note that this service level design results in substantial over-design on a strength basis. The more rational designs with mixed non-prestressed and prestressed reinforcement result in ultimate loads closer to the desired factored load levels.

Since several of these curves represent specimens which had some loading restraint due to the omission of elastomeric bearing pads (steel bearings shown by asterisks on Figure 4.13) there is some question as to whether these curves would be greatly different if elastomeric pads were used on all specimens. The only direct comparisons are CO-PU-100-NA-V and CO-PU-100S-TH-I which have fairly similar shapes. It does not appear that there are big differences at ultimate due to the restraints. These tended to relieve a great deal with large deflections.
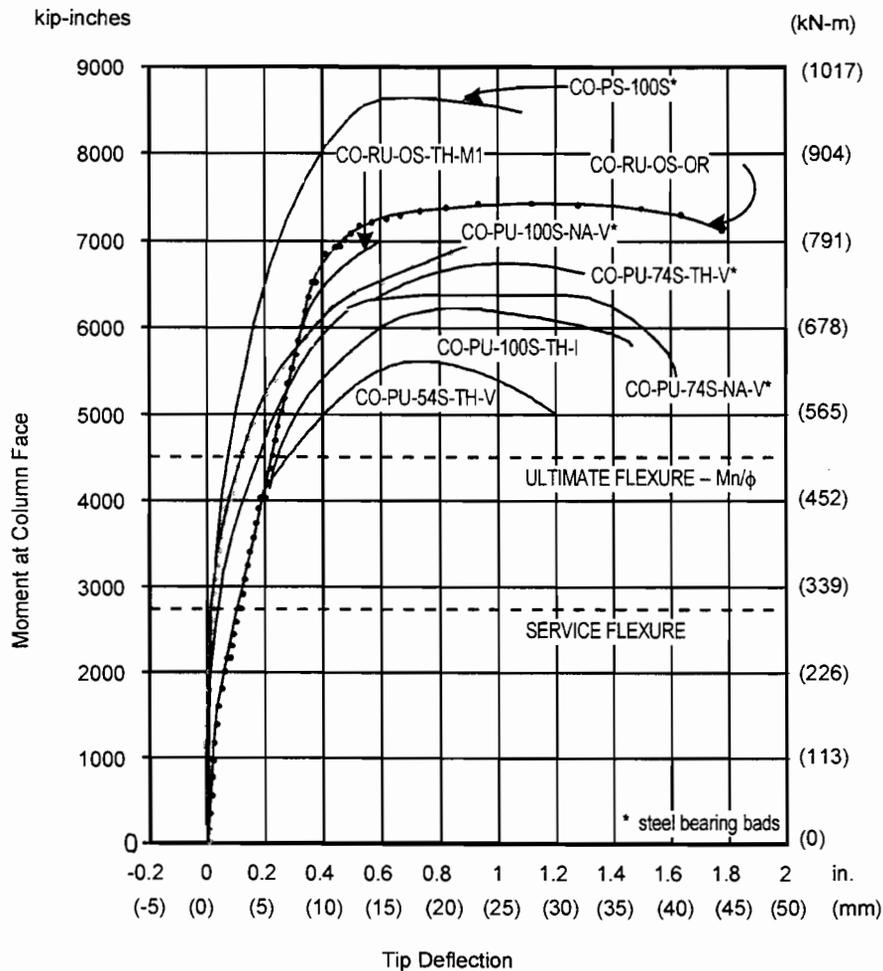
Figure 4. 15 Comparison of moment-deflection for overhangs taken to failure

4.8 ULTIMATE CAPACITY

The eight overhangs which were loaded to failure displayed substantial reserve strength. As shown in Figure 4.16, this varied from a low of about 33 percent excess to a high of over 90 percent excess. Since half of the specimens had elastomeric pads while half had steel bearing pads, and since several of the high ratios had elastomeric pads, this excess is not due to loading problems alone.

The nominal moment capacity for each specimen was calculated on several accepted basis. These ranged from the usual AASHTO flexural capacity equations to a strain compatibility analysis which considered the multiple layers of bars and strands as well as the side face steel which yielded in many cases. The results of these analyses and the ratios $M_{test}/M_{analysis}$ are given in Table 4.6. It can be seen that this calculation

170
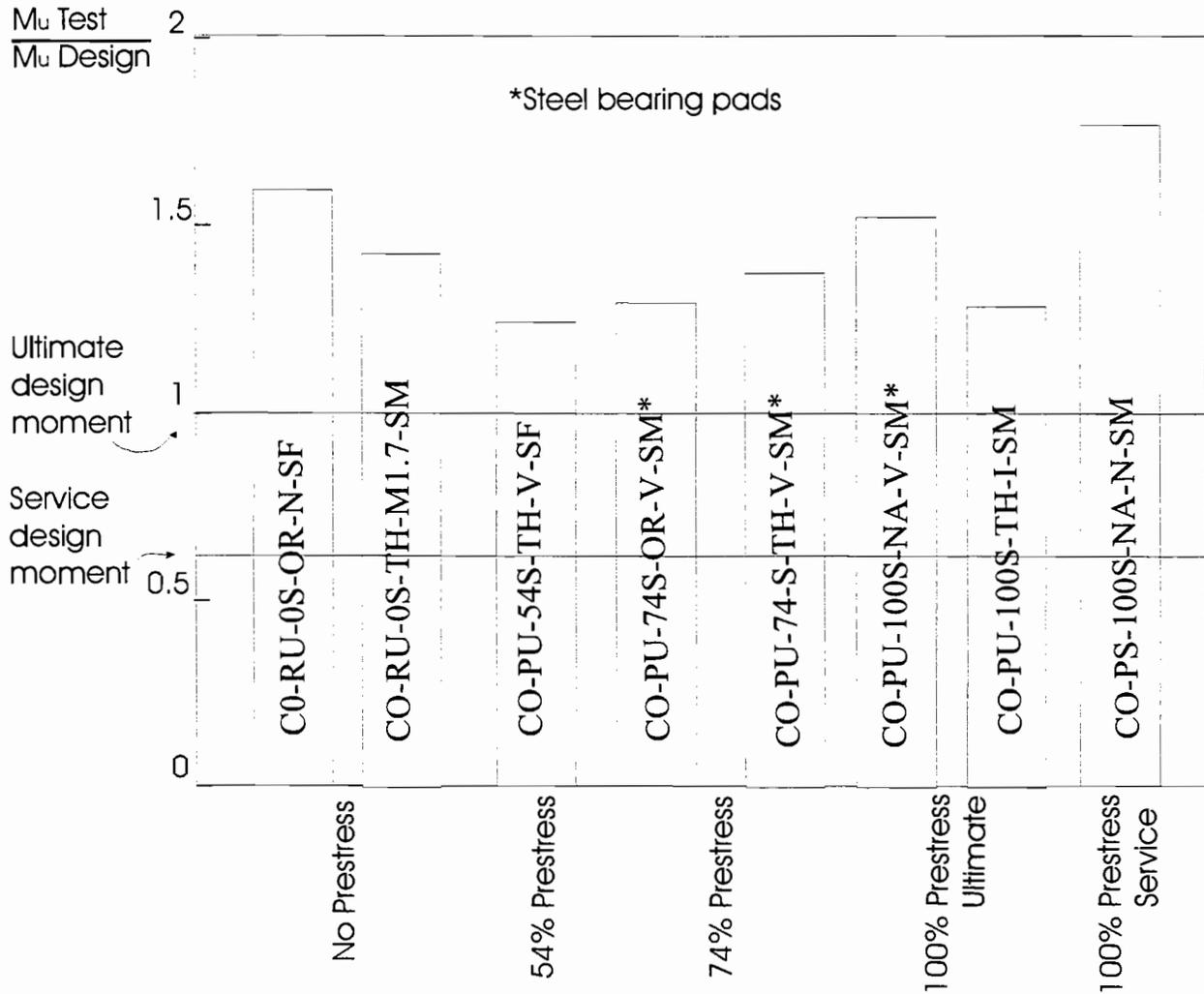
Figure 4. 16 Ratio of test ultimate moment to design ultimate moment

is quite conservative. Excluding the eight specimen which had a shear failure, the average ratio is 1.22 between test and theory. However, the theory neglects strain hardening. Autopsies showed that bars and wires actually meshed and fractured in several specimens. Calculations for several specimens, with strain hardening included in the compatibility analysis, indicated increases in the calculated capacity of around three to eight percent and an average of about five percent (7). This would partly, but not completely, explain the excess. Separate calculations (8) using the much simpler AASHTO equations showed the oversimplified equations gave slightly more accurate results. The effects using strain compatibility are not justified considering the overall conservativeness of the design.

4.9 PERFORMANCE OF T-HEADED REINFORCEMENT

In six of the overhangs, T-headed reinforcing bars were used for the main flexural reinforcement #2 bars, as an alternative for the commonly used standard hooks. The purpose was to evaluate their performance in crack control, in reducing congestion in anchorage areas, and in improving constructibility of the reinforcing cages, when compared to the other overhangs.

To this end, models CO-PU-74S-TH (V&I) were designed, constructed and tested maintaining the same characteristics of models CO-PU-74S-OR-(V&I), but only replacing the standard hooks with T-heads. By maintaining all the other variables in the project without change, performance of T-headed reinforcement could be adequately evaluated.

Evaluating the specimens in terms of constructibility, T-headed reinforcing bars were found to reduce significantly the time necessary to build the reinforcing cages. Additionally, by the removal of the hooks on the longitudinal reinforcement at the ends of the beams, they proved to be very helpful for facilitating placement of the post-tensioning anchorage zone reinforcement. The hooks interfered with the placement of the anchorage zone hoops. Based on elimination of these conflicts and experience from those tying both types of cages, an estimate was made of the general reduction in congestion. It was estimated that congestion in the anchorage area was reduced by approximately 50 percent, resulting in better placement and consolidation of the concrete mix.

With respect to crack control at service load levels, no major improvements were observed. Both specimens CO-PU-74S-TH-(V&I) and CO-PU-74S-OR-(V&I) showed very similar cracking patterns and maximum crack widths. Additionally, the overall behavior up to ultimate loads was very similar. Figure 4.17 shows a comparison of the moment-deflection response of these models.

Table 4. 6   Failure Moments

Specimen		Overhang Designation	Failure Moment Test kip-in.	Failure Moment Test kN-m	Strain Compatibility Analysis kip-in	Strain Compatibility Analysis kN-m	M_{est} / $M_{analysis}$
1	A	CO-RU-0S-OR-N-SF	7440	84	6519	736	1.14
	B	CO-RU-0S-OR-N-SF	----	----	----	----	
2	A	CO-PS-100S-NA-N-SM	8734	986	6935	783	1.26
	B	CO-PS-100S-NA-N-SM	----				
3	A	CO-PU-100S-NA-V-SM	7044	796	5575	630	1.26
	B	CO-PU-100S-NA-I-SM	- - - -				
4	A	CO-PU-54S-OR-V-SM	6364	719	4872	550	1.3
	B	CO-PU-74S-OR-I-SM					
5	A	CO-PU-54S-TH-V-SF	6046	683	5252	594	1.15
	B	CO-PU-54S-TH-I-SM					
6	A	CO-PU-74S-TH-V-SM	6698	751	4799	542	1.38
	B	CO-PU-74S-TH-I-SM					
7	A	CO-PU-100S-TH-V-SF					
	B	CO-PU-100S-TH-I-SM	6232	704	5730	648	1.09
8	A	CO-RU-0S-TH-M1-SM					
	B	CO-RU-0S-TH-M1.7-SM	6813	769	3023	884	0.87*

*shear failure   Average excluding shear failure   1.22

After analyzing the strain gage data, in particular Figures 3.42, 3.51, and 3.59 (gage fx1), it was observed that the strain in the reinforcing bar near the location of the T-head was negligible throughout the entire range of static loading. This showed, as expected, that reinforcing bars were already developed before any tensile force would reach the heads. This was true for all models. Based on these results one could even question the need for any special anchorage system at the end of the non-prestressed reinforcement. In this respect, it has to be recognized that different patterns of cracking may occur during the service life of the structure due to the variable conditions to which this type of overhang structure is exposed, including other load cycles. Should any crack form near the end of the cantilever, it could create additional stresses in the outer regions of the reinforcing bars. This in turn would require more development of the tension force in the bar to avoid any slippage. While it is unlikely to be critical in members of these proportions, additional study might be given to this possibility with other types of overhangs and loadings.

Concentrating on the comparison between the use of standard hooks and T-heads, it can be concluded from the above discussion that in general for this type of application, T-heads:

- improve considerably the constructibility of the cages

- reduce congestion in anchorage areas by approximately 50 percent

- improve placement and consolidation of the concrete mix in the anchorage areas

- do not provide any improvements in terms of crack control

4.10 STRUT-AND-TIE MODELS

A major change from the procedures that TxDOT has traditionally used in the design of large overhangs was the introduction of strut-and-tie models rather than use of more traditional AASHTO shear models with a $V_c + V_s$ combination or a shear-friction model.

The overall success of this approach is indicated in that none of the 14 overhangs designed using strut-and-tie models failed in shear. In contrast, Specimen CO-RU-0S-TH-M1, which included a V_c term, did fail in shear but above factored flexural load levels. At high levels of shear, a V_c term should not be used with strut-and-tie models since the wider crack levels make transfer of forces by aggregate interlock undependable.

There are many problems still existent in the application of STM. Chief among these are the design specification rules for STM application. One of the state-of-the-art uncertainties is the effect of the concrete efficiency factor in the struts. It is important to note that the basic assumption in the assumed strut-and-tie model of a horizontal compression block at the bottom of the overhang with a height of 2.88 inches, leads to compression stresses in that zone that are higher than the maximum levels recommended by Bergmeister et. al. (4). Bergmeister recommends that the maximum
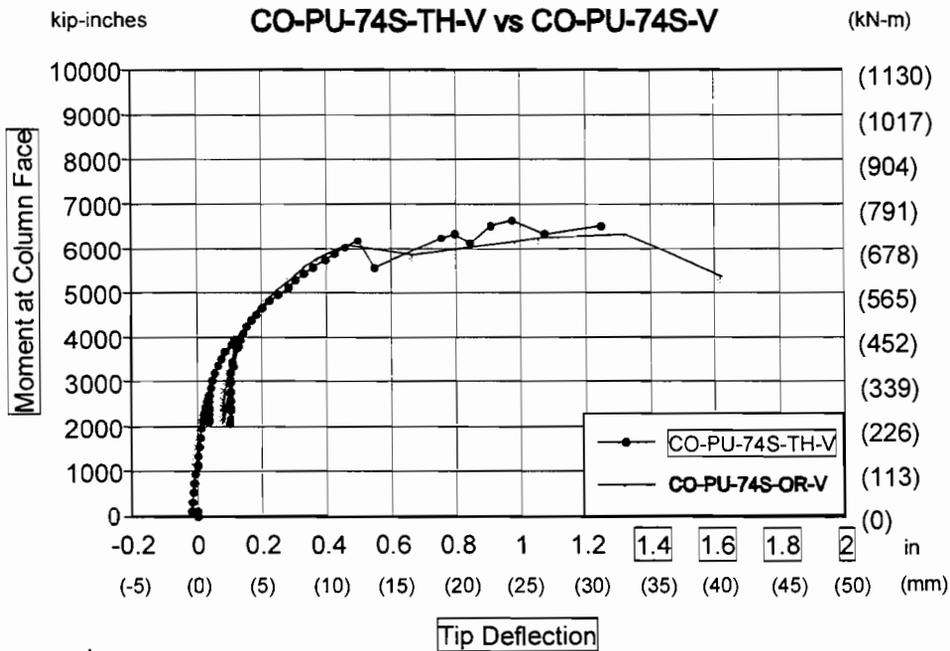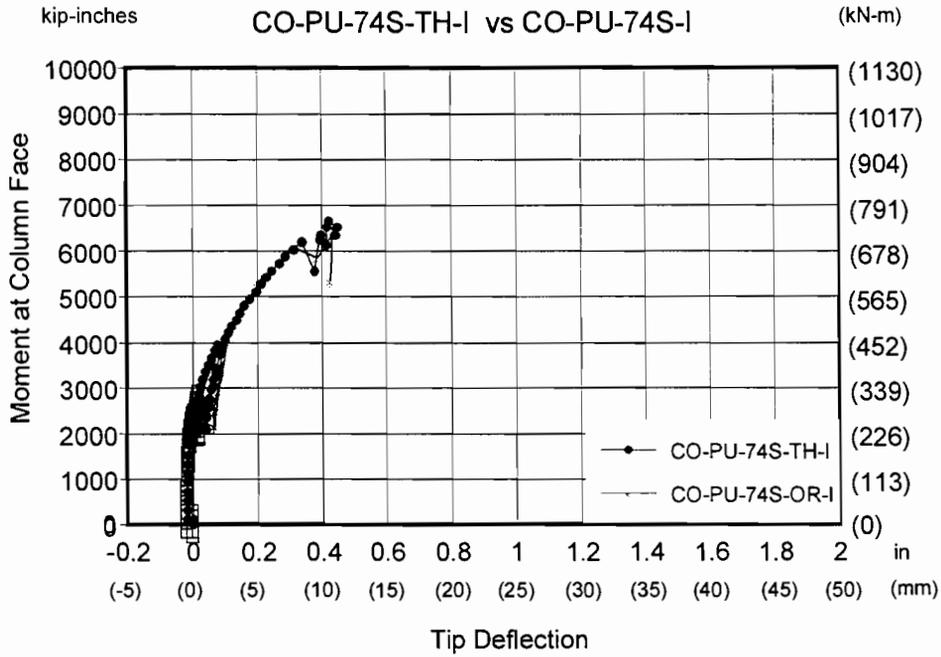
Figure 4. 17 Comparison of moment-deflection responses of Models CO-PU-74S-TH (V&I) using t-heads versus Models CO-PU-74S-OR-(V&I) using standard hooks.

174

concrete compression stress, f_{ce}, in unconfined nodes should be limited to $f_{ce} = v_e f_c'$, where $v_e = 0.9 - 0.25 f_c' / 10000$ for $4000 < f_c' < 10000$ psi. For f_c' equal to 5000 psi (34.4 MPa), the recommended f_{ce} is equal to 3875 psi (26.7 MPa).

If the vertical height of the compression block is limited to 2.88 inches (73 mm), the resultant compression strut (see Figure 4.18) acting against struts C2, C_{SW}, C5 and C6, with factored flexure loads applied to the overhang, has a magnitude of 237.3 kips (1055 kN). From the geometry of the node shown in Figure 4.18, the effective width of the node normal to the resultant compression strut is limited to 2.88 cos∝ = 2.36 inches (60 mm), resulting in a principal compression stress in the node equal to 5586 psi (38.5 MPa). This value is well above the maximum allowable stress of 3875 psi (26.7 MPa).

To limit the compression stress in the node to 3875 psi (26.7 MPa), the vertical height of the node must be increased to approximately 4.3 inches (109 mm). This requires a flatter inclination for struts C2, C_{SW}, C5, and C6 which increases the load in the resultant strut to 243.0 kips (1081 kN).

Making this change to the model would increase the demand on the horizontal steel and lower the overhang capacities. Therefore, the use of the Bergmeister compressive stress limits for concrete efficiency factors is not recommended for predicting the overhang capacities. Further research and tests are needed in this area.
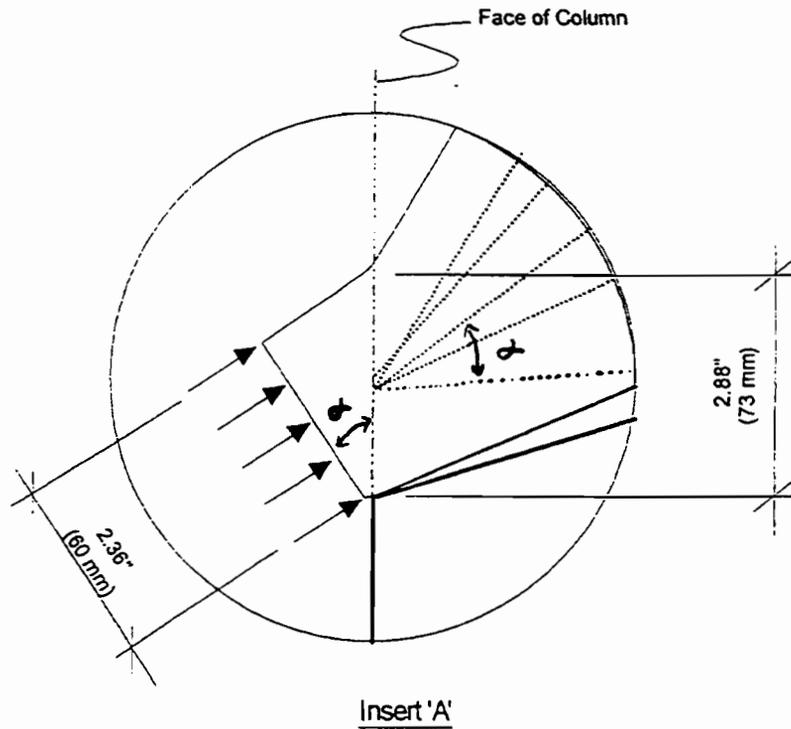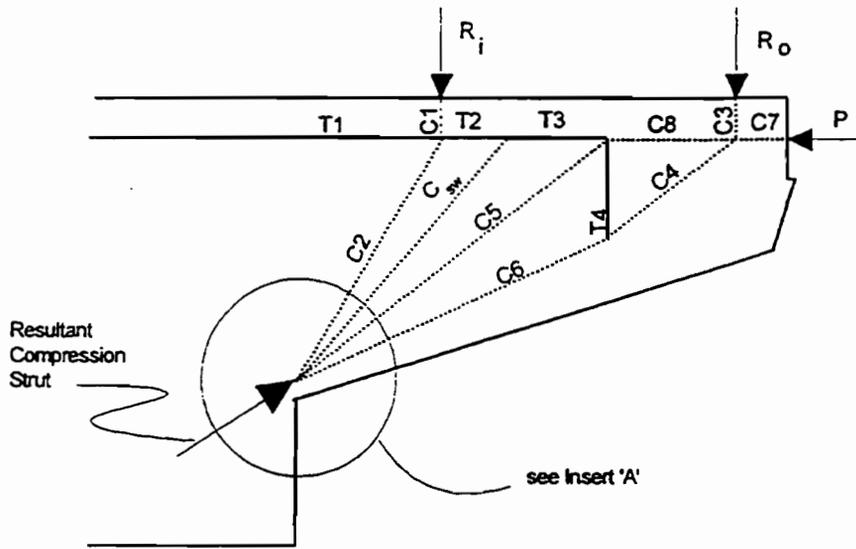
Figure 4. 18   Detail of compression node at bottom of overhang

CHAPTER FIVE

OVERHANG CONSTRUCTIBILITY AND ECONOMICS

5.1 CONSTRUCTIBILITY

Close attention was paid to the ease or difficulty of constructing each overhang. The construction of each overhang involved forming, assembling the reinforcing cage, placing and consolidating the concrete, and the prestressing operation, if applicable. Forming was essentially the same for all overhangs except that the prestressed overhangs required the use of wooden insert forms to create a block-out for the post-tensioning anchorages. In a prototype overhang, this block-out would have to be patched after the post-tensioning operation was completed.

The reinforcing quantities for each 5.5 scale overhang were converted into equivalent prototype quantities. The mild reinforcement quantities were converted according to the relationships between model and prototype reinforcement shown in Table 2.1 and were adjusted for actual and nominal yield point. The post-tensioning strands were converted into equivalent numbers of 19, 12 and 7 strand tendons. Details of the conversions are given in Refs. 7 and 8. A comparison of the total weight of reinforcement (both non-prestressed and prestressed) is given in Figure 5.1. In general, it is fair to say that the difficulty of constructing each specimen was about proportional to the total weight of reinforcement. This reflected not only tying and placing reinforcement, but also the difficulty of placing and compacting concrete in the highly congested cages.

Some work was unique to the post-tensioned specimens. The stressing operation had to be performed, wooden insert forms had to be used to form the block-out for the tendon anchorages, and in a prototype overhang, the block-outs would have to be patched. However, it is felt that the reduction in the congestion of the cage resulting from the use of post-tensioning more than offset the added difficulty of performing these operations. Unfortunately, this tradeoff might not be reflected in bidding by contractors.

The non-prestressed overhang (CO-RU-0S-OR-N), which was based on the TxDOT interpretation of the current AASHTO standards, was by far the most difficult overhang to construct. The cage was very congested and contained multiple levels of horizontal reinforcement and numerous vertical stirrups making it very difficult to assemble. In terms of total poundage and liner feet of reinforcement, this overhang had substantially more than any other overhang, resulting in a very dense reinforcing cage with closely spaced bars throughout. The densely-spaced reinforcement made placement and consolidation of concrete very difficult. This is an important consideration because poorly placed concrete leads to long-term durability problems.

The fully prestressed at service load stress levels overhang (CO-PS-100S), based on the current AASHTO design specifications was also quite difficult to construct. Although the total linear feet and pounds of reinforcement were significantly lower
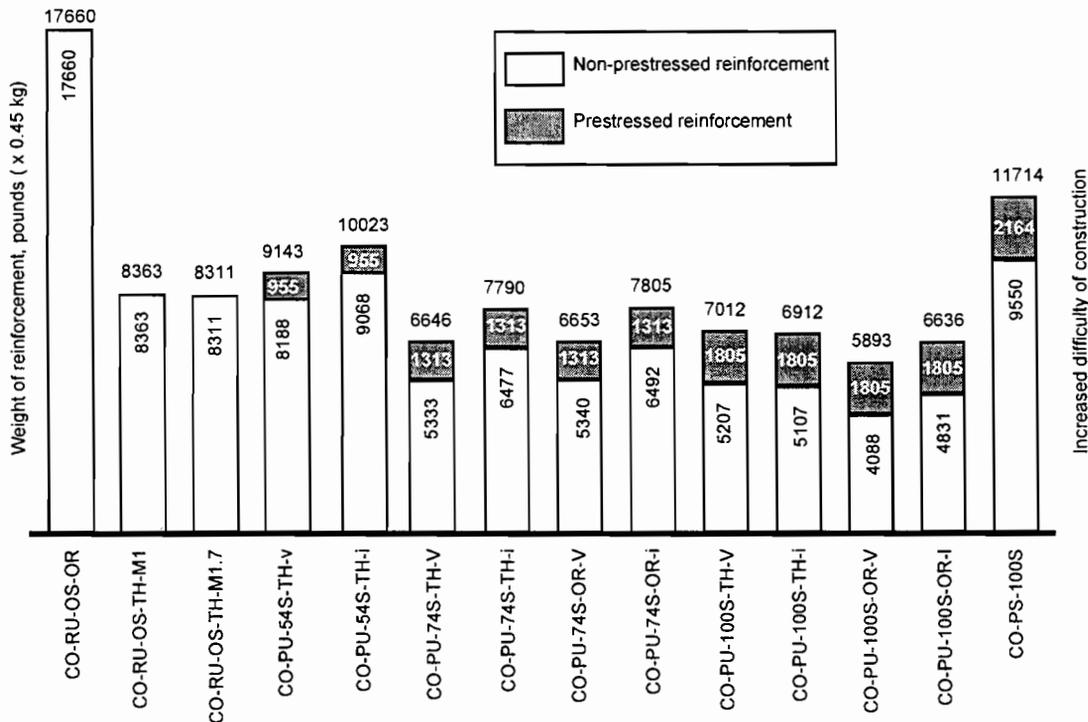
Figure 5. 1   Comparison of total weight of reinforcement for prototype overhangs

than the non-prestressed overhang (CO-RU-0S-OR-N), fabrication of the reinforcing cage was very difficult and the cage was quite congested. This is primarily because of the use of shear-friction steel and because of the large number of vertical stirrups that were used. Good placement and consolidation of the concrete was difficult to achieve because of the highly congested reinforcing cage.

The 100% prestressed overhang based on ultimate with shear design based on a STM with vertical ties (CO-PU-100S-OR-V) was by far the easiest to construct. This overhang had the lowest total poundage of reinforcement of all overhangs. The reduction of reinforcement resulted in greatly simplifying the process of assembling the cage and reducing congestion.

The 100% prestressed overhang based on ultimate with shear design based on a STM with inclined ties (CO-PU-100S-OR-I) was also quite easy to construct. The presence of the horizontal shear steel made it slightly more difficult to construct than the CO-PU-100S-OR-V overhang.

The 74% prestressed overhangs based on ultimate (CO-PU-74S-OR-I & V) were a little more difficult to construct than the 100% prestressed overhangs based on ultimate (CO-PU-100S-OR-I & V), but both were significantly easier to build than either the non-prestressed (CO-RU-0S-OR-N) or 100% prestressed overhangs based on service load conditions (CO-PS-100S).

Results from the T-headed reinforcement showed a similar relationship between constructibility and amount of reinforcement. However, in this case, differences

178

between the various models using T-heads were not very significant. The major difference was found when compared to the non-T-head models since the constructibility of all models was notably improved with the use of T-headed reinforcing bars.

T-headed reinforcement was found to reduce significantly the time necessary to build the reinforcing cages, was shown to ease placement of the post-tensioning anchorage zone reinforcement, and resulted in improved placement and consolidation of the concrete mix in anchorage areas. Conservatively, it was estimated that T-headed bars improved the time of construction of the reinforcing cages by at least 30 percent.

When compared to the other T-head reinforcement models, the 54% prestressed models based on ultimate (CO-PU-54S-TH (V&I)) were the most time-consuming with respect to the construction of the reinforcing cages. However, because of the smaller quantity of post-tensioning reinforcement, these overhangs were the easiest to prestress and grout. As a result, the overall time of construction of these cages including all post-tensioning operations, was just slightly greater than the time of construction of all the other T-head models.

The non-prestressed models with a V_c term used in design (CO-RU-0S-TH-M1&M1.7) had extremely simple cages. The only congestion was in the closely-spaced rows of main flexural reinforcement. The use of T-heads greatly reduced the end hook congestion. Elimination of the shear-friction reinforcement and the heavy stirrups of the conventionally designed non-prestressed model (CO-RU-0S-OR-N) resulted in a dramatic improvement in constructibility.

However, this improvement in constructibility was negated by the service load cracking problems and the final shear failure. The low costs are thus deceptive since the structure failed in performance at service loads and experienced a less desirable brittle failure at ultimate. The 74% prestressed models (CO-PU-74S-TH-(V&I)) were not too different from the 54% prestressed models (CO-PU-54S-TH-(V&I)). These overhangs did not include the skin reinforcement suggested by Frantz and Breen, which resulted in easier construction of the cages, but prestressing operations took more time and effort than the 54% prestressed models (CO-PU-54S-TH-(V&I)).

Reinforcing cages for models with 100% prestressing and T-headed reinforcement (CO-PU-100S-TH (V&I)) were the easiest models to construct. These cages were the least congested. However, placement and tying of the ducts, and placement of the grout tubes was more difficult. Additionally, prestressing operations took double the time to perform when compared with the 54% prestressed models (CO-PU-54S-TH-(V&I)), which suggested a direct relationship between the time to perform prestressing operations and the amount of prestressed reinforcement in the models. As a result, the time to construct these 100% prestressed models was just slightly below the time to construct the 54% and 74% prestressed overhangs (CO-PU-54S-TH (V&I)) and (CO-PU-74S-TH (V&I)).

With respect to the ease of placement and adequate consolidation of the concrete mix, all models of the T-head reinforcement series showed very similar characteristics. The major advantage was in fact the reduction in congestion and reinforcing conflicts.

179

When all specimens are considered, constructibility of the specimens with a mix of non-prestressed and prestressed flexural reinforcement was significantly better than either the non-prestressed specimens following the current AASHTO or the fully prestressed specimens. The non-prestressed specimen with T-headed reinforcement was also very easy to construct. However, its failure in shear rather than flexure and its failure to control service load crack widths indicates undesirable characteristics. These were associated with factors other than the use of T-headed bars.

5.2 ECONOMICS

To evaluate and compare the overhangs with respect to their estimated costs, reinforcing bars and wires in the models were converted into prototype reinforcement. Reinforcing bars were selected depending on the scaled bar area (model bar area multiplied by 5.5^2), and the yield strength that would be used in design, 60 ksi (414 MPa).

Cost estimates were obtained from a representative of a local construction company (25) for each overhang. The estimates are for mild reinforcement and post-tensioning only. The estimator assumed that the cost of forming and supplying and placing concrete would be essentially the same for each overhang. The assumption of no variation in placing costs regardless of type of cage and reinforcement congestion is at great variation with the authors' laboratory observations. It was also assumed that each type of overhang was the only overhang on a project in which 25 overhangs were required. This influenced the cost for tying and erecting the reinforcement which was variable, depending on the quantity of reinforcement used. The unit costs for purchasing materials did not vary with the quantity of usage.

Cost comparisons presented herein correspond to the cost for the prestressed and non-prestressed reinforcement only. This might be less than 30 percent of the total overhang cost. The Austin Bridge & Road, Inc. estimator concluded that the cost of forming and, in spite of the fairly apparent differences in reinforcement congestion, the cost of supplying and placing concrete would be basically the same for all overhangs. This assumption was initially questioned by the authors because the experience in the laboratory showed significant labor differences. It was certainly more difficult to place the concrete mix in the very congested models with higher percentages of reinforcing steel than in those with very light cages. However, a second opinion was sought from a senior engineer with Flatiron Construction who was casting and erecting the large 183 bridge project in Austin. He confirmed that in spite of the obvious difference in degree of congestion, that while he would much rather build the less congested designs, the bid price for concrete including placement would probably be the same for all designs. Thus, the construction cost differences can be judged basically on the differences in cost of reinforcement including all prestressing operations.

T-headed reinforcement costs for all prototype overhangs using T-headed bars were obtained assuming that a project would consist of 25 overhangs with at least 625 T-headed #11 (35 mm dia.) reinforcing bars in total. Based on this information, the price for each 37.5 ft. (11.5 m) long T-headed bar delivered to a job-site in Austin, Texas, was estimated as $53.00 US. This figure was used in determining the material costs for all bars in the estimators calculations.

Figure 5.2 presents the reinforcement material, placement and stressing costs for each specimen. It can be observed that in general those overhangs designed with a mixture of prestressed and non-prestressed reinforcement are, as expected, well below the cost of a prestressed concrete design with allowable stresses governing (overhang CO-PS-100S). Additionally, the 54% and 74% prestressed overhangs (CO-PU-54S-TH (V&I) and CO-PU-74S-TH (V&I)) are only marginally (3 to 10 percent) above the cost for the non-prestressed overhang (CO-RU-0S-OR-N). This non-prestressed specimen is typical of present TxDOT practice. If some recognition was given to those structures with less congested cages, these designs could actually be even less expensive than the conventional reinforced concrete structure. However, the significant reduction in costs associated with the special non-prestressed model (CO-RU-0S-TH-M1) (an over 40 percent reduction from the other non-prestressed model that reflected current TxDOT practice) suggests that if moderate additional shear reinforcement was added by using STM with no V_c term and if side face cracking reinforcement satisfying the Frantz provisions was added, the behavior would be acceptable. Then the least cost would be a reinforced concrete overhang with shear design based on STM and with improved constructibility provided through use of T-headed reinforcement. The reduction in cost would come mainly from the improved shear design.

As shown in Figure 5.2 when the prestressed specimens are compared, there is a trend of increasing price with increasing levels of prestressing. This conclusion was made even when it was realized that the 74% prestressed overhangs (CO-PU-74S-TH-V and CO-PU-74S-TH-I) were less expensive than the 54% prestressed overhangs (CO-PU-54S-TH-V and CO-PU-54S-TH-I), respectively. It is believed that the increased cost in the 54% prestressed overhangs is mainly due to the additional skin steel and the larger amount of T-headed reinforcement. However, the use of T-headed reinforcement would have less influence since it was found that the additional cost due to the use of this reinforcement never exceeded seven percent of the total reinforcing cost of any particular overhang.

As a final observation, it is important to notice that if formwork, concrete material and concrete placement costs are included, the small differences in reinforcement cost between the conventional non-prestressed and mixed prestressed designs would virtually disappear. Then the 74% prestressed overhangs (CO-PU-74S-OR-TH-V) would be highly competitive with the conventionally reinforced concrete design overhang (CO-RU-0S-OR-N).
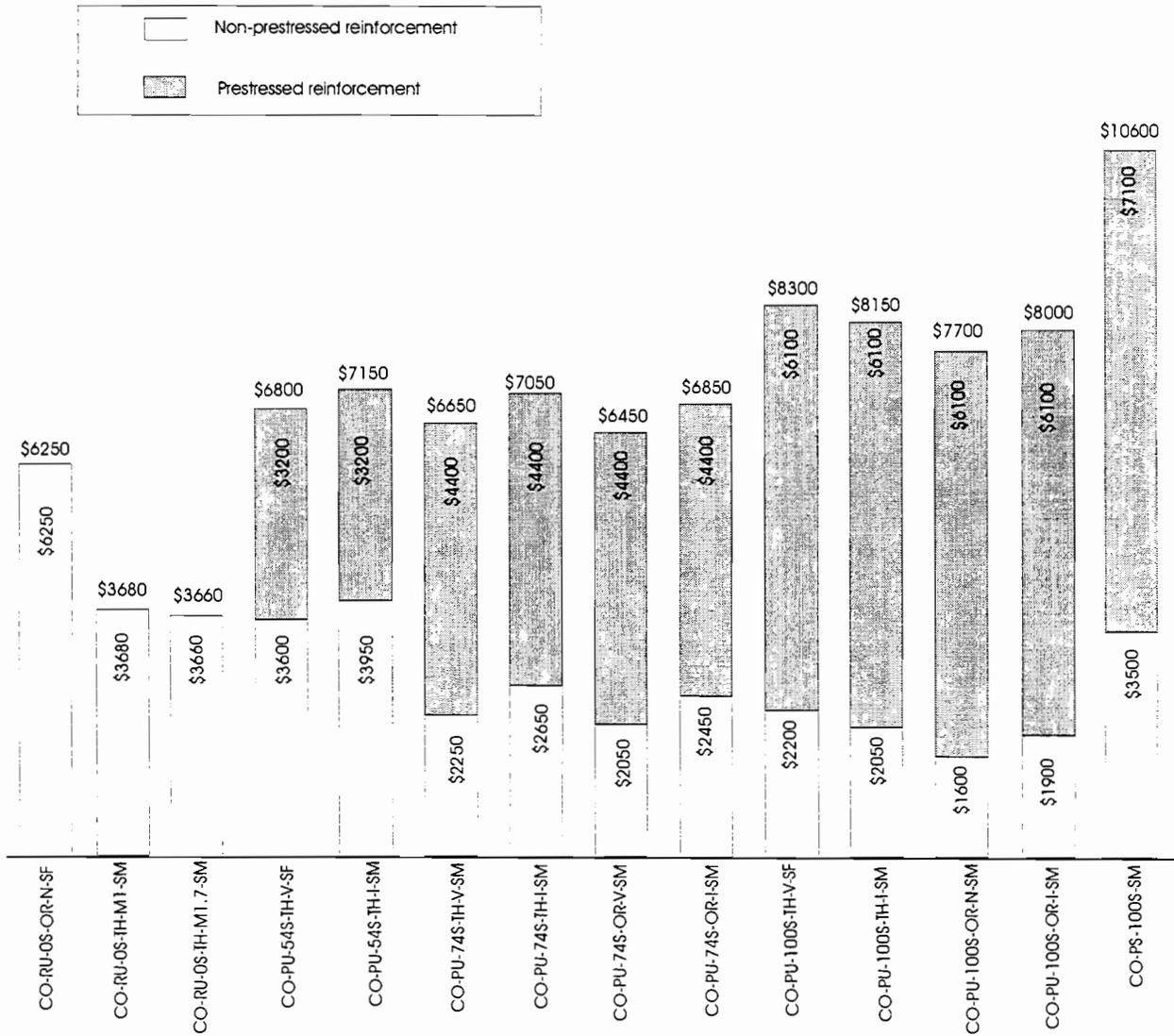
Figure 5. 2   Comparison of total estimated cost for the reinforcement in prototype overhangs

CHAPTER SIX

DESIGN RECOMMENDATIONS

6.1 GENERAL DISCUSSION OF DESIGN RECOMMENDATIONS

Based on the results of this research, it is possible to make several recommendations for the design of large cantilever overhangs. The recommendations are specifically directed at overhangs of intermediate lengths for which application of the current AASHTO specifications are ambiguous and lead to significantly over-designed, difficult to construct, and possibly expensive overhangs. Results of the reinforced concrete specimens designed using strut-and-tie models but allowing a supplementary V_c term (CO-RU-OS-TH-M1 & M1.7) were disappointing in that the final failure occurred brittlely in shear and the crack widths at service level were 80% greater than allowable. The economic studies indicate that a reinforced concrete specimen has the most economic promise but cannot be relied on to satisfy crack control performance requirements unless further reinforcement is added, thus increasing cost. Looking at the overall results of the 16 overhang specimens, the best performance at costs comparable to present costs results from a design procedure similar to that which was used in the design of the fully prestressed or 74% prestressed overhangs using STM modeling with no V_c term (CO-PU-100S-NA-V-SM and CO-PU-74S-OR-V-SM).

Overhangs designed by the proposed approach (summarized in Sec. 6.2) would be easier to construct than current AASHTO designs for either reinforced concrete or fully post-tensioned concrete, and would have significantly less over-design. The resulting overhangs could be provided at a substantially lower cost than the AASHTO fully post-tensioned designs and at about the same cost as the AASHTO reinforced concrete designs. Furthermore, the simplification of the construction process, specifically the placement of concrete, should lead to better consolidation of concrete, more durable structures, and possibly further cost savings.

As demonstrated by this research, such an approach would result in overhangs which have good serviceability and adequate strength. The major variables were summarized in Table 2.5. Two overhangs were designed as reinforced concrete members using traditional AASHTO shear design (CO-RU-0S-OR-N-SF). Two overhangs were designed as fully prestressed concrete members where AASHTO stress limits at service load governed the design and traditional AASHTO shear design was used (CO-PS-100S-NA-N-SM). The other 12 overhang specimens were designed with various combinations of reinforced concrete or prestressed concrete basing bar and strand requirements on ultimate and using strut-and-tie models for shear design. Twelve overhangs were designed and tested in this manner. Ten of these had various combinations of prestressing strand and reinforcing bars based on ultimate requirements. These ranged from 100% prestressed to 54% prestressed. Two specimens had no prestressing, suffered initial brittle shear failures (but above factored load) and had unacceptably large crack widths at service load levels. While each of the other ten new overhang designs had moment capacity substantially above what is required for factored loads, it is important to realize that any reduction in the

amount of reinforcement would probably result in unacceptable service load crack width performance. This is especially true for the 74% prestressed (CO-PU-74S-OR-TH) overhangs which had crack widths right at the maximum acceptable level. It appears that some minimum threshold amount of strength over-design must be provided in order to achieve good serviceability and it is believed that the 74% prestressed overhangs are very close to that amount.

The shear reinforcement design for the 100% prestressed (ultimate) (CO-PU-100S-V) and 74% prestressed (ultimate) (CO-PU-74S-V) overhangs was based on a simple strut-and-tie model incorporating only vertical ties in the webs. This is recommended over the approach taken for the companion 100% prestressed (CO-PU-100S-I) and 74% prestressed (CO-PU-74S-I) overhangs which utilized inclined ties in the web. This is because no significant differences were observed in the service load performance of overhangs designed by the two differing approaches and designs based on the inclined ties were more difficult and expensive to construct.

One-hundred percent of the primary moment reinforcement in the 100% prestressed (CO-PU-100S-V) overhang was provided by post-tensioning while the 74% prestressed (CO-PU-74S-V) overhang utilized a mixture of prestressed and non-prestressed reinforcement. No definitive recommendation of one of these overhangs over the other is suggested because each has its own merits. For example, the 100% prestressed (CO-PU-100S-V) overhang was by far the easiest to construct and had better crack control than the 74% prestressed (CO-PU-74S-V) overhang. However, the 74% prestressed (CO-PU-74S-V) overhang had acceptable crack control and was less costly than the 100% prestressed (CO-PU-100S-V) overhang. Also, the 74% prestressed (CO-PU-74S-V) overhang had better ductility than the 100% prestressed (CO-PU-100S-V) overhang. The design approach used for either overhang would be essentially the same. This decision would be up to the designer, depending on the relative importance given to economics, constructibility, and ductility. If substantial amounts of non-prestressed flexural reinforcement are provided, use of T-headed bars reduces congestion in comparison to the current procedure of providing hooks. End anchorage did not seem a problem since low steel strains were measured near the end anchorage plates.

6.2 SUMMARY OF RECOMMENDED DESIGN PROCEDURES

Currently AASHTO standard design specifications do not explicitly allow the design of prestressed structures with a mixture of prestressed and non-prestressed reinforcement, using the ultimate strength philosophy for flexure. The purpose of this report was to study the behavior of intermediate length overhangs (a/d from 0.67 to 2.5) designed using that methodology, including strut-and-tie modeling for shear, various amounts of skin reinforcement, and exploring the use of T-headed reinforcing bars as flexural reinforcement.

Based on the results from this study, some recommendations can be outlined for the design of similar structures. Before doing this it has to be mentioned that this report summarizes only the first part of CTR Research Project 1364. A more comprehensive report will be presented in the near future including findings of the overall project, which is envisioned to include results on the overall performance of the structure including the overhang, column and footing. These results will be available for

consideration by code and specification-writing bodies as soon as results of the complete research program are approved by TxDOT.

Concentrating on the design of intermediate length cantilever overhangs (a/d from 0.67 to 2.5) some practical design recommendations are:

1. Flexural Design: The quantity of tensile reinforcement required for the critical moment at the face of the column can be determined as the tie force T1 from the strut-and-tie model or from conventional flexural calculations as the designer prefers. The results should be the same. Provision of this tie force should be based on factored load design with mixed prestressed and non-prestressed reinforcement. About 75% of the main tensile force should be provided in the form of prestressing steel. The remainder of the ultimate tensile force should be provided by non-prestressed reinforcement at the yield strength. In addition, as given in Step 6 for serviceability, the amount of non-prestressed reinforcement must be checked and increased if necessary for proper crack control and fatigue stress range control. In cases where the use of prestressing is felt inappropriate, all of the flexural reinforcement can be non-prestressed. All of the following steps are still appropriate and essential.

2. Shear Design: This should be based on a strut-and-tie model as shown in Figures 2.8 and 2.25. The horizontal tie forces are provided by flexural reinforcement from Step 1. The vertical tie force should be provided by the use of vertical stirrups that should be distributed close to the location of the tie as shown in Figure 2.19. When doing this, observance of the minimum spacing limitations set in the AASHTO provisions for adequate placement of the concrete mix is necessary.

3. Skin Reinforcement: Minimum side face skin reinforcement should be proportioned based on recommendations by Frantz and Breen (5).

4. T-Headed Reinforcement: T-head anchorages on reinforcing bars should be used when reinforcement details indicate severe congestion or difficult bar development conditions. In these cases T-headed reinforcement will make the construction process of the reinforcing cages easier and will greatly assist in achieving good consolidation of the concrete mix in anchorage areas. No extra credit should be given to this system for controlling crack widths at service load levels.

5. Post-Tensioning Anchorage Zone Reinforcement: This should be provided in accordance with the NCHRP Report No. 356 provisions (9) which are included in the AASHTO Standard specifications (16).

6. Serviceability Requirements:

   a) Flexural reinforcement should be checked to ensure control of crack widths by meeting the reinforcement distribution provisions (z factor) of AASHTO. These are directly applicable for non-prestressed overhangs. When some or all of the main flexural reinforcement is prestressed, more detailed checks are required. Prediction of the most probable maximum crack width on the tension face of the overhangs should be carried out using any of the Gergely and Lutz expressions discussed in Sections 4.2.2, but modifying them, as recommended in Section 4.2.2 to account for prestressed reinforcement by adding to the actual number of non-

prestressed bars present in the tension zone an equivalent non-prestressed bar for each bonded prestressed strand in the tension zone.

b)   Stress ranges in all post-tensioning tendons should be evaluated at service load levels and compared against recommendations by Wollmann (11).   They may require that supplementary non-prestressed reinforcement be added.   For structures that have to be designed to withstand a fatigue life of two million cycles, Wollmann recommends a stress range limit of 14.5 ksi (96.5 MPa).

c)   Deflections should be calculated by common analytical methods and compared against acceptable values.   A typical limit for cantilever arms for concrete superstructures under service flexure live loads is $L/300$ (24).

d)   Side face cracking is controlled by the skin reinforcement of Step 3.

e)   Minimum area of reinforcement should be provided in any otherwise unreinforced area as per AASHTO provisions for shrinkage and temperature.

CHAPTER SEVEN

SUMMARY AND CONCLUSIONS

7.1 SUMMARY

A number of difficulties were found by the Texas Department of Transportation, TxDOT, when using current AASHTO design specifications for the design of large cantilever bent caps to be used in the San Antonio "Y" project.

The problems arose when designers attempted to satisfy both serviceability and strength requirements which required the use of both reinforced concrete and prestressed concrete specifications found in completely separate chapters of the design standards. Additionally, problems were also found when designing overhangs with concentrated load span-to-depth (a/d) ratios near one. In these cases it was not clear whether corbel design or deep beam design should govern. Designers conservatively tried to satisfy both approaches. This resulted in highly congested reinforcing cages, poor constructibility, and somewhat uneconomical designs.

To this end, with the main purpose of defining a more consistent design approach for structural concrete piers, and upon the request of TxDOT, an experimental program was initiated at The University of Texas at Austin, CTR Project No. 1364, with the general title of *"Design of Large Structural Members Utilizing Partial Prestressing."* This project was divided into several major series of tests. The first reported herein deals with the isolated cantilever pier. Others deal with the design and behavior of two-span continuous pier caps, and with the overall structure including footing, pier and overhang.

This report presents the results of the cantilever overhang series. The objectives of this portion were to evaluate the behavior of large cantilever pier overhangs designed with a non-prestressed reinforcement, with all flexural reinforcement prestressed and with a mixture of prestressed and non-prestressed reinforcement. Both service and ultimate strength approach governing the prestressing was examined. Other objectives were to evaluate the use of T-headed reinforcing bars in flexural reinforcement, and to analyze the performance of different amounts of skin reinforcement in crack control at service levels. In addition, two different patterns of strut-and-tie models were used in design of the specimens. Seven overhangs had vertical ties and five overhangs had inclined ties in the critical shear zone. Considerable detail on selection of a typical STM pattern was given in Section 2.4.4 in order to assist designers unfamiliar with the procedures.

Sixteen concrete overhang structures with mixed reinforcement were tested under static loading. These included four overhangs with no prestressed reinforcement, two overhangs with 54 percent of the main flexural reinforcement prestressed, four with 74 percent of the main flexural reinforcement prestressed and six with nearly 100 percent of the flexural reinforcement prestressed.

The particular characteristics of each of the 16 overhang models can be summarized as:

a) 1A-CO-RU-OS-OR-N-SF (North): Reinforced concrete design using TxDOT interpretation of AASHTO (AASHTO flexure, AASHTO shear, AASHTO corbel design with shear friction, AASHTO skin reinforcement). This results in heavy stirrups and heavy shear friction reinforcement as well as moderate skin reinforcement.

b) 1B-CO-RU-OS-OR-N-SF (South): Same as a)

c) 2A-CO-PS-100S-NA-N-SM (North): Fully prestressed design with amount of prestress strand governed by AASHTO service load considerations, using AASHTO prestressed concrete shear provisions and shear friction reinforcement which were modified for prestressed concrete. TxDOT minimum for side face reinforcement.

d) 2B-CO-PS-100S-NA-N-SM (South): Same as c)

e) 3A - CO-PU-100S-NA-V-SM: Fully prestressed design but allowing prestressing reinforcement to be governed by ultimate requirements, using a STM with vertical ties, no shear friction reinforcement and TxDOT minimum side face steel.

f) 3B-CO-PU-100S-NA-I-SM: Same as e) except the STM used an inclined tie.

g) 4A-CO-PU-74S-OR-V-SM: Mixed reinforcement with 26 percent of tensile force taken by non-prestressed bars. Otherwise like e).

h) 4B-CO-PU-74S-OR-I-SM: Same as g) except the STM used an inclined tie.

i) 5A-CO-PU-54S-TH-V-SF: Mixed reinforcement with 46 percent of tensile force taken by non-prestressed bars with T-headed anchors. STM used vertical tie. No shear friction reinforcement. Skin reinforcement moderate.

j) 5B-CO-PU-54S-TH-I-SM: Same as i) except STM used inclined tie and TxDOT minimum side face reinforcement was used.

k) 6A-CO-PU-74S-TH-V-SM: Same as i) except 26 percent of tensile force taken by non-prestressed reinforcement and TxDOT minimum skin steel used.

l) 6B-CO-PU-74S-TH-I-SM: Same as k) except STM used inclined tension tie.

m) 7A-CO-PU-100S-TH-V-SF: Same as e) except non-prestressed flexural reinforcement anchored with T-heads and moderate side face steel used.

n) 7B-CO-PU-100S-TH-I-SM: Same as m) except STM used inclined tie and TxDOT minimum side face steel used.

o) 8A-CO-RU-OS-TH-M1-SM: Reinforced concrete design using T-headed bars but with no shear-friction reinforcement, with STM with vertical tie supplemented by $1\sqrt{f'_c}\, b\, d$ concrete shear contribution and with TxDOT minimum side face steel.

p) 8B-CO-RU-OS-TH-M1.7-SM: Same as o) except concrete shear contribution $1.7\sqrt{f'_c}\, b\, d$.

One overhang of each specimen was loaded to a complete failure. All failures except one were flexural. The service load performance of all sixteen overhangs was

evaluated on the basis of data collected in the tests. The analysis of test results included evaluation of deflections at service load levels, evaluation of moment-deflection responses, analysis of cracking moments, comparison of predicted maximum crack widths with test results, comparison of cracking patterns, and evaluation of ultimate capacities and behavior. Additionally, analyses based on constructibility and economics associated with all the overhangs were also included. Construction cost estimates based only on reinforcement costs were obtained for each of the overhang types. Comparisons were made between the service load performance, ultimate behavior, and reinforcement economics of each overhang.

The results of this study were used to formulate a design procedure outlined in Section 6.2 which is recommended for use on large cantilever overhangs of intermediate length, (a/d from 0.67 to 2.5).

7.2 CONCLUSIONS

The most important conclusions drawn from the results of this study are:

1. All specimens had substantially more strength than required for factored load design.

2. Overhangs designed according to current AASHTO Standard Specifications as interpreted by TxDOT designers for the San Antonio Y project to include a complete shear design plus complete corbel shear friction reinforcement had significantly excess capacities and utilized excessive quantities of reinforcement. They have highly congested reinforcing cages making them difficult to construct.

3. An attempt to greatly reduce the amount of skin friction and shear reinforcement in the non-prestressed specimen by using a concrete shear contribution to supplement the strut-and-tie model approach was unsuccessful because the failure mode changed to shear and crack widths at service load levels were excessive. At the high shear levels typical in the overhangs, use of a V_c term to supplement the strut-and-tie model is inappropriate because of the fairly wide inclined cracks. However, omission of the shear - friction reinforcement is possible. Design using the strut-and-tie model approach for shear should greatly reduce reinforcement costs and congestion when compared to traditional designs. It might be possible to improve performance at a reasonable cost increase.

4. All overhangs had deflections at service load levels well below the typical service flexure live load limit for cantilevers of L/300. Additionally, a clear trend was observed of decreased deflections with increased effective post-tensioning force in the structures.

5. Most probable maximum crack widths were predicted with very good accuracy using the modified Gergely and Lutz expressions presented in Section 4.2.2. In general, the maximum crack widths in the models decreased as the amount of post-tensioning force increased.

6. At higher post-tensioning forces, fewer cracks were observed, and as a result stiffer structures were attained.

7. With one exception, only flexural failures were observed. These consisted of the wide opening of one or two major cracks close to the face of the column at ultimate

loads, followed by crushing in the compression zone. One reinforced concrete overhang failed with opening of a major diagonal crack, crushing and loss of ductility.

8. Ultimate flexural capacities of all models were in excess of the required capacity at factored loads by approximately 40 to 90 percent. Even in the better designed lower capacity models, this capacity could not be significantly lowered in design because of the requirements for auxiliary reinforcement in terms of minimum skin reinforcement and fatigue related stress ranges in the post-tensioning steel. Stress ranges were found to control the design of the overhangs, especially in those models with low percentages of prestressed steel. Models CO-PU-74S-TH - (V&I) were tested with somewhat higher stress ranges than allowed. This was properly documented and is not recommended. It could be easily adjusted with a relatively small amount of additional non-prestressed reinforcement.

9. For the prediction of ultimate flexural capacity, the current AASHTO expression which takes into account all non-prestressed reinforcement in tension gave good but conservative predictions when compared with test results. The more complex determination of strength using strain compatibility approaches was not justified by improvements in accuracy.

10. The behavior of the overhang (CO-PS-100S-NA-N-SM) designed as 100 percent prestressed based on service design allowable stress values (which is the governing condition under the current AASHTO Standard Bridge Design Specifications) was quite in excess of crack control, deflection, and ultimate capactiy requirements. Such conservative design may have been appropriate in the early days of prestressed concrete usage. This over-conservative design procedure is being replaced in many countries (and in the AASHTO LRF Specifications) with designs allowing mixtures of non-prestressed and prestressed reinforcement based on checks for appropriate limit states. Earlier concepts such as limiting tensile stresses to prevent any cracking at service levels are an effective but over-conservative way to prevent fatigue problems. However, allowing controlled cracks and controlled stress ranges are also effective. While such design is somewhat more complex, substantial savings are possible in construction costs. An alternative design approach, utilizing strut-and-tie modeling and either reductions in the amount of post-tensioning based on ultimate criteria or combinations of about 25 percent non-prestressed and 75 percent prestressed reinforcement based on ultimate criteria, can be successfully employed in the design of large cantilever overhangs. Such designs contain significantly reduced amounts of reinforcement and consequently are much easier to construct.

11. Overhangs designed according to current AASHTO standards and by the alternative approach have acceptable service load performance both with respect to deflections and crack widths.

12. Overhangs designed by the alternative approach have greater strength than required for factored loads, but designing them with less strength may jeopardize their service load performance. This is why the attention to the serviceability requirements in Step 6 of the design recommendations is of such importance.

13. The ductility of an overhang designed with a combination of non-prestressed and prestressed reinforcement can approach that of a reinforced concrete overhang.

14. The STM with vertical ties proved more constructable and economical than those with inclined ties.

15. The Frantz and Breen skin face reinforcement is necessary in non-prestressed overhangs but was not necessary for service load crack control in the prestressed overhangs. The Frantz and Breen skin reinforcement does provide for a great deal of improved crack distribution near ultimate load levels in the prestressed members.

16. T-headed reinforcing bars considerably improved the constructibility of the cages. Placement and tying of bars was improved significantly. Congestion in anchorage areas was judged to be substantially reduced primarily due to the elimination of hooks. This improved the placement and consolidation of the concrete mix. No improvements were observed in terms of crack control at service load levels. Behavior of the specimens using either T-heads or standard hooks in the non-prestressed flexural reinforcement was basically the same over the entire range of loading.

17. Difficulty in constructing reinforcement cages was found to decrease with increased amounts of post-tensioning in the models. On the contrary, and as expected, post-tensioning operations were found to be less time consuming for those overhangs with a lesser amount of prestressed reinforcement.

18. Based on consideration of reinforcement cost only, the construction cost of the overhangs is significantly increased with increasing amounts of post-tensioning. This makes the AASHTO fully prestressed design (CO-PS-100S) the most expensive of the overhangs evaluated. The AASHTO reinforced concrete design (CO-RU-0S-OR-N) had the lowest cost of all overhangs with acceptable behavior. This cost evaluation is based only on the estimated reinforcement cost, including cost of prestressing operation. However, the 74% prestressed overhang (CO-PU-74S-TH-V) had reinforcement costs only 6 percent greater than the reinforced concrete design.

REFERENCES

1. American Association of State Highway Transportation Officials (AASHTO), Standard Specifications for Highway Bridges, Fourteenth Edition, 1989.

2. Schlaich, J., Shafer, K., and Jennewein, M., "Towards a Consistent Design of Structural Concrete," PCI Journal, May-June 1987, pp. 75-150.

3. "Structural Concrete." Summarizing Statement of the IABSE Colloquium on Structural Concrete, Stuttgart, April 10-12, 1991. Structural Engineering International, Vol. 1, No. 3, August 1991, pp. 52-54.

4. Bergmeister, K., Breen, J.E., Jirsa, J.O., and Kreger, M.E., "Detailing for Structural Concrete," Research Report 1127-3F, Center for Transportation Research, The University of Texas at Austin, May 1993.

5. Frantz, G.C., and Breen, J.E., "Control of Cracking on the Side Faces of Large Reinforced Concrete Beams," Research Report 198-1F, Center for Transportation Research, The University of Texas at Austin, September 1978.

6. Leyendecker, E.V., "Behavior of Pan Formed Concrete Slab and Girder Bridges," Ph.D. Dissertation, The University of Texas at Austin, June 1969.

7. Armstrong, S.D., "Design and Behavior of Large Cantilever Overhangs with Combinations of Prestressed and Non-Prestressed Reinforcement," Unpublished Masters Thesis, The University of Texas at Austin, August 1994.

8. Salas Pereira, R. M., "Behavior of Structural Concrete Cantilever Piers Using T-Headed Reinforcing Bars and Varied Prestressing Design Criteria," Unpublished Masters Thesis, The University of Texas at Austin, August 1994.

9. Breen, J.E., Burdet, O., Roberts, C., Sanders, D., and Wollmann, G., "Anchorage Zone Reinforcement for Post-Tensioned Concrete Girders," NCHRP, Report 356, Transportation Research Board, National Research Council, 1994.

10. Breen, J.E., Burdet, O., Roberts, C., Sanders, D., and Wollmann, G., "Anchorage Zone Reinforcement for Post-Tensioned Concrete Girders," National Cooperative Highway Research Program, Report No. 356, August 1991.

11. Wollmann, G.P., Yates, D.L., Breen, J.E., and Kreger, M.E., "Fretting Fatigue in Post-Tensioned Concrete," Report 465-2F, Center for Transportation Research, The University of Texas at Austin, November 1988.

12. American Association of State Highway and Transportation Officials (AASHTO), Standard Specifications for Highway Bridges, Interim Specifications 1990-1991 to the Fourteenth Edition, Washington, D.C., 1991.

13. Dyken, T., and Kepp, B., "Properties of T-Headed Reinforcing Bars in High Strength Concrete," Norway (year not available).

14. Lyngaas Dahl, K., "The Development of Headed-Reinforcement Bar, system." Metalock, Norway (year not available).

15. Camping, M.J., "T-Headed Bars as Shear Reinforcement in High Strength Concrete," Metalock, Norway (year not available).

16. American Association of State Highway and Transportation Officials (AASHTO), Standard Specifications for Highway Bridges, Sixteenth Edtion, Washington, D.C., 1996.

17. American Concrete Institute, Building Code Requirements for Reinforced Concrete (ACI 318-89) and Commentary - 318-89, Detroit, 1989.

18. Gergely, P., and Lutz, L.A., "Maximum Crack Width in Reinforced Concrete Flexural Members," Causes, Mechanism and Control of Cracking in Concrete, ACI Publication SP-20, American Concrete Institute, Detroit, 1973, pp. 87-117.

19. Suri, K.M., and Dilger, W.H., "Crack Width of Partially Prestressed Concrete Members," ACI Journal, September-October 1986.

20. Borges, F., and Lima, A., "Crack and Deformation Similitude in Reinforced Concrete," RILEM, No. 7, June 1960.

21. Canadian Standards Association, Code for the Design of Concrete Structures for Buildings, CAN-A23.3-M84, Ontario, 1984.

22. Comité Euro-International du Béton, CEB-FIP Model Code 1990 (Design Code), Thomas Telford, London, 1993.

23. Comité Euro-International du Béton, CEB-FIP Model Code for Concrete Structurs 1978 (Design Code), London, 1978.

24. American Association of State Highway and Transportation Officials (AASHTO) LRFD Bridge Design Specifications, First Edition, Washington, D.C., 1994.

25. Written correspondence with Michael W. Tanner, P.E., Senior Estimator, Austin Bridge and Road, Inc., Dallas, Tx.

APPENDIX A

CRACK WIDTH AND LOCATIONS

	TABLE	FIGURE
CO-RU-0S-OR-N-SF	A-1, 2	A-1, 2
CO-PS-100S-NA-N-SM	A-3, 4	A-3, 4
CO-PU-100S-NA-V & I-SM	A-5, 6	A-5, 6
CO-PU-74S-OR-V & I-SM	A-7, 8	A-7, 8
CO-PU-54S-TH-V & I-SF & SM	A-9 — A-12	A-9, 10
CO-PU-74S-TH-V & I-SM	A-13 — 16	A-11, 12
CO-PU-100S-TH-V-V&I-SF & SM	A-17 — 20	A-13, 14
CO-RU-0S-TH-M1 & M1.7-SM	A-21 — 24	A-15, 16

195

north east

north west
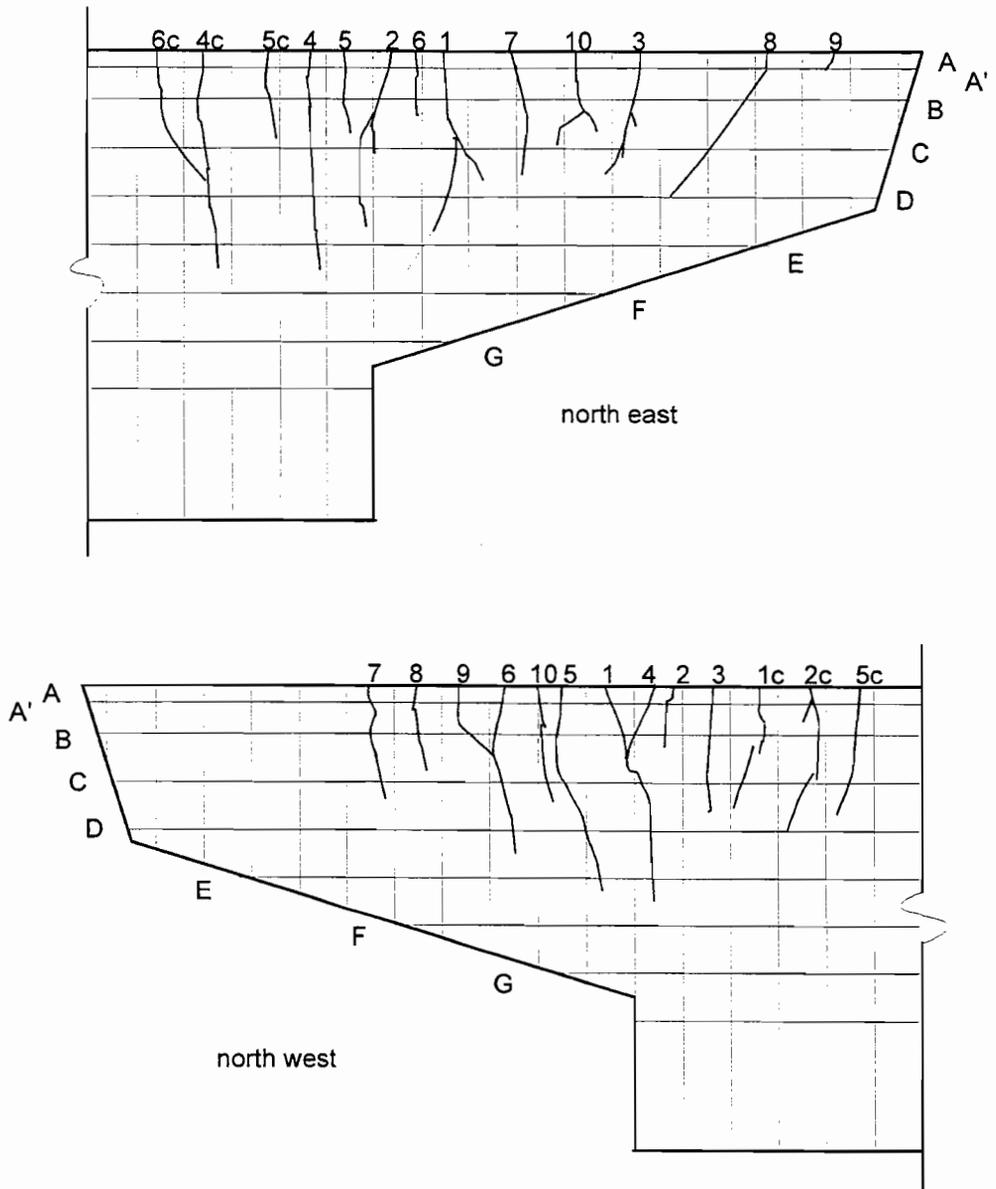
Figure A. 1   *Crack numbers and locations on the north CO-RU-0S-OR-N-SF overhang*
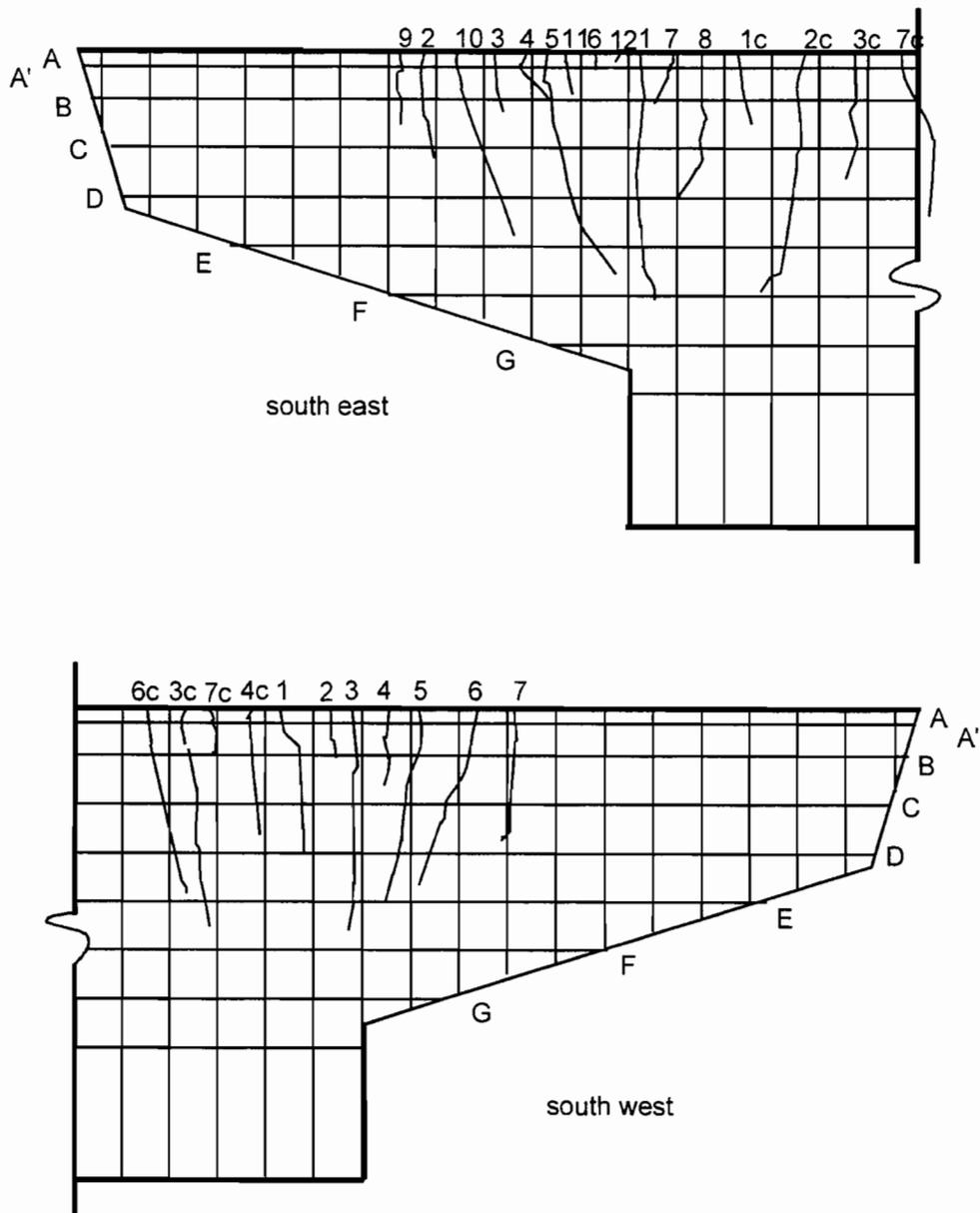
Figure A. 2   Crack numbers and locations on the south CO-RU-0S-OR-N-SF overhang

197

CO - RU North East Side	Ri kips	Ro kips	Moment at Face of Column kip-inches	Maximum Crack Width, inches												
Load Stage				1	2	3	4	5	6	7	8	9	10	4c	5c	6c
cracking loads	28.47	25.59	1394	0.0005	0.0005	0.0005										
(1) Dead Load	43.47	40.47	2169	0.001 A'	0.001	0.0005	0.001	0.0005	0.0005	0.0005	0.0005	0.0005		0.001	0.001	
Dead Load plus	41.15	48.46	2451	0.0025 C	0.002		0.002									
(2) Service Flexure	38.57	56.97	2749	0.0025 B	0.0025	0.002	0.0025	0.002	0.002	0.003	0.0005	0.0015	0.002 A'	0.003 C	0.002	0.001 A'
(4) Service Shear	49.97	46.97	2507	0.002 C	0.003 B	0.0015 B	0.0015 B	0.001	0.0015	0.002 B	0.0005	0.001	0.001 A'	0.002 C	0.002	0.001 A'
(5) Dead Load *	43.47	40.47	2169	0.0005	0.002		0.002			0.0005				0.001	0.001	
(6) Service Flexure *	38.57	56.97	2749	0.001	0.002		0.0025			0.003				0.002	0.002	
Service Flexure plus *	41.51	72.95	3410	0.003	0.0035		0.004		0.002	0.004				0.004	0.0035	
(7) Factored Flexure	46.18	88.52	4078	0.004 B	0.006 B		0.005		0.004	0.006 B				0.0035	0.003	
(8) Dead Load *	43.47	40.47	2169	0.002	0.0025		0.003		0.0015	0.0025				0.003	0.001	
(9) Service Shear *	49.97	46.97	2507	0.002	0.003		0.004		0.003	0.003				0.002	0.0025	0.004
Service Shear plus *	58.00	55.13	2930	0.003	0.003		0.004		0.004	0.003				0.003	0.003	0.004
(10) Factored Shear	70.92	66.82	3554	0.006 B	0.0045 B		0.0045 B		0.0045	0.0055 B				0.003	0.004	0.005

CO - RU North West Side	Ri kips	Ro kips	Moment at Face of Column kip-inches	Maximum Crack Width, inches												
Load Stage				1	2	3	4	5	6	7	8	9	10	1c	2c	5c
cracking loads	28.47	25.59	1394													
(1) Dead Load	43.47	40.47	2169	0.002	0.002	0.002	0.0005	0.002	0.0005					0.005	0.0005	
Dead Load plus	41.15	48.46	2451	0.003		0.002		0.003								
(2) Service Flexure	38.57	56.97	2749	0.003	0.001	0.003	0.001	0.003	0.001	0.001	0.002	0.001		0.001	0.001	0.0005
(4) Service Shear	49.97	46.97	2507	0.003	0.002	0.002	0.0015	0.004**	0.0015	0.0015	0.002 A'	0.001	0.0015	0.0005	0.001	0.0005
(5) Dead Load *	43.47	40.47	2169	0.003		0.002		0.003								
(6) Service Flexure *	38.57	56.97	2749	0.003		0.002		0.003								
Service Flexure plus *	41.51	72.95	3410	0.004		0.003		0.004						0.0015	0.002	
(7) Factored Flexure	46.18	88.52	4078	0.005		0.005		0.005						0.002	0.0025	
(8) Dead Load *	43.47	40.47	2169	0.004		0.002		0.003						0.001	0.001	
(9) Service Shear *	49.97	46.97	2507	0.0035		0.002		0.0045						0.001	0.0015	
Service Shear plus *	58.00	55.13	2930	0.003		0.0025		0.0045						0.001	0.003	
(10) Factored Shear	70.92	66.82	3554	0.0045		0.003		0.005						0.003	0.002	

* crack widths measured only at level A

** omitted

Table A. 2   Maximum crack width readings on the south CO-RU-0S-OR-N-SF overhang

CO - RU	South East Side			Maximum Crack Width, inches													
Load Stage	Ri kips	Ro kips	Moment at Face of Column kip-inches	Crack Number													
				1	2	3	4	5	6	7	8	9	10	11	12	13	1c
cracking loads	28.47	25.59	1394	0.001													
(1) Dead Load	43.47	40.47	2169	0.002 C	0.0005	0.0005	0.0005	0.0005	0.001	0.0005	0.002						0.002
Dead Load plus	41.15	48.46	2451	0.002 C				0.001			0.0015						
(2) Service Flexure	38.57	56.97	2749	0.002 C	0.001	0.002	0.0005	0.002 B	0.001	0.001	0.002	0.001	0.001	0.001	0.0005		0.002
(4) Service Shear	49.97	46.97	2507	0.0025 C	0.001	0.002	0.0005	0.002 B	0.001	0.001	0.0015	0.001	0.001	0.0005	0.0005	0.001 A'	0.002
(5) Dead Load *	43.47	40.47	2169	0.001				0.0005			0.001						0.002
(6) Service Flexure *	38.57	56.97	2749	0.002				0.0015			0.002						0.0025
Service Flexure plus *	41.51	72.95	3410	0.003				0.002			0.004						0.0045
(7) Factored Flexure	46.18	88.52	4078	0.005 C				0.005 C			0.004						0.006
(8) Dead Load *	43.47	40.47	2169	0.002				0.001			0.002						0.004
(9) Service Shear *	49.97	46.97	2507	0.0015				0.001			0.0025						0.005
Service Shear plus *	58.00	55.13	2930	0.002	0.002	0.002		0.002			0.003						0.005
(10) Factored Shear	70.92	66.82	3554	0.0055 C	0.0035	0.003		0.005 C			0.0055 C						0.006

CO - RU	South West Side			Maximum Crack Width, inches										
Load Stage	Ri kips	Ro kips	Moment at Face of Column kip-inches	Crack Number										
				1	2	3	4	5	6	7	3c	4c	6c	7c
cracking loads	28.47	25.59	1394											
(1) Dead Load	43.47	40.47	2169	0.0015 A'	0.0005	0.0015 C	0.0005	0.0005	0.0005		0.0005	0.0005		
Dead Load plus	41.15	48.46	2451	0.001		0.0015 C		0.001 B						
(2) Service Flexure	38.57	56.97	2749	0.002	0.001	0.002 B	0.001	0.001 A'	0.002	0.001	0.001	0.0005	5E-04	0.0005
(4) Service Shear	49.97	46.97	2507	0.002	0.001 A'	0.0015 C	0.001	0.001	0.001	0.001 B	0.0005	0.0005	5E-04	0.0005
(5) Dead Load *	43.47	40.47	2169	0.002		0.001		0.0005						
(6) Service Flexure *	38.57	56.97	2749	0.002		0.0015		0.001						
Service Flexure plus *	41.51	72.95	3410	0.001		0.003		0.004			0.0015			0.003
(7) Factored Flexure	46.18	88.52	4078	0.004 A'		0.004 B		0.004 B			0.003			0.003
(8) Dead Load *	43.47	40.47	2169	0.001		0.001		0.0005			0.001			0.0015
(9) Service Shear *	49.97	46.97	2507	0.002		0.0015		0.001			0.001			0.002
Service Shear plus *	58.00	55.13	2930	0.003		0.002		0.001	0.003		0.001			0.002
(10) Factored Shear	70.92	66.82	3554	0.0045 A'		0.0045 C		0.0045 C	0.003		0.0025			0.003
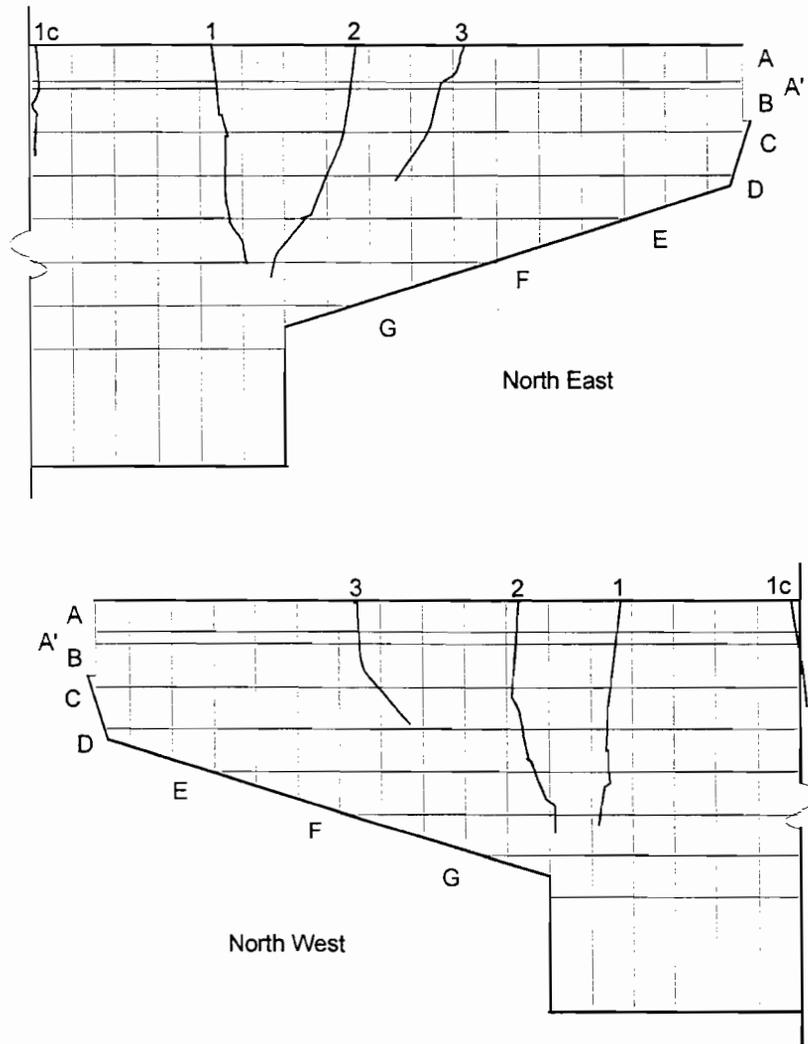
Figure A. 3   Crack numbers and locations on the north CO-PS-100S-NA-N-SM overhang
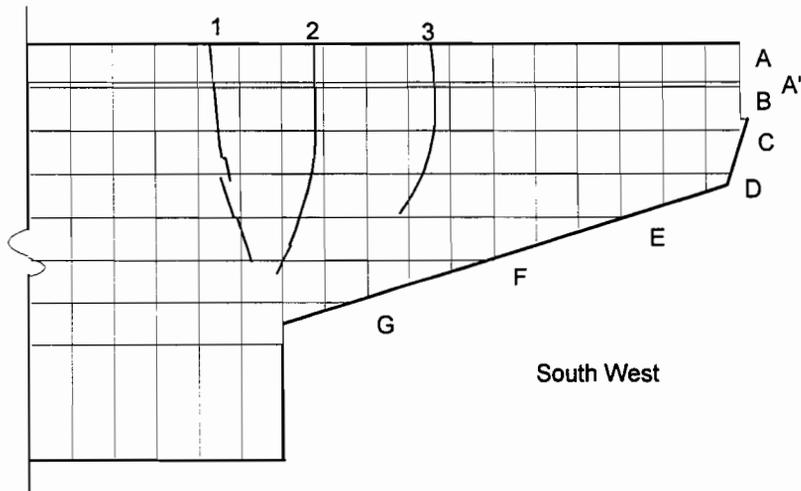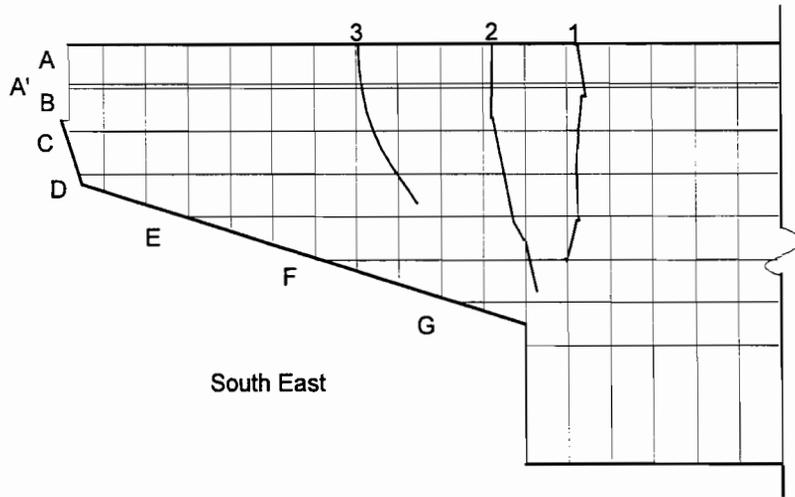
*Figure A. 4   Crack numbers and locations on the south CO-PS-100S-NA-
N-SM overhang*

Table A. 3   Maximum crack width readings on the north CO-PS-100S-NA-N-SM

CO-PS-100S	North East Side			Maximum Crack Width, inches			
Load Stage	Ri	Ro	Moment at Face of Column	Crack Number			
	kips	kips	kip-inches	1	2	3	1c
(7) Factored Flexure	46.18	88.52	4078	0.0045			
(8) Dead Load	43.47	40.47	2169	0.001			
(9) Service Shear	49.97	46.97	2507	0.001			
(10) Factored Shear	70.92	66.82	3554	0.004			
(11) Dead Load	43.47	40.47	2169	0.001			
(12) Service Flexure	38.57	56.97	2749	0.0015			
(13) Factored Flexure	46.18	88.52	4078	0.005			
Factored Flexure plus	51.12	121.25	5419	0.01	0.012		0.003
Factored Flexure plus	61.16	172.90	7564	0.04	0.06 A'	0.007	0.009

CO-PS-100S	North West side			Maximum Crack Width, inches			
Load Stage	Ri	Ro	Moment at Face of Column	Crack Number			
	kips	kips	kip-inches	1	2	3	1c
cracking loads	41.11	69.53	3272	0.0015			
(7) Factored Flexure	46.18	88.52	4078	0.005 A'			
(8) Dead Load	43.47	40.47	2169	0.002			
(9) Service Shear	49.97	46.97	2507	0.002			
(10) Factored Shear	70.92	66.82	3554	0.0055			
(11) Dead Load	43.47	40.47	2169	0.002			
(12) Service Flexure	38.57	56.97	2749	0.003			
(13) Factored Flexure	46.18	88.52	4078	0.006			
Factored Flexure plus	51.12	121.25	5419	0.012	0.011		0.005
Factored Flexure plus	61.16	172.90	7564	0.05	0.06 A'	0.01	0.007

Table A. 4   Maximum crack width readings on the south CO-PS-100S-NA-N-SM overhang

CO-PS-100S	South East side		Moment at Face of Column kip-inches	Maximum Crack Width, inches		
Load Stage	Ri kips	Ro kips		Crack Number		
				1	2	3
(7) Factored Flexure	46.18	88.52	4078	0.004		
(8) Dead Load	43.47	40.47	2169	0.001		
(9) Service Shear	49.97	46.97	2507	0.001		
(10) Factored Shear	70.92	66.82	3554	0.003		
(11) Dead Load	43.47	40.47	2169	0.001		
(12) Service Flexure	38.57	56.97	2749	0.001		
(13) Factored Flexure	46.18	88.52	4078	0.005 B		
Factored Flexure plus	51.12	121.25	5419	0.008	0.016	
Factored Flexure plus	61.16	172.90	7564	0.04	0.05	0.01

| CO-PS-100S	South West side		Moment at Face of Column kip-inches	Maximum Crack Width, inches		
Load Stage	Ri kips	Ro kips		Crack Number		
				1	2	3
(7) Factored Flexure	46.18	88.52	4078	0.005		
(8) Dead Load	43.47	40.47	2169	0.002		
(9) Service Shear	49.97	46.97	2507	0.002		
(10) Factored Shear	70.92	66.82	3554	0.0045		
(11) Dead Load	43.47	40.47	2169	0.002		
(12) Service Flexure	38.57	56.97	2749	0.0025		
(13) Factored Flexure	46.18	88.52	4078	0.007		
Factored Flexure plus	51.12	121.25	5419	0.014	0.014	
Factored Flexure plus	61.16	172.90	7564	0.04	0.06	0.009 B

203
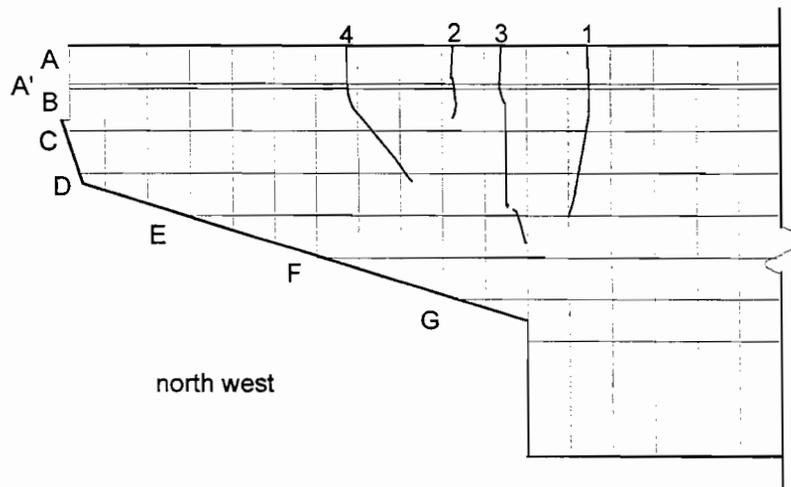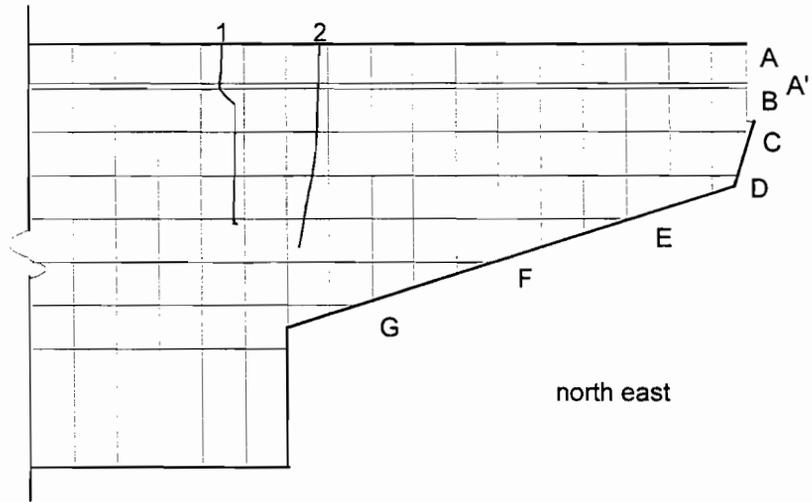
Figure A. 5   Crack numbers and locations on the CO-PU-100S-NA-I-SM overhang
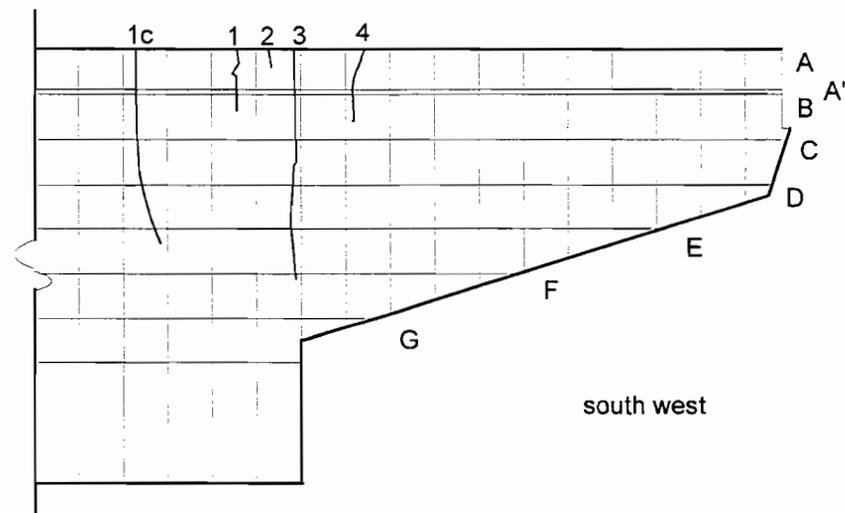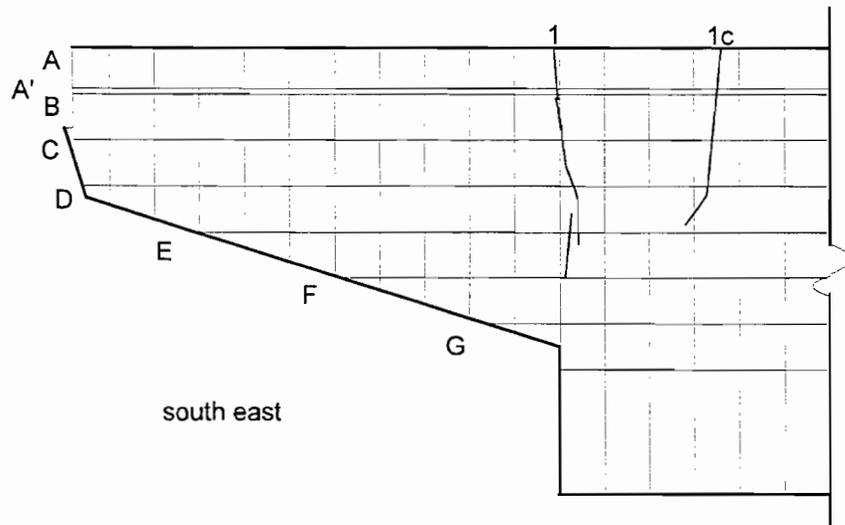
Figure A. 6   Crack numbers and locations on the CO-PU-100S-NA-V-SM overhang

Table A. 5   *Maximum crack width readings on the CO-PU-100S-NA-I-SM overhang*

CO-PU-100S-I North East side				Maximum Crack Width, inches	
Load Stage	Ri kips	Ro kips	Moment at Face of Column kip-inches	Crack Number 1	2
cracking loads	41.48	73.27	3422	0.0015	
(7) Factored Flexure	46.18	88.52	4078	0.005	0.006 A'
(8) Dead Load	43.47	40.47	2169	0.002	0.001
(9) Service Shear	49.97	46.97	2507	0.002	0.003 A'
(10) Factored Shear	70.92	66.82	3554	0.003	0.004 A'
(11) Dead Load	43.47	40.47	2169	0.0015	0.002 A'
(12) Service Flexure	38.57	56.97	2749	0.002	0.003 A'
(13) Factored Flexure	46.18	88.52	4078	0.0055	0.007
Factored Flexure plus	51.12	120.88	5405	0.018	0.025

CO-PU-100S-I North West side				Maximum Crack Width, inches			
Load Stage	Ri kips	Ro kips	Moment at Face of Column kip-inches	Crack Number 1	2	3	4
cracking loads	40.02	65.15	3087	0.002			
cracking NE	41.48	73.27	3422	0.005			
(7) Factored Flexure	46.18	88.52	4078	0.01	0.003	0.003	
(8) Dead Load	43.47	40.47	2169	0.004	0.001	0.001	
(9) Service Shear	49.97	46.97	2507	0.005	0.001	0.002 A'	
(10) Factored Shear	70.92	66.82	3554	0.0065	0.001	0.003	
(11) Dead Load	43.47	40.47	2169	0.004	0.0005	0.001	
(12) Service Flexure	38.57	56.97	2749	0.004	0.001	0.0015	
(13) Factored Flexure	46.18	88.52	4078	0.009	0.003	0.005	
Factored Flexure plus	51.12	120.88	5405		0.002	0.021	0.018

Table A. 6   Maximum crack width readings on the CO-PU-100S-NA-V-SM overhang

CO-PU-100S-V	South East side			Maximum Crack Width, inches	
Load Stage	Ri kips	Ro kips	Moment at Face of Column kip-inches	Crack Number	
				1	1c
cracking loads	40.02	65.15	3087	0.002	
cracking NE	41.48	73.27	3422	0.006	
(7) Factored Flexure	46.18	88.52	4078	0.015	0.004
(8) Dead Load	43.47	40.47	2169	0.006	0.002
(9) Service Shear	49.97	46.97	2507	0.007	0.002
(10) Factored Shear	70.92	66.82	3554	0.013	0.0035
(11) Dead Load	43.47	40.47	2169	0.005	0.001
(12) Service Flexure	38.57	56.97	2749	0.007	0.002
(13) Factored Flexure	46.18	88.52	4078	0.017	0.004
Factored Flexure plus	51.12	120.88	5405	0.074	0.016

CO-PU-100S-V	South West side			Maximum Crack Width, inches				
Load Stage	Ri kips	Ro kips	Moment at Face of Column kip-inches	Crack Number				
				1	2	3	4	1c
cracking loads	39.29	61.20	2923	0.002	0.001			
cracking SE,NW	40.02	65.15	3087	0.0025	0.001			
cracking NE	41.48	73.27	3422	0.003	0.001	0.003		
(7) Factored Flexure	46.18	88.52	4078	0.003	0.001	0.014	0.003	0.005
(8) Dead Load	43.47	40.47	2169	0.0015	0.001	0.005	0.001	0.002
(9) Service Shear	49.97	46.97	2507	0.002	0.001	0.007	0.001	0.002
(10) Factored Shear	70.92	66.82	3554	0.002	0.001	0.011	0.0015	0.004
(11) Dead Load	43.47	40.47	2169	0.002	0.001	0.007	0.001	0.001
(12) Service Flexure	38.57	56.97	2749	0.002	0.001	0.007	0.001	0.002
(13) Factored Flexure	46.18	88.52	4078	0.003	0.001	0.017	0.002	0.005
Factored Flexure plus	51.12	120.88	5405	0.003	0.001	0.077	0.001	0.02
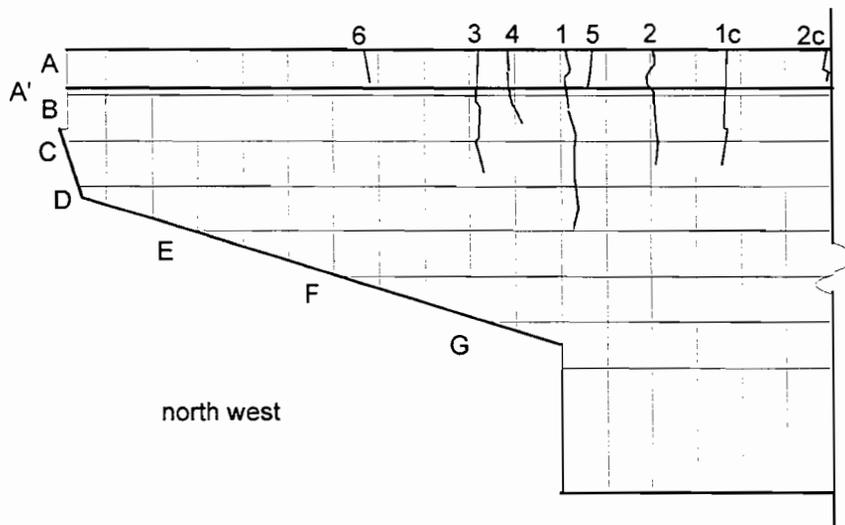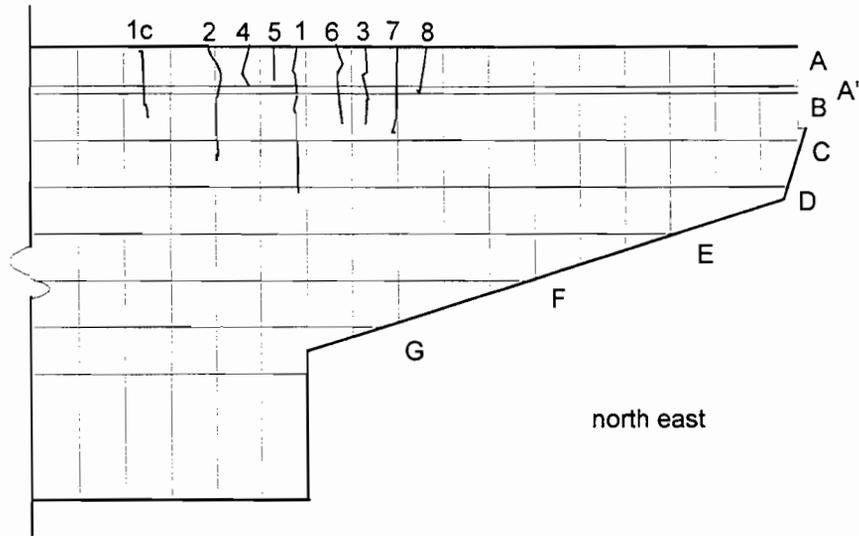
Figure A. 7   Crack numbers and locations on the CO-PU-74S-OR-I-SM overhang
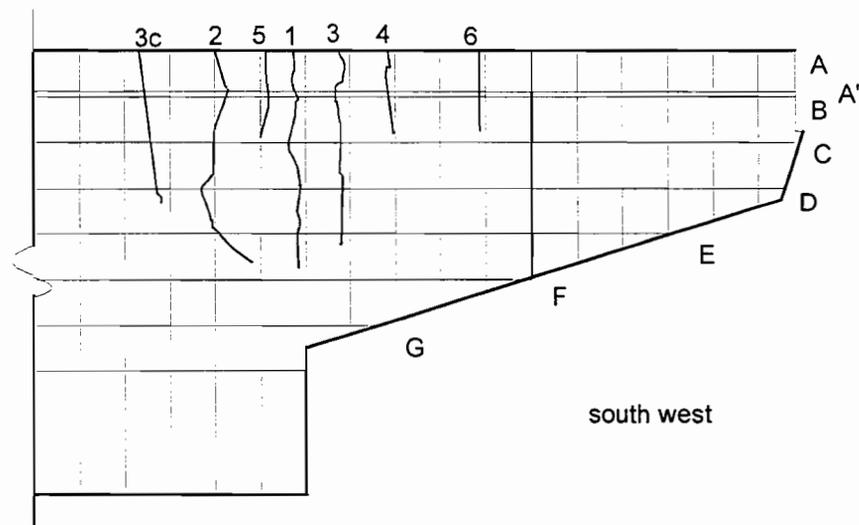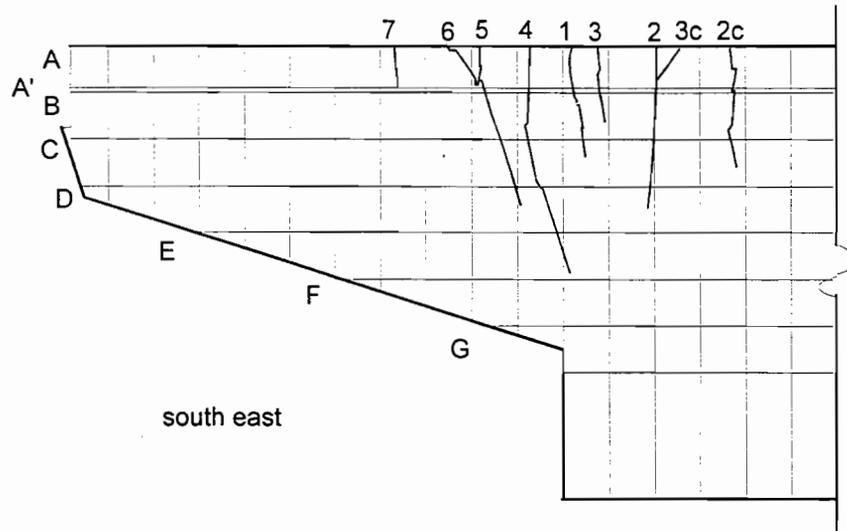
Figure A. 8   Crack numbers and locations on the CO-PU-74S-OR-V-SM overhang

209

Table A. 7   Maximum crack width readings on the CO-PU-74S-OR-I-SM overhang

CO-PU-74S-I	North East side			Maximum Crack Width, inches								
Load Stage	Ri kips	Ro kips	Moment at Face of Column kip-inches	Crack Number								
				1	2	3	4	5	6	7	8	1c
cracking loads	41.29	49.66	2499	0.0015								
(2) Service Flexure	38.57	56.97	2749	0.0025								
(3) Dead Load	43.47	40.47	2169	0.002								
(4) Service Shear	49.97	46.97	2507	0.002								
(5) Dead Load	43.47	40.47	2169	0.002								
(6) Service Flexure	38.57	56.97	2749	0.003	0.0005							
Service Flexure plus	41.91	73.94	3454	0.005	0.003	0.002						
(7) Factored Flexure	46.18	88.52	4078	0.005	0.004	0.0025	0.003	0.002	0.004	0.003	0.003	0.003 A'
(8) Dead Load	43.47	40.47	2169	0.003	0.002	0.0005	0.0005	0.0005	0.002	0.001	0.0005	0.002 A'
(9) Service Shear	49.97	46.97	2507	0.003	0.002	0.0005	0.001	0.0005	0.002	0.001	0.0005	0.002 A'
(10) Factored Shear	70.92	66.82	3554	0.003	0.003	0.002	0.003	0.001	0.003	0.002	0.002	0.003 A'
(12) Service Flexure	38.57	56.97	2749	0.002	0.002	0.001	0.0015	0.0005	0.002	0.001	0.0015	0.002
(13) Factored Flexure	46.18	88.52	4078	0.005	0.004	0.003	0.003	0.002	0.004	0.003	0.003	0.004 A'

CO-PU-74S-I	North West side			Maximum Crack Width, inches							
Load Stage	Ri kips	Ro kips	Moment at Face of Column kip-inches	Crack Number							
				1	2	3	4	5	6	1c	2c
cracking loads	41.29	49.66	2499	0.0005							
(2) Service Flexure	38.57	56.97	2749	0.0025							
(3) Dead Load	43.47	40.47	2169	0.002							
(4) Service Shear	49.97	46.97	2507	0.002	0.0015						
(5) Dead Load	43.47	40.47	2169	0.002	0.0015						
(6) Service Flexure	38.57	56.97	2749	0.003	0.002	0.0005					
Service Flexure plus	41.91	73.94	3454	0.004	0.004 A'	0.007	0.0005				
(7) Factored Flexure	46.18	88.52	4078	0.007 A'	0.004	0.01	0.005	0.004	0.002	0.01	0.002
(8) Dead Load	43.47	40.47	2169	0.0005	0.003 A'	0.006	0.0015	0.001	0.0005	0.003	0.0005
(9) Service Shear	49.97	46.97	2507	0.004 A'	0.003 A'	0.007	0.003	0.002	0.0005	0.003	0.0005
(10) Factored Shear	70.92	66.82	3554	0.005 A'	0.005 A'	0.007	0.004	0.004	0.0015	0.004	0.001
(12) Service Flexure	38.57	56.97	2749	0.004 A'	0.004 A'	0.007	0.003	0.002	0.001	0.0035	0.001
(13) Factored Flexure	46.18	88.52	4078	0.005 A'	0.005 A'	0.009	0.007	0.004	0.003	0.005	0.002

210

Table A. 8   Maximum crack width readings on the CO-PU-74S-OR-V-SM overhang

CO-PU-74S-V		South East side		Maximum Crack Width, inches								
Load Stage	Ri kips	Ro kips	Moment at Face of Column kip-inches	Crack Number								
				1	2	3	4	5	6	7	2c	3c
cracking loads	41.29	49.66	2499	0.001								
(2) Service Flexure	38.57	56.97	2749	0.0028								
(3) Dead Load	43.47	40.47	2169	0.0022								
(4) Service Shear	49.97	46.97	2507	0.0025								
(5) Dead Load	43.47	40.47	2169	0.0022								
Service Flexure plus	41.91	73.94	3454	0.004	0.002	0.004	0.007	0.003				
(7) Factored Flexure	46.18	88.52	4078	0.005	0.005	0.005	0.006	0.005	0.005	0.003	0.004	0.001
(8) Dead Load	43.47	40.47	2169	0.0035	0.001	0.002	0.004	0.0035	0.002	0.0005	0.002	0.0005
(9) Service Shear	49.97	46.97	2507	0.002	0.001	0.002	0.004	0.003	0.002	0.0005	0.003	0.0005
(10) Factored Shear	70.92	66.82	3554	0.003	0.0025	0.003	0.006	0.005	0.003	0.0015	0.0035	0.001
(11) Service Flexure	38.57	56.97	2749	0.003	0.003	0.003	0.004	0.003	0.003	0.001	0.003	0.0005
(12) Factored Flexure	46.18	88.52	4078	0.006	0.005	0.005	0.0065	0.006	0.0045	0.003	0.004	0.002

CO-PU-74S-V		South West side		Maximum Crack Width, inches						
Load Stage	Ri kips	Ro kips	Moment at Face of Column kip-inches	Crack Number						
				1	2	3	4	5	6	3c
cracking loads	43.36	41.86	2222	0.0005						
cracking NW	41.29	49.66	2499	0.002						
(2) Service Flexure	38.57	56.97	2749	0.003	0.0012					
(3) Dead Load	43.47	40.47	2169	0.0025	0.001					
(4) Service Shear	49.97	46.97	2507	0.003	0.001					
(5) Dead Load	43.47	40.47	2169	0.003	0.001					
(6) Service Flexure	38.57	56.97	2749	0.003	0.002					
Service Flexure plus	41.91	73.94	3454	0.0055	0.007	0.005	0.0025			
(7) Factored Flexure	46.18	88.52	4078	0.009	0.009	0.008	0.008	0.005	0.006	0.007
(8) Dead Load	43.47	40.47	2169	0.004	0.004	0.004	0.003	0.004	0.002	0.004
(9) Service Shear	49.97	46.97	2507	0.004	0.006	0.005	0.003	0.003	0.002	0.005
(10) Factored Shear	70.92	66.82	3554	0.0065	0.008	0.007	0.006	0.003	0.0035	0.007
(12) Service Flexure	38.57	56.97	2749	0.005	0.006	0.005	0.006	0.003	0.002	0.005
(13) Factored Flexure	46.18	88.52	4078	0.009	0.011	0.007	0.008	0.006	0.006	0.007

South West

South East
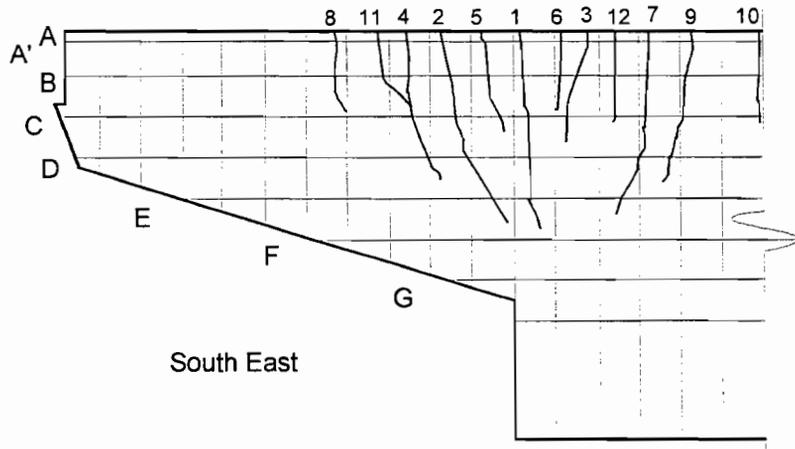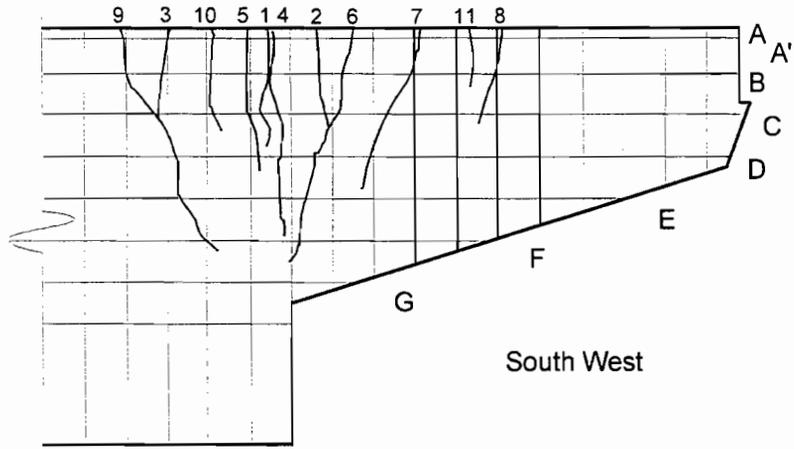
Figure A. 9   *Crack number and location on east and west sides of CO-PU-54S-TH-V-SF*
overhang

North East

North West
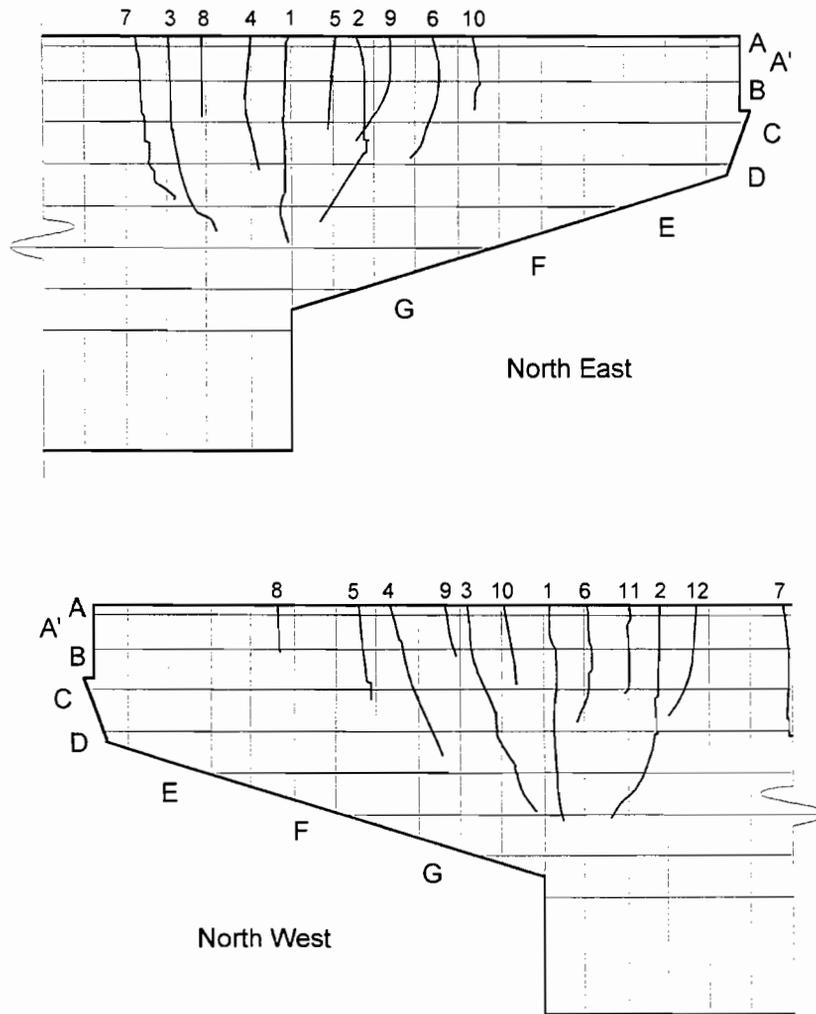
Figure A. 10   Crack number and location on east and west sides of CO-PU-54S-TH-I-SM overhang

213

Table A. 9   Maximum crack width readings for overhang CO-PU-54S-TH-V-SF

CO-PU-54S-TH-V	East Side			Maximum Crack Width, inches											
Load Stage	Ri (kips)	Ro (kips)	Moment at Face of Column (kip-inches)	Crack Number											
				1	2	3	4	5	6	7	8	9	10	11	12
(1) Dead Load	43.47	40.47	2169	0.001A'											
Dead Load plus	42.2	45.46	2322	0.0015											
(2) Service Flexure	38.57	56.97	2749	0.0025	0.001										
(3) Dead Load *	43.47	40.47	2169	0.002	0.001										
(4) Service Shear	49.97	46.97	2507	0.002	0.001										
(5) Dead Load *	43.47	40.47	2169	0.002	0.001										
(6) Service Flexure	38.57	56.97	2749	0.003	0.0015	0.002									
Service Flexure plus *	41.76	73.46	3408	0.003	0.003	0.003	0.002	0.0045	0.0015	0.002					
(7) Factored Flexure *	46.18	88.52	4078	0.005	0.005	0.0035	0.005	0.0055	0.0045	0.0035	0.003	0.0035	0.002	0.002	0.004
(8) Dead Load *	43.47	40.47	2169	0.0025	0.002	0.0015	0.0025	0.0025	0.001	0.002	0.001	0.002	0.0005	0.0005	0.002
(9) Service Shear *	49.97	46.97	2507	0.0025	0.002	0.002	0.003	0.0035	0.002	0.002	0.002	0.002	0.001	0.001	0.002
(10) Factored Shear *	70.92	66.82	3554	0.005	0.005	0.0025	0.003	0.006	0.003	0.003	0.0025	0.003	0.0015	0.0015	0.0035
(12) Service Flexure *	38.57	56.97	2749	0.0025	0.0025	0.0025	0.0035	0.0035	0.002	0.0025	0.0025	0.0025	0.001	0.001	0.0025
(13) Factored Flexure *	46.18	88.52	4078	0.0035	0.0055	0.0035	0.005	0.006	0.004	0.0035	0.005	0.0035	0.0025	0.002	0.004

CO-PU-54S-TH-V	East Side			Maximum Crack Width (mm)											
Load Stage	Ri (kN)	Ro (kN)	Moment at Face of Column (kN-m)	Crack Number											
				1	2	3	4	5	6	7	8	9	10	11	12
(1) Dead Load	(193.4)	(180.0)	(245.1)	(0.025 A')											
Dead Load plus	(187.7)	(202.2)	(262.4)	(0.038)											
(2) Service Flexure	(171.6)	(253.4)	(310.6)	(0.064)	(0.025)										
(3) Dead Load *	(193.4)	(180.0)	(245.1)	(0.051)	(0.025)										
(4) Service Shear	(222.3)	(208.9)	(283.3)	(0.051)	(0.025)										
(5) Dead Load *	(193.4)	(180.0)	(245.1)	(0.051)	(0.025)										
(6) Service Flexure	(171.6)	(253.4)	(310.6)	(0.076)	(0.038)	(0.051)									
Service Flexure plus *	(185.7)	(326.8)	(385.1)	(0.076)	(0.076)	(0.076)	(0.051)	(0.114)	(0.038)	(0.051)					
(7) Factored Flexure *	(205.4)	(393.7)	(460.8)	(0.127)	(0.127)	(0.089)	(0.127)	(0.140)	(0.114)	(0.089)	(0.076)	(0.089)	(0.051)	(0.051)	(0.102)
(8) Dead Load *	(193.4)	(180.0)	(245.1)	(0.064)	(0.051)	(0.038)	(0.064)	(0.064)	(0.025)	(0.051)	(0.025)	(0.051)	(0.013)	(0.013)	(0.051)
(9) Service Shear *	(222.3)	(208.9)	(283.3)	(0.064)	(0.051)	(0.051)	(0.076)	(0.089)	(0.051)	(0.051)	(0.051)	(0.051)	(0.025)	(0.025)	(0.051)
(10) Factored Shear *	(315.5)	(297.2)	(401.6)	(0.127)	(0.127)	(0.064)	(0.076)	(0.152)	(0.076)	(0.076)	(0.064)	(0.076)	(0.038)	(0.038)	(0.089)
(12) Service Flexure *	(171.6)	(253.4)	(310.6)	(0.064)	(0.064)	(0.064)	(0.089)	(0.089)	(0.051)	(0.064)	(0.064)	(0.064)	(0.025)	(0.025)	(0.064)
(13) Factored Flexure *	(205.4)	(393.7)	(460.8)	(0.089)	(0.140)	(0.089)	(0.127)	(0.152)	(0.102)	(0.089)	(0.127)	(0.089)	(0.064)	(0.051)	(0.102)

* Only maximum crack width was measured, usually at level A unless otherwise noted.

Table A. 10   Maximum crack width readings for overhang CO-PU-54S-TH-V-SF (west side)

CO-PU-54S-TH-V West Side				Maximum Crack Width, inches											
Load Stage	Ri kips	Ro kips	Moment at Face of Column kip-inches	Crack Number											
				1	2	3	4	5	6	7	8	9	10	11	12
cracking	40.48	37.46	1987	0.001											
Dead Load plus	42.2	45.46	2322	0.0025											
(2) Service Flexure	38.57	56.97	2749	0.003 A'	0.0025										
(3) Dead Load *	43.47	40.47	2169	0.002	0.0015										
(4) Service Shear	49.97	46.97	2507	0.0025	0.002										
(5) Dead Load *	43.47	40.47	2169	0.0025	0.002										
(6) Service Flexure	38.57	56.97	2749	0.0035	0.0025	0.002	0.001C								
Service Flexure plus *	41.76	73.46	3408	0.005	0.005	0.004	0.003 C	0.0045	0.0035	0.0035	0.002				
(7) Factored Flexure *	46.18	88.52	4078	0.005	0.0065	0.005	0.003 C	0.006	0.006	0.005	0.002	0.0025	0.003	0.002	
(8) Dead Load *	43.47	40.47	2169	0.003	0.004	0.0025	0.0015 C	0.002	0.0025	0.0035	0.001	0.002	0.002	0.001	
(9) Service Shear *	49.97	46.97	2507	0.004	0.0045	0.003	0.0015	0.003	0.003	0.0035	0.001	0.002	0.003	0.001	
(10) Factored Shear *	70.92	66.82	3554	0.005	0.005	0.003	0.002	0.004	0.0055	0.006	0.002	0.0025	0.0025	0.002	
(12) Service Flexure *	38.57	56.97	2749	0.0025	0.0045	0.0035	0.002	0.003	0.0035	0.0045	0.001	0.0025	0.0025	0.0015	
(13) Factored Flexure *	46.18	88.52	4078	0.0035	0.007	0.004	0.003	0.0055	0.006	0.007	0.003	0.0025	0.005	0.0035	

CO-PU-54S-TH-V West Side				Maximum Crack Width (mm)											
Load Stage	Ri (kN)	Ro (kN)	Moment at Face of Column (kN-m)	Crack Number											
				1	2	3	4	5	6	7	8	9	10	11	12
cracking	(180.1)	(166.6)	(224.5)	(0.025)											
Dead Load plus	(187.7)	(202.2)	(262.4)	(0.064)											
(2) Service Flexure	(171.6)	(253.4)	(310.6)	(0.076 A')	(0.064)										
(3) Dead Load *	(193.4)	(180.0)	(245.1)	(0.051)	(0.038)										
(4) Service Shear	(222.3)	(208.9)	(283.3)	(0.064)	(0.051)										
(5) Dead Load *	(193.4)	(180.0)	(245.1)	(0.064)	(0.051)										
(6) Service Flexure	(171.6)	(253.4)	(310.6)	(0.089)	(0.064)	(0.051)	(0.025 C)								
Service Flexure plus *	(185.7)	(326.8)	(385.1)	(0.127)	(0.127)	(0.102)	(0.076 C)	(0.114)	(0.089)	(0.089)	(0.051)				
(7) Factored Flexure *	(205.4)	(393.7)	(460.8)	(0.127)	(0.165)	(0.127)	(0.076 C)	(0.152)	(0.152)	(0.127)	(0.051)	(0.064)	(0.076)	(0.051)	
(8) Dead Load *	(193.4)	(180.0)	(245.1)	(0.076)	(0.102)	(0.064)	(0.0038 C)	(0.051)	(0.064)	(0.089)	(0.025)	(0.051)	(0.051)	(0.025)	
(9) Service Shear *	(222.3)	(208.9)	(283.3)	(0.102)	(0.114)	(0.076)	(0.038)	(0.076)	(0.076)	(0.089)	(0.025)	(0.051)	(0.076)	(0.025)	
(10) Factored Shear *	(315.5)	(297.2)	(401.6)	(0.127)	(0.127)	(0.076)	(0.051)	(0.102)	(0.140)	(0.152)	(0.051)	(0.064)	(0.064)	(0.051)	
(12) Service Flexure *	(171.6)	(253.4)	(310.6)	(0.064)	(0.114)	(0.089)	(0.051)	(0.076)	(0.089)	(0.114)	(0.025)	(0.064)	(0.064)	(0.038)	
(13) Factored Flexure *	(205.4)	(393.7)	(460.8)	(0.089)	(0.178)	(0.102)	(0.076)	(0.140)	(0.152)	(0.178)	(0.076)	(0.064)	(0.127)	(0.089)	

* Only maximum crack width was measured, usually at level A unless otherwise noted.

215

Table A. 11   Maximum crack width readings for overhang CO-PU-54S-TH-I-SM (east side)

CO-PU-54S-TH-I East Side				Maximum Crack Width , inches											
Load Stage	Ri kips	Ro kips	Moment at Face of Column kip-inches	Crack Number											
				1	2	3	4	5	6	7	8	9	10	11	12
Dead Load plus	42.2	45.46	2322	0.001											
(2) Service Flexure	38.57	56.97	2749	0.0025	0.0005	0.0015									
(3) Dead Load *	43.47	40.47	2169	0.002	0.0005	0.001									
(4) Service Shear	49.97	46.97	2507	0.0025 A'	0.0015 A'	0.0015									
(5) Dead Load *	43.47	40.47	2169	0.0015 A'	0.001	0.0015									
(6) Service Flexure	38.57	56.97	2749	0.0025	0.002	0.0015									
Service Flexure plus *	41.76	73.46	3408	0.0035 A'	0.0025	0.0025	0.004	0.003	0.0005						
(7) Factored Flexure *	46.18	88.52	4078	0.005 A'	0.0035	0.005	0.005 A'	0.0035	0.0025	0.003	0.003	0.002	0.0025		
(8) Dead Load *	43.47	40.47	2169	0.0035	0.002	0.0025	0.001	0.001	0.001	0.002	0.001	0.001	0.001		
(9) Service Shear *	49.97	46.97	2507	0.0025 A'	0.002	0.0025	0.0025 A'	0.002	0.001	0.002	0.001	0.001	0.001		
(10) Factored Shear *	70.92	66.82	3554	0.005 A'	0.003	0.003	0.0055 A'	0.003	0.002	0.003	0.0025	0.0035	0.0025		
(12) Service Flexure *	38.57	56.97	2749	0.003 A'	0.0025	0.0025	0.0035 A'	0.002	0.001	0.0015	0.0015	0.0015	0.002		
(13) Factored Flexure *	46.18	88.52	4078	0.006 A'	0.004	0.0035	0.006 A'	0.0045	0.0035	0.005	0.0035	0.0035	0.0035		

CO-PU-54S-TH-I East Side				Maximum Crack Width (mm)											
Load Stage	Ri (kN)	Ro (kN)	Moment at Face of Column (kN-m)	Crack Number											
				1	2	3	4	5	6	7	8	9	10	11	12
Dead Load plus	(187.7)	(202.2)	(262.4)	(0.025)											
(2) Service Flexure	(171.6)	(253.4)	(310.6)	(0.064)	(0.013)	(0.038)									
(3) Dead Load *	(193.4)	(180.0)	(245.1)	(0.051)	(0.013)	(0.025)									
(4) Service Shear	(222.3)	(208.9)	(283.3)	(0.064 A')	(0.038 A')	(0.038)									
(5) Dead Load *	(193.4)	(180.0)	(245.1)	(0.038 A')	(0.025)	(0.038)									
(6) Service Flexure	(171.6)	(253.4)	(310.6)	(0.064)	(0.051)	(0.038)									
Service Flexure plus *	(185.7)	(326.8)	(385.1)	(0.089 A')	(0.064)	(0.064)	(0.102)	(0.076)	(0.013)						
(7) Factored Flexure *	(205.4)	(393.7)	(460.8)	(0.127 A')	(0.089)	(0.127)	(0.127 A')	(0.089)	(0.064)	(0.076)	(0.076)	(0.051)	(0.064)		
(8) Dead Load *	(193.4)	(180.0)	(245.1)	(0.089)	(0.051)	(0.064)	(0.025)	(0.025)	(0.025)	(0.051)	(0.025)	(0.025)	(0.025)		
(9) Service Shear *	(222.3)	(208.9)	(283.3)	(0.064 A')	(0.051)	(0.064)	(0.064 A')	(0.051)	(0.025)	(0.051)	(0.025)	(0.025)	(0.025)		
(10) Factored Shear *	(315.5)	(297.2)	(401.6)	(0.127 A')	(0.076)	(0.076)	(0.140 A')	(0.076)	(0.051)	(0.076)	(0.064)	(0.089)	(0.064)		
(12) Service Flexure *	(171.6)	(253.4)	(310.6)	(0.076 A')	(0.064)	(0.064)	(0.089 A')	(0.051)	(0.025)	(0.038)	(0.038)	(0.038)	(0.051)		
(13) Factored Flexure *	(205.4)	(393.7)	(460.8)	(0.152 A')	(0.102)	(0.089)	(0.152 A')	(0.114)	(0.089)	(0.127)	(0.089)	(0.089)	(0.089)		

* Only maximum crack width was measured, usually at level A unless otherwise noted.

Table A. 12   Maximum crack width readings for overhang CO-PU-54S-TH-I-SM (west side)

CO-PU-54S-TH-I	West Side			Maximum Crack Width (inches)											
Load Stage	Ri kips	Ro kips	Moment at Face of Column kip-inches	Crack Number											
				1	2	3	4	5	6	7	8	9	10	11	12
cracking	40.48	37.46	1987	0.0015											
Dead Load plus	42.2	45.46	2322	0.0025											
(2) Service Flexure	38.57	56.97	2749	0.003	0.0025	0.0025	0.001								
(3) Dead Load *	43.47	40.47	2169	0.002	0.002	0.0015	0.001								
(4) Service Shear	49.97	46.97	2507	0.003	0.002	0.0025	0.001								
(5) Dead Load *	43.47	40.47	2169	0.0025	0.002	0.0025	0.001								
(6) Service Flexure	38.57	56.97	2749	0.0025	0.002	0.0025	0.0015								
Service Flexure plus *	41.76	73.46	3408	0.005	0.002	0.0045	0.002	0.0015	0.004	0.0015					
(7) Factored Flexure *	46.18	88.52	4078	0.006	0.005	0.0065	0.003	0.003	0.006	0.003	0.002	0.0025	0.005	0.004	0.0025
(8) Dead Load *	43.47	40.47	2169	0.0035	0.003	0.0025	0.0025	0.001	0.003	0.002	0.001	0.002	0.002	0.002	0.0015
(9) Service Shear *	49.97	46.97	2507	0.003	0.003	0.0035	0.002	0.001	0.0035	0.002	0.0015	0.001	0.002	0.002	0.002
(10) Factored Shear *	70.92	66.82	3554	0.006	0.0055	0.0045	0.003	0.002	0.005	0.003	0.001	0.003	0.005	0.0045	0.0025
(12) Service Flexure *	38.57	56.97	2749	0.0045	0.004	0.0035	0.003	0.002	0.0045	0.003	0.001	0.0025	0.0035	0.003	0.002
(13) Factored Flexure *	46.18	88.52	4078	0.0065	0.005	0.005	0.004	0.004	0.0065	0.0035	0.0025	0.0035	0.006	0.0065	0.003

CO-PU-54S-TH-I	West Side			Maximum Crack Width (mm)											
Load Stage	Ri (kN)	Ro (kN)	Moment at Face of Column (kN-m)	Crack Number											
				1	2	3	4	5	6	7	8	9	10	11	12
cracking	(180.1)	(166.6)	(224.5)	(0.038)											
Dead Load plus	(187.7)	(202.2)	(262.4)	(0.064)											
(2) Service Flexure	(171.6)	(253.4)	(310.6)	(0.076)	(0.064)	(0.064)	(0.025)								
(3) Dead Load *	(193.4)	(180.0)	(245.1)	(0.051)	(0.051)	(0.038)	(0.025)								
(4) Service Shear	(222.3)	(208.9)	(283.3)	(0.076)	(0.051)	(0.064)	(0.025)								
(5) Dead Load *	(193.4)	(180.0)	(245.1)	(0.064)	(0.051)	(0.064)	(0.025)								
(6) Service Flexure	(171.6)	(253.4)	(310.6)	(0.064)	(0.051)	(0.064)	(0.038)								
Service Flexure plus *	(185.7)	(326.8)	(385.1)	(0.127)	(0.051)	(0.114)	(0.051)	(0.038)	(0.102)	(0.038)					
(7) Factored Flexure *	(205.4)	(393.7)	(460.8)	(0.152)	(0.127)	(0.165)	(0.076)	(0.076)	(0.152)	(0.076)	(0.051)	(0.064)	(0.127)	(0.102)	(0.064)
(8) Dead Load *	(193.4)	(180.0)	(245.1)	(0.089)	(0.076)	(0.064)	(0.064)	(0.025)	(0.076)	(0.051)	(0.025)	(0.051)	(0.051)	(0.051)	(0.038)
(9) Service Shear *	(222.3)	(208.9)	(283.3)	(0.076)	(0.076)	(0.089)	(0.051)	(0.025)	(0.089)	(0.051)	(0.038)	(0.025)	(0.051)	(0.051)	(0.051)
(10) Factored Shear *	(315.5)	(297.2)	(401.6)	(0.152)	(0.140)	(0.114)	(0.076)	(0.051)	(0.127)	(0.076)	(0.025)	(0.076)	(0.127)	(0.114)	(0.064)
(12) Service Flexure *	(171.6)	(253.4)	(310.6)	(0.114)	(0.102)	(0.089)	(0.076)	(0.051)	(0.114)	(0.076)	(0.025)	(0.064)	(0.089)	(0.076)	(0.051)
(13) Factored Flexure *	(205.4)	(393.7)	(460.8)	(0.165)	(0.127)	(0.127)	(0.102)	(0.102)	(0.165)	(0.089)	(0.064)	(0.089)	(0.152)	(0.165)	(0.076)

* Only maximum crack width was measured, usually at level A unless otherwise noted.

217
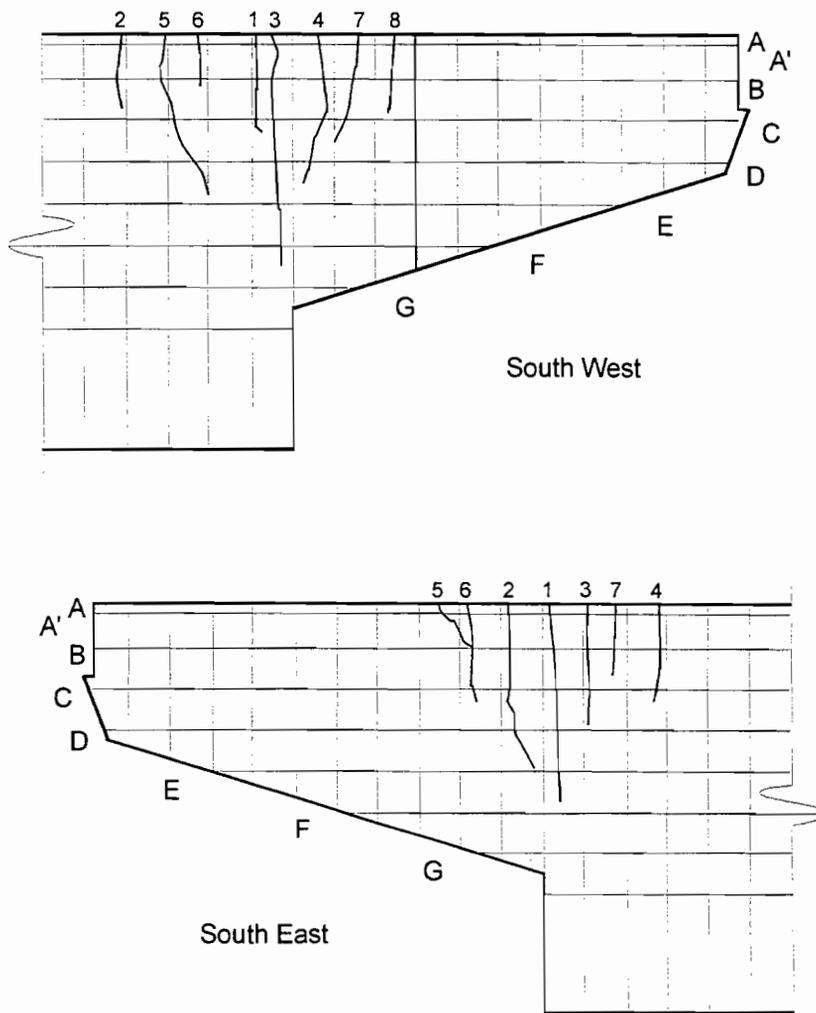
Figure A. 11   *Crack number and location on east and west sides of CO-PU-74S-TH-V-SM overhang*

North East

North West
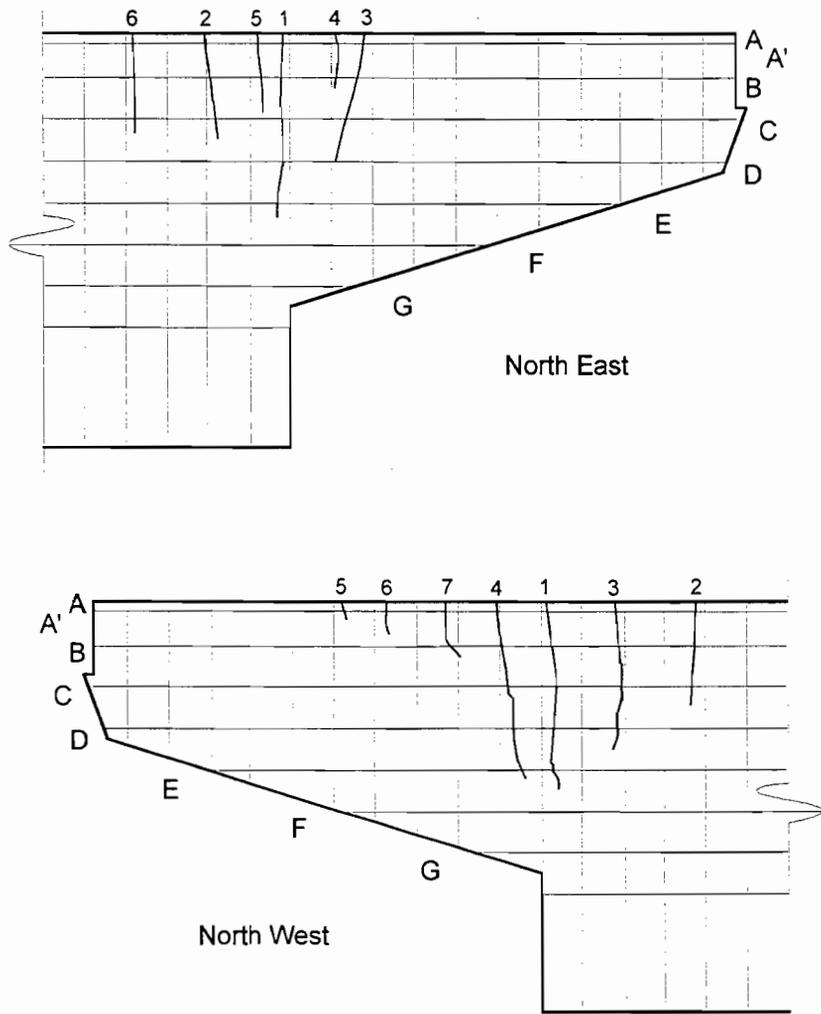
Figure A. 12   Crack number and location on east and west sides of CO-PU-74S-TH-I-SM overhang

219

Table A. 13   Maximum crack width readings for overhang CO-PU-74S-TH-V-SM (east side)

CO-PU-74S-TH-V	East Side			Maximum Crack Width, inches							
Load Stage	Ri kips	Ro kips	Moment at Face of Column kip-inches	Crack Number							
				1	2	3	4	5	6	7	8
cracking	42.2	45.46	2322	0.0005							
Dead Load plus	41.22	49.46	2465	0.0015 A'							
(2) Service Flexure	38.57	56.97	2749	0.003 A'							
(3) Dead Load*	43.47	40.47	2169	0.002 A'							
(4) Service Shear	49.97	46.97	2507	0.0025 A'							
(6) Service Flexure	38.57	56.97	2749	0.003 A'							
Service Flexure plus*	41.76	73.46	3408	0.005 A'	0.004	0.004	0.0005				
(7) Factored Flexure*	46.18	88.52	4078	0.007 A'	0.005	0.006	0.005	0.002	0.005 B	0.0045	
(8) Dead Load	43.47	40.47	2169	0.003	0.0025	0.0025	.002 B	0.0005	0.0015	.0015 B	
(9) Service Shear	49.97	46.97	2507	0.003 A'	0.0025	0.002	0.003	0.001 A'	0.002	0.002	
(10) Factored Shear*	70.92	66.82	3554	0.005 A'	0.005	0.005 A'	0.004 A'	0.0015 A'	0.003	0.002	
(12) Service Flexure*	38.57	56.97	2749	.005 A'	0.004	0.005	0.004	0.001	0.002	0.003	
(13) Factored Flexure*	46.18	88.52	4078	0.006	0.005	0.006	0.005	0.002	0.004	0.004	

CO-PU-74S-TH-V	East Side			Maximum Crack Width (mm)							
Load Stage	Ri (kN)	Ro (kN)	Moment at Face of Column (kN-m)	Crack Number							
				1	2	3	4	5	6	7	8
cracking	(187.7)	(202.2)	(262.4)	(0.013)							
Dead Load plus	(183.3)	(220.0)	(278.5)	(0.038 A')							
(2) Service Flexure	(171.6)	(253.4)	(310.6)	(0.076 A')							
(3) Dead Load*	(193.4)	(180.0)	(245.1)	(0.051A')							
(4) Service Shear	(222.3)	(208.9)	(283.3)	(0.064 A')							
(6) Service Flexure	(171.6)	(253.4)	(310.6)	(0.076 A')							
Service Flexure plus*	(185.7)	(326.8)	(385.1)	(0.127 A')	(0.102)	(0.102)	(0.013)				
(7) Factored Flexure*	(205.4)	(393.7)	(460.8)	(0.178 A')	(0.127)	(0.152)	(0.127)	(0.051)	(0.127 B)	(0.114)	
(8) Dead Load	(193.4)	(180.0)	(245.1)	(0.076)	(0.064)	(0.064)	(0.051B)	(0.013)	(0.038)	(0.038 B)	
(9) Service Shear	(222.3)	(208.9)	(283.3)	(0.176 A')	(0.064)	(0.051)	(0.076)	(0.025 A')	(0.051)	(0.051)	
(10) Factored Shear*	(315.5)	(297.2)	(4016)	(0.127 A')	(0.127)	(0.127 A')	(0.102 A')	(0.038A')	(0.076)	(0.051)	
(12) Service Flexure*	(171.6)	(253.4)	(310.6)	(0.127 A')	(0.102)	(0.127)	(0.102)	(0.025)	(0.051)	(0.076)	
(13) Factored Flexure*	(205.4)	(393.7)	(460.8)	(0.152)	(0.127)	(0.152)	(0.127)	(0.051)	(0.102)	(0.102)	

* Only maximum crack width was measured, usually at level A unless otherwise noted.

Table A. 14   *Maximum crack width readings for overhang CO-PU-74S-TH-V-SM (west side)*

CO-PU-74S-TH-V	West Side			Maximum Crack Width, inches							
Load Stage	Ri kips	Ro kips	Moment at Face of Column kip-inches	Crack Number							
				1	2	3	4	5	6	7	8
cracking	42.2	45.46	2322	0.002							
Dead Load plus	41.22	49.46	2465	0.003	0.0015						
(2) Service Flexure	38.57	56.97	2749	0.004	0.0015 A'						
(3) Dead Load *	43.47	40.47	2169	0.004	0.0015 A'						
(4) Service Shear	49.97	46.97	2507	0.0045	0.0015						
(6) Service Flexure	38.57	56.97	2749	0.0045	0.0015						
Service Flexure plus *	41.76	73.46	3408	0.006	0.003	0.005 A'	0.005				
(7) Factored Flexure *	46.18	88.52	4078	0.008	0.006	0.005 A'	0.006 A'	0.005 A'	0.006	0.005	0.0035
(8) Dead Load	43.47	40.47	2169	0.003 A'	0.002	0.002	0.002	0.002	0.001	0.002 A'	0.001
(9) Service Shear	49.97	46.97	2507	0.004 A'	0.002	0.0025	0.003 A'	0.002	0.002 A'	0.0015	
(10) Factored Shear *	70.92	66.82	3554	0.0075	0.004	0.005 A'	0.005 A'	0.004 B	0.005	0.004	0.002
(12) Service Flexure *	38.57	56.97	2749	0.006	0.003	0.004 A'	0.005 A'	0.003 A'	0.005	0.003 A'	0.0015
(13) Factored Flexure *	46.18	88.52	4078	0.007	0.004	0.005 A'	0.007 A'	0.005 A'	0.006	0.006	0.004

CO-PU-74S-TH-V	West Side			Maximum Crack Width (mm)							
Load Stage	Ri (kN)	Ro (kN)	Moment at Face of Column (kN-m)	Crack Number							
				1	2	3	4	5	6	7	8
cracking	(187.7)	(202.2)	(262.4)	(0.051)							
Dead Load plus	(183.3)	(220.0)	(278.5)	(0.076)	(0.038)						
(2) Service Flexure	(171.6)	(253.4)	(310.6)	(0.102)	(0.038 A')						
(3) Dead Load *	(193.4)	(180.0)	(245.1)	(0.102)	(0.038 A')						
(4) Service Shear	(222.3)	(208.9)	(283.3)	(0.114)	(0.038)						
(6) Service Flexure	(171.6)	(253.4)	(310.6)	(0.114)	(0.038)						
Service Flexure plus *	(185.7)	(326.8)	(385.1)	(0.152)	(0.076)	(0.127 A')	(0.127)				
(7) Factored Flexure *	(205.4)	(393.7)	(460.8)	(0.203)	(0.152)	(0.127 A')	(0.152 A')	(0.127 A')	(0.152)	(0.127)	(0.089)
(8) Dead Load	(193.4)	(180.0)	(245.1)	(0.076 A')	(0.051)	(0.051)	(0.051)	(0.051)	(0.025)	(0.051A')	(0.025)
(9) Service Shear	(222.3)	(208.9)	(283.3)	(0.102 A')	(0.051)	(0.064)	(0.076 A')	(0.051)	(0.051A')	(0.038)	
(10) Factored Shear *	(315.5)	(297.2)	(401.6)	(0.191)	(0.102)	(0.127 A')	(0.127 A')	(0.102 B)	(0.127)	(0.102)	(0.051)
(12) Service Flexure *	(171.6)	(253.4)	(310.6)	(0.152)	(0.076)	(0.102 A')	(0.127 A')	(0.076 A')	(0.127)	(0.076 A')	(0.038)
(13) Factored Flexure *	(205.4)	(393.7)	(460.8)	(0.178)	(0.102)	(0.127 A')	(0.178 A')	(0.127 A')	(0.152)	(0.152)	(0.102)

* Only maximum crack width was measured, usually at level A unless otherwise noted.

Table A. 15   Maximum crack width readings for overhang CO-PU-74S-TH-I-SM

CO-PU-74S-TH-I	East Side			Maximum Crack Width, inches						
Load Stage	Ri kips	Ro kips	Moment at Face of Column kip-inches	Crack Number						
				1	2	3	4	5	6	7
cracking	41.22	49.46	2465	0.001						
(2) Service Flexure	38.57	56.97	2749	0.002						
(3) Dead Load	43.47	40.47	2169	0.002						
(4) Service Shear	49.97	46.97	2507	0.0025						
(6) Service Flexure	38.57	56.97	2749	0.0025						
Service Flexure plus *	41.76	73.46	3408	0.005	0.0035	0.002				
(7) Factored Flexure *	46.18	88.52	4078	0.006	0.0045	0.005	0.004 A'	0.0035	0.003 A'	
(8) Dead Load	43.47	40.47	2169	0.0025 A'	0.002	.0015 B	0.001	0.001	0.0015 A'	
(9) Service Shear	49.97	46.97	2507	0.002	0.002	0.002 A'	0.001	0.001	0.0015 A'	
(10) Factored Shear *	70.92	66.82	3554	0.005	0.004	0.004 A'	0.003 C	0.0035 C	0.003 A'	
(12) Service Flexure *	38.57	56.97	2749	0.004	0.003	0.003	0.002 A'	0.002	0.002 A'	
(13) Factored Flexure *	46.18	88.52	4078	0.005	0.004	0.004	0.004 A'	0.004	0.003	

CO-PU-74S-TH-I	East Side			Maximum Crack Width (mm)						
Load Stage	Ri (kN)	Ro (kN)	Moment at Face of Column (kN-m)	Crack Number						
				1	2	3	4	5	6	7
cracking	(183.3)	(220.0)	(278.5)	(0.025)						
(2) Service Flexure	(171.6)	(253.4)	(310.6)	(0.051)						
(3) Dead Load	(193.4)	(180.0)	(245.1)	(0.051)						
(4) Service Shear	(222.3)	(208.9)	(283.3)	(0.064)						
(6) Service Flexure	(171.6)	(253.4)	(310.6)	(0.064)						
Service Flexure plus *	(185.7)	(326.8)	(385.1)	(0.127)	(0.089)	(0.051)				
(7) Factored Flexure *	(205.4)	(393.7)	(460.8)	(0.152)	(0.114)	(0.127)	(0.102 A')	(0.089)	(0.076 A')	
(8) Dead Load	(193.4)	(180.0)	(245.1)	(0.064 A')	(0.051)	(0.038 B)	(0.025)	(0.025)	(0.038 A')	
(9) Service Shear	(222.3)	(208.9)	(283.3)	(0.051)	(0.051)	(0.051 A')	(0.025)	(0.025)	(0.038 A')	
(10) Factored Shear *	(315.5)	(297.2)	(401.6)	(0.127)	(0.102)	(0.102 A')	(0.076 C)	(0.089 C)	(0.076 A')	
(12) Service Flexure *	(171.6)	(253.4)	(310.6)	(0.102)	(0.076)	(0.076)	(0.051 A')	(0.051)	(0.051 A')	
(13) Factored Flexure *	(205.4)	(393.7)	(460.8)	(0.127)	(0.102)	(0.102)	(0.102 A')	(0.102)	(0.076)	

* Only maximum crack width was measured, usually at level A unless otherwise noted.

Table A. 16   Maximum crack width readings for overhang CO-PU-74S-TH-I-SM (west side)

CO-PU-74S-TH-I	West Side			Maximum Crack Width, inches						
Load Stage	Ri kips	Ro kips	Moment at Face of Column kip-inches	Crack Number						
				1	2	3	4	5	6	7
cracking	41.22	49.46	2465	0.0015						
(2) Service Flexure	38.57	56.97	2749	0.0025	0.001					
(3) Dead Load	43.47	40.47	2169	0.002	0.0015					
(4) Service Shear	49.97	46.97	2507	0.002	0.002					
(6) Service Flexure	38.57	56.97	2749	0.003	0.002					
Service Flexure plus *	41.76	73.46	3408	0.0045	0.002	0.004	0.003	0.002		
(7) Factored Flexure *	46.18	88.52	4078	0.007	0.005	0.007	0.009	0.0025	0.0015	0.0035
(8) Dead Load	43.47	40.47	2169	0.002	0.001	0.002	0.004	0.002	0.001A'	0.0015
(9) Service Shear	49.97	46.97	2507	0.0035	0.003	0.0025	0.004	0.002	0.001A'	0.001
(10) Factored Shear *	70.92	66.82	3554	0.006	0.004	0.006	0.005	0.001	0.0015	0.002 A'
(12) Service Flexure *	38.57	56.97	2749	0.005	0.004	0.0045	0.006	0.0015	0.001	0.002
(13) Factored Flexure *	46.18	88.52	4078	0.008	0.006	0.006	0.009	0.002	0.002	0.003

CO-PU-74S-TH-I	West Side			Maximum Crack Width (mm)						
Load Stage	Ri (kN)	Ro (kN)	Moment at Face of Column (kN-m)	Crack Number						
				1	2	3	4	5	6	7
cracking	(183.3)	(220.0)	(278.5)	(0.038)						
(2) Service Flexure	(171.6)	(253.4)	(310.6)	(0.064)	(0.025)					
(3) Dead Load	(193.4)	(180.0)	(245.1)	(0.051)	(0.038)					
(4) Service Shear	(222.3)	(208.9)	(283.3)	(0.051)	(0.051)					
(6) Service Flexure	(171.6)	(253.4)	(310.6)	(0.076)	(0.051)					
Service Flexure plus *	(185.7)	(326.8)	(385.1)	(0.114)	(0.051)	(0.102)	(0.076)	(0.051)		
(7) Factored Flexure *	(205.4)	(393.7)	(460.8)	(0.178)	(0.127)	(0.178)	(0.229)	(0.064)	(0.038)	(0.089)
(8) Dead Load	(193.4)	(180.0)	(245.1)	(0.051)	(0.025)	(0.051)	(0.102)	(0.051)	(0.025 A')	(0.038)
(9) Service Shear	(222.3)	(208.9)	(283.3)	(0.089)	(0.076)	(0.064)	(0.102)	(0.051)	(0.025 A')	(0.025)
(10) Factored Shear *	(315.5)	(297.2)	(401.6)	(0.152)	(0.102)	(0.152)	(0.127)	(0.025)	(0.038)	(0.051A')
(12) Service Flexure *	(171.6)	(253.4)	(310.6)	(0.127)	(0.102)	(0.114)	(0.152)	(0.038)	(0.025)	(0.051)
(13) Factored Flexure *	(205.4)	(393.7)	(460.8)	(0.203)	(0.152)	(0.152)	(0.229)	(0.051)	(0.051)	(0.076)

* Only maximum crack width was measured, usually at level A unless otherwise noted.
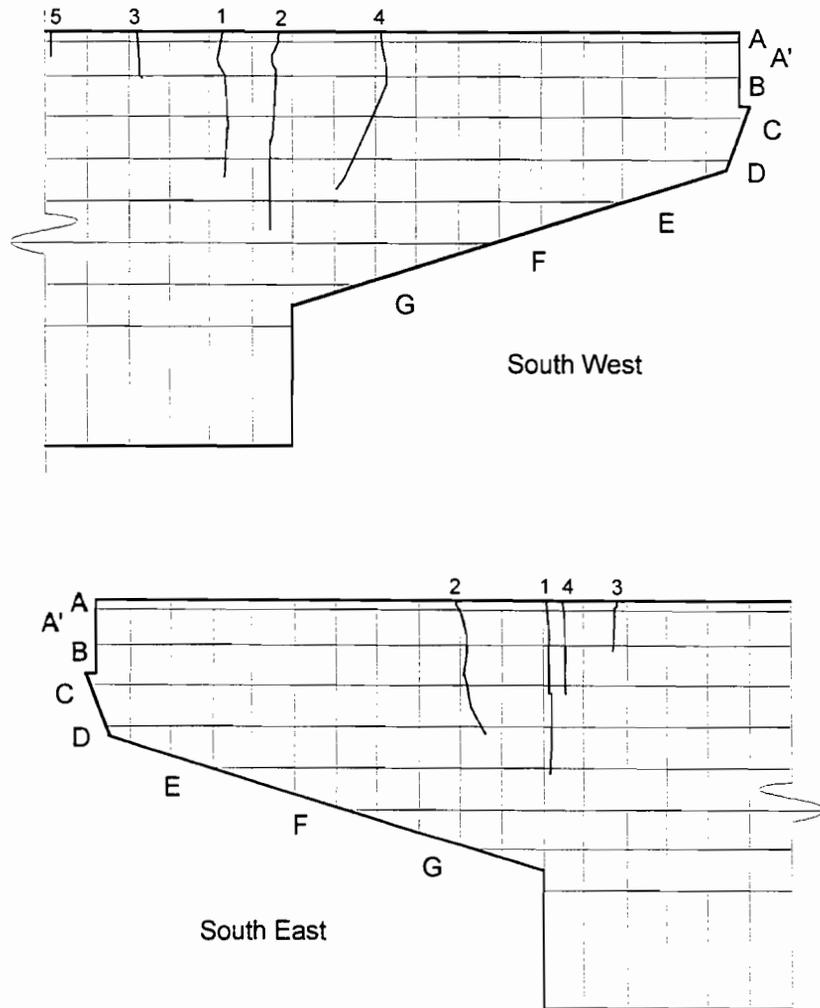
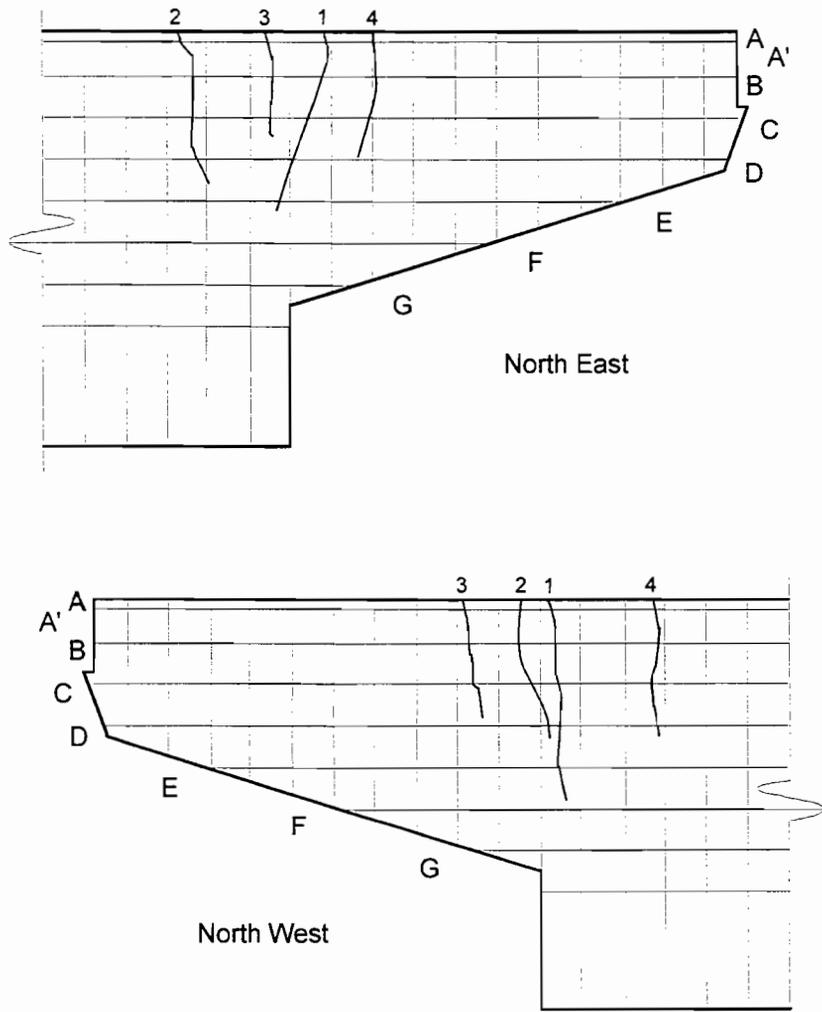*Figure A. 13   Crack number and location on east and west sides of CO-PU-100S-TH-V-SF overhang*

North East

North West

Figure A. 14   Crack number and location on east and west sides of CO-PU-100S-TH-I-SM overhang

225

Table A. 17   Maximum crack width readings for overhang CO-PU-100S-TH-V-SF (east side)

CO-PU-100S-TH-V	East Side			Maximum Crack Width, inches				
Load Stage	Ri	Ro	Moment at Face of Column	Crack Number				
	kips	kips	kip-inches	1	2	3	4	5
service flexure plus	40.99	69.46	3242	0.0015				
Dead Load * **	43.47	40.47	2169	0.0005				
Service Flexure * **	38.57	56.97	2749	0.001				
Service Flexure plus * **	40.99	69.46	3242	0.0025				
(7) Factored Flexure *	46.18	88.52	4078	0.003	0.001	0.0005		
(8) Dead Load *	43.47	40.47	2169	0.0005	0.0005	0.0005		
(9) Service Shear *	49.97	46.97	2507	0.0005	0.0005	0.0005		
(10) Factored Shear *	70.92	66.82	3554	0.001	0.001	0.0005		
(11) Dead Load*	43.47	40.47	2169	0.001	0.001	0.001		
(12) Service Flexure *	38.57	56.97	2749	0.001	0.001	0.001		
(13) Factored Flexure *	46.18	88.52	4078	0.0025	0.003	0.0005	0.002	

CO-PU-100S-TH-V	East Side			Maximum Crack Width (mm)				
Load Stage	Ri	Ro	Moment at Face of Column	Crack Number				
	(kN)	(kN)	(kN-m)	1	2	3	4	5
service flexure plus	(182.3)	(309.0)	(366.3)	(0.038)				
Dead Load * **	(193.4)	(180.0)	(245.1)	(0.013)				
Service Flexure * **	(171.6)	(253.4)	(310.6)	(0.025)				
Service Flexure plus * **	(182.3)	(309.0)	(366.3)	(0.064)				
(7) Factored Flexure *	(205.4)	(393.7)	(460.8)	(0.076)	(0.025)	(0.013)		
(8) Dead Load *	(193.4)	(180.0)	(245.1)	(0.013)	(0.013)	(0.013)		
(9) Service Shear *	(222.3)	(208.9)	(283.3)	(0.013)	(0.013)	(0.013)		
(10) Factored Shear *	(315.5)	(297.2)	(401.6)	(0.025)	(0.025)	(0.013)		
(11) Dead Load*	(193.4)	(180.0)	(245.1)	(0.025)	(0.025)	(0.025)		
(12) Service Flexure *	(171.6)	(253.4)	(310.6)	(0.025)	(0.025)	(0.025)		
(13) Factored Flexure *	(205.4)	(393.7)	(460.8)	(0.064)	(0.076)	(0.013)	(0.051)	

* Only maximum crack width was measured, usually at level A unless otherwise noted.
** This load sequence was followed in specimen CO-PU-100S-TH only.

226

Table A. 18   Maximum crack width readings for overhang CO-PU-100S-TH-V-SF (west side)

CO-PU-100S-TH-V	West Side			Maximum Crack Width, inches				
Load Stage	Ri	Ro	Moment at Face of Column	Crack Number				
	kips	kips	kip-inches	1	2	3	4	5
cracking	40.22	65.46	3076	0.0015				
Dead Load **	43.47	40.47	2169	0.0005				
Dead Load plus **	42.2	45.46	2322	0.0005				
Service Flexure **	38.57	56.97	2749	0.001				
Service Flexure plus **	40.22	65.46	3076	0.002				
Service Flexure plus plus **	40.99	69.46	3242	0.002	0.0025			
Dead Load * **	43.47	40.47	2169	0.001	0.0015			
Service Flexure * **	38.57	56.97	2749	0.0015	0.002			
Service Flexure plus * **	40.99	69.46	3242	0.002	0.003			
(7) Factored Flexure *	46.18	88.52	4078	0.006 A'	0.006	0.001	0.005	
(8) Dead Load *	43.47	40.47	2169	0.002 A'	0.002 A'	0.0005	0.001	
(9) Service Shear *	49.97	46.97	2507	0.002 A'	0.002	0.0005	0.001	
(10) Factored Shear *	70.92	66.82	3554	0.005 A'	0.006	0.0005	0.003	0.0005
(11) Dead Load *	43.47	40.47	2169	0.002 A'	0.002	0.0005	0.001	0.0005
(12) Service Flexure *	38.57	56.97	2749	0.003 A'	0.003	0.0005	0.0015	0.0005
(13) Factored Flexure *	46.18	88.52	4078	0.0075 A'	0.0065	0.0005	0.005	0.0005

CO-PU-100S-TH-V	West Side			Maximum Crack Width (mm)				
Load Stage	Ri	Ro	Moment at Face of Column	Crack Number				
	(kN)	(kN)	(kN-m)	1	2	3	4	5
cracking	(178.9)	(291.2)	(347.6)	(0.038)				
Dead Load **	(193.4)	(180.0)	(245.1)	(0.013)				
Dead Load plus **	(187.7)	(202.2)	(262.4)	(0.013)				
Service Flexure **	(171.6)	(253.4)	(310.6)	(0.025)				
Service Flexure plus **	(178.9)	(291.2)	(347.6)	(0.051)				
Service Flexure plus plus **	(182.3)	(309.0)	(366.3)	(0.051)	(0.064)			
Dead Load * **	(193.4)	(180.0)	(245.1)	(0.025)	(0.038)			
Service Flexure * **	(171.6)	(253.4)	(310.6)	(0.038)	(0.051)			
Service Flexure plus * **	(182.3)	(309.0)	(366.3)	(0.051)	(0.076)			
(7) Factored Flexure *	(205.4)	(393.7)	(460.8)	(0.152 A')	(0.152)	(0.025)	(0.127)	
(8) Dead Load *	(193.4)	(180.0)	(245.1)	(0.051A')	(0.051A')	(0.013)	(0.025)	
(9) Service Shear *	(222.3)	(208.9)	(283.3)	(0.051A')	(0.051)	(0.013)	(0.025)	
(10) Factored Shear *	(315.5)	(297.2)	(401.6)	(0.127 A')	(0.152)	(0.013)	(0.076)	(0.013)
(11) Dead Load *	(193.4)	(180.0)	(245.1)	(0.051A')	(0.051)	(0.013)	(0.025)	(0.013)
(12) Service Flexure *	(171.6)	(253.4)	(310.6)	(0.076 A')	(0.076)	(0.013)	(0.038)	(0.013)
(13) Factored Flexure *	(205.4)	(393.7)	(460.8)	(0.191A')	(0.165)	(0.013)	(0.127)	(0.013)

* Only maximum crack width was measured, usually at level A unless otherwise noted.
** This load sequence was followed in specimen CO-PU-100S-TH only.

227

Table A. 19   Maximum crack width readings for overhang CO-PU-100S-TH-I-SM (east side)

CO-PU-100S-TH-I	East Side			Maximum Crack Width, inches			
Load Stage	Ri	Ro	Moment at Face of Column	Crack Number			
	kips	kips	kip-inches	1	2	3	4
service flexure plus	40.99	69.46	3242	0.002			
Dead Load * **	43.47	40.47	2169	0.0005			
Service Flexure * **	38.57	56.97	2749	0.0015			
Service Flexure plus * **	40.99	69.46	3242	0.003			
(7) Factored Flexure *	46.18	88.52	4078	0.006 A'	0.0025	0.0055 A'	0.007
(8) Dead Load *	43.47	40.47	2169	0.001A'	0.0005	0.001A'	0.0015
(9) Service Shear*	49.97	46.97	2507	0.002 A'	0.001A'	0.0015 A'	0.001
(10) Factored Shear*	70.92	66.82	3554	0.0035 A'	0.003 A'	0.005 A	0.003
(11) Dead Load*	43.47	40.47	2169	0.001	0.0005	0.001A'	0.001
(12) Service Flexure *	38.57	56.97	2749	0.0015	0.001A'	0.002 A'	0.0015
(13) Factored Flexure *	46.18	88.52	4078	0.006	0.004 A'	0.0065 A'	0.0065

CO-PU-100S-TH-I	East Side			Maximum Crack Width (mm)			
Load Stage	Ri	Ro	Moment at Face of Column	Crack Number			
	(kN)	(kN)	(kN-m)	1	2	3	4
service flexure plus	(182.3)	(309.0)	(366.3)	(0.051)			
Dead Load * **	(193.4)	(180.0)	(245.1)	(0.013)			
Service Flexure * **	(171.6)	(253.4)	(310.6)	(0.038)			
Service Flexure plus * **	(182.3)	(309.0)	(366.3)	(0.076)			
(7) Factored Flexure *	(205.4)	(393.7)	(460.8)	(0.152 A')	(0.064)	(0.140 A')	(0.178)
(8) Dead Load *	(193.4)	(180.0)	(245.1)	(0.025 A')	(0.013)	(0.025 A')	(0.038)
(9) Service Shear*	(222.3)	(208.9)	(283.3)	(0.051 A')	(0.025 A')	(0.038 A')	(0.025)
(10) Factored Shear*	(315.5)	(297.2)	(401.6)	(0.089 A')	(0.076 A')	(0.127 A')	(0.076)
(11) Dead Load*	(193.4)	(180.0)	(245.1)	(0.025)	(0.013)	(0.025 A')	(0.025)
(12) Service Flexure *	(171.6)	(253.4)	(310.6)	(0.038)	(0.025 A')	(0.051 A')	(0.038)
(13) Factored Flexure *	(205.4)	(393.7)	(460.8)	(0.152)	(0.102 A')	(0.165 A')	(0.165)

* Only maximum crack width was measured, usually at level A unless otherwise noted.
** This load sequence was followed in specimen CO-PU-100S-TH only.

228

Table A. 20   Maximum crack width readings for overhang CO-PU-100S-TH-I-SM (west side)

CO-PU-100S-TH-I	West Side		Moment at	Maximum Crack Width, inches			
Load Stage	Ri	Ro	Face of Column	Crack Number			
	kips	kips	kip-inches	1	2	3	4
cracking	38.68	57.46	2750	0.001			
service flexure plus **	39.45	61.46	2910	0.0015			
service flexure plus plus **	40.22	65.46	3076	0.002	0.0015		
Dead Load **	43.47	40.47	2169	0.0005	0.0005		
Dead Load plus **	42.2	45.46	2322	0.0005	0.0005		
Service Flexure **	38.57	56.97	2749	0.001	0.001		
Service Flexure plus **	40.22	65.46	3076	0.002	0.0015		
Service Flexure plus plus **	40.99	69.46	3242	0.002	0.0025		
Dead Load * **	43.47	40.47	2169	0.001	0.001		
Service Flexure * **	38.57	56.97	2749	0.0015	0.002		
Service Flexure plus * **	40.99	69.46	3242	0.0025	0.002		
(7) Factored Flexure *	46.18	88.52	4078	0.007	0.0075 A'	0.003	0.0075
(8) Dead Load *	43.47	40.47	2169	0.0015	0.002 A'	0.0005	0.0015
(9) Service Shear *	49.97	46.97	2507	0.002	0.002 A'	0.001	0.003
(10) Factored Shear *	70.92	66.82	3554	0.0065	0.006 A'	0.002	0.005
(11) Dead Load *	43.47	40.47	2169	0.003	0.0025 A'	0.001	0.002
(12) Service Flexure *	38.57	56.97	2749	0.0035	0.003 A'	0.002	0.003
(13) Factored Flexure *	46.18	88.52	4078	0.01	0.0075 A'	0.006	0.006

CO-PU-100S-TH-I	West Side		Moment at	Maximum Crack Width (mm)			
Load Stage	Ri	Ro	Face of Column	Crack Number			
	(kN)	(kN)	(kN-m)	1	2	3	4
cracking	(172.0)	(255.6)	(310.8)	(0.025)			
service flexure plus **	(175.5)	(273.4)	(328.8)	(0.038)			
service flexure plus plus **	(178.9)	(291.2)	(347.6)	(0.051)	(0.038)		
Dead Load **	(193.4)	(180.0)	(245.1)	(0.013)	(0.013)		
Dead Load plus **	(187.7)	(202.2)	(262.4)	(0.013)	(0.013)		
Service Flexure **	(171.6)	(253.4)	(310.6)	(0.025)	(0.025)		
Service Flexure plus **	(178.9)	(291.2)	(347.6)	(0.051)	(0.038)		
Service Flexure plus plus **	(182.3)	(309.0)	(366.3)	(0.051)	(0.064)		
Dead Load * **	(193.4)	(180.0)	(245.1)	(0.025)	(0.025)		
Service Flexure * **	(171.6)	(253.4)	(310.6)	(0.038)	(0.051)		
Service Flexure plus * **	(182.3)	(309.0)	(366.3)	(0.064)	(0.051)		
(7) Factored Flexure *	(205.4)	(393.7)	(460.8)	(0.178)	(0.191 A')	(0.076)	(0.191)
(8) Dead Load *	(193.4)	(180.0)	(245.1)	(0.038)	(0.051 A')	(0.013)	(0.038)
(9) Service Shear *	(222.3)	(208.9)	(283.3)	(0.051)	(0.051 A')	(0.025)	(0.076)
(10) Factored Shear *	(315.5)	(297.2)	(401.6)	(0.165)	(0.152 A')	(0.051)	(0.127)
(11) Dead Load *	(193.4)	(180.0)	(245.1)	(0.076)	(0.064 A')	(0.025)	(0.051)
(12) Service Flexure *	(171.6)	(253.4)	(310.6)	(0.089)	(0.076 A')	(0.051)	(0.076)
(13) Factored Flexure *	(205.4)	(393.7)	(460.8)	(0.254)	(0.191 A')	(0.152)	(0.152)

* Only maximum crack width was measured, usually at level A unless otherwise noted.
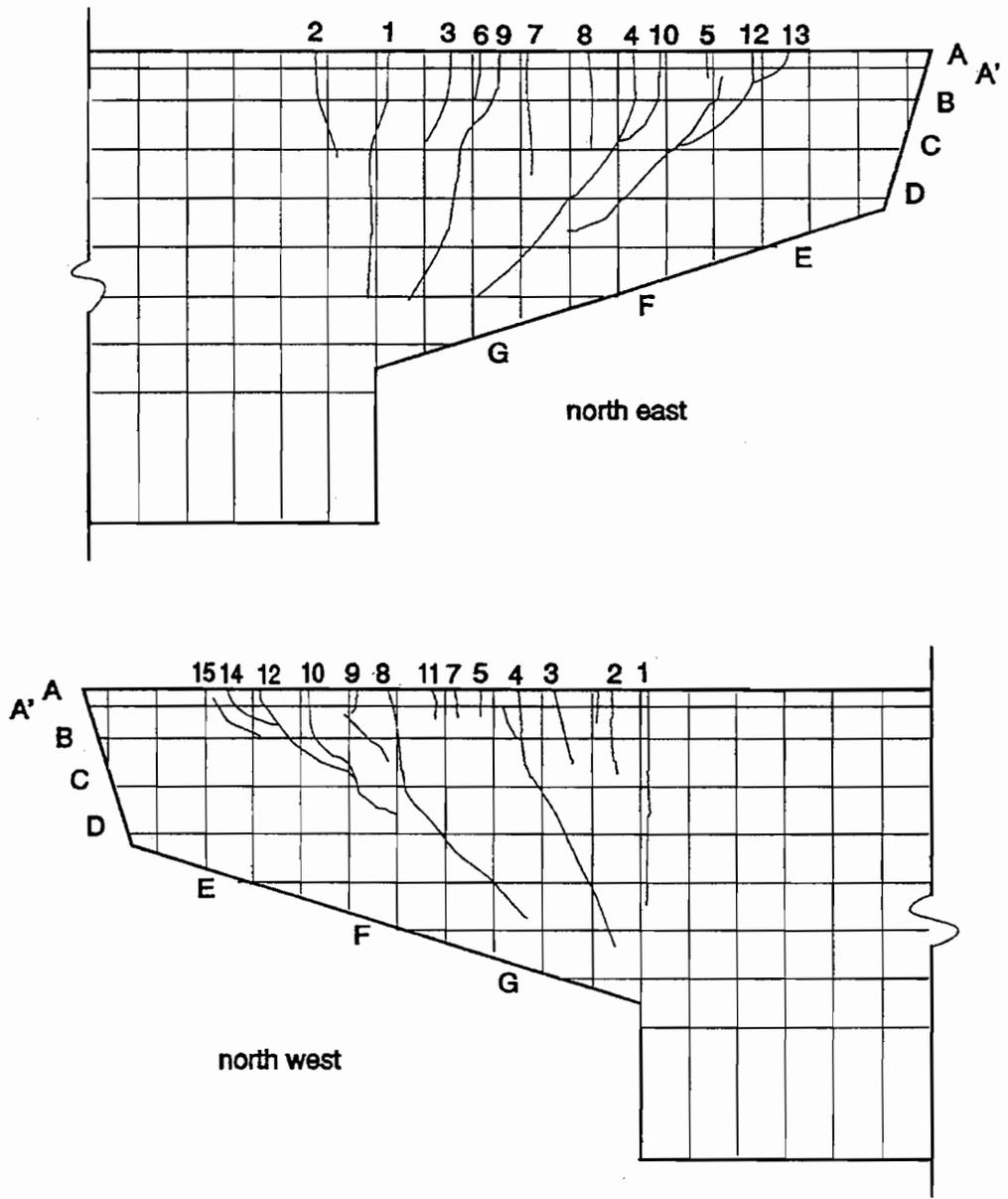** This load sequence was followed in specimen CO-PU-100S-TH only.

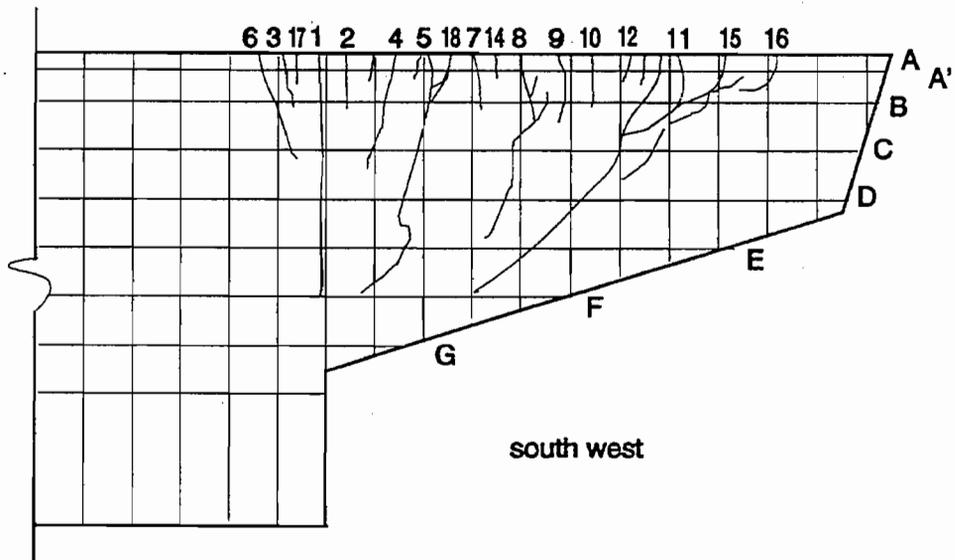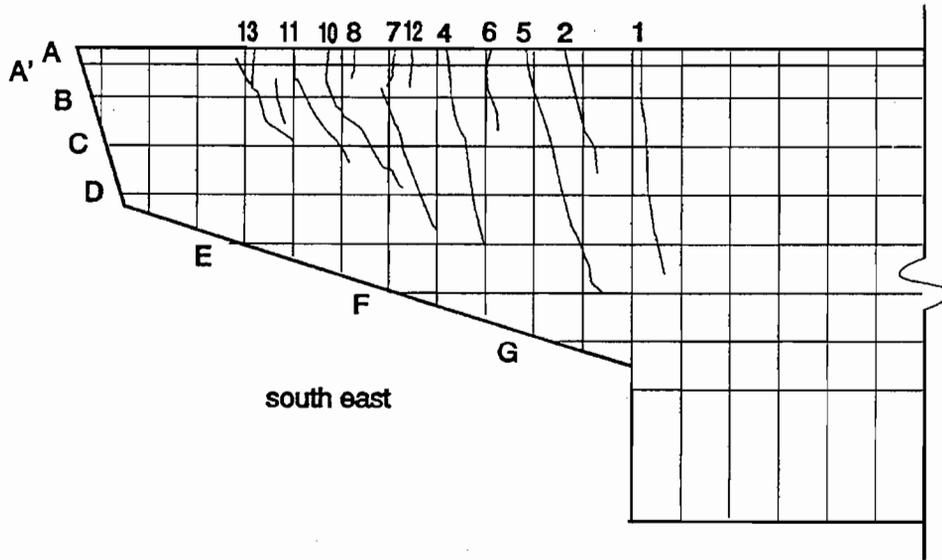*Figure A. 15   Crack number and location on east and west sides of CO-RU-0S-TH-M1-SM*

230

*Figure A. 16   Crack number and location on east and west sides of CO-RU-0S-TH-M1.7-
2M overhang*

231

Table A. 21   Maximum crack width readings for overhang CO-RU-0S-TH-M1-SM (east side)

CO-RC-TH-M	East Side			Maximum Crack Width, (inches)											
Load Stage	RI (kips)	Ro (kips)	Moment at Face of Column (kip-inches)	Crack Number											
				1	2	3	4	5	6	7	8	9	10	11	12
cracking	(28.48)	(25.46)	(1363)	(0.002)	(0.001)										
(1) Dead Load	(43.48)	(40.46)	(2143)	(0.003)	(0.002)	(0.002)									
Dead Load Plus	(41.22)	(49.46)	(2465)	(0.005 a')	(0.002)	(0.003)	(0.001)	(0.001)	(0.001)	(0.001)					
(2) Service Flexure	(38.57)	(56.97)	(2749)	(0.005 c)	(0.004)	(0.003)	(0.001)	(0.001)	(0.003)	(0.003 a')	(0.002)	(0.0015 b)	(0.001)	(0.002)	
(3) Dead Load *	(43.47)	(40.47)	(2169)	(0.005 c)											
(4) Service Shear	(49.97)	(46.97)	(2507)	(0.006 c)	(0.003)	(0.003)	(0.001)	(0.001)	(0.001)	(0.003 a')	(0.002)	(0.0015 a')	(0.001)	(0.003)	
(5) Dead Load *	(43.47)	(40.47)	(2169)	(0.0055 c)	(0.003)	(0.003)	(0.001)	(0.001)	(0.001)	(0.0025 a')	(0.002)	(0.002 a')	(0.001)	(0.003)	
(6) Service Flexure	(38.57)	(56.97)	(2749)	(0.006 c)	(0.003)	(0.003)	(0.001)	(0.001)	(0.001)	(0.0025 a')	(0.003)	(0.0025 a')	(0.001)	(0.003)	
Service Flexure Plus	(46.18)	(73.46)	(3408)	(0.0075 c)	(0.004)	(0.002 c)				(0.003)	(0.004)	(0.005 c)	(0.001)	(0.003)	

CO-RC-TH-M	East Side			Maximum Crack Width mm											
Load Stage	RI kN	Ro kN	Moment at Face of Column kN-m	Crack Number											
				1	2	3	4	5	6	7	8	9	10	11	12
cracking	126.7	113.2	154.0	0.05	0.03										
(1) Dead Load	193.4	180.0	242.2	0.08	0.05	0.05									
Dead Load Plus	183.3	220.0	278.5	0.13 a	0.05	0.06	0.01	0.01	0.03	0.03					
(2) Service Flexure	171.6	253.4	310.6	0.13 c	0.09	0.08	0.01	0.01	0.08	0.08 a'	0.05	0.04 b	0.01	0.05	
(3) Dead Load *	193.4	180.0	245.1	0.15 c											
(4) Service Shear	222.3	208.9	283.3	0.15 c	0.08	0.08	0.01	0.01	0.03	0.08 a'	0.04	0.04 a'	0.01	0.08	
(5) Dead Load *	193.4	180.0	245.1	0.14 c	0.06	0.06	0.01	0.01	0.03	0.06 a'	0.05	0.05 a'	0.01	0.06	
(6) Service Flexure	171.6	253.4	310.6	0.15 c	0.06	0.06	0.01	0.01	0.03	0.06 a'	0.06	0.06 a'	0.01	0.08	
Service Flexure Plus	205.4	326.8	385.1	0.19 c	0.09	0.05 c				0.06	0.10	0.13 c	0.01	0.08	

* Only maximum crack width was measured, usually at level A unless otherwise noted.

Table A. 22   Maximum crack width readings for overhang CO-RU-0S-TH-M1-SM

CO-RC-TH-M	West Side			Maximum Crack Width, (inches)											
Load Stage	RI (kips)	Ro (kips)	Moment at Face of Column (kip-inches)	Crack Number											
				1	2	3	4	5	6	7	8	9	10	11	12
cracking	(28.48)	(25.46)	(1383)	(0.0015 c)	(0.001)	(0.001)									
(1) Dead Load	(43.48)	(40.46)	(2143)	(0.0025 c)	(0.002)	(0.002)									
Dead Load Plus	(41.22)	(49.46)	(2465)	(0.0045 c)	(0.003)	(0.003)	(0.003 b)	(0.002)	(0.002)						
(2) Service Flexure	(38.57)	(56.97)	(2723)	(0.0045 c)	(0.003)	(0.003)	(0.003 b')	(0.002)	(0.002)						
(3) Dead Load *	(43.47)	(40.47)	(2143)	(0.0035 c)											
(4) Service Shear	(49.97)	(46.97)	(2455)	(0.0035 d)	(0.002)	(0.003)	(0.003 b')	(0.002)	(0.001)						
(5) Dead Load *	(43.47)	(40.47)	(2143)	(0.004 d)	(0.003)	(0.003)	(0.0035 b')	(0.002)	(0.002)						
(6) Service Flexure	(38.57)	(56.97)	(2722)	(0.005 d)	(0.002)	(0.003)	(0.003 b')	(0.002)	(0.002)						
Service Flexure plus *	(41.76)	(73.46)	(3408)	(0.005 d)	(0.004)	(0.004)	(0.005 b')	(0.003)	(0.002)						

CO-RC-TH-M	West Side			Maximum Crack Width mm											
Load Stage	RI kN	Ro kN	Moment at Face of Column kN-m	Crack Number											
				1	2	3	4	5	6	7	8	9	10	11	12
cracking	126.7	113.2	154.0	0.04 c	0.03	0.03									
Dead Load	126.7	113.2	154.0	0.04 c	0.05	0.04									
Dead Load plus	193.4	180.0	242.2	0.06 d	0.08	0.06	0.08 b	0.04	0.05						
(2) Service Flexure	171.6	253.4	307.7	0.11 c	0.08	0.06	0.08 b'	0.04	0.05						
(3) Dead Load *	193.4	180.0	242.2	0.09 c											
(4) Service Shear	222.3	208.9	277.4	0.09 d	0.05	0.06	0.08 b'	0.04	0.03						
(5) Dead Load *	193.4	180.0	242.2	0.10 d	0.06	0.06	0.09 b'	0.04	0.04						
(6) Service Flexure	171.6	253.4	307.6	0.13 c	0.05	0.08	0.08 b'	0.05	0.04						
Service Flexure plus	171.6	253.4	307.6	0.15 c	0.05	0.09	0.13 b'	0.06	0.05						

* Only maximum crack width was measured, usually at level A unless otherwise noted.

Table A. 23   Maximum crack width readings for overhang CO-RU-0S-TH-M1.7-SM

CO-RC-TH-O	East Side			Maximum Crack Width, (inches)											
Load Stage	Ri (kips)	Ro (kips)	Moment at Face of Column (kip-inches)	Crack Number											
				1	2	3	4	5	6	7	8	9	10	11	12
cracking	(28.48)	(25.48)	(1383)	(0.002 b)	(0.001)	(0.001)									
(1) Dead Load	(43.48)	(40.46)	(2143)	(0.0035 b)	(0.002)	(0.002)									
Dead Load Plus	(41.22)	(49.46)	(2465)	(0.005 b)	(0.002)	(0.002)	(0.002)	(0.002)							
(2) Service Flexure	(38.57)	(56.97)	(2749)	(0.005 b)	(0.003 a')	(0.004)	(0.002)	(0.003)	(0.0015 a')						
(3) Dead Load *	(43.47)	(40.47)	(2169)	(0.005 c)											
(4) Service Shear	(49.97)	(46.97)	(2507)	(0.006 c)	(0.002)	(0.003)	(0.002)	(0.002)	(0.002)						
(5) Dead Load *	(43.47)	(40.47)	(2169)	(0.005 c')	(0.002)	(0.003)	(0.002)	(0.002)	(0.002)						
(6) Service Flexure	(38.57)	(56.97)	(2749)	(0.0065 c)	(0.002)	(0.003)	(0.002)	(0.002)	(0.002)						
Service Flexure Plus	(46.18)	(73.46)	(3408)	(0.008 c)	(0.004)			(0.003 b)	(0.003)	(0.0025 b)					

CO-RC-TH-O	East Side			Maximum Crack Width mm											
Load Stage	Ri kN	Ro kN	Moment at Face of Column kN-m	Crack Number											
				1	2	3	4	5	6	7	8	9	10	11	12
cracking	126.7	113.2	154.0	0.05 b	0.03	0.03									
(1) Dead Load	193.4	180.0	242.2	0.09 b	0.05	0.05									
Dead Load Plus	183.3	220.0	278.5	0.13 b	0.05	0.05	0.04	0.05							
(2) Service Flexure	171.6	253.4	310.6	0.13 b	0.08 a'	0.09	0.04	0.08	0.04 a'						
(3) Dead Load *	193.4	180.0	245.1	0.13 c											
(4) Service Shear	222.3	208.9	283.3	0.15 c	0.05	0.08	0.04	0.05							
(5) Dead Load *	193.4	180.0	245.1	0.13 c'	0.05	0.08	0.04	0.05	0.05						
(6) Service Flexure	171.6	253.4	310.6	0.17 c	0.05	0.08	0.05	0.05	0.05						
Service Flexure Plus	205.4	326.8	385.1	0.20 c	0.09			0.08 b	0.08	0.06 b					

* Only maximum crack width was measured, usually at level A unless otherwise noted.

234

Table A. 24   Maximum crack width readings for overhang CO-RU-0S-TH-M1.7-SM

CO-RC-TH-O	West Side			Maximum Crack Width, (inches)											
Load Stage	RI (kips)	Ro (kips)	Moment at Face of Column (kip-inches)	Crack Number											
				1	2	3	4	5	6	7	8	9	10	11	12
cracking	(28.48)	(25.46)	(1363)	(0.0015 b)		(0.001)									
(1) Dead Load	(43.48)	(40.46)	(2143)	(0.0025 c)	(0.002)	(0.002)	(0.001 b)								
Dead Load Plus	(41.22)	(49.46)	(2465)	(0.0035 c)	(0.002)	(0.002)	(0.0015 c)	(0.001)	(0.002)						
(2) Service Flexure	(38.57)	(56.97)	(2723)	(0.005 c)	(0.002)	(0.003)	(0.0015 b)	(0.002)	(0.002)	(0.001)	(0.002)				
(3) Dead Load *	(43.47)	(40.47)	(2143)	(0.0045 c)											
(4) Service Shear	(49.97)	(46.97)	(2455)	(0.005 c)	(0.003)	(0.003)	(0.002 b)	(0.002 b)	(0.002)	(0.001)	(0.001)				
(5) Dead Load *	(43.47)	(40.47)	(2143)	(0.005 c)	(0.002)	(0.002)	(0.002 b)	(0.002 b)	(0.001)	(0.001)	(0.001)				
(6) Service Flexure	(38.57)	(56.97)	(2722)	(0.006 c)	(0.002)	(0.003)	(0.0025 b)	(0.003 b)	(0.001)	(0.001)	(0.001)				
Service Flexure plus *	(41.76)	(73.46)	(3408)	(0.007 c)	(0.003)		(0.003 b)	(0.0035 c)		(0.002)	(0.004)				

CO-RC-TH-O	West Side			Maximum Crack Width mm											
Load Stage	RI kN	Ro kN	Moment at Face of Column kN-m	Crack Number											
				1	2	3	4	5	6	7	8	9	10	11	12
cracking	126.7	113.2	154.0	0.038 b		0.03									
Dead Load	126.7	113.2	154.0	0.038 c	0.04	0.04	0.025 b								
Dead Load plus	193.4	180.0	242.2	0.063 c	0.05	0.05	0.038 c	0.01	0.05						
(2) Service Flexure	171.6	253.4	307.7	0.089 c	0.05	0.06	0.038 b	0.04	0.04	0.03	0.04				
(3) Dead Load *	193.4	180.0	242.2	0.11 c											
(4) Service Shear	222.3	208.9	277.4	0.13 c	0.06	0.06	0.050 b	0.051 b	0.04	0.03	0.03				
(5) Dead Load *	193.4	180.0	242.2	0.13 c	0.05	0.05	0.050 b	0.051 b	0.03	0.03	0.01				
(6) Service Flexure	171.6	253.4	307.6	0.15 c	0.05	0.08	0.063 b	0.076 b	0.03	0.03	0.03				
Service Flexure plus	171.6	253.4	307.6	0.15 c	0.05		0.076 b	0.089 c	0.00	0.05	0.10				

* Only maximum crack width was measured, usually at level A unless otherwise noted.

235

APPENDIX B

MAJOR CRACK PLOTS AND CRACK WIDTH ENVELOPES

SPECIMEN	FIGURE
CO-PS-100S-NA-N-SM	B1
CO-PU-100S-NA-I-SM	B2
CO-PU-100S-NA-V-SM	B3, B4
CO-PU-74S-OR-I-SM	B5, B6
CO-PU-74S-OR-V-SM	B7, B8
CO-PU-54S-TH-V-SF *(VIRGIN LOADING)*	B9
CO-PU-54S-TH-I-SM *(VIRGIN LOADING)*	B10
CO-PU-74S-TH-V-SM *(VIRGIN LOADING)*	B11
CO-PU-74S-TH-I-SM *(VIRGIN LOADING)*	B12
CO-PU-100S-TH-V-SF *(VIRGIN LOADING)*	B13
CO-PU-100S-TH-I-SM *(VIRGIN LOADING)*	B14
CO-RU-0S-TH-M1-SM *(VIRGIN LOADING)*	B15
CO-RU-0S-TH-M1.7-SM *(VIRGIN LOADING)*	B16
CO-PU-54S-TH-V-SF *(COMPLETE LOADING)*	B17
CO-PU-54S-TH-I-SM *(COMPLETE LOADING)*	B18
CO-PU-74S-TH-V-SM *(COMPLETE LOADING)*	B19
CO-PU-74S-TH-I-SM *(COMPLETE LOADING)*	B20
CO-PU-100S-TH-V-SF *(COMPLETE LOADING)*	B21
CO-PU-100S-TH-I-SM *(COMPLETE LOADING)*	B22
CO-RU-0S-TH-M1-SM *(COMPLETE LOADING)*	B23
CO-RU-0S-TH-M1.7-SM *(COMPLETE LOADING)*	B24
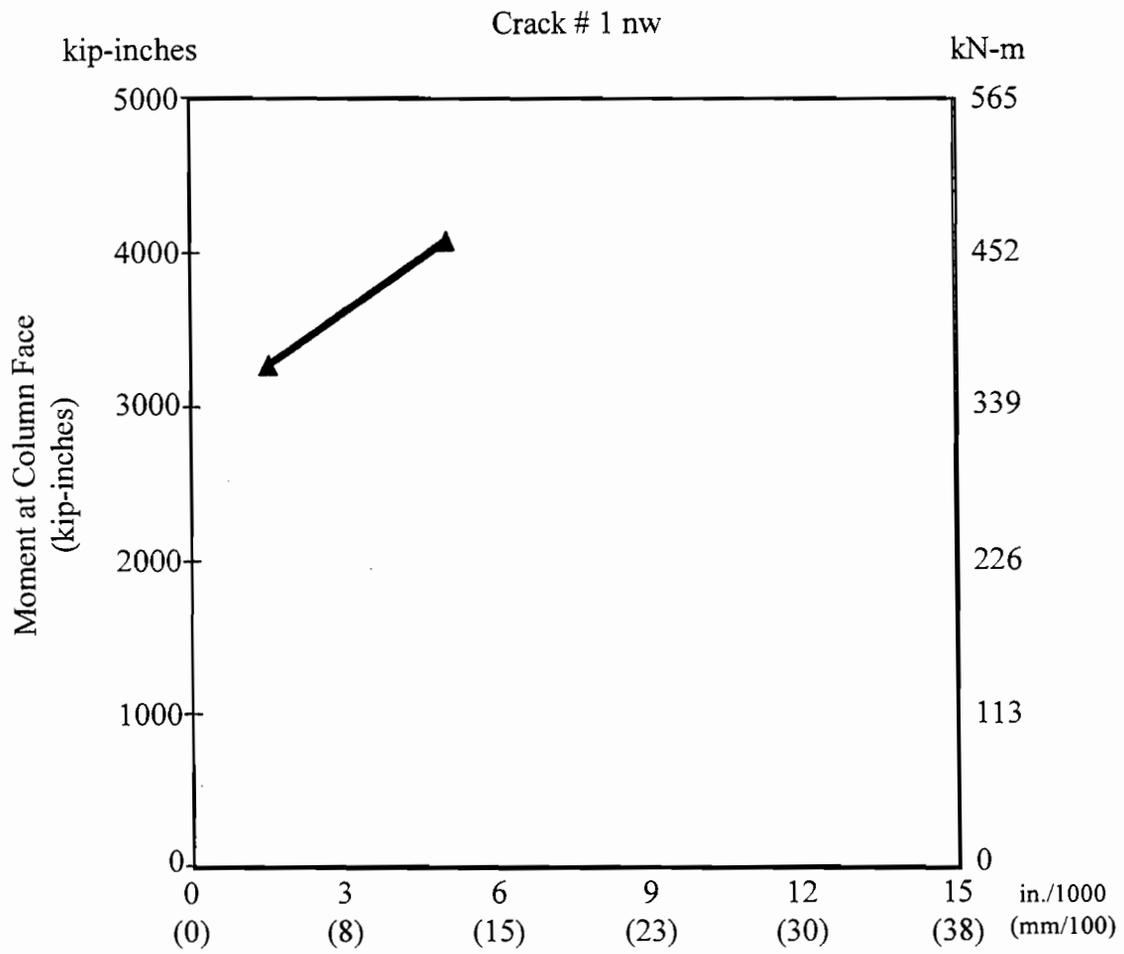
Figure B. 1   *"Crack Width Envelope" for the CO-PS-100S-NA-N-SM overhang*

238
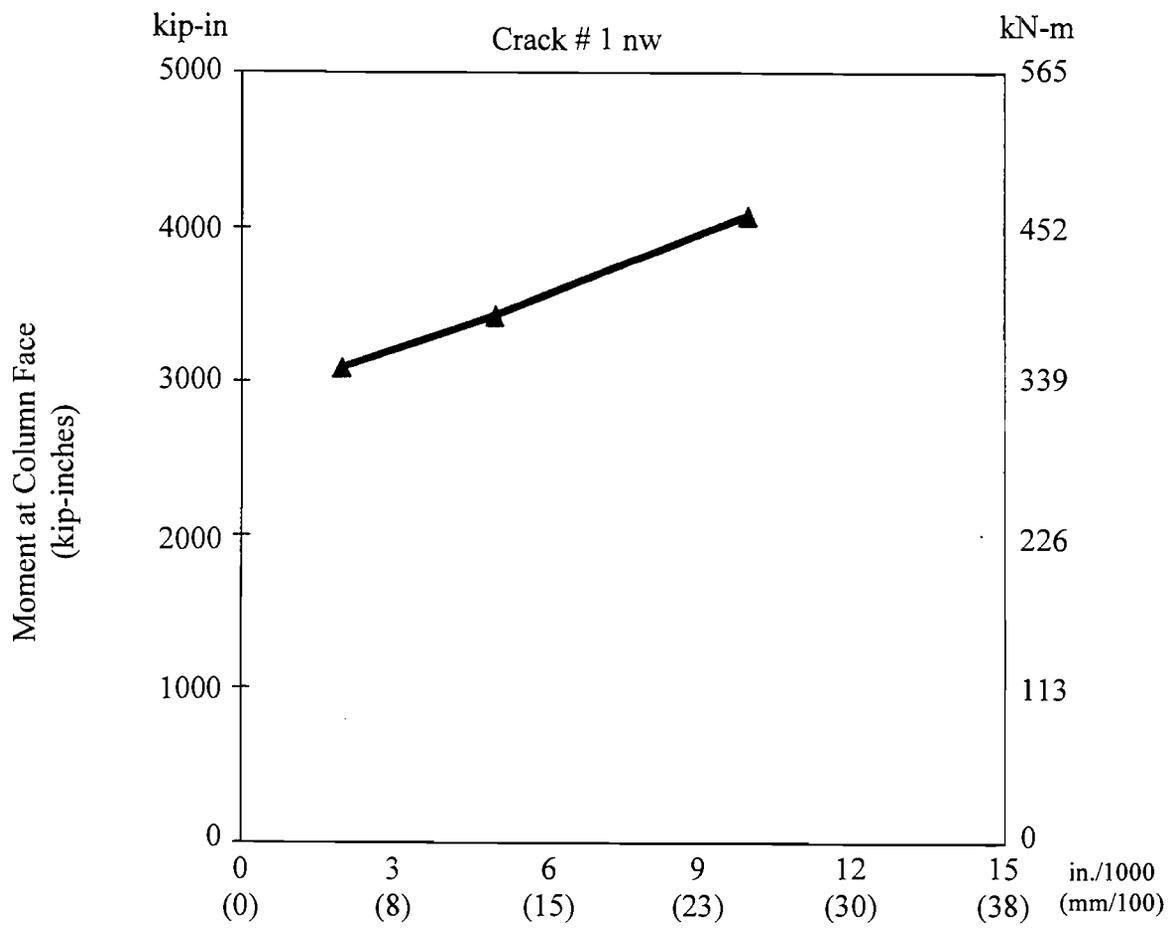
Figure B. 2 "*Crack Width Envelope*" *for the CO-PU-100S-NA-I-SM overhang*
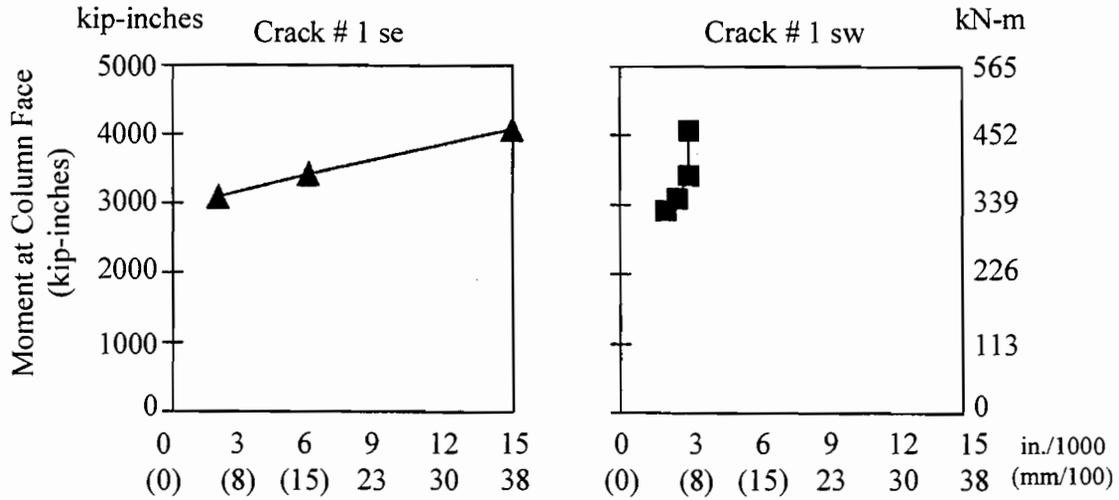
Figure B. 3   *"Major" crack plots for the CO-PU-100S-NA-V-SM overhang*
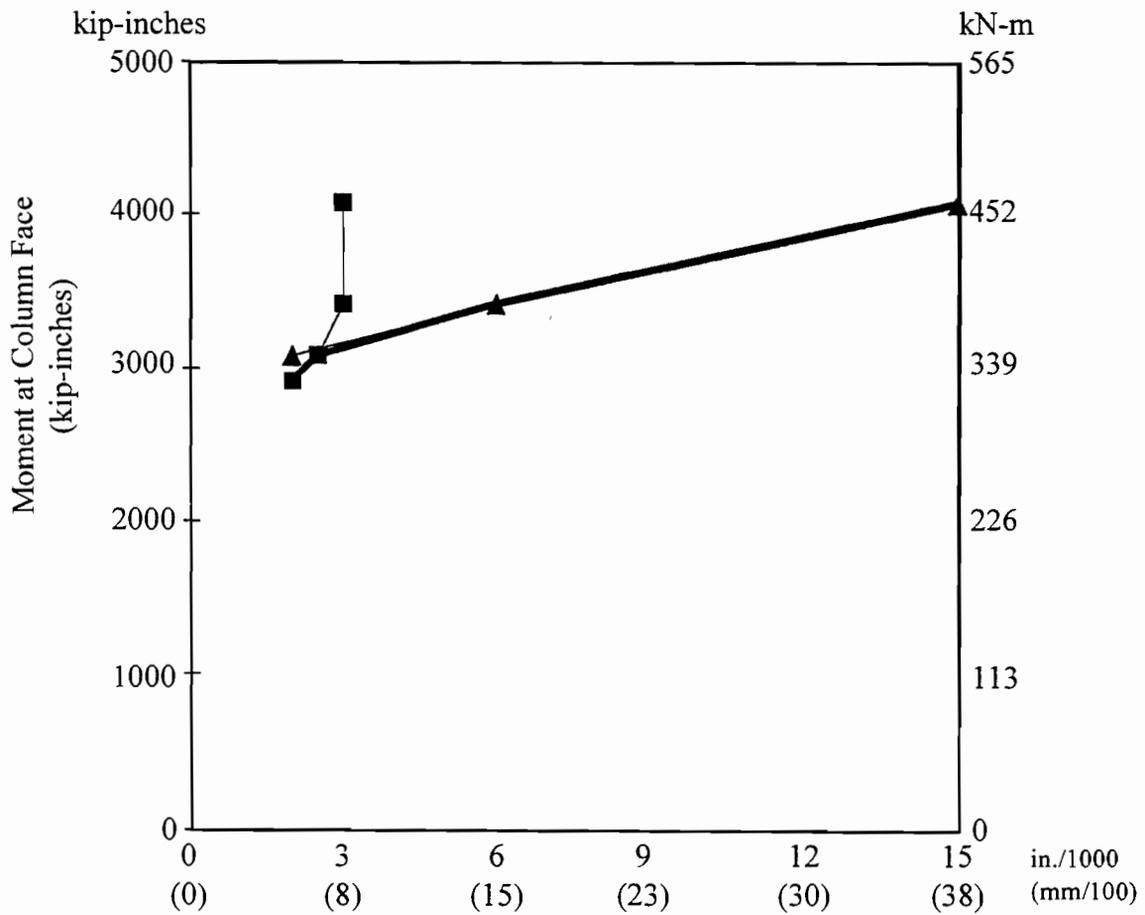
Figure B. 4   *"Crack Width Envelope" for the CO-PU-100S-NA-V-SM overhang*

240
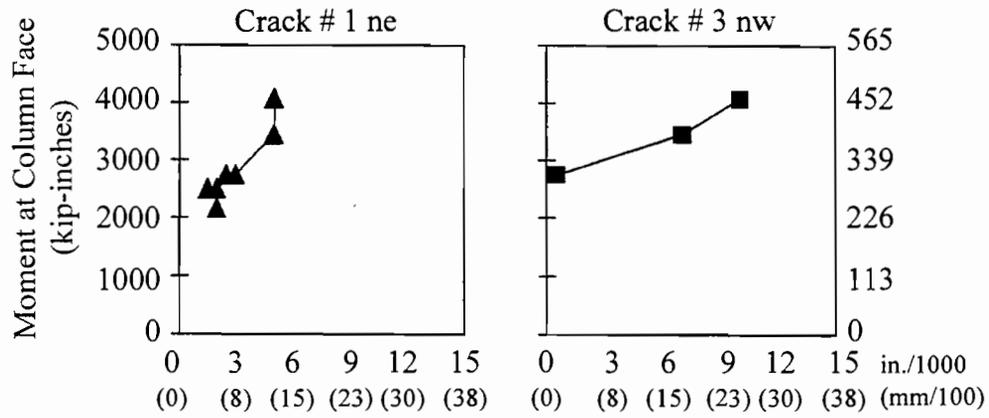
Figure B. 5   *"Major" crack plots for the CO-PU-74S-OR-I-SM overhang*
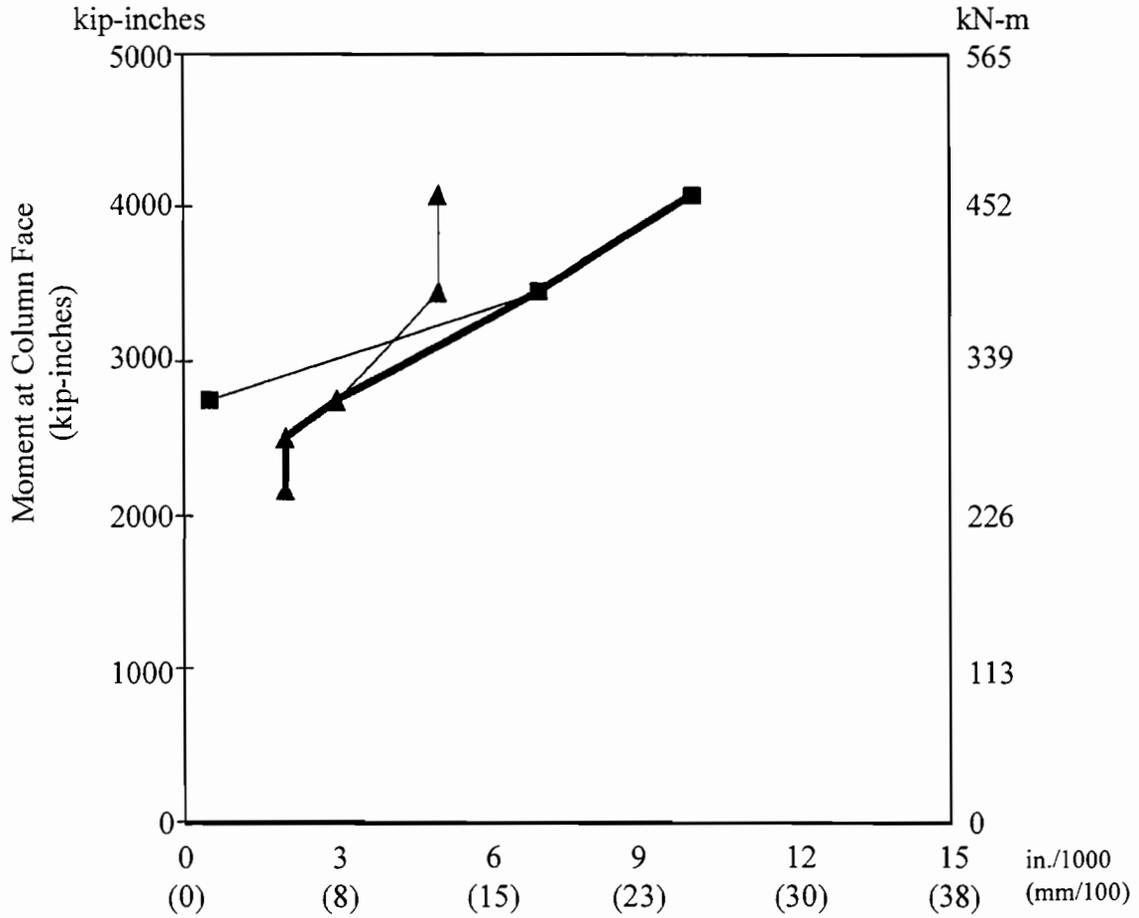
Figure B. 6   *"Crack Width Envelope" for the CO-PU-74S-OR-I-SM overhang*

241
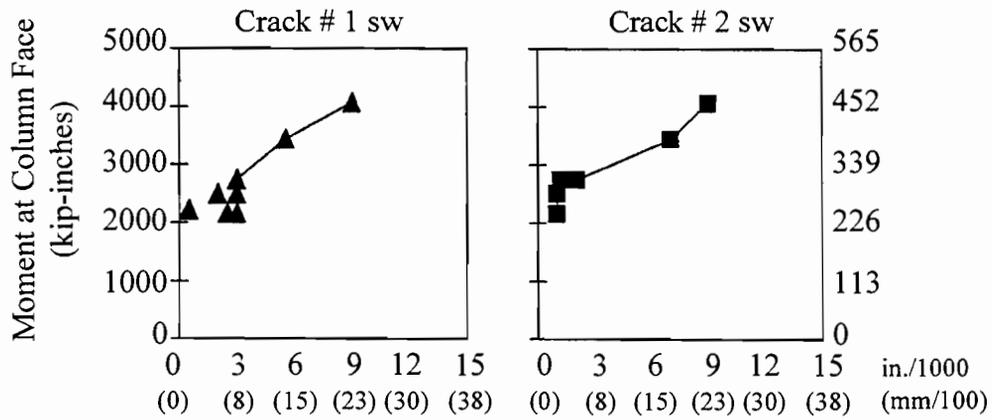
Figure B. 7   *"Major" crack plots for the CO-PU-74S-OR-V-SM overhang*
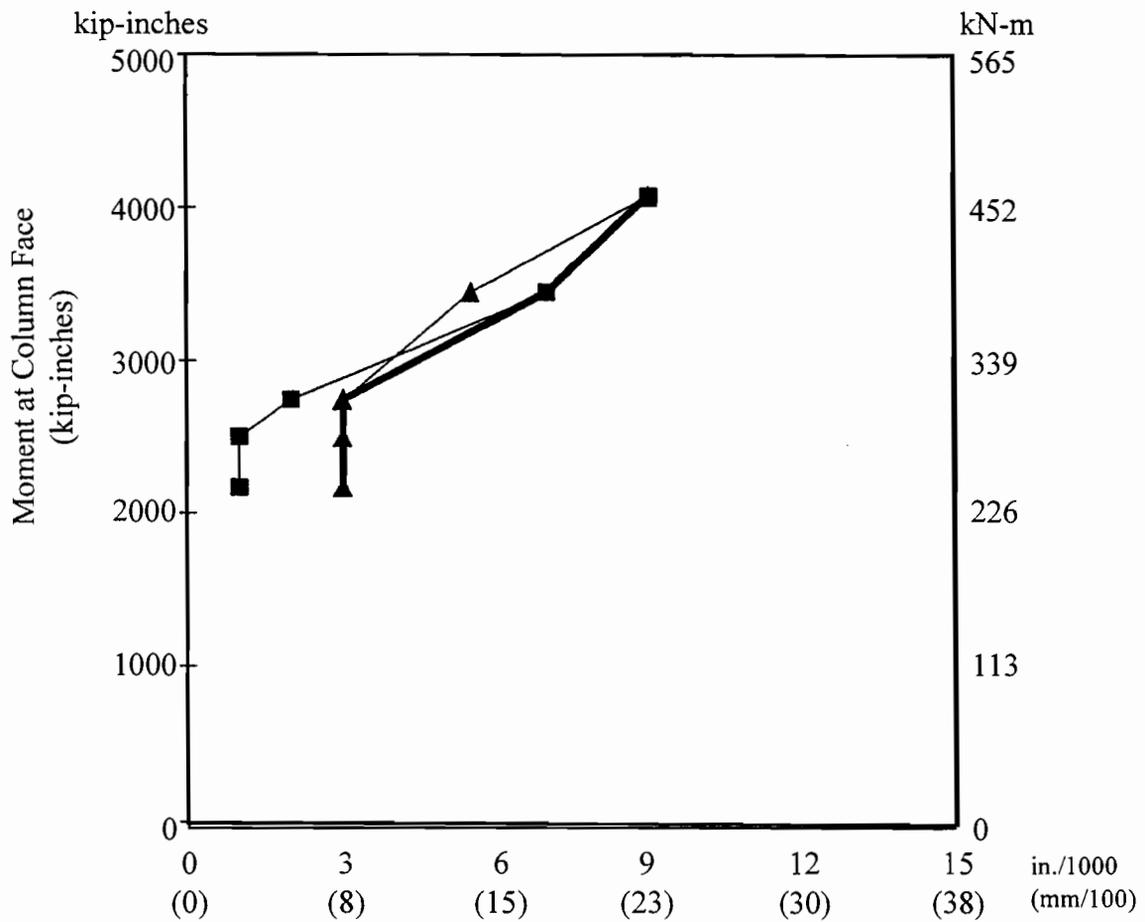
Figure B. 8   *"Crack Width Envelope" for the CO-PU-74S-OR-V-SM overhang*
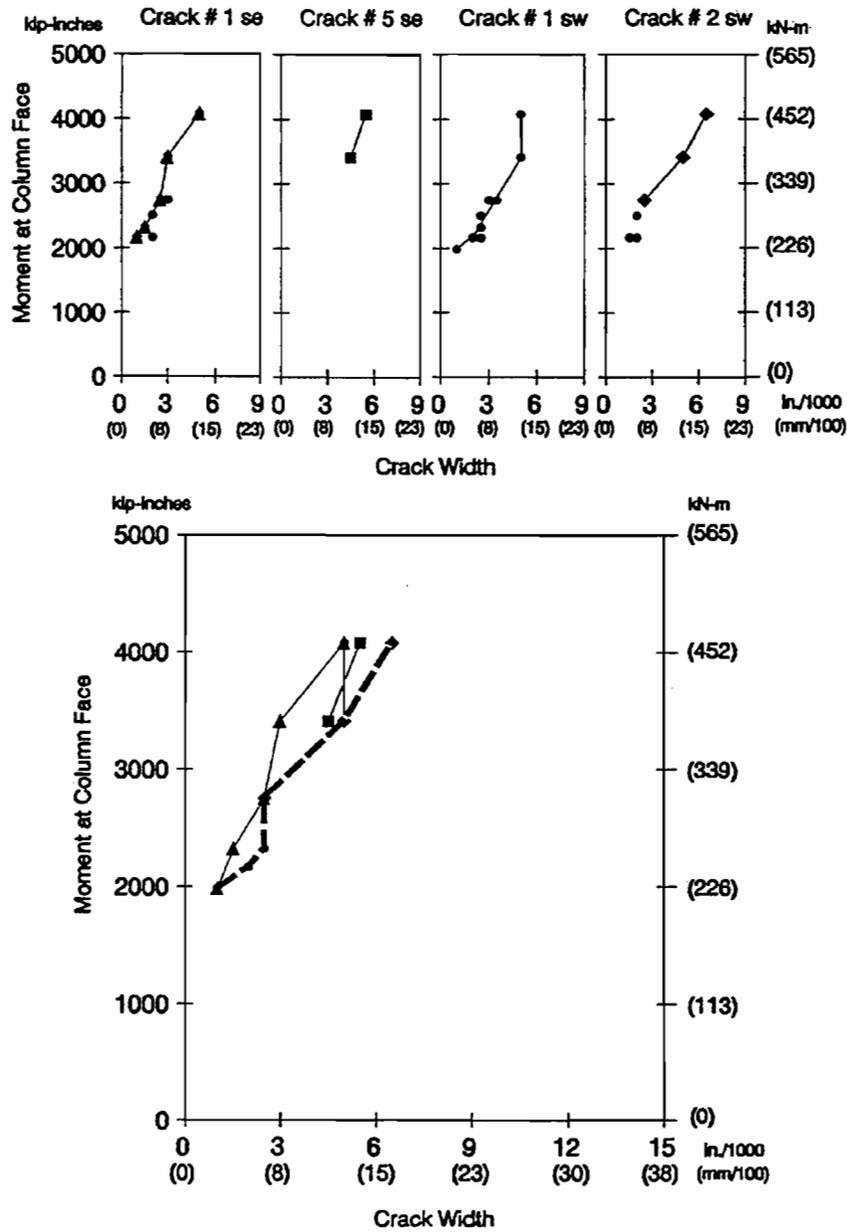
Figure B. 9   *Crack plots for CO-PU-54S-TH-V-SF overhang with "virgin" loading curves: (above) "Major" crack plots; (below) "Crack Width Envelope"*
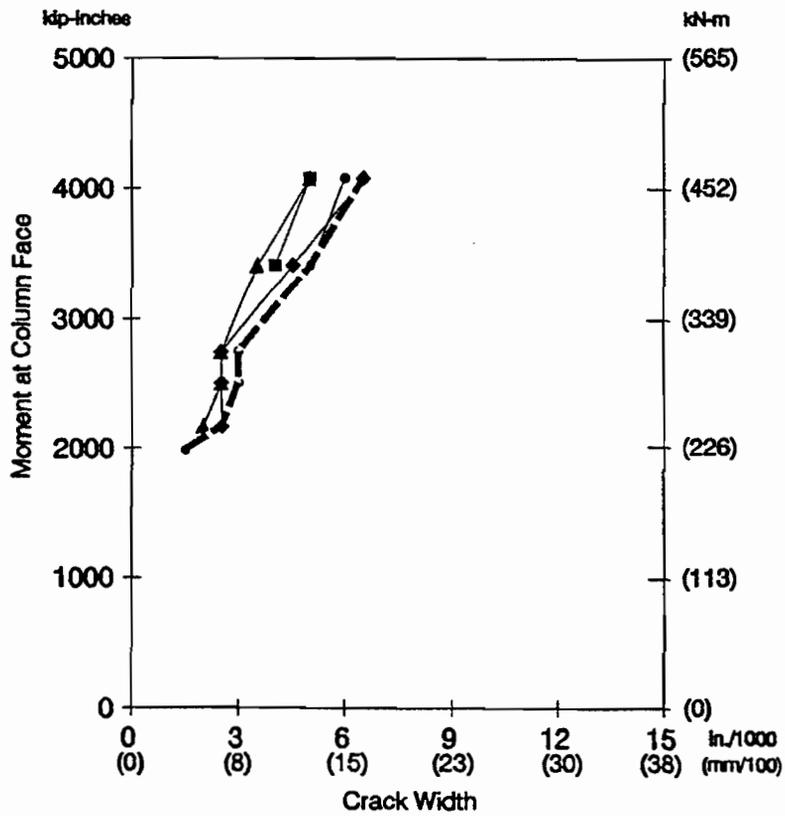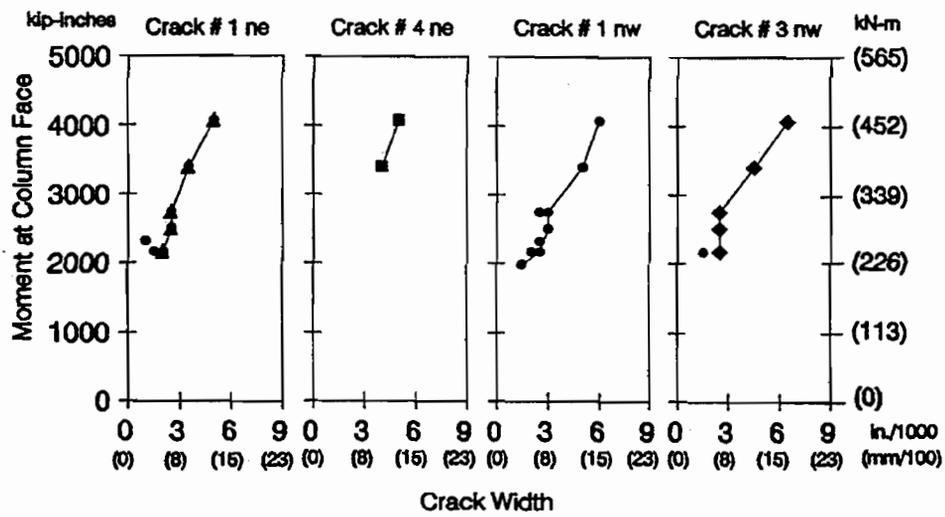
243
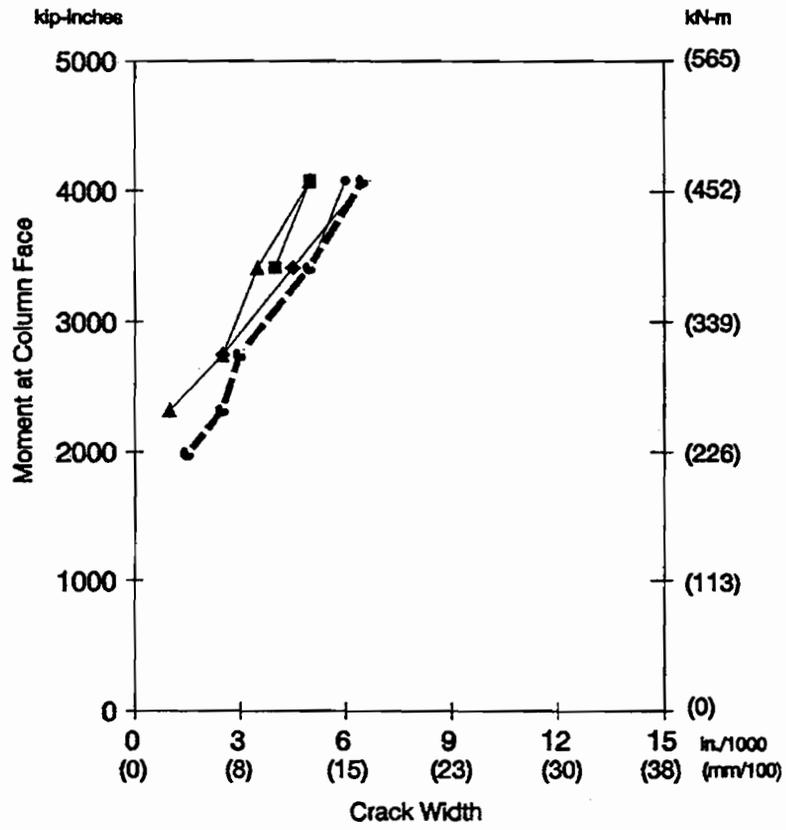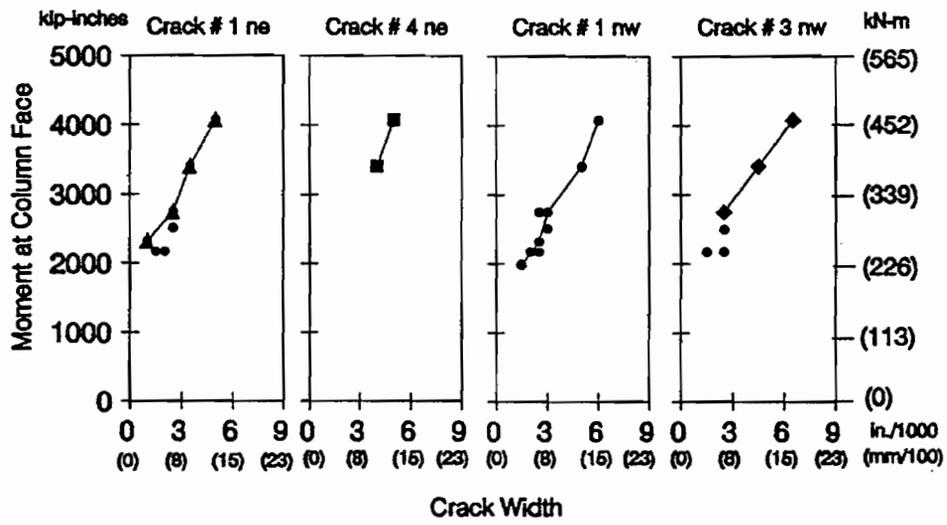
Figure B. 10   Crack plots for CO-PU-54S-TH-I-SM overhang with "virgin" loading curves: (above) "Major" crack plots; (below) "Crack Width Envelope"
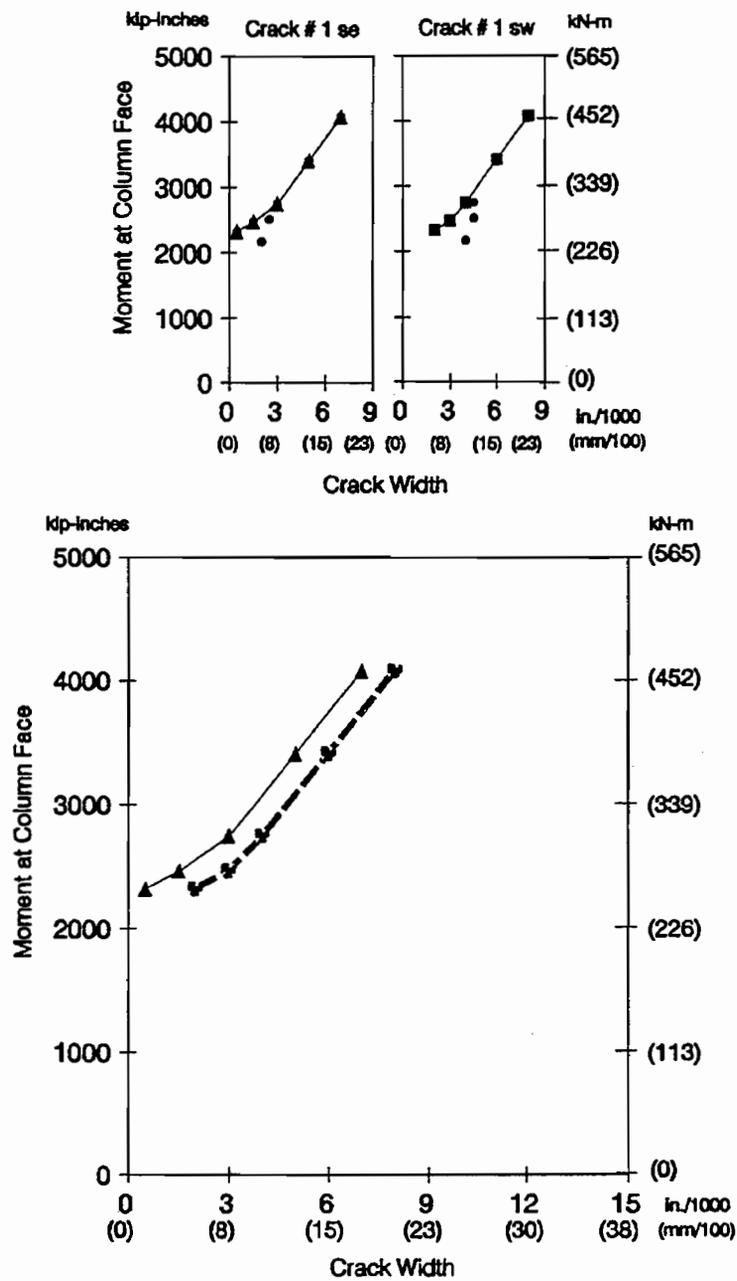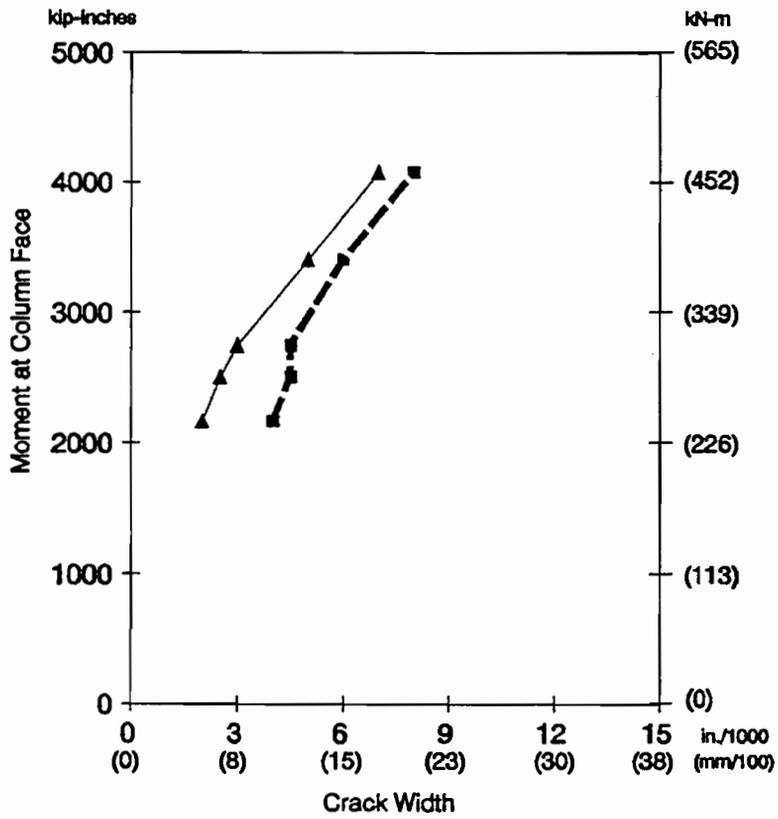
Figure B. 11   Crack plots for CO-PU-74S-TH-V-SM overhang with "virgin" loading curves: (above) "Major" crack plots; (below) "Crack Width Envelope"
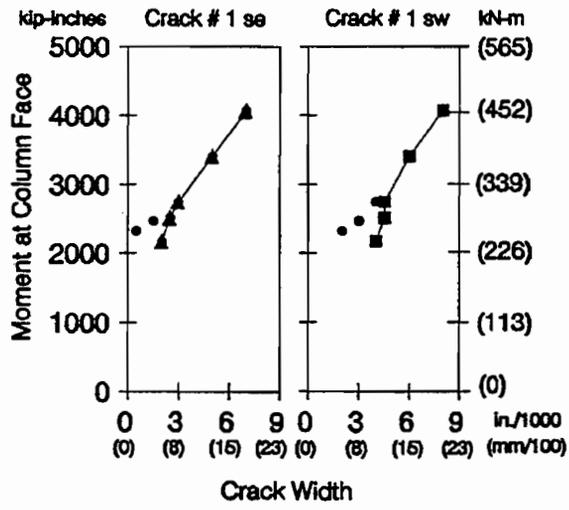
245
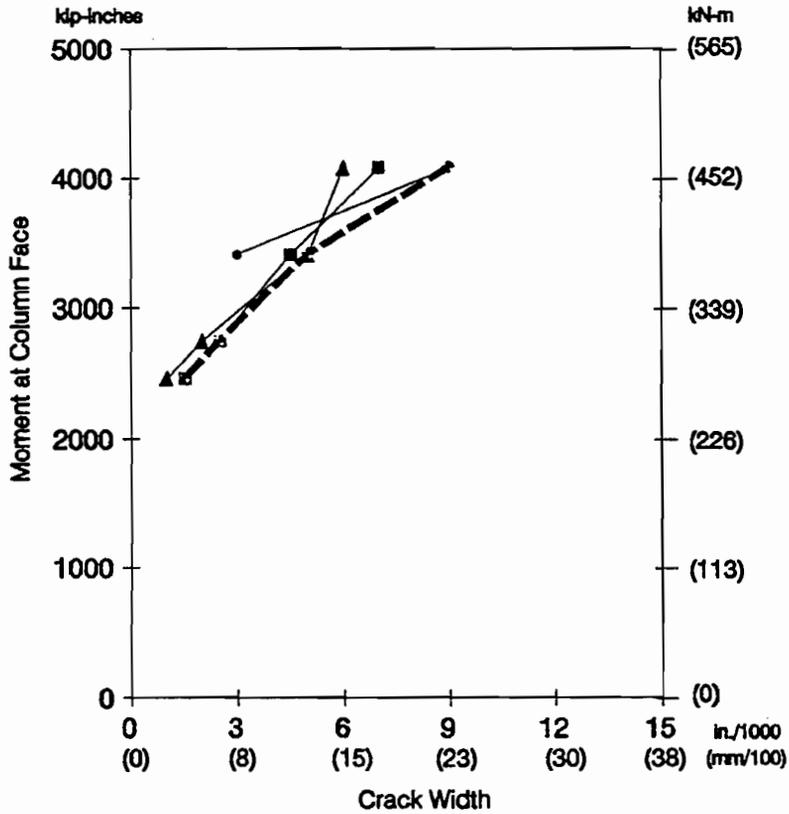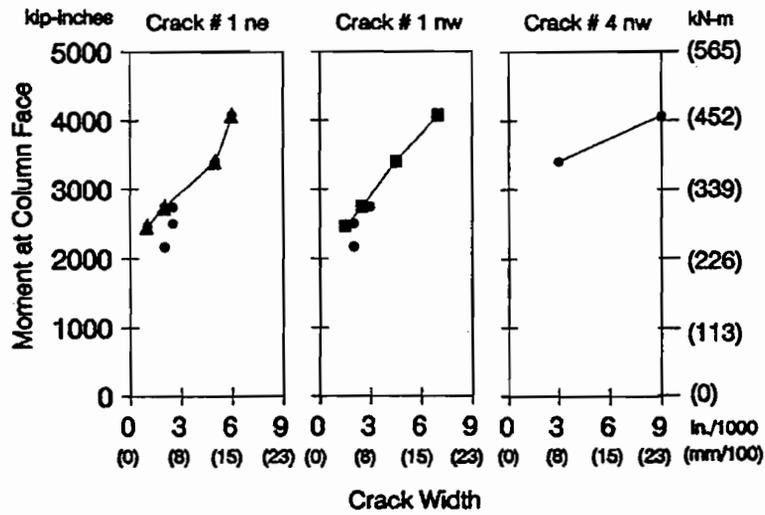
Figure B. 12   Crack plots for CO-PU-74S-TH-I-SM overhang with "virgin" loading curves: (above) "Major" crack plots; (below) "Crack Width Envelope"
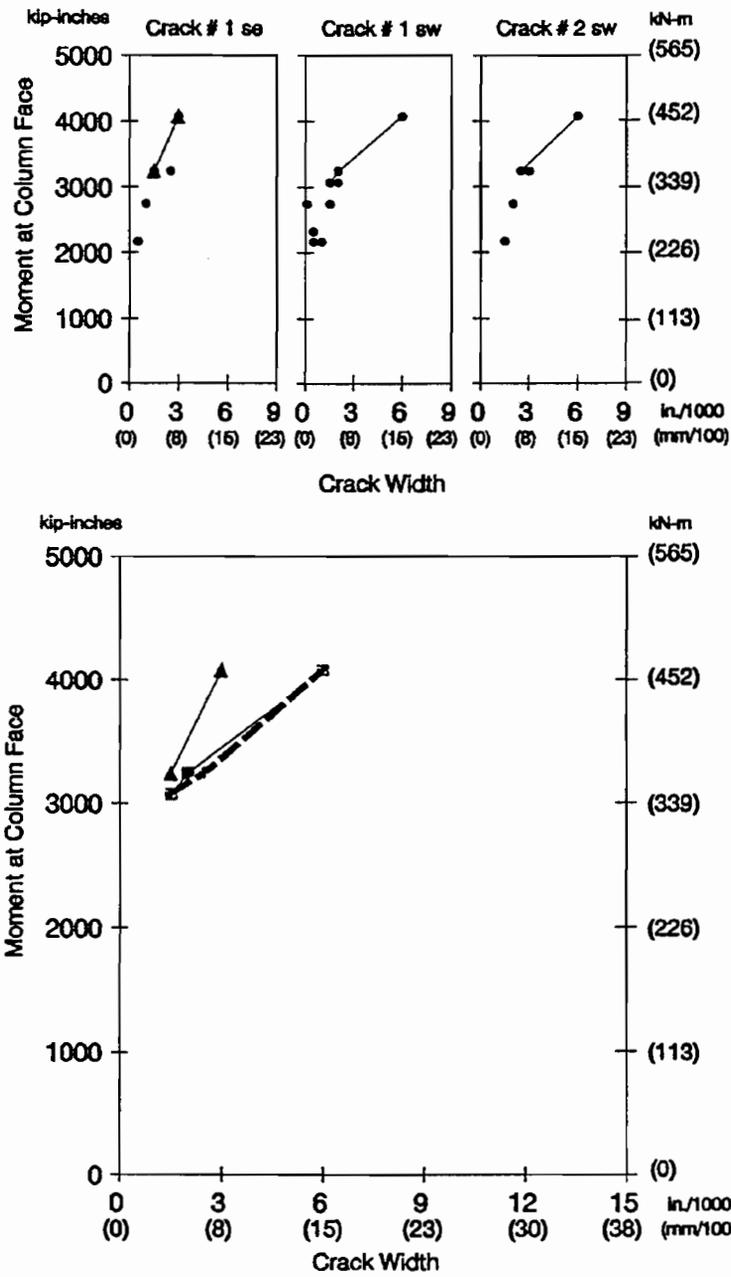
Figure B. 13   Crack plots for CO-PU-100S-TH-V-SF overhang with "virgin" loading curves: (above) "Major" crack plots; (below) "Crack Width Envelope"

247
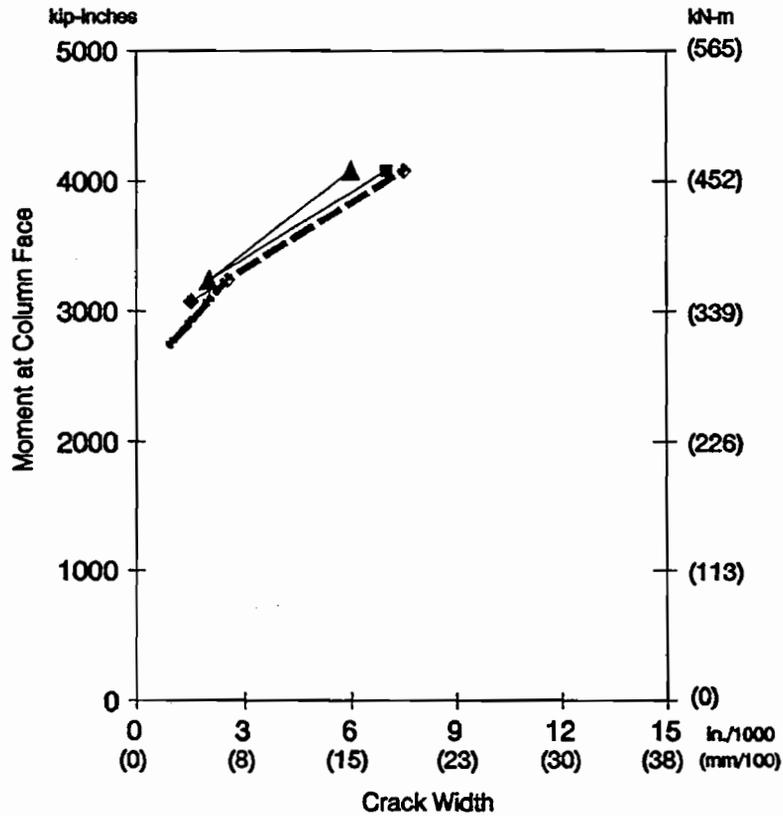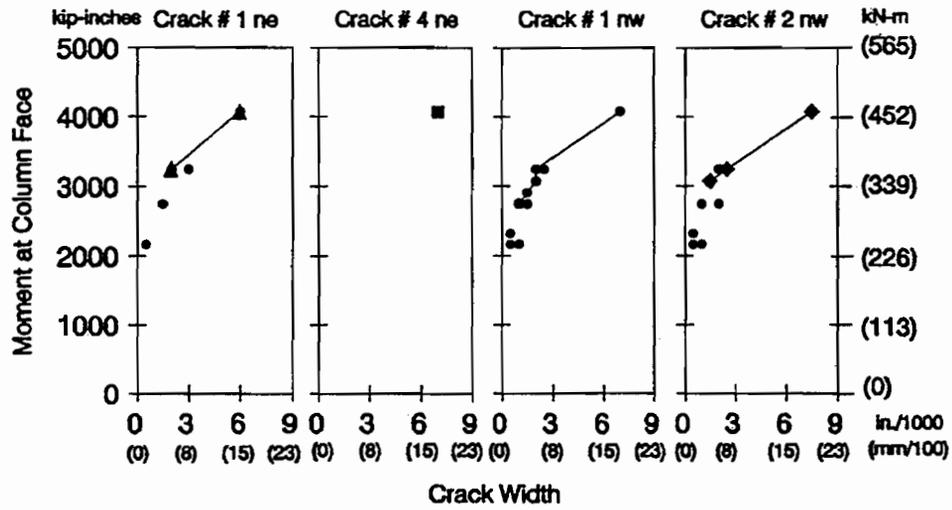
Figure B. 14   Crack plots for CO-PU-100S-TH-I-SM overhang with "virgin" loading curves: (above) "Major" crack plots; (below) "Crack Width Envelope"
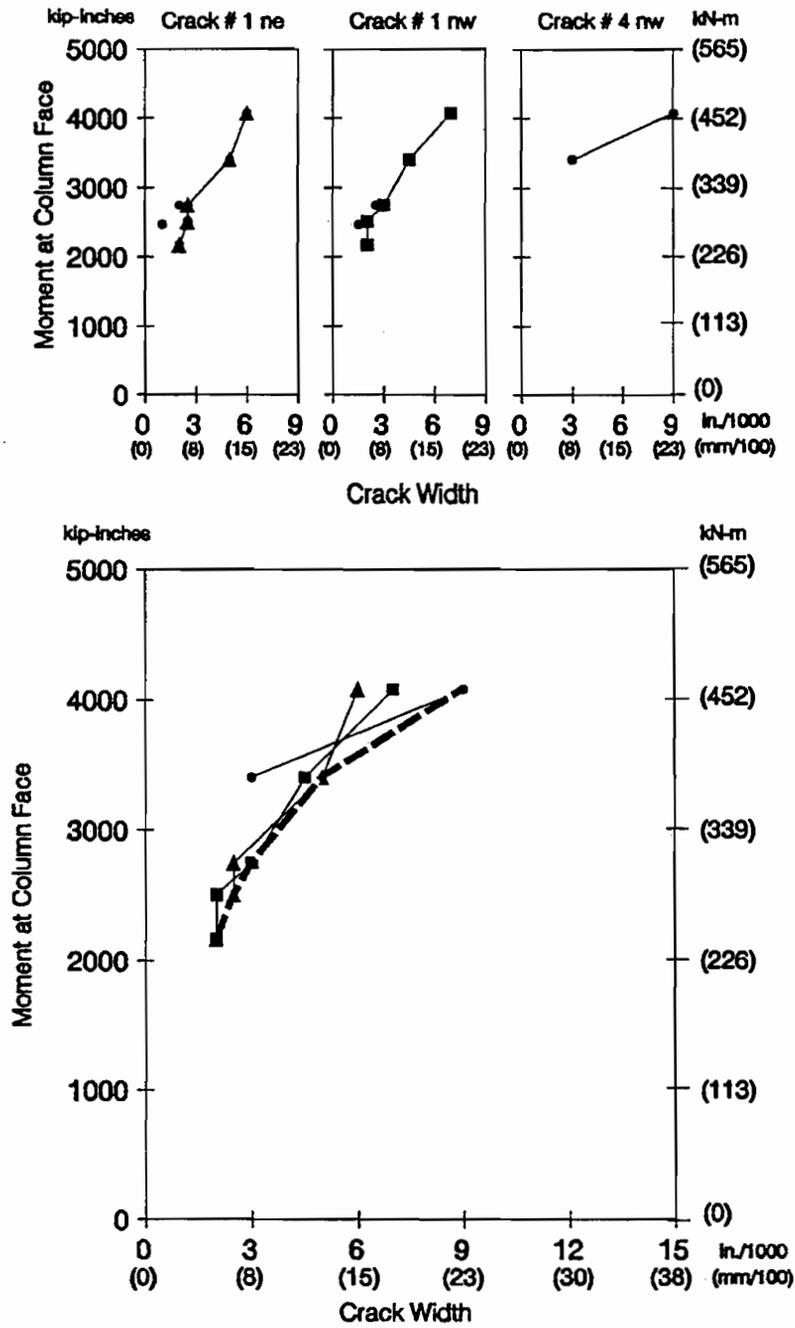
248
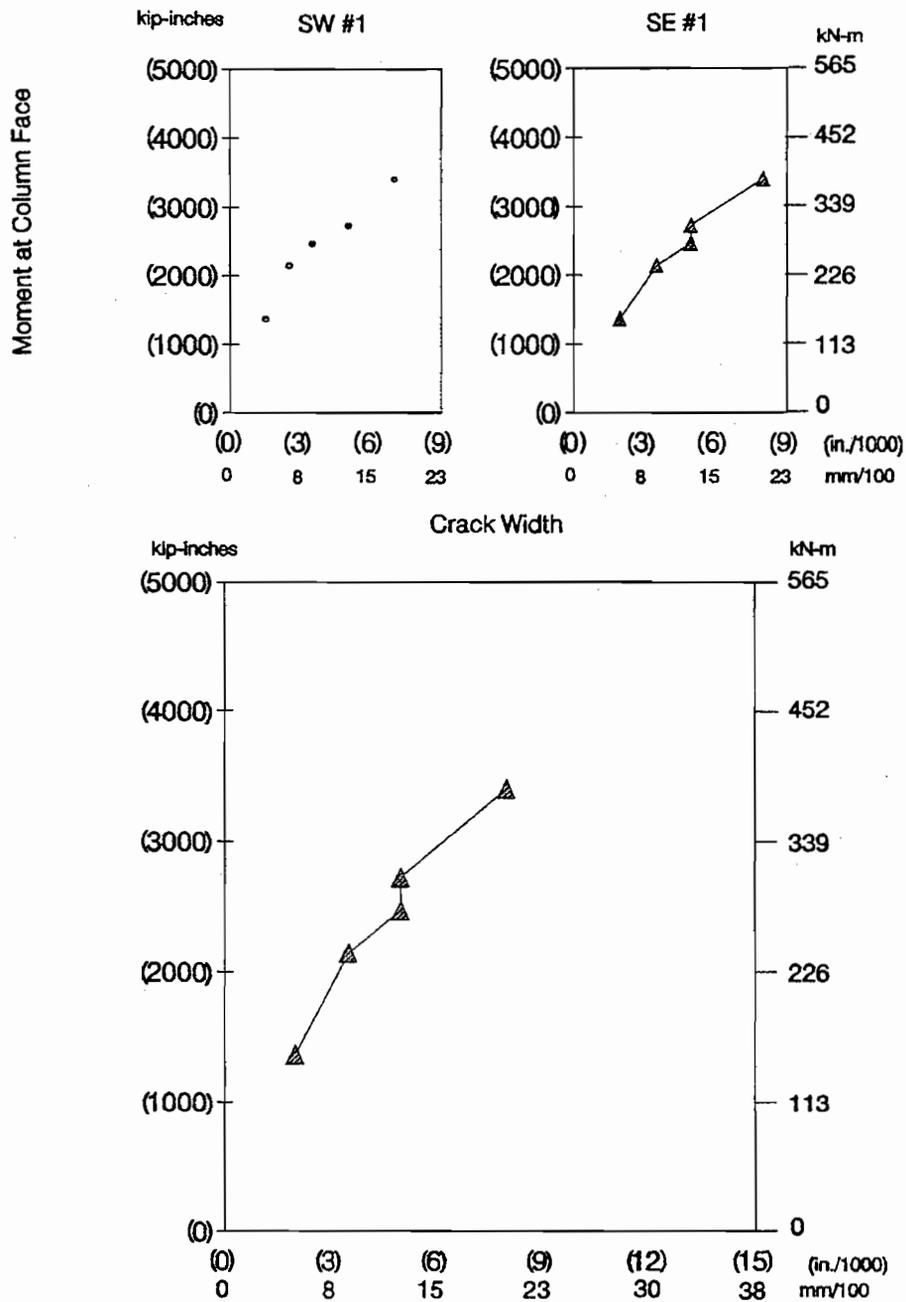
Figure B. 15   Crack plots for CO-RU-0S-TH-M1.7-SM overhang with "virgin" loading curve: (above) "Major" crack plots; (below) "Crack Width Envelope"
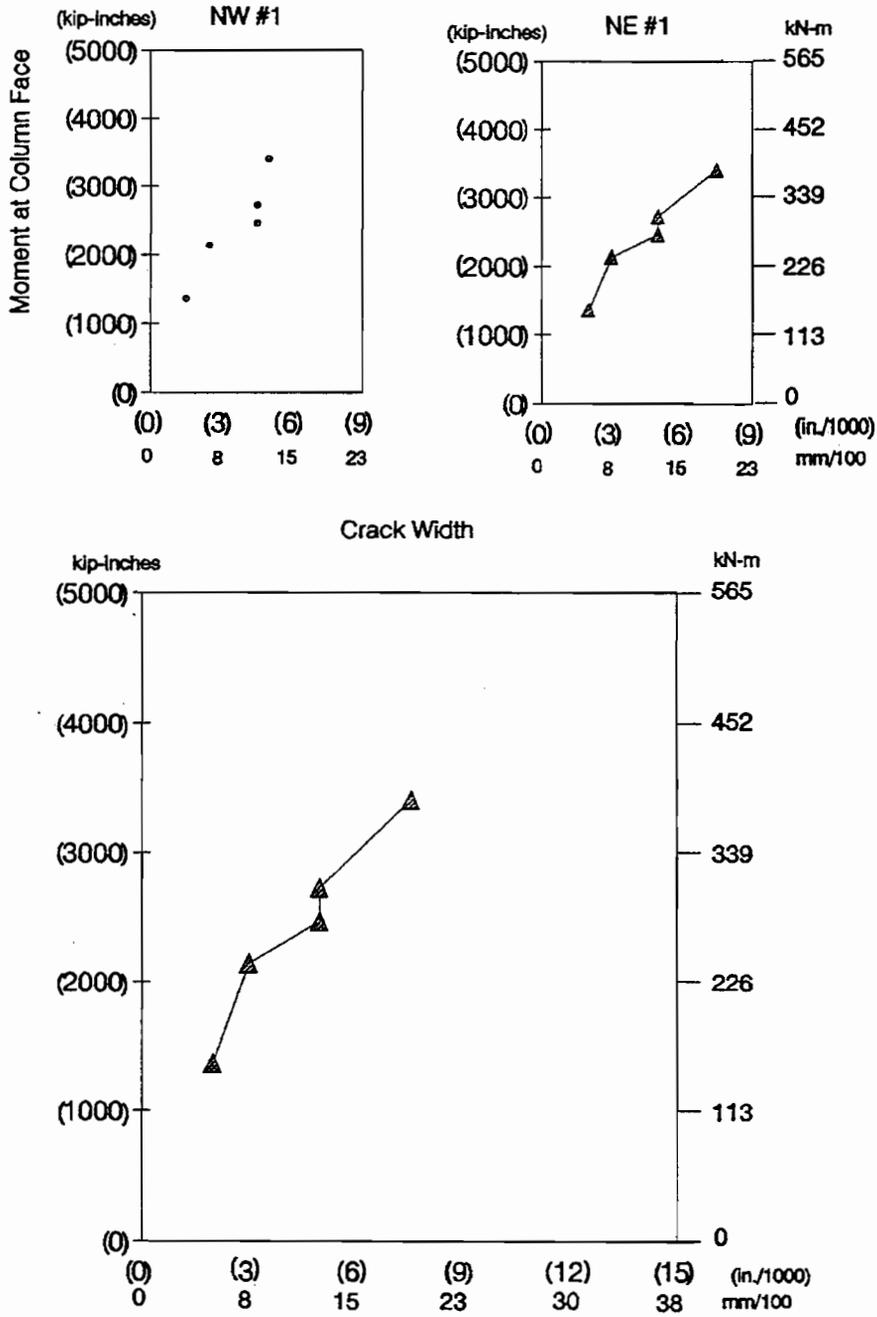
Figure B. 16   Crack plots for CO-RU-0S-TH-M1-SM overhang with "virgin" loading curve: (above) "Major" crack plots; (below) "Crack Width Envelope"
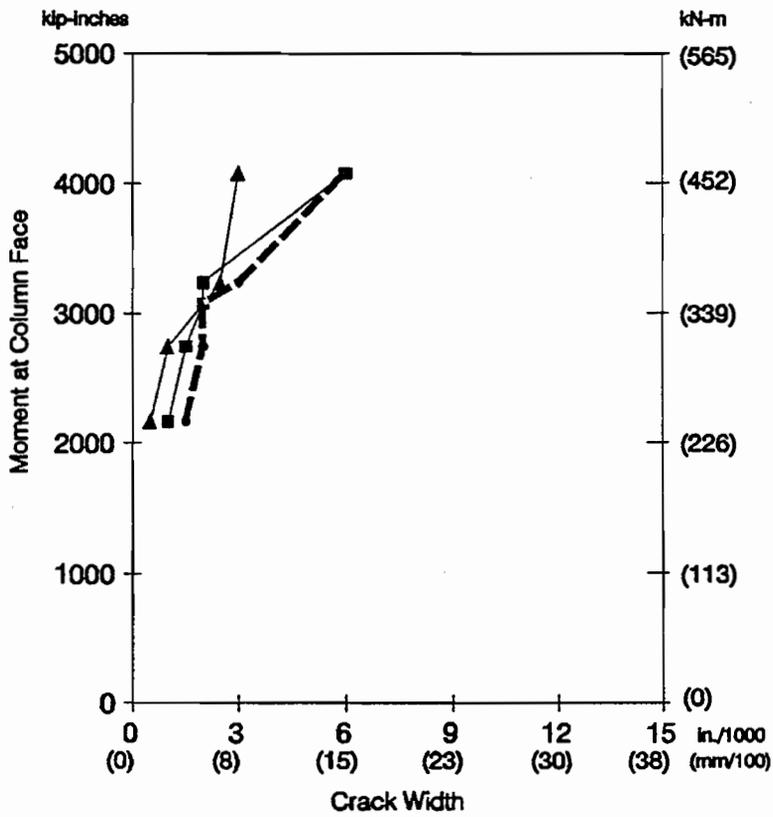
250
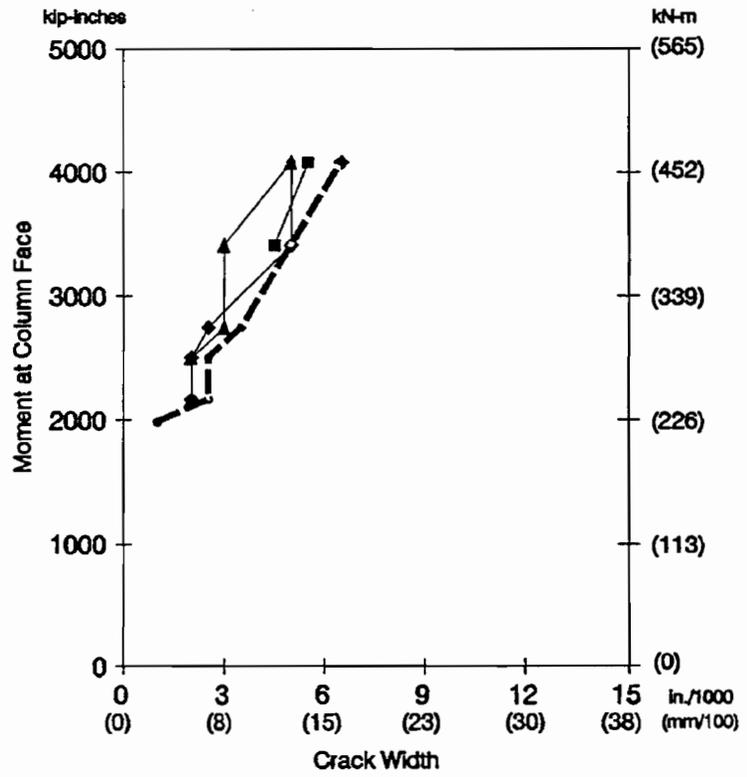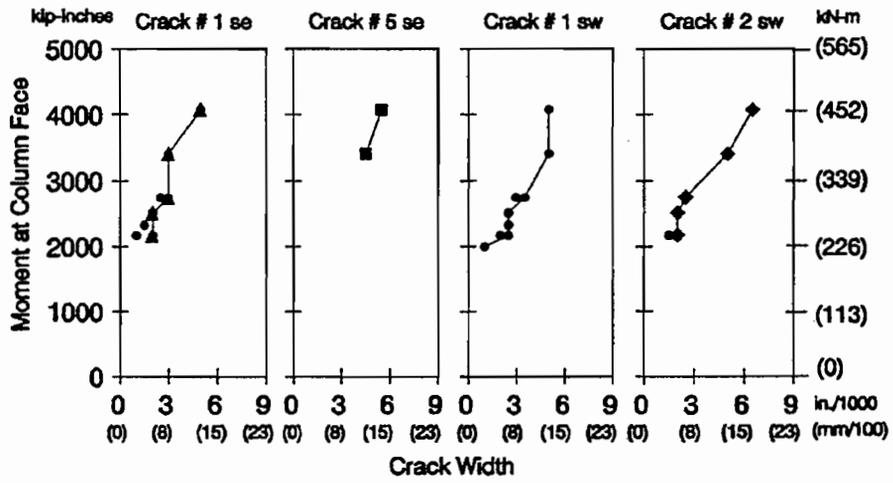
Figure B. 17   Crack plots for CO-PU-54S-TH-V-SF overhang with "complete" loading curves: (above) "Major" crack plots; (below) "Crack Width Envelope"

251

Figure B. 18   Crack plots for CO-PU-54S-TH-I-SM overhang with "complete" loading curves: (above) "Major" crack plots; (below) "Crack Width Envelope"
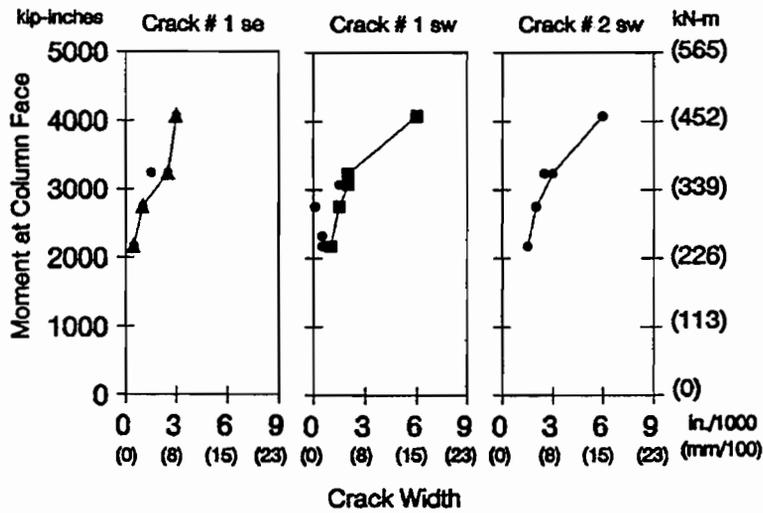
252

Figure B. 19   Crack plots for CO-PU-74S-TH-V-SM overhang with "complete" loading curves: (above) "Major" crack plots; (below) "Crack Width Envelope"
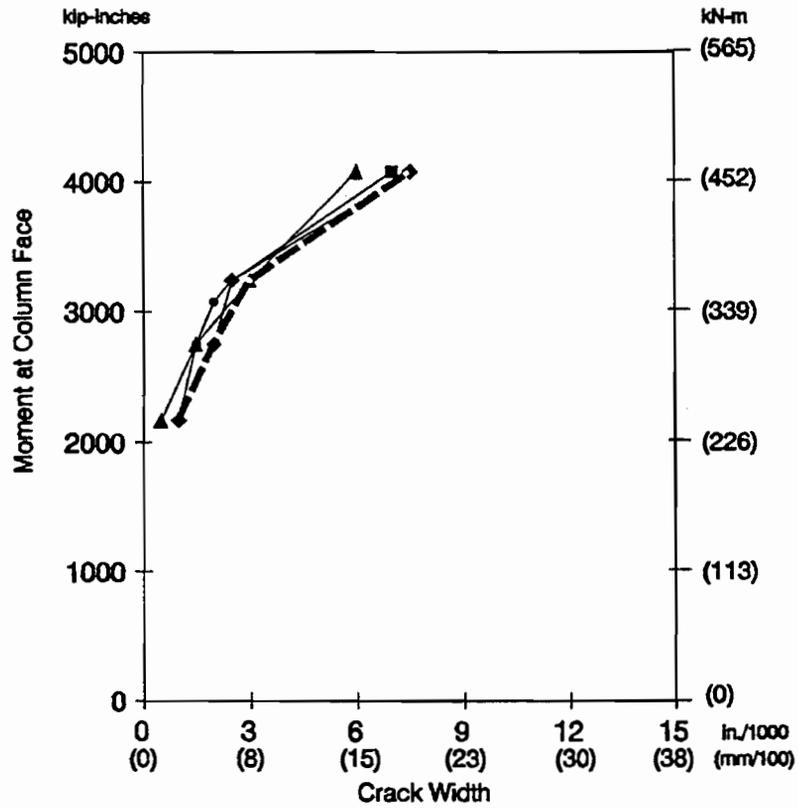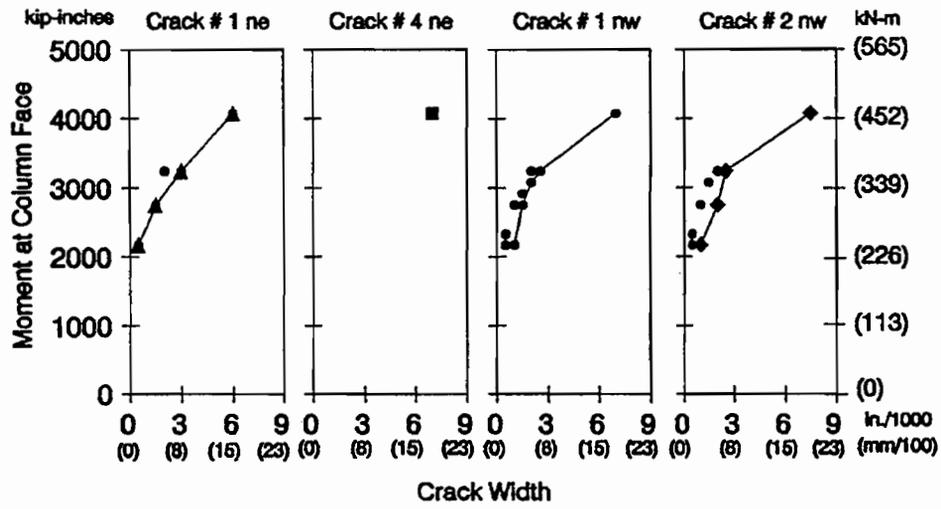
253

Figure B. 20   *Crack plots for CO-PU-74S-TH-I-SM overhang with "complete" loading curves: (above) "Major" crack plots; (below) "Crack Width Envelope"*

Figure B. 21   Crack plots for CO-PU-100S-TH-V-SF overhang with "complete" loading curves: (above) "Major" crack plots; (below) "Crack Width Envelope"

255

Figure B. 22   Crack plots for CO-PU-100S-TH-I-SM overhang with "complete" loading curves: (above) "Major" crack plots; (below) "Crack Width Envelope"
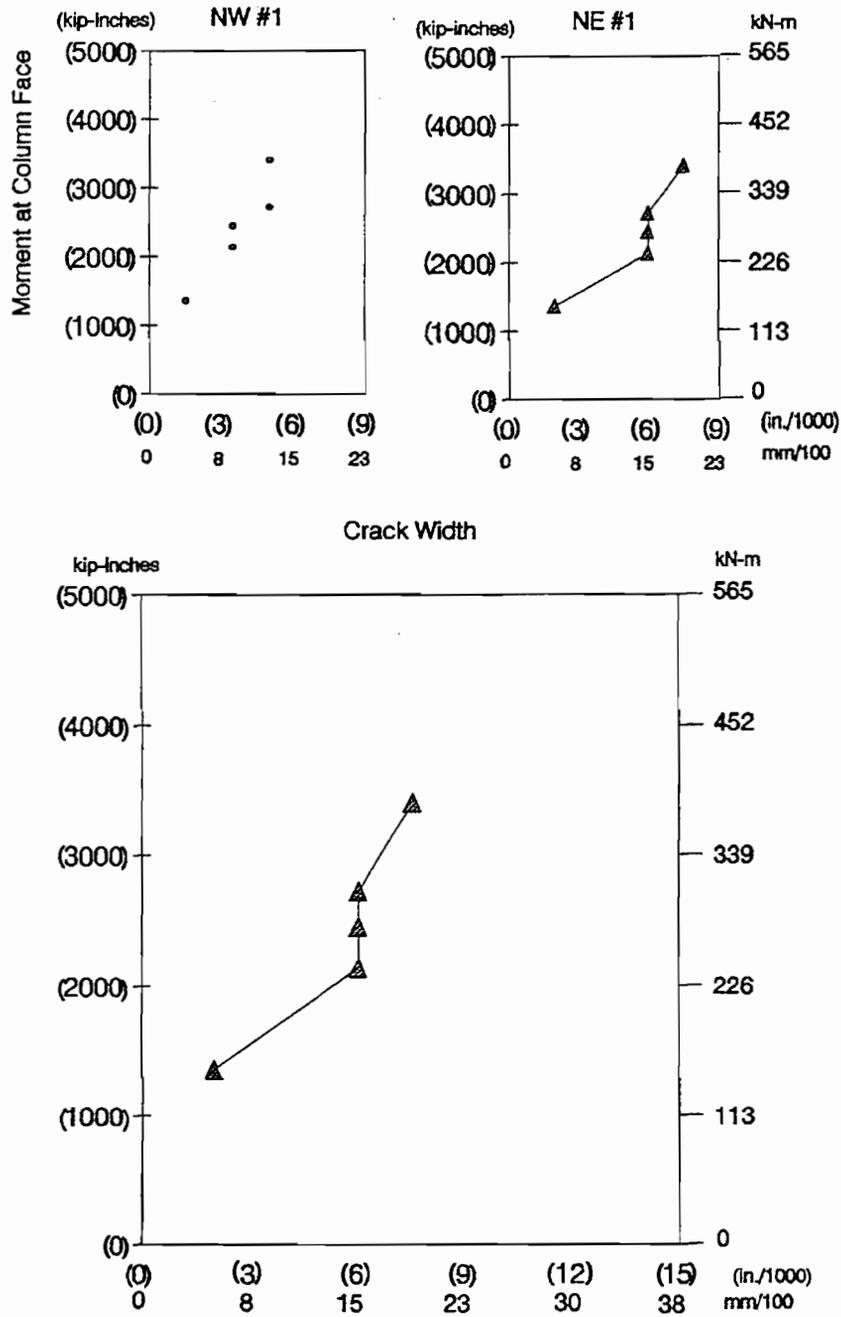
Figure B. 23   *Crack plots for CO-RU-0S-TH-M1-SM overhang with "complete" loading curve: (above) "Major" crack plots; (below) "Crack Width Envelope"*
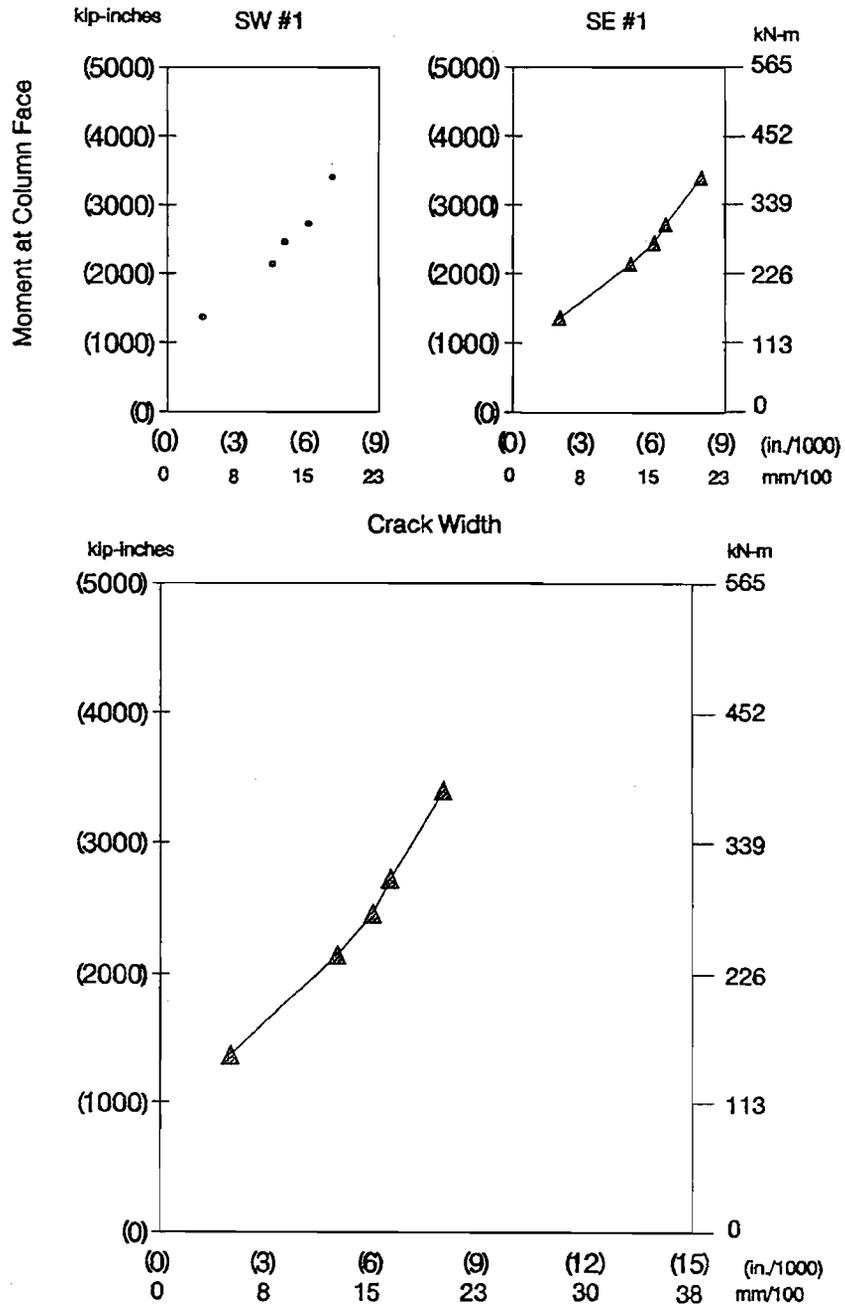
Figure B. 24   Crack plots for CO-RU-0S-TH-M1.7-SM overhang with "complete" loading curve: (above) "Major" crack plots; (below) "Crack Width Envelope"

258